Development of Computer-Aided Molecular Design Methods for Bioengineering Applications

By

Brock C. Roughton

Submitted to the graduate degree program in Bioengineering and the Graduate Faculty of the University of Kansas in partial fulfillment of the requirements for the degree of Doctor of Philosophy.

____

Chairperson Dr. Kyle Camarda

____

Dr. Stevin Gehrke

____

Dr. Luke Huan

____

Dr. Sarah Kieweg

____

Dr. Jennifer Laurence

Date Defended: December 9th, 2013

The Dissertation Committee for Brock C. Roughton

certifies that this is the approved version of the following dissertation:

Development of Computer-Aided Molecular Design Methods for Bioengineering Applications

Chairperson Dr. Kyle Camarda

Date Approved: December 13th, 2013

ABSTRACT

Computer-aided molecular design (CAMD) offers a methodology for rational product design. The CAMD procedure consists of pre-design, design and post-design phases. CAMD was used to address two bioengineering problems: design of excipients for lyophilized protein formulations and design of ionic liquids for use in bioseparations. Protein stability remains a major concern during protein drug development. Lyophilization, or freeze-drying, is often sought to improve chemical stability. However, lyophilization can result in protein aggregation. Excipients, or additives, are included to stabilize proteins in lyophilized formulations. CAMD was used to rationally select or design excipients for lyophilized protein formulations. The use of solvents to aid separation is common in chemical processes. Ionic liquids offer a class of molecules with tunable properties that can be altered to find optimal solvents for a given application. CAMD was used to design ionic liquids for extractive distillation and *in situ* extractive fermentation processes.

The pre-design phase involves experimental data gathering and problem formulation. When available, data was obtained from literature sources. For excipient design, data of percent protein monomer remaining post-lyophilization was measured for a variety of protein-excipient combinations. In problem formulation, the objective was to minimize the difference between the properties of the designed molecule and the target property values. Problem formulations resulted in either mixed-integer linear programs (MILPs) or mixed-integer non-linear programs (MINLPs).

The design phase consists of the forward problem and the reverse problem. In the forward problem, linear quantitative structure-property relationships (QSPRs) were developed using connectivity indices. Chiral connectivity indices were used for excipient property models to improve fit and incorporate three-dimensional structural information. Descriptor selection methods were employed to find models that minimized Mallow's C_p statistic, obtaining models with good fit while avoiding overfitting. Cross-validation was performed to access predictive capabilities. Model development was also performed to develop group contribution models and non-linear QSPRs. A UNIFAC model was developed to predict the thermodynamic properties of ionic liquids.

In the reverse problem of the design phase, molecules were proposed with optimal property values. Deterministic methods were used to design ionic liquids entrainers for azeotropic distillation. Tabu search, a stochastic optimization method, was applied to both ionic liquid and excipient design to provide novel molecular candidates. Tabu search was also compared to a genetic algorithm for CAMD applications. Tuning was performed using a test case to determine parameter values for both methods. After tuning, both stochastic methods were used with design cases to provide optimal excipient stabilizers for lyophilized protein formulations. Results suggested that the genetic algorithm provided a faster time to solution while the tabu search provides quality solutions more consistently.

The post-design phase provides solution analysis and verification. Process simulation was used to evaluate the energy requirements of azeotropic separations using designed ionic liquids. Results demonstrated that less energy was required than processes using conventional entrainers or ionic liquids that were not optimally designed. Molecular simulation was used to guide protein formulation design and may prove to be a useful tool in post-design verification. Finally, prediction intervals were used for properties predicted from linear QSPRs to quantify the prediction error in the CAMD solutions. Overlapping prediction intervals indicate solutions with statistically similar property values. Prediction interval analysis showed that tabu search returns many results with statistically similar property values in the design of carbohydrate glass formers for lyophilized protein formulations. The best solutions from tabu search and the genetic algorithm were shown to be statistically similar for all design cases considered. Overall the CAMD method developed here provide a comprehensive framework for the design of novel molecules for bioengineering approaches.

ACKNOWLEDGEMENTS

While only one name appears as author, my dissertation would not be possible without the help and support of many different individuals. First and foremost, I would like to express my gratitude towards God for providing perspective and direction in my life. I have been very blessed to have the experiences that graduate school as provided me. My wife Mary has been a constant source of affirmation for me. I thank her for being my partner throughout my years in graduate school despite any discomfort the weird hours and extended absences may have caused her. I have enjoyed her constant company as I journeyed from Colorado to Kansas, then Denmark, back to Kansas, to Indiana and a final return to Kansas in pursuit of my degree. I also thank my son Charlie for being a part of nearly the last two years of my graduate studies. He has brought a deeper meaning to my life and I enjoy spending every day with him. I appreciate all that my dad Bryan, mom Marie, sister Jessica and brother-in-law Matt have done to welcome us to the Sunflower State and the assistance they have offered us. I can't thank Mary's parents Hilary and Robert and her siblings Samuel and Grace enough for welcoming me into their family. They have provided continual support to Mary and I. Both Mary and my mom provided excellent editorial advice while writing my dissertation, providing the outside eye that is sometimes necessary to catch the most obvious mistakes.

My time in graduate school has exceeded my expectations and that is due in no small part to my advisor Dr. Kyle Camarda. I appreciate all that he has done to progress my professional development. He has provided me with numerous opportunities and allowed me the freedom to become confident in my own abilities. Besides an advisor, I am glad to count Kyle as a true friend. I would like to thank my dissertation committee for all that I have learned from them through courses and my comprehensive exam. Their instruction has improved the work that follows. I appreciate the guidance that Dr. Liz Topp from Purdue University has provided. She helped me to look at my work from a different perspective. I am especially

grateful for her providing me the opportunity to spend a semester at Purdue learning the experimental side of proteins. My education would be incomplete without the lessons I learned while in her lab.

I would like to extend a special thank you to all the members of the Camarda lab for their help and support over the years. Thanks go to John Eslick and JR Hacker for proving that graduation is possible! Thank you to Thora Whitmore, Rajib Anwar and Farhana Abedin for making my time in graduate school better. My appreciation goes out to the members of the Topp lab that made me feel welcome at Purdue: Lavanya Iyer, Saradha Chandrasekhar, Jainik Panchal, Bo Xie, Moorthy Balakrishnan and Andreas Sophocleous. I would also like to acknowledge all the hard-working undergraduates that I have had the pleasure to work with: Qi Chen, Haider Tarar, Briana Christian, John White, Anthony Pokphanh, Taylor Wilson and Steele Reynolds. I have met many great people while at KU and am very grateful to all the friends that I have made. You have all made my time here more worthwhile.

CONTENTS

Abstract iii

Acknowledgements v

List of Figures xi

List of Tables xiii

1.0 Introduction 1

1.1 Motivation 2

1.2 Overview 6

2.0 Background 8

Lyophilized Protein Formulation Design 8

2.1 Proteins as Drugs 8

2.2 Lyophilization 11

2.3 Protein Aggregation – Mechanisms, Measurement and Prediction 12

2.4 Approaches to Aggregation Minimization 18

2.5 Vitrification – Glass Transitions in Lyophilization 23

2.6 Protein-Excipient Interactions in the Dried State 27

Ionic Liquid Solvent Design 29

2.7 Use of Separation Media for Azeotropic Distillation and *in situ* Fermentation 29

2.8 Ionic Liquids as Separation Media 31

Forward Problem 33

2.9 Descriptors Used in Structure-Property Models 33

2.10 Property Model Development 35

2.11 Thermodynamic Property Modeling and Prediction 37

Reverse Problem 38

2.12 Computer-Aided Molecular Design (CAMD) Overview and Problem Formulation 38

2.13 Enumeration Solution Methods 41

2.14 Deterministic Solution Methods 42

2.15 Stochastic Solution Methods 43

2.16 Integrated Product-Process Design 45

2.17 Post-Design Methods 46

3.0 Experimental Methods 48

3.1 Experimental Overview 48

3.1.1 Materials 49

3.1.2 Sample Preparation 50

3.1.3 Lyophilization 51

3.2 Ultraviolet-Visible Light Spectrophotometry (UV-Vis) 52

3.2.1 Theory 52

3.2.2 Experimental Procedure 54

3.3 Size-Exclusion Chromatography (SEC) 55

3.3.1 Theory 55

3.3.2 Experimental Procedure 57

3.4 Sodium-Dodecyl-Sulfate Polyacrylamide Gel Electrophoresis (SDS-PAGE) 57

3.4.1 Theory 57

3.4.2 Experimental Procedure 58

3.5 Powder X-ray Diffraction (pxrd) 59

3.5.1 Theory 59

3.5.2 Experimental Procedure 62

3.6 Hydrogen-Deuterium Exchange Mass Spectroscopy (HX-MS) 63

3.6.1 Theory 63

3.6.2 Use in Lyophilized Solids 65

4.0 Property Model Development: The Forward Problem 67

4.1 Calculation of Molecular Descriptors 70

4.1.1 Group Contribution 70

4.1.2 Connectivity Indices 71

4.1.3 Protein-Based Descriptors 74

4.1.4 Principal Component Analysis 75

4.2 Development of Linear QSPRs 76

4.2.1 Glass Transition Properties 76

4.2.2 Percent Monomer Remaining Following Lyophilization 76

4.2.3 Properties for in situ NDHD recovery 77

4.2.4 Descriptor selection 78

4.2.5 Cross-Validation 80

4.3 Development of Non-Linear QSPRs 81

4.3.1 Selection of Functional Forms 81

4.3.2 Parameter Fitting 82

4.3.3 Parameter Sensitivity 82

4.3.4 Statistical Verification 83

4.4 Group Contribution Methods 84

4.4.1 Hildebrand Solubility Parameter 84

4.4.2 Thermal Decomposition Temperature 86

4.4.3 Group Contribution Model Development 86

4.5 UNIFAC-IL Model Development 93

4.5.1 Theory 93

4.5.2 Determination of Groups and Group Parameters 96

4.5.3 Determination of Interaction Parameters 97

5.0 Molecular Design Methods: The Reverse Problem 98

5.1 Deterministic Design of Ionic Liquid Entrainers 98

5.2 Use of Tabu Search in Design of Ionic Liquid Extractants and Carbohydrate Glass-Formers 101

5.3 Development of Stochastic Design Methods for Carbohydrate Excipients in Lyophilized Protein Formulations 102

5.4 Tuning of Stochastic Design Methods for Carbohydrate Excipients in Lyophilized Protein Formulations 117

5.4.2 Genetic Algorithm 119

5.5 Comparison of Stochastic Design Methods for Carbohydrate Excipients in Lyophilized Protein Formulations 119

6.0 Simultaneous Product and Process Design 122

6.1 Driving Force Based Design 123

6.2 Azeotrope Separation Process Simulation 125

7.0 Molecular Simulation for Design and Post-Design Stages 128

7.1 Use of AutoDock for Blind Docking Simulations 129

7.2 Determination of Protein-Excipient Interactions 129

7.3 Optimal Selection of Excipients 130

7.4 Docking Simulation Results 132

7.5 Formulation Selection for Maximizing Protein-Excipient Interactions 134

8.0 Results for Ionic Liquid Design 136

8.1 Hildebrand Solubility Parameter Group Contribution Model 136
8.2 UNIFAC-IL Model 138
8.3 CAMD Results for Ionic Liquid Entrainers 144
8.4 Design of Ionic Liquid-Based Azeotropic Separation Processes 149
8.5 Prediction of Relevant Properties for in situ Extractive Fermentation 154
8.6 CAMD results for in situ Extractants 156
9.0 Results for Lyophilized Excipient Design 158
9.1 Glass Transition Temperature Property Models 158
9.2 Results for Optimal Glass Former Design 163
9.3 Experimental Results for Post-Lyophilization Protein Loss 167
9.4 Post-Lyophilization Protein Loss Models: As a Function of Protein Structure 170
9.5 Post-Lyophilization Protein Loss Models: As a Function of Excipient Structure 181
9.5.1 Principal Component Analysis and Descriptor Comparison 182
9.5.2 Correlation and K-Fold Cross-Validation 184
9.6 Post-Lyophilization Protein Loss Models: As a Function of Both Protein and Excipient Structure 190
9.7 Stochastic Optimization Tuning Results 195
9.8 Results for Optimal Design of Stabilizers for Lyophilized Protein Formulations 207
10.0 Conclusions and Future Recommendations 217
References 221
A. Nomenclature 232
B. R Procedure For Model Development 236
C. Polymer Designer Procedure 244
Ionic Liquid Groups Used in Polymer Designer 246
Excipient Groups Used in Polymer Designer 247
D. CAMD Excipient Designer Source Code 249
CAMD Module Code 249
Property Module Code 257
Connectivity Indices Calculator Code 264
Tabu Search Code 269
Genetic Algorithm Code 276
E. UNIFAC-IL Interaction Parameters 282
F. Summary of Experimental Data 285

LIST OF FIGURES

Figure 1.1 Computer-aided molecular design methodology 4
Figure 2.1 Hierarchy of protein structure 10
Figure 2.2 Vial containing lyophilized protein formulation 11
Figure 2.3 Solutions containing aggregated protein 13
Figure 2.4 Pathway for the formation of aggregates through conformation instability 14
Figure 2.5 Preformulation and formulation development process diagram 22
Figure 2.6 The phase transitions that occur during the lyophilization process 26
Figure 2.7 Hydroxyl groups on sucrose 28
Figure 2.8 Block flow diagram of azeotropic distillation process 30
Figure 2.9 Block flow diagram of *in situ* extractive fermentation 31
Figure 2.10 The ionic liquid 1,3-dimethylimidazolium dimethylphosphate (MMIm DMP) 32
Figure 2.11 A general procedure for the solution of the CAMD reverse problem 39
Figure 2.12 Overview of integrated product and process design 46
Figure 3.1 Overview of experimental procedure used by author 49
Figure 3.2 Chromophores commonly present in proteins 53
Figure 3.3 Typical UV-Vis spectra for a protein 54
Figure 3.4 Overview of size-exclusion chromatography (SEC) 56
Figure 3.5 Representative gel following SDS-PAGE 58
Figure 3.6 Diagram of typical powder x-ray diffraction setup 60
Figure 3.7 Representative x-ray diffraction patterns 62
Figure 3.8 A peptide bond, which forms between amino acids to construct the protein backbone 63
Figure 3.9 General experimental procedure for HX-MS experiments performed in aqueous solution 65
Figure 4.1 Procedure for experimental data acquisition and model development for rational lyophilized formulation development 68
Figure 4.2 Example group contributions for (A) ethanol, (B) acetone and (C) benzene 70
Figure 4.3 Comparison of the chiral structures of stereoisomers (A) glucose and (B) mannose 73
Figure 4.4 Oxidation of naphthalene to (1R,2S)-1,2-naphthalene dihydrodiol (NDHD) 77
Figure 4.5 Values for Mallow's Cp statistic versus model size (number of connectivity indices used) 79
Figure 5.1 CAMD framework developed to design carbohydrate excipients using either tabu search or a genetic algorithm 103
Figure 5.2 Number of possible combinations of groups that would provide solutions to a CAMD problem 106
Figure 5.3 Tabu search algorithm as implemented in the CAMD framework 111
Figure 5.4 Genetic algorithm as implemented in the CAMD framework 115
Figure 6.1 Overall methodology for simultaneous design of ionic liquid entrainers and IL-based separation processes 122

Figure 6.2 Proposed ionic liquid-based azeotropic separation process 125
Figure 7.1 Frequency of amino acid residues of calmodulin in contact with trehalose 133
Figure 7.2 Trehalose interaction regions mapped to the surface of calmodulin 133
Figure 8.1 Comparison between experimental and predicted solubility parameter values 137
Figure 8.2 Acetone-methanol-[emim][triflate] x-y diagram at 100 kPa 141
Figure 8.3 1-propanol-water-[emim][triflate] x-y diagram at 100 kPa 141
Figure 8.4 Ethyl acetate-ethanol-[emim][triflate] x-y diagram at 100 kPa... 142
Figure 8.5 Ethanol-water-[emim][triflate] x-y diagram at 100 kPa 142
Figure 8.6 1-propanol-water-[mmim][dmp] P-T diagram... 143
Figure 8.7 2-propanol- water-[mmim][dmp] P-T diagram.. 143
Figure 8.8 x-y diagram showing the performance of several ionic liquid entrainers on the acetone-methanol azeotrope at 101.325 kPa... 146
Figure 8.9 x-y diagram showing the performance of several ionic liquid entrainers on the ethanol-water azeotrope at 101.325 kPa 147
Figure 8.10 Reboiler heat duty as a function of feed stage location for separation of the ethanol-water azeotrope using various amounts of [mmim][dmp] as an entrainer.. 150
Figure 8.11 Reboiler heat duty as a function of ionic liquid flow rate for separation of the ethanol-water azeotrope using [mmim][dmp] as an entrainer.. 150
Figure 8.12 1-octyl-4-methylpyridinium trifluoromethane sulfonate ([ompy][triflate])......................... 153
Figure 8.13 1,3-dimethylimidazolium dimethylphosphate ([mmim][dmp])... 153
Figure 8.14 Comparison of correlation coefficient values belong to different model sizes for the partition coefficient model (K_x).. 155
Figure 8.15 The best cation candidates for the design cases (A) and (B) 156
Figure 9.1 Comparison of measured experimental values to QSPR predicted values for the glass transition temperature of the anhydrous solute (T_g) 160
Figure 9.2 Comparison of measured experimental values to QSPR predicted values for the glass transition temperature of the maximally freeze-concentrated solute (T_g') 161
Figure 9.3 Comparison of measured experimental values to QSPR predicted values for the melting point of ice (T_m') 162
Figure 9.4 Comparison of measured experimental values to QSPR predicted values for the Gordon-Taylor constant (k) 163
Figure 9.5 Optimal carbohydrate excipient candidate 1 proposed by CAMD using tabu search............ 165
Figure 9.6 Optimal carbohydrate excipient candidate 2 proposed by CAMD using tabu search............ 165
Figure 9.7 Optimal carbohydrate excipient candidate 3 proposed by CAMD using tabu serach............ 166
Figure 9.8 Parity plots of experimental percent monomeric protein values (%Monomer) from SEC versus predicted %Monomer values... 177
Figure 9.9 Principal component analysis of descriptor space for excipients used in study 182
Figure 9.10 Comparison of chiral and simple connectivity indices for BSA and RNAse carbohydrate models.. 183
Figure 9.11 Parity plots of percent monomer remaining after lyophilization as a function of carbohydrate excipient choice for (A) BSA, (B) RNAse A, (C) α-Amylase, (D) Ovalbumin and (E) Trypsin Inhibitor....... 185

Figure 9.12 Parity plots of percent monomer remaining after lyophilization as a function of amino acid excipient choice for (A) BSA and (B) RNAse A 186
Figure 9.13 Parity plots of percent monomer remaining after lyophilization as a function of both protein and excipient structure 193
Figure 9.14 Tuning results for tabu search with varying maximum number of non-improving iterations 196
Figure 9.15 Tuning results for tabu search with varying maximum number of neighbors considered at each iteration 197
Figure 9.16 Tuning results for tabu search with varying tabu list length of stored solution 198
Figure 9.17 Tuning results for tabu search with varying tabu criteria 199
Figure 9.18 Tuning results for genetic algorithm with varying maximum number of generations 201
Figure 9.19 Tuning results for genetic algorithm with population size per generation 202
Figure 9.20 Tuning results for genetic algorithm with varying maximum probability that a member will be selected as a parent 203
Figure 9.21 Comparison between objective function values obtained for all 100 trial solutions of the test case by (A) tabu search and (B) the genetic algorithm 205
Figure 9.22 Comparison between times to solution observed for all 100 trial solutions of the test case during (A) tabu search and (B) the genetic algorithm 206
Figure 9.23 Optimal carbohydrate stabilizer candidates for BSA, as determined by (A) tabu search and (B) genetic algorithm 209
Figure 9.24 Optimal carbohydrate stabilizer candidates for RNAse A, as determined by (A) tabu search and (B) genetic algorithm 210
Figure 9.25 Optimal carbohydrate stabilizer candidates for α-amylase, as determined by (A) tabu search and (B) genetic algorithm 211
Figure 9.26 Optimal carbohydrate stabilizer candidates for ovalbumin, as determined by (A) tabu search and (B) genetic algorithm 212
Figure 9.27 Optimal carbohydrate stabilizer candidates for trypsin inhibitor, as determined by (A) tabu search and (B) genetic algorithm 213
Figure 9.28 Comparison across protein models of average chemical information for solutions derived by both tabu search and genetic algorithm 215
Figure F.1 Pxrd results for subset of formulations selected 287

LIST OF TABLES

Table 2.1 Summary of experimental techniques commonly utilized in the detection of protein aggregates 16
Table 2.2 Common protein engineering targets for property improvement 20
Table 2.3 Overview of stochastic approaches commonly used in CAMD 44
Table 3.1 Biophysical descriptors for the proteins considered 50
Table 4.1 Summary of property models developed for both lyophilized protein formulation design and ionic liquid design for use in separations of bio-products 69

Table 4.2 Biophysical descriptors for the proteins considered 74
Table 4.3 Descriptors obtained and derived from aggregation propensity prediction methods 75
Table 4.4 Ionic liquid groups used for GC model development 87
Table 5.1 Property targets for molecular design using tabu search 101
Table 5.2 Building block groups and chiral subgroups available for design of new excipient candidates 104
Table 5.3 Description of VBA functions and subroutines used for molecular representation 108
Table 5.4 Moves used to generate neighbors to current solution in tabu search 112
Table 5.5 Moves used to generate offspring to selected parents in the genetic algorithm 116
Table 5.6 Parameter values used for the base case during tuning of the tabu search 118
Table 5.7 Parameter values used for the base case during tuning of the genetic algorithm 119
Table 6.1 Fixed parameters and free variables for ionic liquid-based extractive distillation processes .. 127
Table 7.1 Sugar-surfactant formulations selected for maximum interaction with hot spot regions 134
Table 8.1 Group contribution values for ionic liquid Hildebrand solubility parameter model 138
Table 8.2 Volume (R_k) and surface area (Q_k) parameters for the UNIFAC-IL model 139
Table 8.3 UNIFAC-IL binary interaction parameters for the groups used for the final design candidates in the acetone-methanol and ethanol-water examples 140
Table 8.4 Comparison of minimum amount of designed and experimentally selected ionic liquids required to break the acetone-methanol and ethanol-water azeotropes at 101.325 kPa 148
Table 8.5 Simulation results for ionic liquid-based azeotropic separation processes 151
Table 9.1 Summary of glass transition-related QSPRs developed 159
Table 9.2 Property values of candidate carbohydrate excipients designed using tabu search 164
Table 9.3 Descriptors selected using an exhaustive search method with model size selected by minimizing C_p score 171
Table 9.4 Correlation results for all four formulations 173
Table 9.5 Descriptors selected using a forward search method with AIC evaluation 174
Table 9.6 Summary of covariance analysis 179
Table 9.7 Comparison of model size (including intercept), R2 and Q2 values for final protein-specific models selected 187
Table 9.8 Protein-by-protein model parameters determined by multiple linear regression following descriptor selection 189
Table 9.9 List of descriptors considered for non-linear model development 191
Table 9.10 Summary statistics of non-protein specific model 192
Table 9.11 Final tuned values for tabu search and the genetic algorithm 204
Table E.1 UNIFAC-IL group interaction parameters 283
Table F.1 Summary of experimental measures of protein aggregation via SEC (% monomer), UV- Vis (AI) and SDS-PAGE 286
Table F.2 Experimental SEC results 291
Table F.3 SDS-PAGE Results under non-reducing and reducing conditions 292

1.0 INTRODUCTION

Chemical product design is an important, yet often overlooked, aspect of chemical engineering. Traditionally, chemical engineering has focused on process design, yet the aim of any process is to manufacture a product of value. The objective of process design is to maximize output and profit while minimizing material and energy inputs. Additional factors, such as safety and environmental concerns, further constrain the process design. The same design principles can be applied to chemical product design, where a molecule requires specific chemical or physical properties for a certain task. Other properties can be used as constraints to further ensure the designed product works to the correct specifications. Chemical product design has been defined as the process in which needs are determined, candidates are generated to meet needs, screening and selection of candidates identifies the best candidate and the final candidate is manufactured into a finished product (Cussler and Moggridge 2011). The product design problem is often addressed by extensive experimental generate-and-test approaches. Such approaches would not be feasible in many process design problems, and thus systems engineering and process design developed to identify solutions from a modeling, simulation and optimization perspective. Computer-aided molecular design (CAMD) offers a methodology that aims to reduce trial-and-error and rationally design and select candidates in chemical product design using systems engineering principles. In general, CAMD aims to solve the chemical product design problem by determining a molecule or formulation (mixture of molecules) that best matches a set of target properties given an assortment of chemical groups (Gani 2004). The advent of engineering approaches to biological systems presents many new opportunities for the application and further development of computer-aided molecular design. The work that follows describes the development and use of CAMD approaches towards two applications of biological relevance: design of lyophilized protein formulations and design of ionic liquid solvents for use in separation of bio-products.

1.1 MOTIVATION

Protein drugs are a fast growing pharmaceutical market. Global spending on biologics, which include protein drugs and cell-based therapies, in 2011 was \$157Bn and is expected to grow to \$200Bn by 2016 (source: IMS Health, http://www.imshealth.com). In relation to traditional pharmaceutical molecules, biologics are gaining market share. Of the top 100 drugs by U.S. sales in the fourth quarter of 2012, 28 were protein drugs or other biologics (source: IMS Health, http://www.imshealth.com). Lyophilization, or freeze-drying, is a common process used to increase the stability of protein drug products through the removal of water. Despite improvements to chemical stability, lyophilization can induce protein aggregation. Protein aggregation is undesirable in drug products as it can reduce efficacy, cause immunogenicity and/or result in product losses during production. Thus, reduction of protein aggregation is a topic of extreme interest and concern in the pharmaceutical industry. The two general approaches taken to minimize aggregation are protein engineering and formulation development. The work detailed here focuses on use of CAMD for the design of a molecule or set of molecules for inclusion in a lyophilized formulation with the aim of minimizing aggregation.

Another class of molecules receiving increased attention both in research and industry is ionic liquids. The number of publications concerning ionic liquids has jumped from less than 100 in 2000 to nearly 2,500 in 2011 (Ann, Nicholas *et al.* 2012). Ionic liquids are attractive as environmentally friendly, or "green", solvents due to their extremely low vapor pressure and tunable properties through alteration of the cation and anion selected (Marsh, Boxall *et al.* 2004; Zhao, Xia *et al.* 2005). Two bio-based applications of ionic liquids as solvents are used as the basis for CAMD in this work: ionic liquids as entrainers in azeotropic distillation and ionic liquids as extraction media for *in situ* fermentation processes.

Distillation is a commonly used unit operation that allows for separation of products based on differences in volatility. Azeotropic distillation allows separation of azeotropes through use of an entrainer, further increasing the applications of distillation. A major drawback to distillation is the energy requirements. Distillation processes are estimated to account for 40% of the entire energy usage of the chemical processing industry in North America (U.S. Dept. of Energy 2001). The use of ionic liquids as entrainers has shown improvements in energy requirements in comparison to conventional entrainers used in azeotropic distillation (Seiler, Jork *et al.* 2004).

Fermentation is a common method which utilizes microorganisms for the production of chemicals. Substrate/product inhibition and separation of chemical products are two main concerns that reduce the efficiency of fermentation processes. By removing the product as it is produced, *in situ* fermentation offers a solution to these concerns. Ionic liquids have been proposed for use as extractive media for *in situ* fermentation processes due to their flexible properties obtained by altering the cation and anion used (Gangu, Weatherley *et al.* 2009). Through CAMD methods, optimal ionic liquids can be identified for azeotropic distillation and *in situ* fermentation resulting in increasingly efficient separation processes.

CAMD provides a methodology for the rational design or selection of molecules for a specific task. CAMD methodology consists of a forward and a reverse problem (Venkatasubramanian, Chan *et al.* 1994). In the forward problem, property models are developed which relate chemical structure to properties of interest. The reverse problem determines a molecular structure which best matches a set of target property values and property constraints. The overall design methodology is outlined by Figure 1.1.

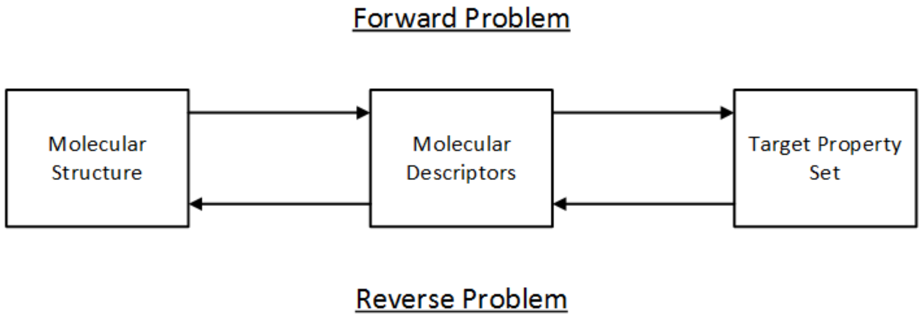

Figure 1.1 Computer-aided molecular design methodology The forward problem relates molecular structure to property values through molecular descriptors. The reverse problem determines the molecular descriptor values and hence molecular structure that provides an optimal match to target property values.

While much research has been spent on the reverse problem, little effort has been spent on the forward problem (Patel, Ng *et al.* 2009). Many CAMD methods utilize group contribution (GC) property models (Gani, Nielsen *et al.* 1991; Harper and Gani 2000). Group contribution methods describe molecular structure as a collection of chemical fragments of groups. The number and type of groups are correlated to properties of interest. GC methods generally do not account for the connectivity of the molecule and provide a low level of molecular representation (Patel, Ng *et al.* 2009). The work here largely uses connectivity indices to represent molecular structure to provide higher level molecular representation and increased accuracy in property modeling. Connectivity indices and other topological indices are becoming more widespread in the development of property models for CAMD (Raman and Maranas 1998; Camarda and Maranas 1999; Siddhaye, Camarda et al. 2000; Lin, Chavali et al. 2005; Eslick, Ye et al. 2009; McLeese, Eslick et al. 2010; Roughton, Topp et al. 2012). The following work advances the level of molecular representation used in CAMD approaches through the integration of chirality information in the calculation of connectivity indices.

Descriptor selection is trivial in the development of GC property models as the descriptors needed are defined by the types of chemical groups present in the model building set. GC models run the risk of over-fitting as a result, potentially leading to poor property prediction. By using connectivity indices, descriptor selection techniques become available to ensure the development of models with good fits and predictive ability. The work here integrates established statistical techniques for descriptor selection with CAMD model development for the first time. Additionally, model cross-validation methods used previously in CAMD (Eslick, Ye et al. 2009) are further advanced.

Given a set of predictive property models, a CAMD solution technique is employed to design or select candidate molecules for a given task in the reverse problem. Three main solution approaches have been used in CAMD: enumeration techniques, mathematical programming and stochastic optimization (Eljack and Eden 2008). Enumeration techniques use a set of chemical groups to generate all chemical combinations and then screen the combinations using property targets and constraints. As the number of groups and/or the maximum allowable molecule size becomes large, enumeration techniques can suffer from combinatorial explosion. Enumeration approaches are also reliant on a predefined chemical group set that may preclude the consideration of many novel molecules. Mathematical programming poses the CAMD problem as a mixed integer linear program (MILP) or mixed integer nonlinear program (MINLP). While solution of a MILP ensures that a globally optimal solution is found, many CAMD problems require a MINLP representation. Solution of a MINLP can be computationally expensive and does not guarantee that the solution found is the global optimum (Eljack and Eden 2008). Furthermore, a global optimum may not be necessary or even meaningful for CAMD approaches due to uncertainties in property prediction. CAMD methods which employ stochastic optimization algorithms are iterative procedures which aim to find multiple near-optimal or locally optimal solutions. The speed in generation of a set of many good candidate molecules makes stochastic optimization approaches attractive for CAMD and stochastic approaches are the focus of this work. Genetic algorithm CAMD approaches mimic evolution to refine a population of candidate molecules through a series of generations, until candidates are identified that provide the best match to a set of target properties (Venkatasubramanian, Chan *et al.* 1994). Tabu search CAMD approaches use a local search to identify candidate molecules while maintaining a history of previous solutions (Lin, Chavali *et al.* 2005). The solution history, stored in tabu lists, is used to guide the local search and determine when the search should be expanded to consider other, more diverse molecular structures (Lin, Chavali *et al.* 2005). While both methods have advantages – multiple initial solutions (seed population) in genetic algorithms and memory guided search (via tabu lists) in tabu search – the utility of one stochastic method over another for CAMD is not established. The work that follows details the development, tuning and comparison of genetic algorithms and Tabu search for CAMD to identify the strengths and weaknesses in both approaches. Finally, as stochastic methods generate many locally optimal solutions, a comparison method would provide a tool to determine the best subset of solutions for further consideration. The work here demonstrates a novel application of prediction intervals to provide statistical comparisons of CAMD solutions obtained from stochastic solution methods. The prediction interval comparisons are made between solutions found using the same method and also between the best solutions found using different methods.

1.2 Overview

The following chapter (Section 2) will offer further background into both the lyophilized protein formulation and ionic liquid solvent design problems being considered, along with a detailed explanation of CAMD methodology and state-of-the-art. In addition to the use of CAMD towards novel applications, the work concerned here also presents new approaches for CAMD model development, solution and final candidate selection. To design a molecule with target properties, models must exist for prediction of the targeted properties. Experimental data is needed for model development. The experimental methods used in the work are detailed in Section 3. Development of reliable property models is imperative as the validity of a CAMD solution rests on the predicted properties being accurate. The work described in Section 4 details the efforts made to improve property prediction by uniting established statistical techniques to model development for CAMD problems. Solution of the CAMD problem provides candidate molecules for a given application. The CAMD solution approaches presented here are based on optimization frameworks and are detailed in Section 5. Solution of the optimization problems are approached through both deterministic and stochastic methods, with the use of stochastic methods being emphasized. Additional computational tools have been utilized and are detailed in Section 6 (process design) and Section 7 (molecular simulation). Results are presented in Section 8 (ionic liquid design) and Section 9 (excipient design). Finally, conclusions and future recommendations are given in Section 10.

For further clarification, nomenclature is given in Appendix A. The procedure used for model development is provided in Appendix B. Appendix C provides guidelines for using a previously existing CAMD framework while Appendix D provides the source code for a new CAMD framework proposed here. Additional interaction parameters for a UNIFAC model developed by this work are available in Appendix E. All experimental data obtained by the author are summarized in Appendix F.

2.0 BACKGROUND

CAMD requires a product design problem for solution. Two different problems related to bioengineering have been addressed here: design of lyophilized protein formulations to minimize aggregation and design of ionic liquids for separation of bio-products. Background on lyophilization and protein aggregation is given in Sections 2.1-2.6. Background regarding ionic liquids and their use in separations is given in Sections 2.7-2.8. Once a design problem of interest has been identified, property models are needed to link key properties for design to molecular structure (the forward problem). Sections 2.9-2.11 describe model development for both structure-property relationships as well as thermodynamic property models. Upon creation of reliable property models, CAMD is used to generate candidates that optimally match a given set of target properties (the reverse problem). The CAMD methodology and its historical development are detailed in Sections 2.12-2.17.

LYOPHILIZED PROTEIN FORMULATION DESIGN

2.1 PROTEINS AS DRUGS

Proteins are increasingly being considered as therapeutic candidates. Proteins fulfill a multitude of biological functions including catalysis, transport and structural support and consequently have been indicated in numerous disease states (Leader, Baca *et al.* 2008). Currently, approved protein drugs are available for treatment of a wide range of diseases including diabetes, multiple sclerosis, rheumatoid arthritis, cancer and hepatitis (Marshall, Lazar *et al.* 2003). Compared to traditional small molecule pharmaceuticals, protein molecules have increased complexity.

Proteins are biopolymers comprised of amino acids. The main structure of an amino acid involves an amino group and carbonyl group common to all amino acids along with a side group that defines the amino acid. There are twenty common amino acids used in the biosynthesis of proteins, which can be arranged in classes of non-polar or hydrophobic, polar, acidic and basic amino acids. Two amino acids bond covalently to form a peptide bond between the amide nitrogen of one amino acid and carbonyl carbon of another amino acid. The formation of peptide bonds creates the polypeptide backbone which is common among all proteins with structural diversity arising from the amino acid side groups. The amino acid sequence of the protein is referred to as the primary structure. Proteins do not exist as linear molecules but instead fold into a variety of three-dimensional conformations. Structural motifs known as α-helices and β-sheets (pleated sheets) form the secondary structure of a protein. Such motifs are formed by hydrogen bonding between the amide hydrogen of one amino acid and the carbonyl oxygen of another amino acid. The three-dimensional arrangement of secondary structural elements and unfolded regions constitutes the tertiary structure of the protein, which is driven by the amino acid sequence (Anfinsen 1972). Minimization of exposed non-polar or hydrophobic surface area and formation of intramolecular contacts are two main driving forces in the tertiary structure adopted by a protein (Pace, Shirley *et al.* 1996; Rose, Fleming *et al.* 2006). Quaternary structure is derived from arrangement of single folded polypeptide chains into multi-protein complexes. An overview of the structural hierarchy in proteins is given by Figure 2.1. The biological function of proteins is derived from protein structure. As a result, preservation of native structure is essential for proper function of therapeutic proteins.

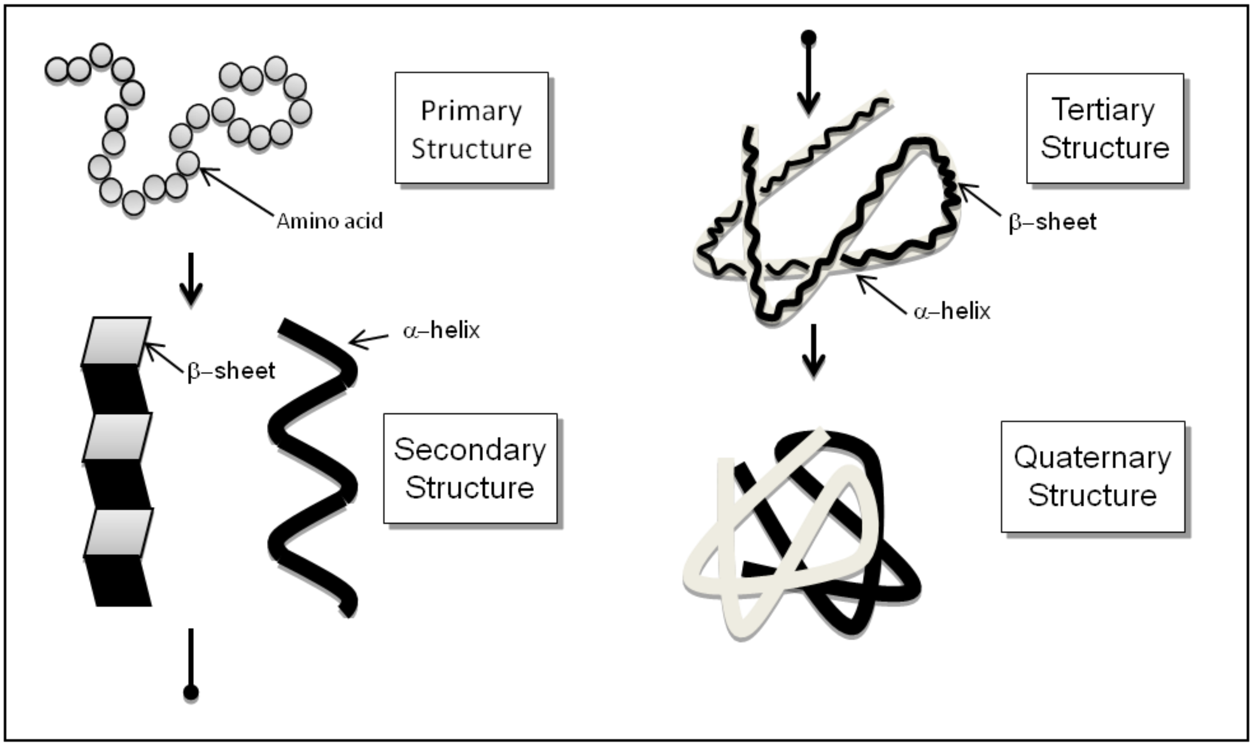

Figure 2.1 Hierarchy of protein structure Figure adapted from (University of Massachusetts, accessed 1 June 2013).

When a protein is identified as a therapeutic candidate, a formulation must be developed for administration. Due to degradation processes in the body, protein drug products generally require injectable routes of administration (intravenous, intramuscular or subcutaneous). Thus the final product requires an injectable solution for patient use. Additives, or excipients, are included in the formulation to attain desirable properties, including stabilization of the final drug product. Stability is a major concern, as many degradation routes exist for proteins. For example, degradation can occur via aggregation, deamidation, isomerization, oxidation, glycation, and thioldisulphide exchange (Cleland, Langer *et al.* 1994; Manning, Chou *et al.* 2010). Degradation not only results in product loss, but also can lead to issues in regulatory approval. In most cases, the FDA requires pharmaceutical product degradation to be below 10% of the product's final weight (Cleland, Langer *et al.* 1994).

2.2 Lyophilization

For proteins that prove unstable under aqueous conditions, lyophilization is often employed. Lyophilization removes water from the formulation by sublimation via a freezing step and then by evaporation through primary and secondary drying steps (Cleland, Langer *et al.* 1994; Costantino and Pikal 2004). During the lyophilization process, the protein experiences several temperature and pressure changes. By removing water, the mobility of the protein is reduced and stability is improved by elimination of many reactions that are facilitated by water. The desired resulting product is an amorphous solid with minimal water content (see Figure 2.2). Lyophilization is among the most common formulation choices for protein drugs, representing 46% of the biopharmaceuticals approved by the FDA through December 2003 (Costantino and Pikal 2004). For administration, lyophilized protein drug products are reconstituted and subsequently injected.

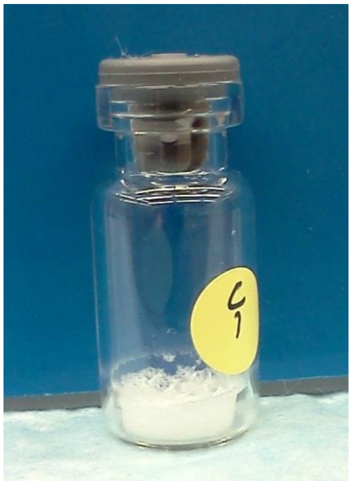

Figure 2.2 Vial containing lyophilized protein formulation The resulting formulation is an amorphous solid.

Despite improvements to stability, degradation can still occur in lyophilized proteins. Of particular interest here is degradation due to protein aggregation, which is an often irreversible self-association resulting in a protein complex (Cleland, Langer *et al.* 1994; Wang 2005; Wang, Nema *et al.* 2010). The aggregation process can occur due to physical interactions between protein surfaces or can result from chemical interactions of the amino acids, forming covalent bonds between proteins (Wang 2005). The detection of aggregates is difficult, as the protein complexes may be soluble (Wang 2005). Aggregation not only results in product loss and lowered efficacy of the protein drug, but can also lead to severe and life threatening immunogenic responses (Rosenberg 2006). One aim of a lyophilized formulation should be to minimize aggregation, ensuring the safety and efficacy of the final product.

2.3 Protein Aggregation – Mechanisms, Measurement and Prediction

Protein aggregation is defined as the self-association of monomeric protein leading to the formation of multi-protein complexes. Aggregation can be either reversible or irreversible, arising from the formation of covalent bonds or through physical interactions (Wang 2005). An example of chemical reaction leading to aggregation is the formation of intermolecular disulfide bonds. Interactions between hydrophobic regions of proteins represent a physical pathway that results in aggregation. Protein aggregates can either be soluble or insoluble (Wang 2005). Insoluble protein aggregates precipitate out of solution. Soluble aggregates are further characterized as visible or sub-visible. An example of visible soluble aggregates is provided by Figure 2.3. The formation of visible soluble aggregates results in solution turbidity and can be detected through optical methods (Katayama, Nayar *et al.* 2005). The presence of sub-visible aggregates is receiving increasing attention in protein formulation development (Carpenter, Randolph *et al.* 2009).

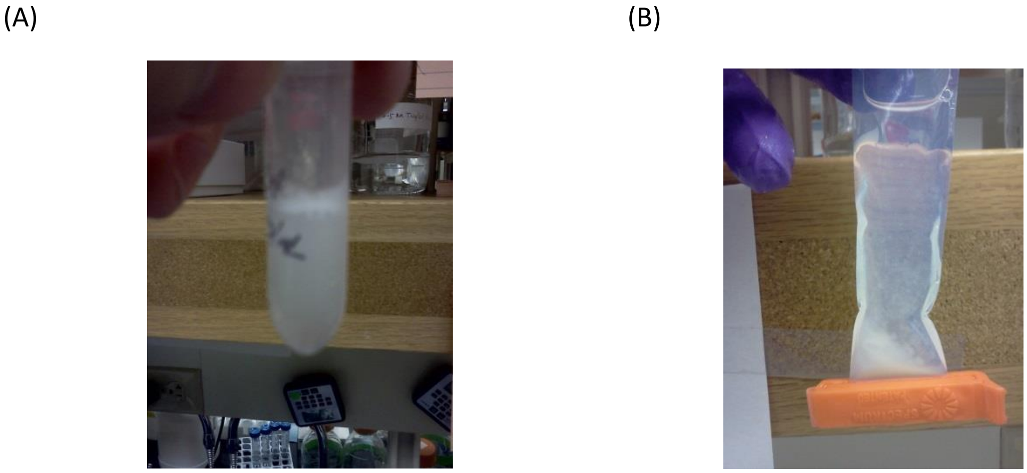

Figure 2.3 Solutions containing aggregated protein (A) The presence of visible aggregates leads to turbidity in the solution. (B) Protein aggregates can precipitate out of solution.

The formation of protein aggregates is primarily driving by two factors: colloidal instability and conformation instability (Chi, Krishnan et al. 2003). Colloidal instability results in aggregation through direct interaction of properly folded proteins. Of special concern for colloidal instability is the exposure of hydrophobic surfaces on the protein which may drive aggregation and has been implicated in a variety of disease states resulting from protein aggregation (Münch and Bertolotti 2010). The mechanism behind colloidal instability is rather straightforward (*i.e.*, direct protein-protein interactions), yet the prediction of colloidal instability for any given protein remains a challenge.

Conformational instability involves a change in native conformation that leads to aggregation. Partial unfolding may expose regions of the protein that increase aggregation propensity (Wang 2005). A general pathway for the formation of aggregates is outlined in Figure 2.4. The progression of protein from native state to partially unfolded states is driving by the free energy landscape and can result in an ensemble of intermediate structures (Gsponer and Vendruscolo 2006). The free energy landscape has both entropic and enthalpic contributions. It has been suggested that individual unfolded monomers are favorable by increasing entropy while aggregated states are favorable by decreasing enthalpy (Gsponer and Vendruscolo 2006). In many cases, aggregation may be driven through a combination of colloidal and conformation instabilities leading to a more complicated set of pathways than that proposed in Figure 2.4 (Wang, Nema *et al.* 2010).

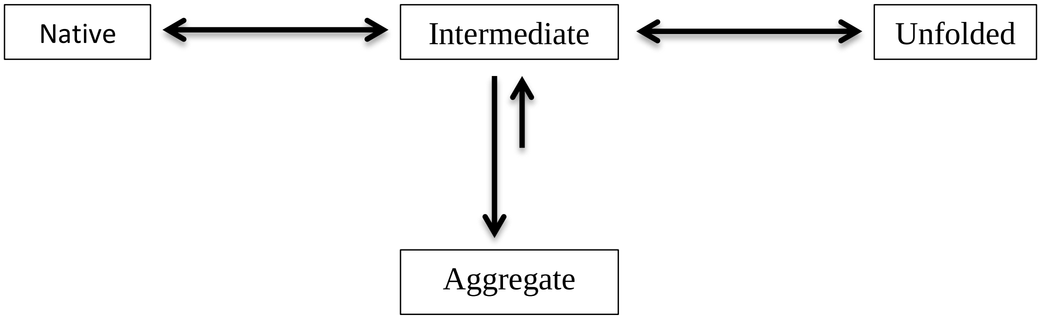

Figure 2.4 Pathway for the formation of aggregates through conformation instability Partial unfolding of the native protein lead to aggregation-prone intermediates. The intermediates can aggregate or further unfolded. Figure adapted from (Wang 2005).

A variety of experimental techniques exist for the detection and assessment of protein aggregates which can be classified as particle-based methods, separation-based methods and indirect methods (Engelsman, Garidel *et al.* 2011). Particle-based methods aim to detect aggregates through identification of particles in solution. Separation-based methods aim to separate aggregates from native protein in solution through basis of size, following by aggregate detection. Indirect methods often utilize spectroscopy methods to detect structural changes that are associated with protein aggregation. Overall, experimental techniques either provide qualitative information on protein aggregation or quantitative information such as the percentage of protein that is monomeric as opposed to aggregated. A summary of some common experimental techniques is provided by Table 2.1. The list provided is by means exhaustive and continual work is being performed to both improve existing aggregate detection methods as well as develop novel techniques for aggregate detection.

Understanding the structural properties of proteins that lead to aggregation is critical to the design of safe and effective protein drug products, and an ability to predict aggregation propensity (i.e., the likelihood and extent to which a protein will aggregate) with reasonable accuracy would accelerate development. Several approaches have been developed to estimate aggregation propensity for a given protein, which can classified into two main methods: heuristic-based methods and simulation-based methods.

Table 2.1 Summary of experimental techniques commonly utilized in the detection of protein aggregates Techniques are classified as either particle-based methods, separation-based methods or indirect methods. The quantitative indication is with regards to the number of aggregates present in the system. Table adapted from (Liu, Andya *et al.* 2006; Carpenter, Randolph *et al.* 2010; Engelsman, Garidel *et al.* 2011).

		Particle-Based Methods		
Technique	*Principle*	*Quantitative?*	*Advantages*	*Disadvantages*
Light obscuration	Light is blocked by particles present in solution	Yes	Quickly provides number and size of particles	Requires large sample volume. Sensitive to contamination.
Dynamic light scattering	Intensity of scattering light due to Brownian motion	No	High sensitivity. Requires low sample volume.	Low resolution. Data analysis is complicated. Sensitive to contamination
		Size-Based Methods		
Technique	*Principle*	*Quantitative?*	*Advantages*	*Disadvantages*
Size-exclusion chromatography	Separation by size	Yes	Sensitive. Can be utilized with online detectors (*e.g.*, UV-Vis)	Dilution of sample. Column matrix interactions may interfere with separation.
SDS-PAGE	Separation by size and charge	Potentially	Can detect aggregates formed by disulfide bonds.	Quantification can be difficult.
Analytical Ultracentrifugation	Separation due to sedimentation velocity	Yes	High resolution. Provides size and shape information.	Data analysis is complicated. Time consuming.
		Indirect Methods		
Technique	*Principle*	*Quantitative?*	*Advantages*	*Disadvantages*
Infrared spectroscopy	Absorbance of infrared light	No	Provides solid-state analysis. Does not consume sample.	Low sensitivity. Moderate protein concentrations are required.
Derivative UV-Vis Spectrophotometry	Absorbance and scattering of light	No	Easy to perform. Does not consume sample.	Data interpretation is complicated.
Circular dichroism spectroscopy	Difference in absorption of polarized light	No	Easy to perform. Does not consume sample.	Light scattering can cause interference. Data interpretation is complicated.

Heuristic-based approaches attempt to use prior history on aggregation or causes of aggregation in proteins to develop predictors for aggregation propensity. The aim of a heuristic-based approach is to relate protein properties to experimental data on protein aggregation, with the end result being a predictive model or algorithm that returns aggregation propensity given a measure of protein structure. Several algorithms have been developed to predict protein aggregation in solution as a function of structural parameters. For example, AGGRESCAN utilizes the intrinsic aggregation propensity of amino acids obtained from an experimental aggregation database of mutated β-amyloid peptides (Conchillo-Sole, de Groot et al. 2007). PASTA predicts the likelihood of amino acid sequences being involved in intermolecular β-sheet formation, based on minimization of β-pairing energies (Trovato, Seno et al. 2007). Zyggregator uses factors such as protein hydrophobicity, electrostatic interactions and alternating stretches of polar and non-polar residues to predict aggregation propensity (Tartaglia and Vendruscolo 2008). For all of these methods, protein primary structure (amino acid sequence) is used to return one or more scoring parameters which are indicative of the propensity of a protein to aggregate. For instance, AGGRESCAN returns the number of aggregation prone regions, or “hot spots” in a protein. The number of hot spots is then used to qualitatively indicate the likelihood of protein aggregation occurring, with a larger number of hot spots corresponding to a higher likelihood. Therefore, a hallmark of current methods is qualitative results in the form of aggregation predictors that must be interpreted.

Simulation-based methods use any of the many available molecular simulation software packages or newly-developed tools to investigate interactions between protein molecules or dynamics within a single protein molecule. The aim of simulation-based methods is to determine if aggregation is likely to happen based on the energetics of protein-protein interactions (Ma and Nussinov 2006). Alternatively, simulation-based methods can investigate the dynamics of a single protein molecule to determine if the properties of the protein could become amenable to aggregation (Irbäck and Mohanty 2006). For example, the spatial aggregation propensity (SAP) algorithm uses molecular simulations to determine the average exposed hydrophobic surface area for a given protein, with larger exposed hydrophobic surface areas representing increased aggregation propensity (Chennamsetty, Voynov et al. 2009). In general, simulations are more computationally expensive than use of a model or algorithm to predict aggregation propensity. Simulations are usually required for every system of interest. Simulation-based methods necessitate three-dimensional structure of a protein for determination of aggregation propensity and thus require more structural information than the heuristic-based methods described previously. Simulation-based approaches offer advantages over current heuristic-based approaches due to the ability for qualitative assessments (e.g., free energy calculations of protein-protein interactions) and inclusion of formulation conditions via explicit solvent and solute modeling. Recently, hybrid approaches have been developed to combine simulation results with heuristic model-based predictions. The Developability Index has been constructed for monoclonal antibodies utilizing net charge and SAP (Lauer, Agrawal et al. 2012). Additionally, the osmotic second virial coefficient (B22) has also been used to predict protein self-association in aggregation (Chi, Krishnan et al. 2003; Printz, Kalonia et al. 2012), though it is based on experimental measurement and not on *a priori* descriptors of protein structure.

2.4 Approaches to Aggregation Minimization

Two basic approaches are taken to minimize protein aggregation in therapeutics: protein engineering and formulation development. Protein engineering focuses on modifications to the structure of the protein which result in reduced aggregation propensity. Formulation development attempts to minimize aggregation through the inclusion of excipients, resulting in a multi-component product. The two approaches differ in that protein engineering is focused on the protein molecule itself (active compound) while formulation development is concerned with selection of excipient molecules (inactive compounds).

The basis behind protein engineering is that structure of the protein determines function. Consequently, modification of protein structure can offer improvement of certain properties while still maintaining the intended therapeutic function. Key properties of interest for protein drugs, and therefore areas for desired improvement, include mechanism of action, stability, bioavailability, toxicity or occurrence of side effects, ability for production at economically viable scales and dosing/delivery requirements (Marshall, Lazar *et al.* 2003). Table 2.2 provides an overview of the common targets of protein engineering approaches. With regards to preventing aggregation, common protein engineering strategies include replacement of cysteine residues, replacement of exposed hydrophobic residues, charge modification and post-translation modification (Marshall, Lazar *et al.* 2003). Replacing free cysteine residues can prevent aggregation that occurs due to disulfide bond formation and has been shown to successfully reduce aggregation for commercially available protein drugs such as Proleukin (aldesleukin, produced by Chiron) and Betaseron (interferon beta-1b, produced by Berlex/Chiron) (Marshall, Lazar *et al.* 2003). Yet aggregation can still occur from the scrambling of disulfide bonds formed from paired cysteine residues (Wang 2005). Replacement of hydrophobic residues through site-directed mutagenesis offers an increasingly popular choice for protein engineering, including rational protein design. For example, the SAP algorithm has been developed to identify amino acids in antibodies with high aggregation propensity as targets for mutagenesis (Chennamsetty, Voynov *et al.* 2009). SAP has also been used with total charge to provide a developability index for monoclonal antibodies (Lauer, Agrawal et al. 2012). Protein engineering approaches may improve the stability of lyophilized protein drugs or offer sufficient stability improvements such that lyophilization is no longer necessary.

Table 2.2 Common protein engineering targets for property improvement Table adapted from (Marshall, Lazar et al. 2003).

Protein Structural Target	**Desired Improvement**
Exposed hydrophobic residues	Solubility
Binding site	Interaction affinity and specificity
Loops	Protease susceptibility
Core	Stability and conformational control
Linear epitopes	Immunogenicity
Termini	Attachment of fusion partners or polyethylene glycol (PEG)

Formulation development assumes a fixed protein molecule and selects excipients to improve the drug product properties. Figure 2.5 illustrates the general preformulation and formulation development process. Excipients provide a variety of roles in protein drug formulation including solubilizing compounds, stabilizers and bulking agents for lyophilized formulations (Costantino and Pikal 2004; Strickley 2004). If possible, excipients are added to ensure stability in the aqueous solution, bypassing the need for a lyophilized formulation. For reduction of aggregation, a common strategy is to create favorable conditions for the native state of the protein through addition of excipients to prevent protein-surface interactions and/or improve conformational stability. Surfactants are employed to prevent denaturation and adherence of proteins to the surface of any variety of containers that the protein is exposed to during manufacturing and storage, as the surfactants are more likely to bind to the surfaces (Chang, Kendrick et al. 1996; Chi, Krishnan et al. 2003). Other excipients, such as sugars, are added to improve conformational stability via preferential exclusion (Arakawa and Timasheff 1982). According to preferential exclusion, sugars and other weakly interacting excipients are excluded from the protein's surface. The exclusion leads to an increase in free energy that is proportional to the protein's surface area (Arakawa and Timasheff 1982; Timasheff 1998). As a result, a compact form of the protein is energetically more favorable and the native state is preferred to an unfolded or denatured state. Excipients that bind with strong affinity to the protein surface can also affect protein stability. Excipients that bind to the native state increase conformational stability, while excipients that have an affinity for the unfolded state drive denaturation (Chi, Krishnan et al. 2003). Examples of molecules that affect protein stability through binding include heme with myoglobin (increased stability) and guanidine hydrochloride with proteins in general (decreased stability, denaturation). During formulation development, stability concerns may justify the use of lyophilization.

Several classes of molecules are employed in lyophilized protein formulations including amino acids, carbohydrates, polymers and surfactants (Costantino and Pikal 2004). Of special interest are carbohydrate excipients, such as sucrose and trehalose, which have been shown repeatedly in literature to stabilize lyophilized protein structure (Fung, Darabie *et al.* 2005; Li, Williams *et al.* 2008; Sinha, Li *et al.* 2008). Many lyophilized protein formulations utilize simple sugars, disaccharides, oligosaccharides, or sugar alcohols as stabilizers (Cleland, Langer *et al.* 1994). Two main theories have been proposed for describing an excipient's ability to stabilize biomolecules during lyophilization: water replacement and vitrification. In the water replacement theory, stabilizing excipients are those that can substitute for water in the dried state through hydrogen bonding with the protein (Cleland, Langer *et al.* 1994). The vitrification hypothesis proposes that stabilizing excipients are those that form glasses during lyophilization (Crowe, Carpenter *et al.* 1998). Vitrification is described in more detail in Section 2.4, while water-replacement is further addressed in Section 2.5.

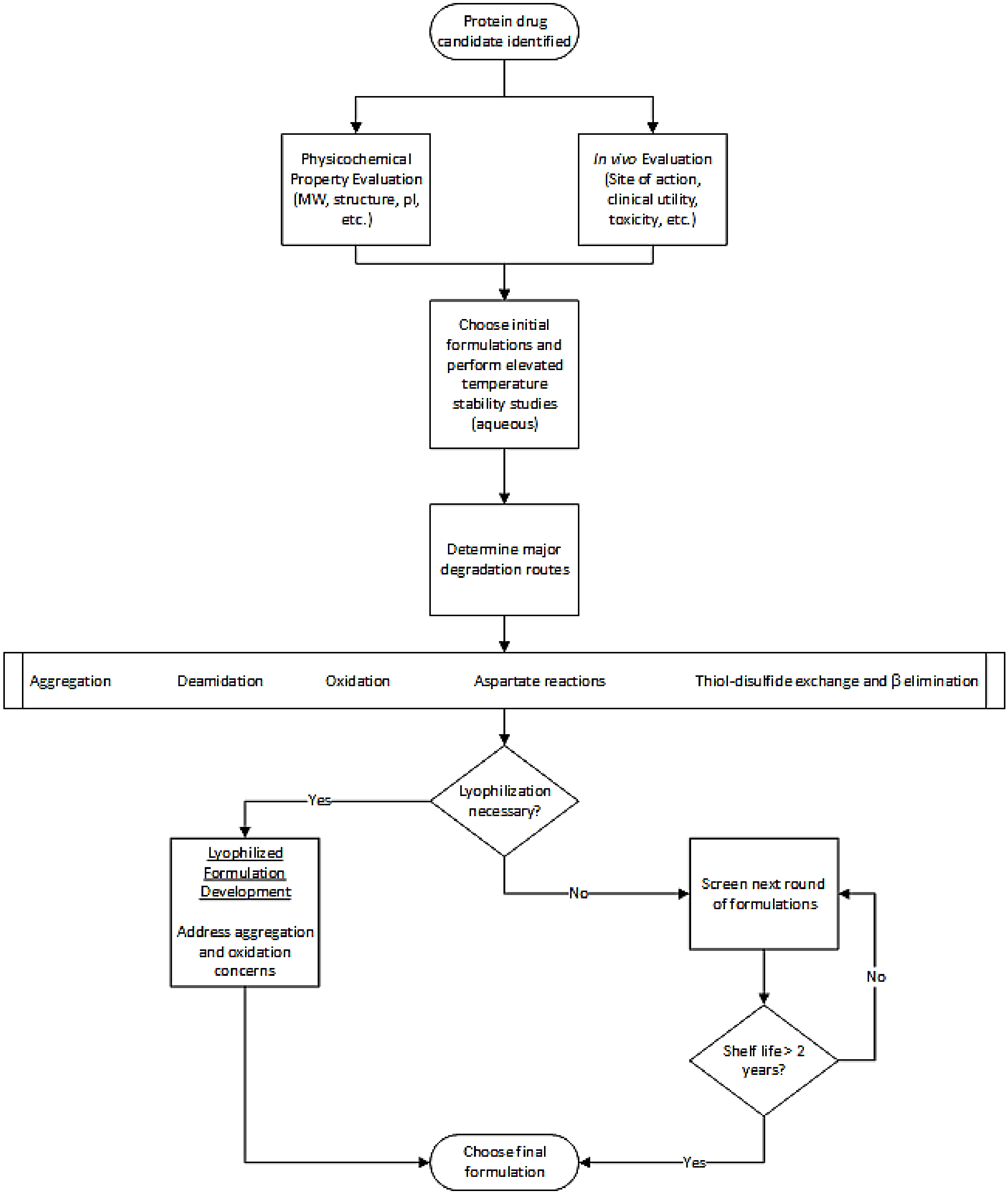
Protein drug candidate identified
Physicochemical Property Evaluation (MW, structure, pI, etc.)
In vivo Evaluation (Site of action, clinical utility, toxicity, etc.)
Choose initial formulations and perform elevated temperature stability studies (aqueous)
Determine major degradation routes
Aggregation
Deamidation
Oxidation
Aspartate reactions
Thiol-disulfide exchange and β elimination
Lyophilization necessary?
Yes
No
Lyophilized Formulation Development
Address aggregation and oxidation concerns
Screen next round of formulations
No
Shelf life> 2 years?
Yes
Choose final formulation

Figure 2.5 Preformulation and formulation development process diagram Adapted from (Cleland, Langer et al. 1994).

2.5 Vitrification – Glass Transitions in Lyophilization

In general, the glass transition temperature marks the change between a liquid/rubbery state and an amorphous solid/glass state. The glass transition temperature can be measured by a variety of methods including differential mechanical thermal analysis (DMTA) and differential scanning calorimetry (DSC) (Rahman, Al-Marhubi *et al.* 2007). Due to the different features used by each method, the exact transition temperature measured varies by method (Rahman, Al-Marhubi *et al.* 2007) or even by procedure or data interpretation used for a particular method (Roos 1997). Regardless of method, the change in features attributed to the glass transition indicate the point or region where α-relaxation processes are arrested when cooling a liquid/rubber into a glass (Gangasharan and Murthy 1995). The transition is not a true glass-transition as defined for polymers; however, the language used to describe the transition noted in sugars is borrowed from literature concerned with polymers. In reality, the glass transition of sugars is related to mobility and does not describe a thermodynamic event.

For carbohydrates, α-relaxation involves both structural and dielectric changes. The dielectric changes involve the rotation of dipoles resulting in polarization while structural changes arise from local spatial reorientations of chemical groups on the molecule (Gangasharan and Murthy 1995). The dielectric and structural modes are coupled in carbohydrates, mainly due to the presence of hydroxyl (-OH) groups (Gangasharan and Murthy 1995). The hydroxyl groups are polarizable and also constrain structural rearrangements through the need to form hydrogen bonds. Every rearrangement that occurs during α-relaxation requires a hydrogen bond to be broken and then subsequently remade. The glass transition temperature then marks the point when cooling a rubber/liquid at which there is not enough random kinetic energy present for the necessary vibrations, reorientations and hydrogen bond shuffling resulting in the cessation of α-relaxation (Meste, Champion *et al.* 2002). As the molecule size increases, large intermolecular and intramolecular cooperation is needed to make and break hydrogen bonds

(Gangasharan and Murthy 1995). As a result, glass transition temperatures are generally higher in trisaccharides as compared to disaccharides and higher in disaccharides as compared to monosaccharides. Segmental rotation also occurs during α-relaxation. For carbohydrates, ring-chain and chair-boat transformations increase the number of modes of relaxation (Gangasharan and Murthy 1995). Such modes generally require more energy and thus monosaccharides tend to have higher glass transition temperatures than sugar alcohols that exist solely in chain conformations due to the lack of a carbonyl moiety.

Often in biological or pharmaceutical contexts, water is present in the system. Water acts as a plasticizer and effectively lowers the glass transition temperature. The glass transition temperature for a binary mixture is often represented by the Gordon-Taylor expression, given by Equation 2.1 (Meste, Champion *et al.* 2002):

$$T_g = \frac{m_2 T_{g,2} + k m_1 T_{g,1}}{m_2 + k m_1}$$

(Equation 2.1)

Where $T_{g,1}$ and $T_{g,2}$ represent the pure component glass transition temperature of components 1 and 2, m_1 and m_2 represent the weight fractions of components 1 and 2 and k is the Gorbon-Taylor constant for the mixture of interest.

A specific temperature may be reached during cooling of carbohydrate-water mixtures, known as the maximally freeze-concentrated glass transition temperature (T_g'), where a glass transition of the solute occurs. The solute compound is the carbohydrate excipient and the solvent is water. The result is an amorphous solid composed of the carbohydrate and water, where the carbohydrate is at the maximal freeze concentration (C_g') (Roos 1997). The glass transition temperature of the anhydrous solute is used for $T_{g,1}$ and the glass transition temperature of water (-135°C) is used for $T_{g,2}$ (Roos 1993). By rearrangement of Equation 2.1, the solute concentration (weight fraction) of the maximally freeze concentrated matrix (C_g') can be solved for, as shown in Equation 2.2.

$$C_g' = \frac{k\left(T_{g,water} - T_g'\right)}{\left(T_g' - T_{g,carb} + k\left(T_{g,water} - T_g'\right)\right)}$$

(Equation 2.2)

If the solution is not at the proper or maximal concentration, glass formation occurs sub-T_g' (Meste, Champion *et al.* 2002). The glass transition of the anhydrous carbohydrate (T_g), the glass transition temperature of the maximally freeze-concentrated solute (T_g') and the maximal freeze concentration (C_g') are all parameters of interest when developing lyophilized protein formulations.

During lyophilization, a concentrated amorphous glass is produced during the freezing step and a mostly water free glass is produced during the drying steps (Costantino and Pikal 2004). Initially, as a solution with excipients is cooled, a concentrated supercooled liquid or rubbery state is formed. The melting point of ice occurs first and represents the point where ice begins to form in the concentrated rubbery phase (Roos 1997). Upon further cooling, the concentrated rubbery phase transitions into a concentrated glass phase, marked by the glass transition temperature of the maximally concentrated solute (Roos 1997). The ice is removed via sublimation as a vacuum is applied to the system (Costantino and Pikal 2004). The amount of water remaining in the maximally freeze-concentrated glass matrix can be estimated by Equation 2.2 (Roos 1993; Costantino and Pikal 2004). The lyophilized product temperature is then raised and residual water in the maximally freeze-concentrated glass matrix is removed during the drying steps. The phase transitions that occur in a lyophilized formulation are summarized in Figure 2.6.

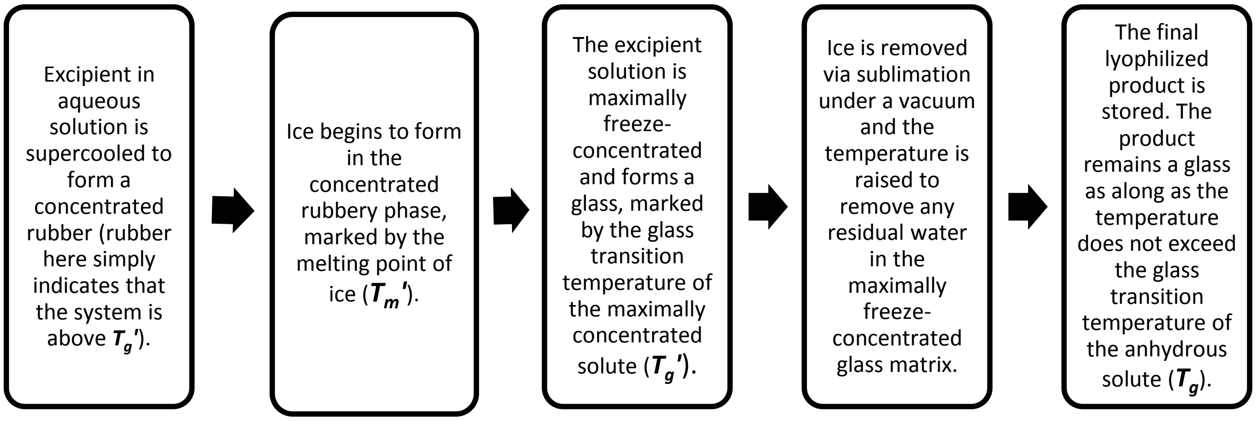
Excipient in aqueous solution is supercooled to form a concentrated rubber (rubber here simply indicates that the system is above T_g').
Ice begins to form in the concentrated rubbery phase, marked by the melting point of ice (T_m').
The excipient solution is maximally freeze-concentrated and forms a glass, marked by the glass transition temperature of the maximally concentrated solute (T_g').
Ice is removed via sublimation under a vacuum and the temperature is raised to remove any residual water in the maximally freeze-concentrated glass matrix.
The final lyophilized product is stored. The product remains a glass as along as the temperature does not exceed the glass transition temperature of the anhydrous solute (T_g).

Figure 2.6 The phase transitions that occur during the lyophilization process Figure adapted from (Roughton, Topp *et al.* 2012).

Roos suggested that the increase of transition temperatures could be "used in product development to improve freeze-drying behavior and stability of dehydrated materials" (1997). A lyophilized product must reach a temperature below both the glass transition temperature of the maximally concentrated solute and the melting point of ice to ensure minimal water content and glass formation, restricting protein mobility. By restricting mobility, the protein's potential to aggregate is reduced. An appreciable temperature difference between the glass transition temperature of the maximally concentrated solute and the melting point of ice is also desired, as the freeze-concentrated solution is annealed between these temperatures to ensure maximal solute concentration and minimal water content (Roos 1997). The glass transition temperature of the anhydrous solute is important for long-term storage stability as well, as lyophilized formulations are usually stored at temperatures at least 50°C below their glass transition temperature (Costantino and Pikal 2004). The literature has shown glass transitions to be dependent on chemical structure (Slade and Levine 1995), providing motivation for structure-property model development. An ideal excipient will form a freeze-concentrate with minimal water content and will remain a glass during drying and storage, restricting protein mobility and reducing the potential for aggregation.

2.6 Protein-Excipient Interactions in the Dried State

As water is the key factor in the structure that proteins adopt, dehydration or removal of water is predicted to have a large effect on protein structure (Kuntz Jr and Kauzmann 1974). Using a poly-L-lysine model, dehydration has been shown to result in loss of hydrogen bonds that are present in solution (Prestrelski, Tedeschi *et al.* 1993). To compensate for the loss of hydrogen bonds, intermolecular hydrogen bonds are formed and a β-sheet conformation is adopted over the native random coil conformation (Prestrelski, Tedeschi *et al.* 1993). A possible approach to stabilization in the dried state is to prevent protein conformational adjustments due to the removal of water. The water replacement hypothesis attributes protein stabilization to the replacement of protein-water interactions in aqueous solution with protein-excipient interactions in the dried state following lyophilization.

Addition of so-called stabilizer excipients achieves partial or full preservation of protein native structure. In particular, carbohydrate excipients have shown success when used as stabilizers. It has been proposed that stabilization arises from a direct effect of the excipient on protein conformation (Prestrelski, Tedeschi *et al.* 1993; Manning, Chou *et al.* 2010). Infrared spectra results have suggested that carbohydrates hydrogen bond with proteins in the dried state and may be a requirement for the preservation of lyophilized/dried proteins by carbohydrates (Carpenter and Crowe 1989; Prestrelski, Tedeschi *et al.* 1993). The water-replacement hypothesis postulates that hydrogen bonds form between the hydroxyl groups of carbohydrates (see Figure 2.7) and the protein backbone, mimicking the hydrogen bonding that occurs between water and the protein backbone. Recent hydrogen-deuterium exchange mass spectroscopy experiments support the water-replacement hypothesis, with the results showing that certain excipients can reduce deuterium exchange in a site-specific manner (Li, Williams et al. 2007; Li, Williams et al. 2008). Reduction of deuterium exchange indicates that the protein backbone is protected by the inclusion of stabilizing excipients. Such protection could arise from hydrogen bonding between the protein backbone and excipients. Hydrogen bonding is attributed to reduced deuterium exchange (Tsutsui and Wintrode 2007).

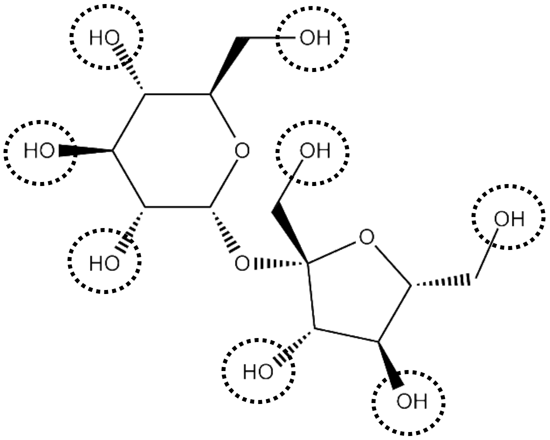

Figure 2.7 Hydroxyl groups on sucrose Groups are circled. Hydroxyl groups form hydrogen bonds with the protein backbone in dried proteins. Such interaction may have a stabilizing effect on protein conformation.

An alternative to the water replacement hypothesis has been proposed recently. Known as the water entrapment hypothesis, the hypothesis proposes that water molecules are entrapped between the protein surface and sugar matrix in lyophilized solids (Hackel, Zinkevich *et al.* 2012). Thus the water needed to maintain the protein conformation is still available to the protein, with stabilizing excipients aiding in the maintenance of the water layer. Evidence from nuclear magnetic resonance spectroscopy (NMR) and molecular dynamics (MD) simulations indicate that there is the formation of sugar-water-protein structures, indicating that water is maintaining the protein conformation and that the sugar is maintaining the hydration layer of the protein (Cottone, Ciccotti *et al.* 2002; Hackel, Zinkevich *et al.* 2012). A combination of both the water replacement hypothesis and the water entrapment hypothesis is likely as dehydration can prevent the formation of a fully hydrated layer and NMR and MD results both indicate that contacts between the protein surface and sugar matrix are formed (Cottone, Ciccotti *et al.* 2002; Hackel, Zinkevich *et al.* 2012). While water may still play a role in preservation of native protein structure in the dried state, stabilizers clearly play a role in maintaining protein conformation including the formation of some direct protein-excipient interactions.

IONIC LIQUID SOLVENT DESIGN

2.7 USE OF SEPARATION MEDIA FOR AZEOTROPIC DISTILLATION AND *IN SITU* FERMENTATION

Solvents represent chemicals that are used to solubilize molecules of interest and may or may not be present in the final chemical product. Of particular concern here is the use of solvents as mass separating agents (MSA). An MSA is a chemical that aids in the separation of two or more compounds of interest to high levels of purity. In general, an MSA is not a component of the final chemical product and is removed and recycled following separation. Two applications for separation media are azeotropic distillation and *in situ* fermentation.

Numerous binary azeotropes are encountered in chemical systems (Gmehling 1994). An azeotrope is defined as a mixture where the liquid composition is equal to the vapor composition, resulting in a lack of driving force for further separation to pure or mostly pure compositions. Separation of azeotropic mixtures affects many industrial sectors due to the prevalence of such mixtures, yet separation remains a challenging task. Azeotropes may be encountered in the solvent recovery stage following the downstream separation of pharmaceutical and/or biochemical processes (Barton 2000; Simoni, Chapeaux *et al.* 2010). Separation of azeotropic mixtures also contributes to many of the separation tasks in the petrochemical and chemical industries (Trotta and Miracca 1997). An entrainer can selectively interact with one of the components in an azeotrope, allowing the azeotrope to be broken and the components separated. An basic process diagram for azeotropic distillation is presented in Figure 2.8. A common concern with the design and operation of separation processes is the selection of the entrainer.

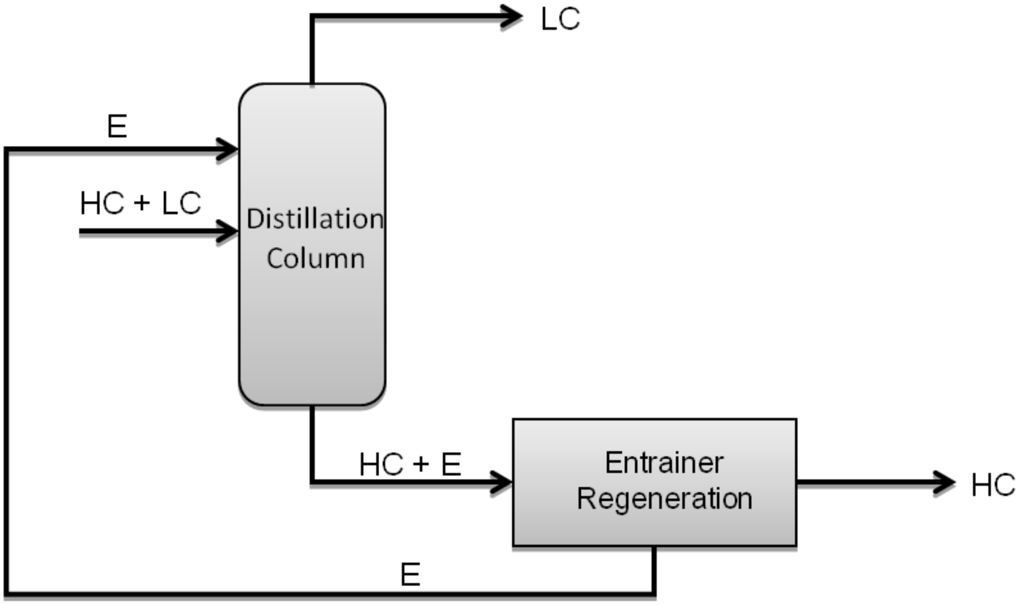

Figure 2.8 Block flow diagram of azeotropic distillation process HC refers to the heavy component, LC refers to the light component and E refers to the entrainer.

Industrial processes can utilize fermentation, where microorganisms convert sugars to other chemicals, to produce chemicals of interest. A major concern in fermentation processes is separation of product from the fermentation broth as downstream separation often requires a high energy input. Additionally, product yield is often low in fermentation due to product inhibition. *In situ* product recovery during fermentation offers a means to improve fermentation processes by reducing product inhibition and enabling more efficient separations (Gangu, Weatherley *et al.* 2009). Three main *in situ* product recovery processes exist: volatility-based methods, membrane-based methods and solvent-based methods (Huang, Ramaswamy *et al.* 2008). Solvent-based methods provide a pathway to tunable separations based on solvent selection. Major considerations when selecting a solvent include toxicity towards fermentation microorganism, immiscibility with water and increased solubility of solute (product) in solvent compared to water (Huang, Ramaswamy *et al.* 2008; Gangu, Weatherley *et al.* 2009). Figure 2.9 presents the basic process diagram for *in situ* extractive fermentation.

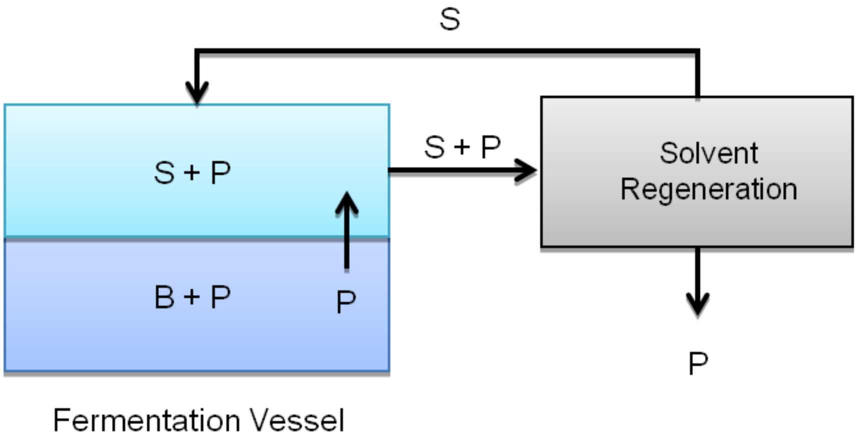

Figure 2.9 Block flow diagram of *in situ* extractive fermentation P refers to the desired product, B refers to the fermentation broth and S refers to the solvent used for extraction.

Increasingly, the environmental impact of solvent selection must be minimized (Kerton 2009). Additionally, material and energy inputs need to be minimized to improve process economics. Ionic liquids represent a class of molecules that possess many desirable solvent properties and are increasingly being considered for industrial applications. For separation processes, an optimal ionic liquid solvent can be designed to reduce material and energy inputs and ensure feasible separation or extraction.

2.8 Ionic Liquids as Separation Media

Ionic liquids (ILs) have become increasingly attractive options in solvent selection, especially for separations. Ionic liquids are defined as salts with melting points below 100°C (Marsh, Boxall *et al.* 2004). Due to negligible vapor pressure, environmental concerns are reduced in comparison to many conventional solvents (Marsh, Boxall *et al.* 2004). Ionic liquids can be recycled in separation processes, reducing the material demands and improving the economics (Zhao, Xia *et al.* 2005). As a class of chemicals, ionic liquids are soluble with a wide range of organic compounds (Marsh, Boxall *et al.* 2004). Ionic liquids can be composed of many different cation and anion combinations, resulting in different thermophysical properties (Zhao, Xia *et al.* 2005). The properties of an ionic liquid can be tuned for use in a particular application by rational design or selection of the cation, anion, and cation alkyl chain length. An example of a commonly studied ionic liquid is shown in Figure 2.10.

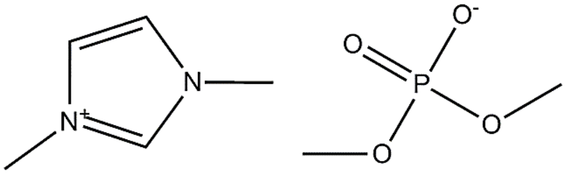

Figure 2.10 The ionic liquid 1,3-dimethylimidazolium dimethylphosphate (MMIm DMP)

Ionic liquids are promising candidates for entrainers due to their adjustable properties and negligible vapor pressure. Extractive distillation processes using ionic liquids as entrainers have be proposed and designed for common binary azeotropes, showing reduced energy requirements when compared to processes using conventional entrainers (Seiler, Jork *et al.* 2004). Energy requirements may further be reduced through correct selection or design of the ionic liquid entrainer.

Ionic liquids are a class of molecules that have been shown to exhibit immiscibility with water and high organic solute solubility, providing viable candidates for solvents used for *in situ* fermentation and product recovery processes (Gangu, Weatherley *et al.* 2009). Additionally, toxicity towards the fermentation organism can be adjusted through cation and anion selection (Matsumoto, Mochiduki *et* *al.* 2004; Gangu, Weatherley *et al.* 2009). Thus the design of an ionic liquid for in situ fermentation processes offers several, often competing, targets for required solvent properties.

Forward Problem

2.9 Descriptors Used in Structure-Property Models

The impetus for CAMD is the need for a chemical or formulation to fulfill certain characteristics. Ideally, product characteristics can be directly linked to chemical properties. Upon identification of key properties, property models are required for the design of molecules matching target properties. Properties are linked to molecular structure through molecular descriptors by the generation of structure-property models in the forward problem of CAMD.

The representation of molecule via molecular descriptors that capture relevant information is a key step in the forward problem. Many different molecular descriptors have been considered for CAMD: group contribution (GC) methods, graph theoretical approaches (including connectivity indices), three-dimensional descriptors and other so-called "DRAGON" descriptors (Consonni and Todeschini 2000). In addition to the descriptor class chosen, the functional form of the structure-property model must also be determined. More treatment to model development is given in Section 2.10.

Group contribution models have often been used for CAMD methods as they are considered to be simple, accurate and predictive (Harper, Gani *et al.* 1999). However, while GC models are commonly applied to solvents, reliability can be a concern for classes of molecules that are inherently larger in size (Harper, Gani *et al.* 1999). For example, carbohydrates can be an order of magnitude larger in molecular weight than common organic solvents. Additionally, the types of properties that can be predicted by GC methods has commonly been limited to thermophysical properties (Harper, Gani *et al.* 1999). Properties that are dependent on three-dimensional molecular structure are not amenable to GC methods.

Graph theoretical methods, especially connectivity indices, have been used in quantitative structure-property relationship (QSPR) models for a variety of systems including polymers (Camarda and Maranas 1999; Bicerano 2002) and pharmaceutical compounds (Kier, Hall *et al.* 1975). In graph theoretical methods, a molecular structure is interpreted as a graph where atoms are represented by vertices and bonds are represented by edges. Therefore, graph-based approaches capture the two-dimensional topology of a molecular structure. Apart from bonding configuration, some graph-based descriptors (including valence connectivity indices) capture information pertaining to the electronic configuration of a molecule. Descriptors derived from graph theoretical approaches can be calculated with low computational effort. In general, graph-based descriptors do not capture three-dimensional or conformational information.

Three-dimensional based descriptors have received increase attention in the development of 3-D quantitative structure-activity relationships (QSAR) for prediction of interaction energies for a variety of biologically relevant systems (Cheng, Shen *et al.* 2002). Additionally, use of 3-D QSAR models coupled with molecular simulation has proven fruitful in guiding computer-aided drug design efforts (Cheng, Shen *et al.* 2002). A variety of 3-D descriptors can be calculated through use of computational packages such as DRAGON (Consonni and Todeschini 2000). The advantage of 3-D descriptors is increased information about molecular structure which can help discriminate between stereoisomers. However, 3-D QSARs are usually limited to very defined molecular spaces and requires large computational effort for calculation of necessary descriptors (Golbraikh, Bonchev *et al.* 2001). Incorporation of chirality information in graph-based topological descriptors has been proposed as a bridge between the efficient of graph theoretical methods and the detailed structural information provided by 3-D descriptors (Golbraikh, Bonchev *et al.* 2001).

2.10 Property Model Development

Development of property models requires a function form. The most basic function form is a linear model, which can be determined through use of linear regression. Linear regression (or multiple linear regression for multiple dependent variables) essentially utilizes optimization to provide a model with maximum fit to the provided data. Equation 2.3 gives the general multiple linear regression model form (Wasserman 2004).

$$Y = X\beta$$

(Equation 2.3)

Where *Y* is an array of independent, or response, variable values, *X* is a matrix of dependent variable values and β is an array of coefficient values. To maximize fit, coefficients for all dependent variables are varied to achieve minimization of the residual sum of the squares (*RSS*). Equation 2.4 is used to calculate RSS (Wasserman 2004).

$$RSS = \sum_{i=1}^{n} \left(\hat{Y}_i - Y_i\right)^2$$

(Equation 2.4)

Where $\hat{Y}_i$ is the predicted value for observation *i*, Y_i is the observed value for observation *i* and *n* is the number of observations. Determination of the coefficient values is achieved through matrix inversion of Equation 2.3, as given by Equation 2.5 (Wasserman 2004).

$$\beta = (X^T X)^{-1} X^T Y$$

(Equation 2.5)

For functional forms utilizing non-linear model forms, the determination of coefficient values is still determined through optimization by minimizing either *RSS* or another suitable indicate of fit.

While model development, especially for linear models, is relatively straightforward, the selection of descriptors used in the model remains a subject of interest and debate. Model selection aims to choose descriptors that maximize fit and minimize variance and prediction errors due to overfitting (Wasserman 2004). Model selection requires a score to be assigned to each model and also requires a method of searching for models with the best score (Wasserman 2004).

Several methods exist for scoring a model. In nearly all cases, the score is based on the lack of fit provide by the model and the number of descriptors used to generate the model. As fit will increase (albeit usually at a decreasing rate) with the addition of more descriptors, a trade-off between underfitting and overfitting is sought. Several common methods for scoring models include Mallow's C_p statistic, Akaike Information Criterion (AIC) and Bayesian Information Criterion (BIC) (Wasserman 2004). Each method utilizes slightly different penalties for lack of fit and number of descriptors. For all cases, the model with the minimal score is selected. Cross-validation and sensitivity analysis also provide methods of scoring and selecting models on the basis of predictive ability and can provide further justification for the selection of a model.

To select a model, a search must be performed for the model with the minimal score. Three methods are used to search for models: exhaustive search, forward search and backward search (Wasserman 2004). Exhaustive search looks at all possible model combinations (number and type of descriptors). Therefore, exhaustive search is guaranteed to return the model with the optimal score. For models with large data sets and/or descriptor sets, exhaustive search may be too computationally expensive. In such cases, forward search or backward search are useful. In forward search, a null model provides the starting point. Descriptors are added one by one, selecting the descriptor that provides the lowest score at each step. Once a model size is encountered that cannot provide an improvement in score compared to the previous model size, the search is ended and the best model from the previous size is selected. Backward search operates in a similar manner with the difference being the initial model is generated using all available descriptors. Descriptors are then removed one by one until no further improvement can be gained. Backward search is not possible when the number of considered descriptors exceeds the number of observations used to develop the model.

2.11 Thermodynamic Property Modeling and Prediction

Thermodynamic property models seek to represent phase equilibria through mathematical means. The determination of phase equilibria is paramount in the design of separation processes. Accordingly, accurate and predictive models are needed for reliable separation process design. In essence, all phase equilibria problems seek to find the solution to Equation 2.6 (Prausnitz, Lichtenthaler *et al.* 1999).

$$\mu_i^\alpha = \mu_i^\beta$$

(Equation 2.6)

Where μ is the chemical potential of species *i* and α and β represent the two phases considered. For the work presented here, fluid phases are the phases of interest. For fluid phases, Equation 2.6 can be represented in a more useful form for species *i*, as provided by Equation 2.7 (Prausnitz, Lichtenthaler *et al.* 1999).

$$\varphi_i y_i P = \gamma_i x_i f_i^0$$

(Equation 2.7)

Where φ_i is the fugacity coefficient, y_i is vapor mole fraction, P is system pressure, γ_i is activity coefficient, x_i is liquid mole fraction and f_i^0 is the fugacity at standard conditions. Of interest to the work here is the determination of the activity coefficient, as provided by activity coefficient models. Activity coefficient models provide estimation or prediction of the activity coefficient as a function of temperature, pressure and compositon. A variety of activity coefficient models exist with the most commonly utilized including Wilson, NRTL and UNIQUAC (Prausnitz, Lichtenthaler *et al.* 1999). Every activity coefficient model is developed with certain assumptions, which can limit applicability. Of particular interest for CAMD approaches is the UNIFAC model, a predictive group-contribution based extension of UNIQUAC (Fredenslund, Gmehling *et al.* 1977). The UNIFAC model is given further treatment in Section 4.5.

Reverse Problem

2.12 Computer-Aided Molecular Design (CAMD) Overview and Problem Formulation

The reverse problem in CAMD entails the actual design phase, where either known molecular structures are selected from a database or novel molecular structures are proposed. In the reverse problem, target properties values are set and molecular structures are generated which best match the target properties. Property constraints may be employed to guide candidate selection, either during design as rigid constraints or after design as screening criteria. The intermediary between structure and property are the molecular descriptors used in the property models. As candidates are determined, molecular descriptors must be calculated and used in property models to evaluate the suitability of the candidate. Thus, a potential limiting factor in CAMD is that molecules can only be designed which are enclosed by the chosen descriptor class.

Three steps comprise the CAMD procedure (Harper and Gani 2000):

1. *Pre-design step* – problem formulation
2. *Design step* – model development and solution of problem leading to compound identification
3. *Post-design step* – results analysis and screening

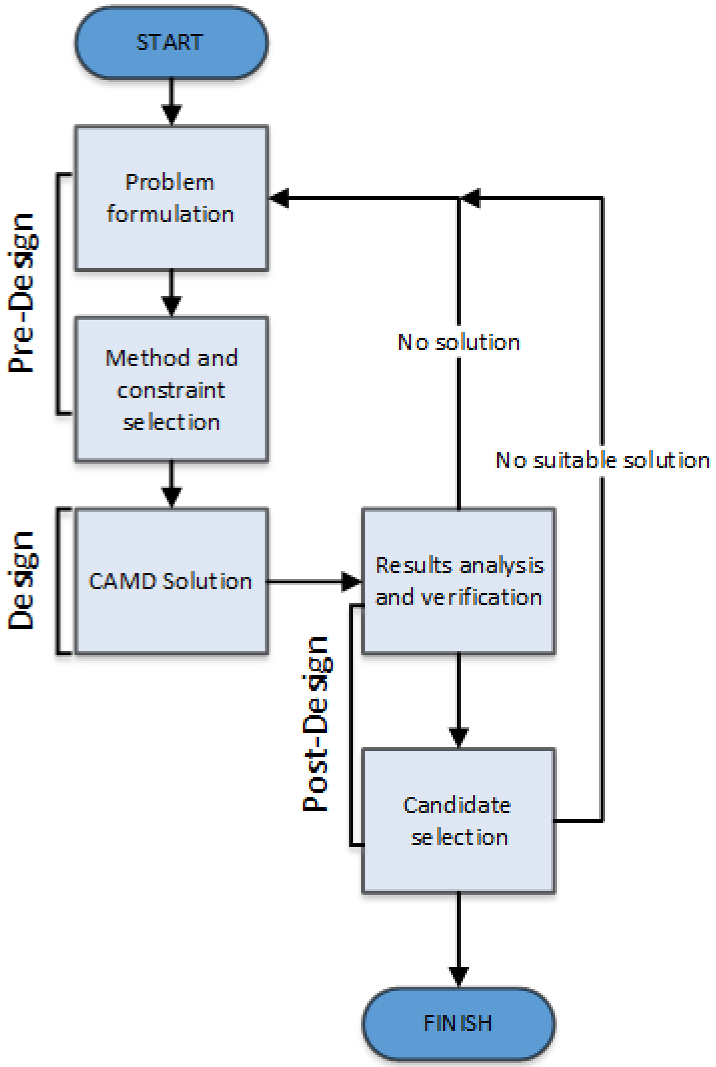

Figure 2.11 A general procedure for the solution of the CAMD reverse problem Interplay between the main steps of the CAMD methodology is highlighted. Figure adapted from (Gani 2004).

The general procedure used for the reverse problem solution and the interplay between the steps of the CAMD procedure are illustrated in Figure 2.11. The design step is the dominant step, influencing the problem formulation as well as the options for post-design analysis. The methodology concerning the actual design step is outlined in Figure 1.1 (see 1.0 Introduction).

The main concerns with CAMD approaches during the design step are as follows (Gani 2004):

- How will new molecular structures be generated?
- How will the molecular structure be represented?
- What level of structural information is required?
- How are target properties obtained?

The problem formulation, solution method used in design and the availability of post-design screening methods are impacted by the answers given for the above questions. A general problem formulation is given by Equation 2.8 (Camarda and Sunderesan 2005).

$$\min z = \sum\nolimits_{M} \frac{1}{P_m^{scale}} \left|P_m - P_m^{target}\right|$$

s.t.

$$P_m = f_m(y)$$

$$y = g\left(a_{ijk}, w_i\right)$$

$$h_c\left(a_{ijk}, w_i\right) \geq 0$$

(Equation 2.8)

Where *z* is the objective function, which consists of the sum of the absolute differences between solution properties (P_m) and target properties (P_m^{target}) for the set of properties *M*. Each difference can be scaled (via P_m^{scale}) to place more or less emphasis on the target property, as determined by the molecular properties with the highest priorities. The properties are functions of the molecular structure (*y*), where the structure is provided by the chemical groups (w_i) and the adjacency matrix (a_{ijk}) of the groups. Structural constraints (h_c) are employed to ensure solutions are feasible. Molecular structure representation may vary according to implementation of CAMD. Additionally, some property models may be used as constraints rather than targets. Property models and/or constraints often introduce non-linearities, resulting in a mixed-integer non-linear program (MINLP).

Historically, three main approaches have been used for the solution of CAMD problems (Harper, Gani *et al.* 1999; Eljack and Eden 2008):

- Enumeration techniques/database search
- Deterministic optimization/mathematical programming
- Stochastic optimization/iterative search

Each approach has seen success in certain applications of CAMD. The approach chosen should be taken with consideration towards the advantages and disadvantages of each approach. The three approaches are given further attention in the following sections (2.13-2.15). A subset of CAMD involves simultaneous product and process design and is detailed in section 2.16. Post-design methods are examined in section 2.17.

2.13 Enumeration Solution Methods

The first CAMD methods employed relied on enumeration of possible solutions followed by selection of molecules that best matched a set of target property values (Gani and Brignole 1983). Enumeration solution methods have historically used group contribution property models. The approach of enumeration methods is to determine the number and types of functional groups that best satisfy a set of target properties. Given the functional groups determined, molecular structures are identified that are comprised of all the functional groups selected.

A general procedure for CAMD by enumeration follows (Gani, Nielsen *et al.* 1991):

1. Preselect the types of groups that will be used to provide solutions. Additionally, the properties of interest with set target values must be identified. Rules for the formation of feasible compounds from the groups selected must be established.
2. All chemically feasible molecules are generated.
3. Solution reduction is performed by property screening. Properties are predicted for the set of chemically feasible molecules. Molecules that match the target properties are retained while all other solutions are discarded.
4. Post-design methods such as process simulation are utilized to rank remaining solutions on basis of performance index. Screening of secondary properties may also be used to reduce the amount of solutions considered.

Vital to the use of enumeration solution methods is the ability to generate all feasible chemical structures. For design cases with large numbers of possible solutions, the generation of all possible solutions may prove computationally restrictive. However, for small cases the enumeration approach can identify optimal solution. Incorporation of multi-level molecular representation (*e.g.*, higher order group contribution methods) provides opportunities for more rigorous property prediction (Harper and Gani 2000).

2.14 Deterministic Solution Methods

Deterministic methods seek to find a global optimum to a mixed-integer linear program (MILP) or mixed-integer non-linear program (MINLP) through derivative-based solutions. Use of deterministic methods requires mathematical constraints to effectively limit the search space. Solution of a MILP is almost always performed by branch and bound methods (Edgar, Himmelblau *et al.* 2001). Often a MINLP results from problem formulation. When a MINLP results, the determination of a global optimum is not guaranteed. By far, the most commonly used method to solve MINLPs in CAMD utilizes the optimization solver DICOPT (http://www.gams.com/dd/docs/solvers/dicopt.pdf), which is available in the optimization software GAMS (http://www.gams.com/).

DICOPT solves MINLPs through the use of outer approximation, which is an iterative process that solves two sub-problems each iteration (Duran and Grossmann 1986; Floudas 1995). The first sub-problem is the solution of a non-linear program (NLP), which is formed by fixing the integer values of the original MINLP problem. Optimization is then performed over the continuous variables, with the provided solution being a lower bound to the original MINLP problem (Edgar, Himmelblau *et al.* 2001). The next sub-problem is the solution of a MILP. The continuous variable portion of the objective function is replaced with a constant. The constant is constrained to maintain equivalence to the original MINLP formulation. Solution of the MILP sub-problem optimizes over both the integer and continuous variables, with the provided solution being an upper bound to the original MINLP problem (Edgar, Himmelblau *et al.* 2001). If the problem is convex, the upper and lower bounds will converge to the optimal solution for the original MINLP problem in a finite number of iterations (Duran and Grossmann 1986; Floudas 1995). In addition to outer approximation, other approaches have also been considered for solution of MINLPs in CAMD problems, but are not given further treatment here (Sahinidis and Tawarmalani 2000; Karunanithi, Achenie *et al.* 2006).

2.15 Stochastic Solution Methods

Stochastic methods employ iterative processes to determine locally optimal solutions. Depending on the method, different rules or moves are used to proceed from one solution to another. Stochastic methods do not require derivatives for solution and are not guaranteed to return the global optimum. Two stochastic approaches have featured prominently in CAMD: genetic algorithms and tabu search. They are summarized in Table 2.3. In addition to genetic algorithms and tabu search, simulated annealing has also been used to solve CAMD problem (Ourique and Silva Telles 1998).

Table 2.3 Overview of stochastic approaches commonly used in CAMD

Method	Characteristics	Advantages	Disadvantages
Genetic Algorithm (GA)	Mimics evolution by improving a population of solutions incrementally over several generations	• Many solutions evaluated at each generation • Random moves can help to escape local minima	• No guarantee that moves will be significant enough to escape local minima • Storage of many current solutions may be memory intensive
Tabu Search	Use of previous solutions stored in a tabu list to guide search for new solutions	• Random moves can help to escape local minima • History of previous solutions further helps avoid local minima traps	• May disregard good solutions as tabu • Storage of past solutions may be memory intensive

Genetic algorithms are search methods that simulate natural progression through evolution (Holland 1975). Given an initial set of solutions, or *seed population*, adaptive and reproductive strategies are used to advance the solutions (Holland 1975). The classical genetic algorithm is not well suited for combinatorial solution spaces, leading to the development of special data structures on an application by application basis (Bäck 1996). One such application is CAMD, where molecular groups are represented by genes, a molecule represents a chromosome and a set of molecules represents the *population* (Venkatasubramanian, Chan *et al.* 1994). Moves mimicking adaptation and reproduction are used to alter the population in each iteration or *generation*. Moves mimicking adaption can be thought of as local moves, while reproductive-inspired moves are global moves. The suitability of solutions is determined by their *fitness*, which in turn determines the likelihood of a solution to become a *parent* (Venkatasubramanian, Chan *et al.* 1994). Parents are used to generate the population for the next generation. The search continues until a predetermined number of generations is reached. The search is then terminated, returning the solution with the highest fitness.

Tabu search is a heuristic approach which guides a local search through use of previous solution history (Glover 1989; Lin, Chavali *et al.* 2005). Tabu search relies on recently visited solutions, which are stored in a tabu list. Local moves are made to change a previous solution to a new solution. If a new solution is too similar to a solution stored in the tabu list, it is deemed *tabu* and discarded (Glover 1989; Lin, Chavali *et al.* 2005). Similarity is determined by the tabu criterion. In this manner, the search for solutions is a constrained search (Glover 1989). The search space is more effectively scanned and local minima can be escaped to search for better solutions. If a tabu solution is the best solution yet encountered, the tabu criterion can be overridden via *aspiration* (Glover 1989). After a predetermined number of non-improving iterations, the search is terminated and the best solution is returned (Glover 1989).

2.16 Integrated Product-Process Design

Product and process design employ similar solution methods and are both utilized to improve chemical production processes. Consequently the simultaneous design of both product and process has been pursued for various applications, especially for separation design (Eden, Jørgensen *et al.* 2004; Roughton, Christian *et al.* 2012). For separation design, the designed product is often a solvent for use in achieving the desired separation. The desired process performance is used to determine molecule property targets and constraints. The properties are in turn used to determine optimal chemical structures. In effect, integrated process design involves solving two reverse problems (see Figure 2.12). The final solution contains the design variables for the process as well as the molecules that satisfy the necessary property targets. By coupling molecular design with process design, process performance can be expected to improve as optimal solvents are identified and used in the necessary separations.

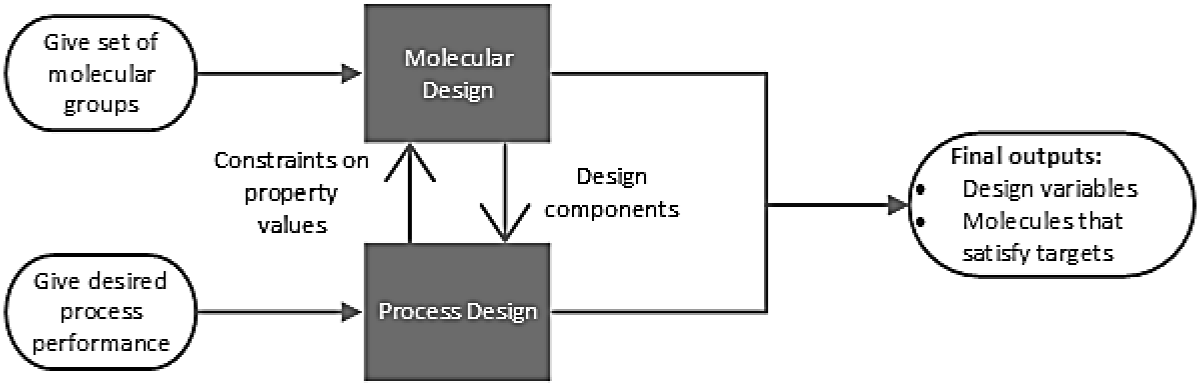
Give set of molecular groups
Molecular Design
Constraints on property values
Design components
Give desired process performance
Process Design
Final outputs:
Design variables
Molecules that satisfy targets

Figure 2.12 Overview of integrated product and process design Each design process generates parameters that are used to constrain the other design problem. Adapted from (Eden, Jørgensen *et al.* 2004).

2.17 Post-Design Methods

Post-design methods are used in CAMD to further screen the candidates generated in the design phase. The simplest post-design method is the use of secondary properties to screen the candidates. Such properties may require higher-dimensional structural information than is utilized during the design phase due to computational limitations (Harper and Gani 2000). A more detailed analysis of candidates is provided by the use of molecular modeling. A three-dimensional model is generated for a given candidate through the use of energy minimization. The end result is a 3-D molecular structure that can be used to obtain values for properties that require 3-D structural information (Harper, Gani *et al.* 1999).

An common example is toxicity towards various organisms, which is often predicted via a 3-D QSAR (Akamatsu 2002). Experimental verification is needed for final candidate selection and is beginning to be implemented in CAMD frameworks (Conte, Gani *et al.* 2011; Conte, Gani *et al.* 2012).

3.0 EXPERIMENTAL METHODS

The following chapter describes in detail the experimental plan used in the work as well as all relevant experimental methods that were used to generate data for the forward problem. Methods that were performed by the author include the experimental procedure used for generation of the data. The theory behind hydrogen-deuterium exchange mass spectroscopy is detailed as experimental data obtained from the method is used in conjunction with simulations to investigate protein-excipient interactions (See Section 7.0). Refer to the references cited for detailed information concerning the experimental setup and procedure.

3.1 EXPERIMENTAL OVERVIEW

The experiments done by the author were performed to evaluate the effect of excipient selection on aggregation following lyophilization. The following methods were performed by the author and all data pertaining to the methods were generated by the author for the data set used to generate models describing post-lyophilization protein loss as a function of excipient structure: ultraviolet-visible light spectrophotometry, size-exclusion chromatography, sodium-dodecyl-sulfate polyacrylamide gel electrophoresis and powder x-ray diffraction. Figure 3.1 displays the overall experimental approach.

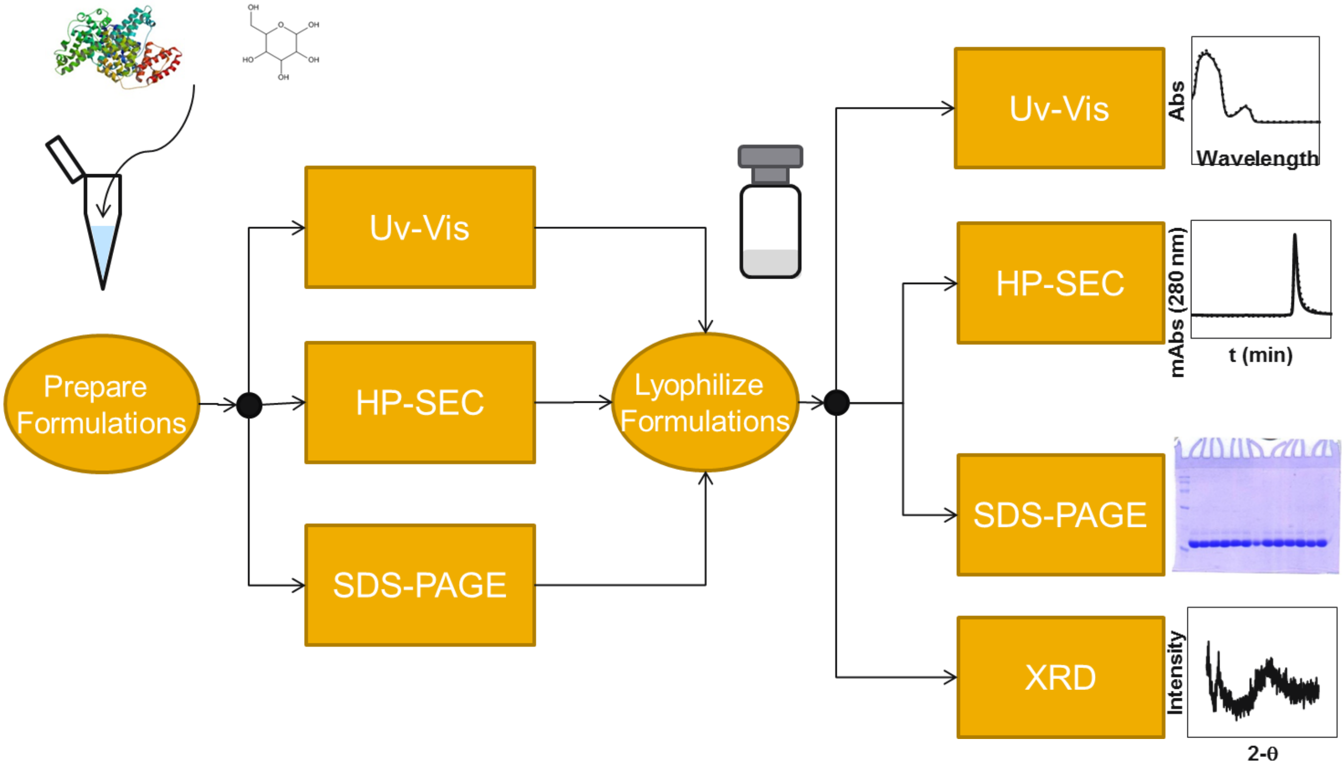

Figure 3.1 Overview of experimental procedure used by author The aim of the experiments was to characterize aggregation following lyophilization for several different excipient and protein choices.

Additional experimental results were obtained from literature for use in modeling building for the forward problem. The corresponding references contain information concerning the experimental setup and procedure. Material procurement, sample preparation and lyophilization for the experiments done by the author follow.

3.1.1 Materials

The following proteins were considered in the study: α-amylase, bovine serum albumin (BSA), ovalbumin, ribonuclease A (RNAse A) and soybean trypsin inhibitor. All proteins were acquired from Sigma-Aldrich (St. Louis, MO) except trypsin inhibitor, which was obtained from Worthington Biochemical Corporation (Lakewood, NJ). Table 3.1 lists key biophysical properties for each protein.

Table 3.1 Biophysical descriptors for the proteins considered

Protein	PDB code	MW (kDa)	pI	ASA[a] (Å^2)	f_{ASA}[b]	% α helix	% β sheet	# SS bonds	# free thiols	T_m (°C)
Ovalbumin	1ova	44.3	5.19	34237	0.63	30.8	31.3	1	4	76[c]
RNase A	5rsa	16.5	8.93	4052	0.60	21	33	4	0	62.5[d]
α-amylase	1bli	58	6.33	10480	0.60	26.2	25.6	0	0	102[e]
BSA	3v03	66	5.82	35921	0.68	67	0	17	1	59[f]
Trypsin inhibitor	1avu	20.1	4.95	4986	0.60	1.4	97.2	2	0	65[g]

a – ASA=apolar surface area
b – fASA = apolar surface area / total surface area
Melting temperature (T_m) values were obtained from literature: c (Tani, Shirai *et al.* 1997), d (TAKAHASHI, IRIE *et al.* 1969), e (Duy and Fitter 2005), f (Arakawa and Kita 2000), g (Roychaudhuri, Sarath *et al.* 2003)

A broad range of readily available molecules for use as excipients were considered, which can be broken into the two main classes of amino acids and carbohydrates. The following amino acids and amino acid derivatives were considered: N-acetylglycine, N-ethylglycine, glycine-alanine (glu-ala), glycine-glycine (gly-gly), glycine-leucine (gly-leu) and glycine-serine (gly-ser). The following carbohydrates and carbohydrate derivatives were considered: mannitol, sorbitol, maltitol, glucose, mannose, fructose, psicose, 2-deoxyglucose, 2-deoxyribose, xylose, rhamnose, α-methylglucopyranoside, trehalose, maltose, palatinose, melibiose, raffinose, N-methylglucamine, N-acetylglucosamine and N-acetylneuraminic acid. All chemicals were acquired from Sigma-Aldrich. While all of the molecules used may not have suitable properties for protein formulation, the entire set provides a broad sampling of molecular structures which is desirable for model development purposes.

3.1.2 Sample Preparation

Protein solutions were prepared by dissolving protein in 20 mM potassium phosphate pH 7.4 buffer to a concentration of 2 mg/mL. The protein solution was then dialyzed using Biotech cellulose ester dialysis tubing (MWCO 8,000-10,000 Da, Spectrum Laboratories, Rancho Dominguez, CA) against a 20 mM potassium phosphate pH 7.4 buffer at 4°C. Following dialysis, the protein solutions were passed through a 20 μm syringe filter (Gelman Nylon Acrodisc 13, Sigma-Aldrich). Dialyzed and filtered solutions were stored at 4°C for use within 24 hours.

In a similar manner, excipient solutions were prepared by dissolving excipient in 20 mM potassium phosphate pH 7.4 buffer to a concentration of 2 mg/mL. The excipient solutions were passed through a 20 μm syringe filter and stored at 4°C.

Formulations were prepared for each protein-excipient pair by mixing equal volumes of protein solution and excipient solution to yield a solution with 1 mg/mL protein and 1 mg/mL excipient (1:1 excipient to protein weight ratio). Immediately following preparation of a formulation, 400 μL of the solution was added to a lyophilization vial (Worthington Biochemical Corporation). Vials were prepared in triplicate for each protein-excipient pair. After the solution was transferred to the vial, the samples were immediately lyophilized. Additional samples of non-lyophilized control solutions were prepared in triplicate for each protein-excipient pair using the same procedure.

3.1.3 Lyophilization

Each formulation (protein-excipient pair) was lyophilized in triplicate through use of a VirTis adVantage Plus lyophilizer (SP Industries, Inc., Gardiner, NY). The following lyophilization cycle was used for all samples: shelves were pre-cooled to -2°C (15 minutes), sample freezing at -40°C (50 minutes) was performed, primary drying under vacuum (70 mTorr) occurred at -35°C for 10 hours, -20°C for 8 hours, -5°C for 6 hours, with secondary drying (100 mTorr) at 10°C for 6 hours, 25°C for 6 hours and 4°C for 30 minutes (Sophocleous, Zhang *et al.* 2012). After completion of the lyophilization cycle, samples were held at 4°C for no more than 2 hours before reconstitution and subsequent analysis. No attempt was made to optimize the lyophilization cycle based on the formulation properties, such as the glass transition temperature of the maximally freeze-concentrated solute (T_g').

3.2 Ultraviolet-Visible Light Spectrophotometry (UV-Vis)

3.2.1 Theory

UV-Vis is a technique that measures absorbance of light by a molecule at any given wavelength. The absorption of light is accompanied by a transition in the molecule from lower energy state to a higher energy state, via energy provided by the photon of light (Van Holde, Johnson *et al.* 2006). The transitions typically associated with ultraviolet and visible light absorption are electronic transitions of the valence shell electrons, where electrons are excited from an occupied or ground state orbital to an unoccupied or excited state orbital (Van Holde, Johnson *et al.* 2006). Absorption occurs if the energy of the photon at a particular wavelength is equal to the difference in energy between the ground state and the excited state. The energy absorbed from the photon is usually lost as heat. By comparing the emission of light through a sample and a control, differences observed are used to construct the absorption spectra of the sample. Chromophores are chemical groups that absorb light at particular wavelengths and thus have characteristic absorption spectra (Van Holde, Johnson *et al.* 2006).

Proteins contain several chromophores: peptide bond, aromatic residues (phenylalanine, tryptophan and tyrosine), prosthetic groups and metal cations (see Figure 3.2). Absorbance due to the peptide bond is the strongest observed and occurs around a wavelength of 185-195 nm, depending on the protein's secondary structure (Martin, Sinko *et al.* 2011). Absorbance from the range of 250-300 nm corresponds to absorbance by the aromatic residues in the protein. Prosthetic groups and metal cations may have absorbance at varying wavelengths according to the species of interest. Absorbance past 300 nm is associated with light scattering (Martin, Sinko *et al.* 2011). A typical UV-vis spectrum for a protein is shown in Figure 3.3.

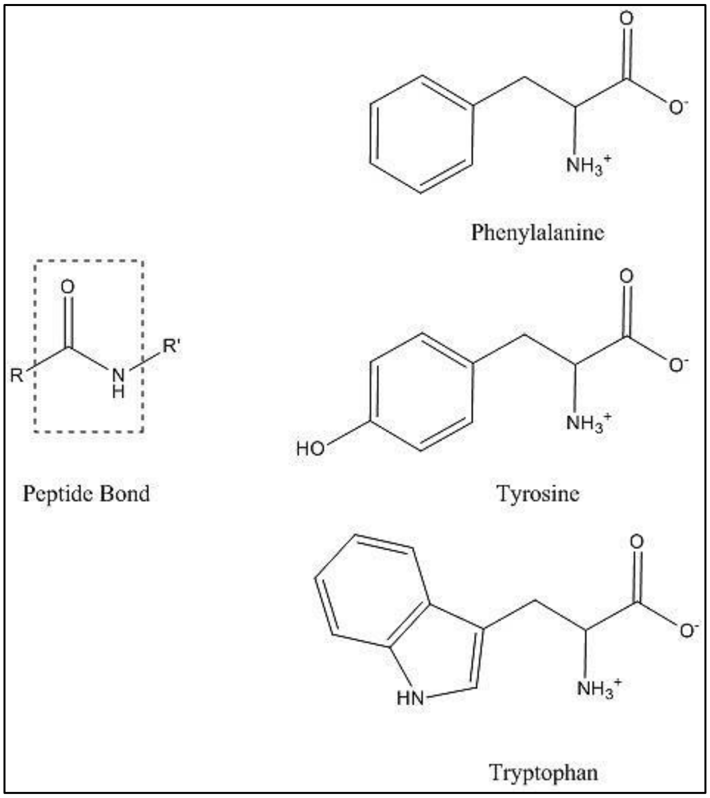

Figure 3.2 Chromophores commonly present in proteins

Absorbance (*A*) allows calculation of concentration of a species through Beer's law (Equation 3.1):

$$A = \varepsilon c l$$

(Equation 3.1)

where c is concentration, l is path length and ε is the extinction coefficient. The value of ε for proteins is estimated from the amino acid sequence (Martin, Sinko *et al.* 2011). In practice the pure absorbance is not usually measured but rather the optical density (O.D.), which is defined as the absorbance plus any other extinction processes such as light scattering.

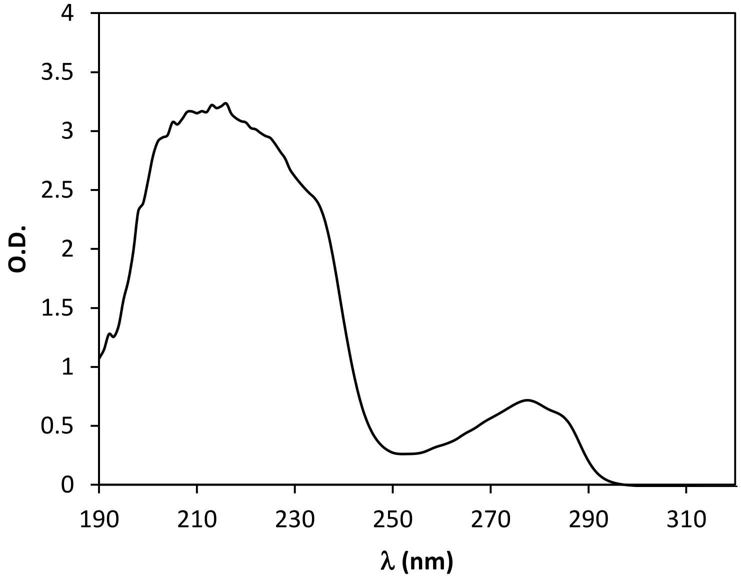

Figure 3.3 Typical UV-Vis spectra for a protein The large peak is due to absorbance by the peptide bond. The smaller peak arises from absorbance by the aromatic amino acid residues (phenylalanine, tryptophan and tyrosine).

Information about protein structure can be obtained through a derivative analysis of the UV-vis spectra, focusing on the absorbance due to the aromatic residues (Martin, Sinko *et al.* 2011). The calculation of aggregation index (AI) compares the O.D. values at two different wavelengths (*i.e.*, 280 nm and 350 nm) to check for the presence of larger particles or aggregates (Equation 3.2). AI is affected by light scattering of particles and increases with larger aggregates (Katayama, Nayar *et al.* 2005).

$$AI = 100 * \frac{OD_{350}}{OD_{280} - OD_{350}}$$

(Equation 3.2)

3.2.2 Experimental Procedure

UV-visible spectra were obtained for all lyophilized and non-lyophilized samples using an Agilent 8453 UV-Vis spectrophotometer. For each spectrum, 400 μL of sample solution was added to a low volume cuvette. Wavelengths were collected from 200-600 nm using an integration time of 10 seconds and an interval of 1 nm. The aggregation index (AI) was calculated for each sample given the optical density values at 280 and 350 nm (see Equation 3.2).

3.3 Size-Exclusion Chromatography (SEC)

3.3.1 Theory

SEC is used to separate molecules on the basis of size and shape (see Figure 3.4). A sample containing molecular species of varying sizes is injected upstream of the column. The sample flows through the system through use of a mobile phase, which is pumped at a constant rate. The mobile phase often contains a buffer to maintain the pH of the sample. The column used in SEC is packed with a porous matrix which provides the separation ability. Gel beads comprise the matrix or fixed phase of the column, resulting in a cross-linked network of pores (Rosenberg 2005). Separation of molecules is based on the size of the pores in the beads, with larger molecules being unable to enter the pores and thus eluting at a faster time. Both molecular weight (size) and the three-dimensional conformation (shape) of the molecule contribute to a protein’s ability to enter a pore. Adsorption of protein to the column matrix is a concern in SEC, preventing protein from eluting in a timely manner if at all. For analysis of protein samples, high salt concentrations are used in the mobile phase to curtail protein adsorption to the column matrix (Arakawa, Ejima *et al.* 2010).

SEC is often coupled with UV-vis spectrophotometry through inclusion of an inline UV detector following the SEC column. Determination of UV absorption immediately following elution form the column allows for quantitative measurement of the amount of molecules eluting at a given time. UV absorption values are either taken at a few specific wavelengths (e.g., 280 nm for proteins) or an entire absorption spectrum can be obtained. Sample volume should be kept minimal to ensure high signal resolution and avoid peak broadening (Rosenberg 2005).

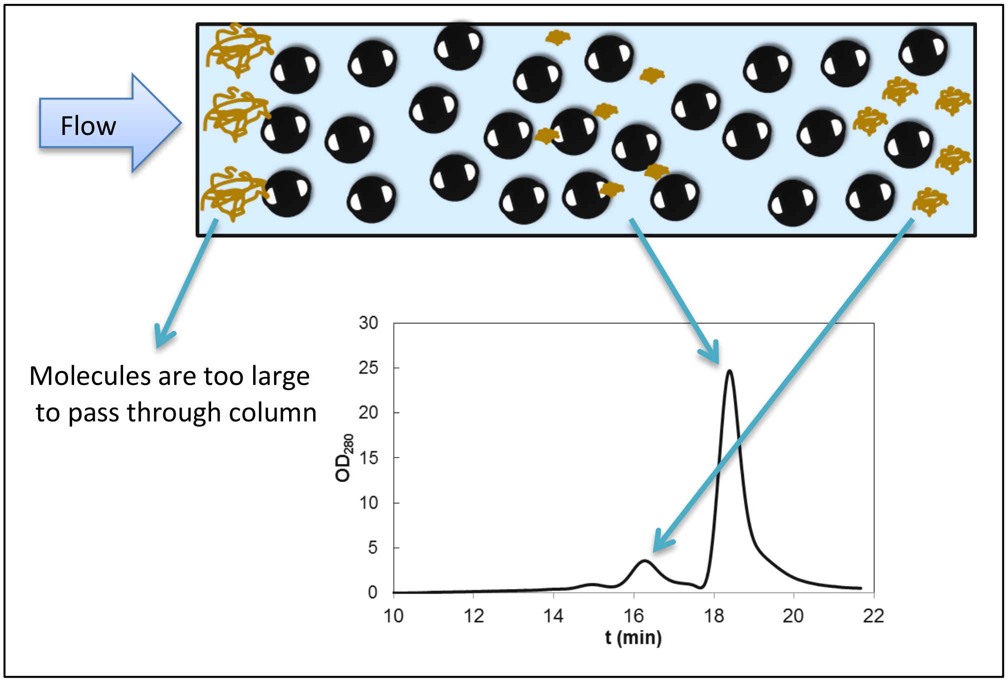

Figure 3.4 Overview of size-exclusion chromatography (SEC) Molecules are separated by the column based on size, with smaller molecules experiencing a more tortuous path and hence longer times to elution. As molecules elute, they are detected using UV absorption. Some molecules may be too large to pass through the column and are retained.

The use of SEC in analysis of protein aggregates is common due to the advantages offered by the fast analysis time, ability to be performed at high-throughput, the quantitative information on the abundance of monomeric and multimeric protein species and the high precision that is obtainable in the results (Carpenter, Randolph *et al.* 2010). However, a need for orthogonal methods for aggregation analysis has been established due to numerous concerns including the inability of large aggregates to pass through the frit and enter the column, adsorption of aggregates on the column walls and the dissociation of aggregates in the column prior to elution (Carpenter, Randolph *et al.* 2010).

3.3.2 Experimental Procedure

Quantitative aggregation analysis was performed using size exclusion chromatography (SEC) for both reconstituted lyophilized and non-lyophilized control samples. SEC was performed using an Agilent 1200 Series LC system (Agilent Technologies, Santa Clara, CA) with a TSKgel G3000SWxl column (Tosh Bioscience LLC, King of Prussia, PA). A mobile phase of 50 mM potassium phosphate pH 7.0 buffer with 200 mM NaCl was used. The flow rate was set to 0.5 mL/min and UV signals were collected at 215 nm and 280 nm. Using the 280 nm signal, peak area was calculated for each chromatogram. The peak area was used to determine the percent monomer remaining after lyophilization, assuming that the peak area for the non-lyophilized control corresponded to 100% monomer.

$$\%Monomer = \frac{PeakArea_{280\,nm,\ lyo}}{PeakArea_{280\,nm,\ non-lyo}}$$

(Equation 3.3)

3.4 Sodium-Dodecyl-Sulfate Polyacrylamide Gel Electrophoresis (SDS-PAGE)

3.4.1 Theory

Electrophoresis separates molecules on the basis of size and charge. Molecules are separated in a cross-linked gel network in polyacrylamide gel electrophoresis (PAGE). Pore size is controlled by concentration of polyacrylamide with higher concentrations of polyacrylamide leading to smaller pore sizes (Rosenberg 2005). Commonly, gels are comprised of a stacking gel with low polyacrylamide content where the sample is injected and the resolving gel with higher polyacrylamide content where separation occurs (Rosenberg 2005).

Sodium-dodecyl-sulfate (SDS) is a detergent which is used to denature the protein prior to electrophoresis. SDS also causes protein to carry an overall net negative charge. Additionally, proteins may be treated with reducing agents to eliminate disulfide bonds. After injection of samples, an electric field is applied to the gel which causes the protein to migrate through the gel. The speed of migration is proportionally to the molecular weight of the protein (Rosenberg 2005). Following electrophoresis, protein is deposited in bands throughout the gel according to its molecular weight. A reference ladder of known proteins can be used to provide molecular weight references for comparison. Figure 3.5 provides a representative gel following SDS-PAGE.

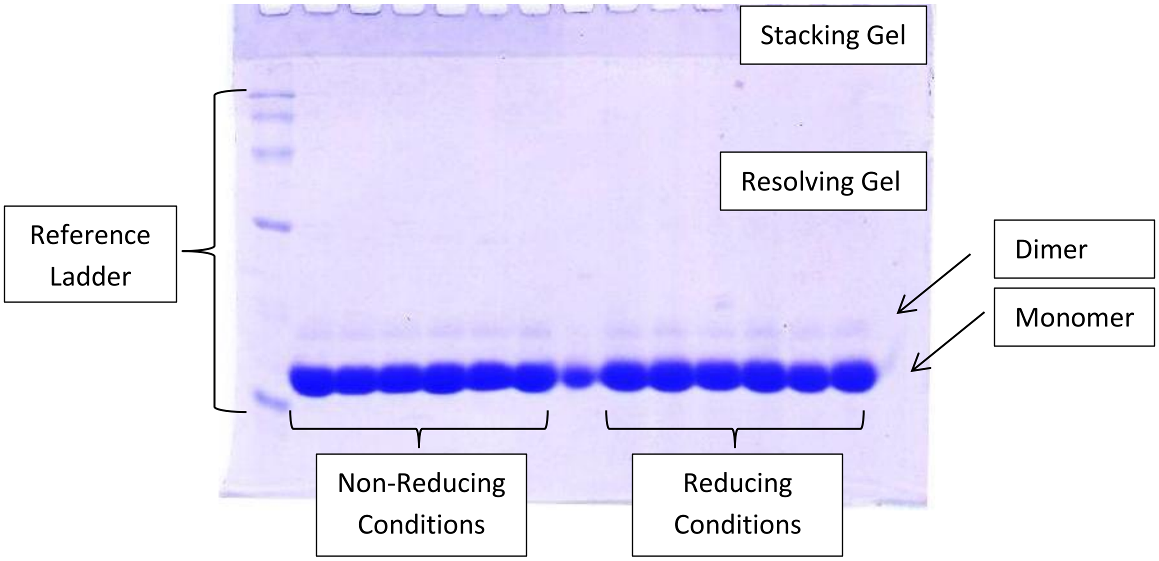

Figure 3.5 Representative gel following SDS-PAGE The leftmost lane shows a reference ladder. The protein used is RNAse A.

Staining following SDS-PAGE allows for visual detection of protein within the gel. SDS-PAGE can be used to qualitatively detect the presence of species of different molecular weight, including aggregates. Alternatively, quantitative methods such as radio-labeling and autoradiography allow the quantification of different protein species or protein size distribution following SDS-PAGE (Rosenberg 2005).

3.4.2 Experimental Procedure

Qualitative aggregation analysis was performed using SDS-PAGE for both reconstituted lyophilized and non-lyophilized control samples. Samples were divided and mixed with either non-reducing or reducing (containing β-mercaptoethanol) loading buffer containing bromophenol blue for staining. Samples were vortexed for 10 min and then heated for 5 min at 95°C. Samples were allowed to cool and were then loaded into 10% or 12% polyacrylamide gels. Precision Plus Protein Dual Xtra Standards (Bio-Rad, Hercules, CA) were used as a reference ladder. SDS-PAGE was performed using a Mini-PROTEAN Tetra cell electrophoresis instrument attached to a PowerPac Basic power supply (Bio-Rad). After completion of electrophoresis, the gels were removed and stained with Coomassie Brilliant Blue R-250 staining solution for 30 min and then destained for approximately 24 hrs on a rocking platform (VWR International, Radnor, PA).

3.5 Powder X-ray Diffraction (pxrd)

3.5.1 Theory

Powder x-ray diffraction emits x-rays at a powdered solid sample and measures the resulting diffraction pattern. X-rays are sent from a source (e.g., x-ray tube) and collide with the sample at a specified incident angle (θ). As the x-rays collide with atoms in the solid, the x-rays are scattered. An x-ray detector is used to detect any x-rays that are deflected at an angle of twice the incident angle (in reference to the x-ray beam sent from the source), referred to as 2θ. The detection of x-rays is represented as the intensity. The incident angle is changed repeatedly to allow detection of diffraction patterns across a range of 2θ values. A typical PXRD setup is shown in Figure 3.6.

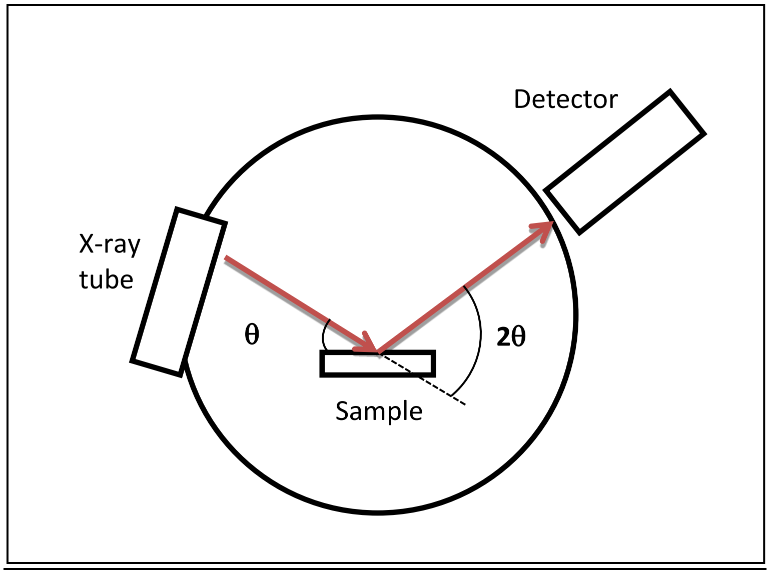

Figure 3.6 Diagram of typical powder x-ray diffraction setup X-rays are sent from the source (x-ray tube) and are reflected back to the detector at an angle referred to as the incident angle (θ). 2θ is equal to two times θ. Figure adapted from (Speakman).

Arrangement of the atoms in a sample produces a characteristic diffraction pattern. Bragg's law describes the conditions that must be satisfied for diffraction to occur at a given incident angle (θ):

$$\boldsymbol{\lambda = 2d_{hkl}sin\theta}$$

(Equation 3.4)

Where λ is the wavelength of the x-ray and is fixed and d_{hkl} is a characteristic vector defined by the crystal geometry. A crystal has repeating units of atomic structure, referred to as unit cells (Shackelford 2009). The unit cell represents the maximal symmetric unit in the material and has a characteristic shape and size that determines d_{hkl} (Speakman ; Shackelford 2009). The unit cell in a crystal has atomic planes which are attributed to the diffraction peaks observed in a sample. As the unit cell is repeated, diffraction at the angle incident to the plane occurs frequently resulting in a sharp peak with high intensity in the observed diffraction pattern.

While pxrd has several applications, the focus here is the use of pxrd to determine whether a sample is crystalline or amorphous. On a qualitative basis, a sample can be classified as either largely amorphous or largely crystalline based on the overall diffraction pattern observed. Amorphous solids have no long range order and thus show no diffraction pattern, instead displaying what is referred to as an "amorphous halo" (see Figure 3.7). Crystalline solids are highly ordered and only show diffraction at certain wavelengths based on the crystal structure. The resulting diffraction pattern is characterized by a few sharp peaks of high intensity (see Figure 3.7). The discernible visual differences in the diffraction patterns often allows for a general qualitative classification of either largely amorphous or largely crystalline. Quantitatively, pxrd can be used to calculate the percent crystallinity of a sample by dividing the intensity of a peak observed in a given sample by the intensity of the peak in a pure crystalline control (Clas, Faizer *et al.* 1995). For multiple peaks, the intensities are summed for both the sample and the pure crystalline control and then the ratio is determined. Low percent crystallinity corresponds to a sample that is largely amorphous. For small molecule drug development, the exact percent crystallinity is often of interest as it relates to bioavailability (Clas, Faizer *et al.* 1995). However for the experiments conducted here, the main concern was whether any given formulation was largely amorphous following lyophilization for which a qualitative approach was sufficient.

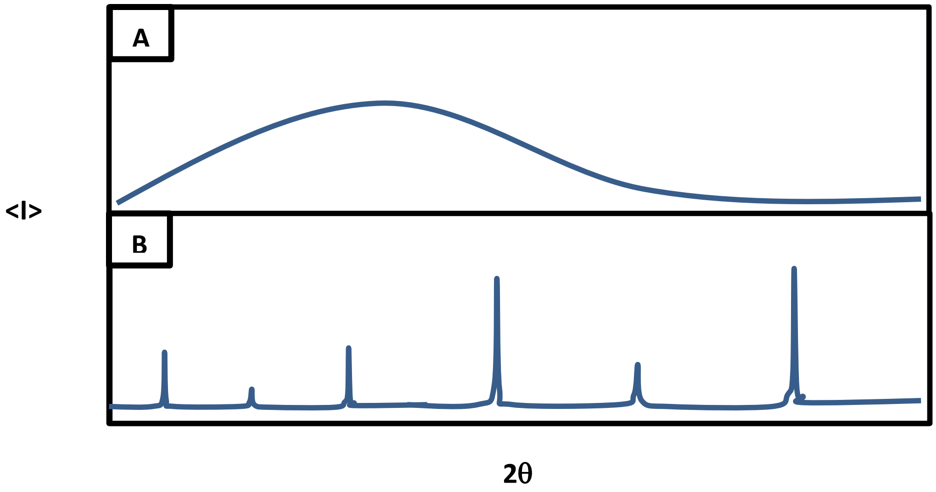

Figure 3.7 Representative x-ray diffraction patterns (A) amorphous material and (B) crystalline material showing intensity (<I>) versus 2θ. Figure adapted from (Speakman).

3.5.2 Experimental Procedure

Samples for PXRD analysis were prepared similarly to the method stated previously except protein and excipient solutions were made to concentrations of 10 mg/mL, yielding formulation concentrations of 5 mg/mL protein and 5 mg/mL excipient (1:1 excipient to protein weight ratio). The same sample volume of 400 μL was transferred to the lyophilization vials for each protein-excipient pair. Samples were lyophilized using the previously mentioned lyophilization cycle. Following lyophilization, confirmation that the samples were amorphous was performed by collecting X-ray diffractograms using a Scintag X2 θ-θ diffractometer (Scintag Inc., Cupertino, CA) equipped with a Cu Kα anode operating at a wavelength of 1.5406 Å.

Due to the large amount of formulations considered, a smaller subset was selected for PXRD analysis. JMP statistical software (SAS, www.jmp.com) was used to randomly select a minimal number of formulations for analysis such that each protein was selected at least once, each excipient was selected at least once and each sugar alcohol excipient was selected at least twice. 20 formulations were selected and from the set of 20, 6 were randomly selected to be done in replicate. Only carbohydrate excipients were considered.

3.6 Hydrogen-Deuterium Exchange Mass Spectroscopy (HX-MS)

3.6.1 Theory

Hydrogens bonded to the amide nitrogen (See Figure 3.8) in the protein backbone can exchange with deuteriums when exposed to deuterated water (D_2O). The reaction can be catalyzed either acid (D_3O^+) or base (OD^-). The exchange rate of the amide hydrogens can occur over a wide range of time, with some exchanging in milliseconds and others in days.

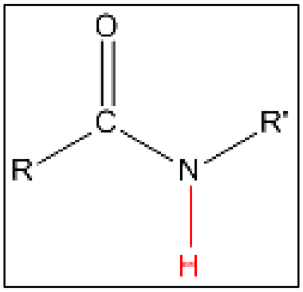

Figure 3.8 A peptide bond, which forms between amino acids to construct the protein backbone The hydrogen bonded to the amide nitrogen is highlighted in red. The hydrogen participates in exchange with deuterium during HX experiments.

The exchange rate is highly dependent on the degree of solvent protection and hydrogen bonding. Buried residues or residues with an amide hydrogen that participating in hydrogen bonding are resistant to exchange, where surface residue freely exchange hydrogen for deuterium (Tsutsui and Wintrode 2007). Hydrogen exchange is also impacted by the flexibility of the protein's conformation, both locally and overall. Fluctuations in the protein's structure allow solvent penetration and subsequent exchange. The exchange rate is given by Equation 3.5 (Tsutsui and Wintrode 2007):

$$k_{obs} = \frac{k_1 k_2}{k_{-1} + k_2}$$

(Equation 3.5)

Where k_1 is the rate of conformational changes that result in unfolding, k_{-1} is the rate of conformational changes that result in folding, k_2 is the chemical rate of exchange between a hydrogen and a deuterium and k_{obs} is the observed rate of exchange. The overall observed exchange can be divided into two regimes: the EX1 regime (k_2 >> k_{-1}) and the EX2 regime (k_{-1} >> k_2). In EX1, the protein exhibits multiple conformations and slowly interconverts between conformations, allow exchange to occur (Tsutsui and Wintrode 2007). The observed exchange rate depends only on the rate of unfolding. The EX1 regime is often induced through use of denaturants. More frequently the EX2 regime is observed, where local conformational changes exposing amide hydrogens may occur multiple times before exchange can occur (Tsutsui and Wintrode 2007). The observed rate is therefore mostly dependent on the equilibrium of local unfolded and folded states. In regions where local unfolding occurs more frequently, more exchange will occur. The observation of local exchange rates gives an indication of the stability of the region.

Exchange at individual residues can be determined with Nuclear Magnetic Resonance (NMR), but the approach is limited due to the large protein amounts needed, the size of the protein is restricted, and the difficult and time consuming assessment of peaks (Tsutsui and Wintrode 2007). In 1990, mass spectroscopy was shown to be a viable tool for the study conformational changes in proteins (Chowdhury, Katta *et al.* 1990). Mass spectroscopy and proteolysis have since been coupled with hydrogen/deuterium exchange to provide a medium resolution tool (5-10 residues) for probing the structural changes of proteins (Katta, Chait *et al.* 1991; Tsutsui and Wintrode 2007). An overview of the HX-MS experimental procedure is given in Figure 3.9.

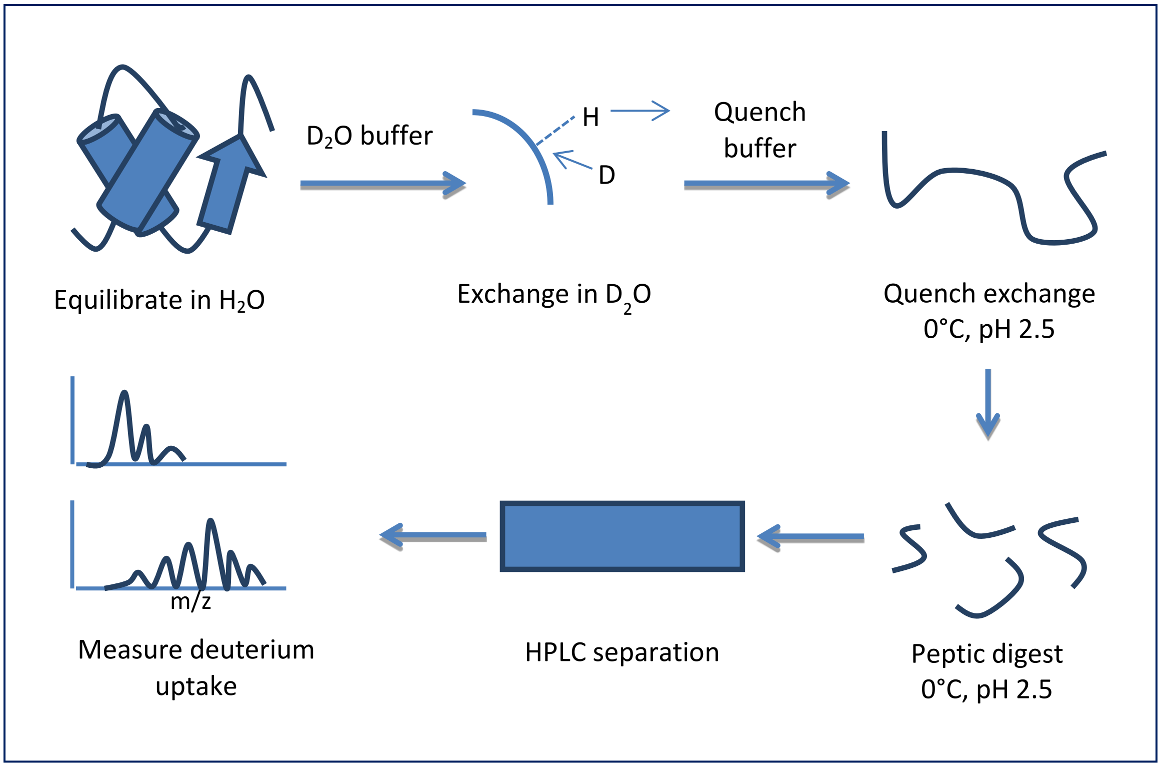

Figure 3.9 General experimental procedure for HX-MS experiments performed in aqueous solution Figure adapted from (Tsutsui and Wintrode 2007).

3.6.2 Use in Lyophilized Solids

HX-MS has been extended to lyophilized solids as a method to elucidate protein structure and formulation effects (Li, Williams et al. 2007; Li, Williams et al. 2007; Li, Williams et al. 2008). Some modification to the procedure outlined in Figure 3.9 is required to adapt the process to lyophilized solids. Following equilibration in aqueous solution, the protein is lyophilized to produce an amorphous solid. Exchange with deuterium is then carried out by exposing the solid to deuterated water vapor. Following exchange, the lyophilized protein is reconstituted with quenching and peptic digestion following as performed for aqueous samples.

The results given by HX-MS with lyophilized solids provides site-specific information on interactions between protein and the solid environment (Li, Williams et al. 2007). Factors influencing in the solid state include relative humidity during exchange, inclusion of salts and inclusion of stabilizing excipients (Li, Williams et al. 2007; Li, Williams et al. 2007). HX-MS with lyophilized proteins provides a quantitative and site-specific tool for the study of protein-excipient interactions in amorphous solids.

4.0 PROPERTY MODEL DEVELOPMENT: THE FORWARD PROBLEM

CAMD requires accurate and predictive property models for design or selection of candidate molecules. For development of property models, molecular descriptors are needed for correlation between molecular structure and properties of interest. For example, an overview of the experimental procedure and model development steps in the design of lyophilized protein formulation is given by Figure 4.1 with the steps relevant to property model development highlighted.

The property models considered here are classified either as quantitative structure-property relationships (QSPRs), group contribution (GC) methods or thermodynamic property models. The property models developed here are given in Table 4.1, along with the corresponding descriptor type and model type. Additional property models available in literature were used where applicable.

The types of molecular descriptors used are discussed in Section 4.1. Development of linear QSPRs is described in Section 4.2 and development of non-linear QSPRs is described in Section 4.3. Group contribution methods are detailed in Section 4.4. Finally, the development of a UNIFAC thermodynamic property model for ionic liquids (UNIFAC-IL) is outlined in Section 4.5.

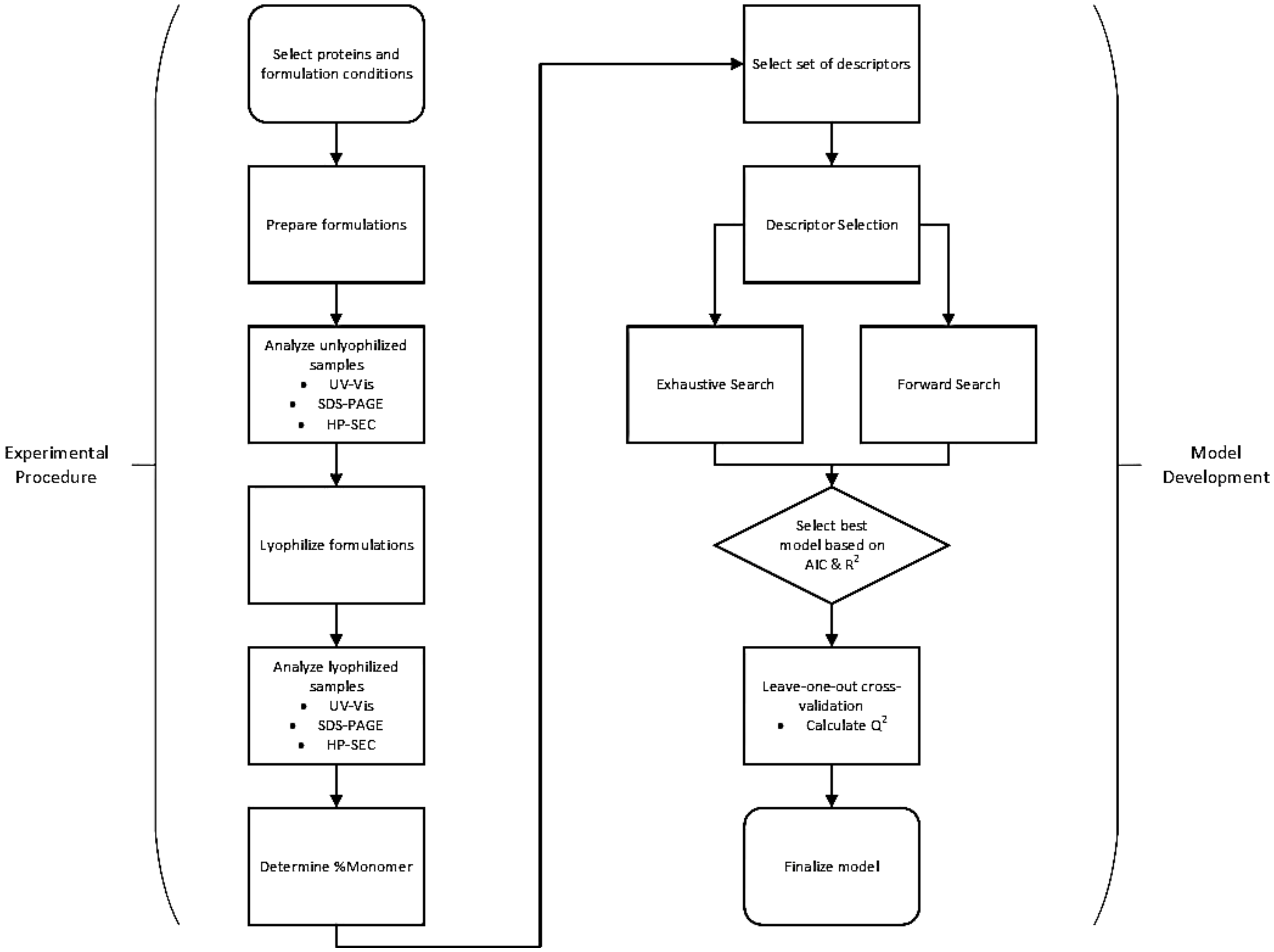

Figure 4.1 Procedure for experimental data acquisition and model development for rational lyophilized formulation development The part of the process that describes the model development process is detailed in Section 4.0. The experimental procedure is described in Section 3.0. Figure adapted from (Roughton, Iyer *et al.* 2013).

Table 4.1 Summary of property models developed for both lyophilized protein formulation design and ionic liquid design for use in separations of bio-products

Property	Descriptors Used	Model Type
LYOPHILIZED PROTEIN FORMULATION DESIGN		
Anhydrous glass transition temperature (T_g)	Connectivity indices	Linear QSPR
Freeze-concentrated glass transition temperature (T_g')	Connectivity indices	Linear QSPR
Maximal concentration in freeze-concentrated matrix (Cg')	Connectivity indices	Linear QSPR
Gordon-Taylor constant (k)	Connectivity indices	Linear QSPR
Percent monomer remaining after lyophilization (*%Monomer*; on a formulation-by-formulation basis)	Protein-based descriptors	Linear QSPR
Percent monomer remaining after lyophilization (*%Monomer*; on a protein-by-protein basis)	Chiral connectivity indices	Linear QSPR
Percent monomer remaining after lyophilization (*%Monomer*; as a function of protein and excipient choice)	Chiral connectivity indices Protein-based descriptors	Non-linear QSPR
IONIC LIQUID DESIGN		
Property	**Descriptors Used**	**Model Type**
Hildebrand solubility parameter (δ)	Group contribution	Group contribution method
Thermal decomposition temperature (T_d)	Group contribution	Group contribution method
Partition Coefficient for NDHD (K_x)	Connectivity indices	Linear QSPR
Toxicity towards *E. coli* (EC_{50})	Connectivity indices	Linear QSPR
Activity coefficients (γ)	Group contribution	UNIFAC thermodynamic model

4.1 Calculation of Molecular Descriptors

Three classes of molecular descriptors were considered. Group contribution is described in Section 4.1.1, connectivity indices are discussed in Section 4.1.2 and protein-based descriptors are detailed in Section 4.1.3.

4.1.1 Group Contribution

Group contribution methods identify common molecular groups, which are then used to build the molecule of interest. Group contribution (GC) methods have been utilized successfully to predict many physical properties of organic compounds, including boiling point and freezing point (Joback and Reid 1987). GC approaches have seen success in the prediction of vapor-liquid equilibria (VLE) (Gani, Tzouvaras et al. 1989). The UNIFAC method uses group contributions to predict activity coefficients for mixtures, which are subsequently used to predict VLE (Fredenslund, Gmehling *et al.* 1977).

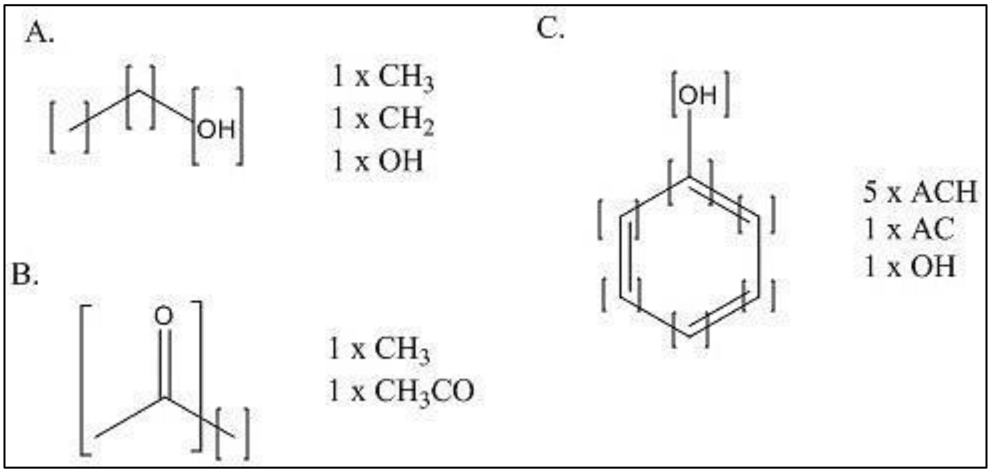

Figure 4.2 Example group contributions for (A) ethanol, (B) acetone and (C) benzene Groups used are the main groups used in UNIFAC.

In general, groups are determined by the author of the method and can vary from method to method. An example of the groups present in several molecules as defined by UNIFAC is given by Figure 4.2. As every chemical group needs to be accounted for, descriptor selection methods (cf. Section 4.2.4) cannot be utilized in the development of GC methods. The motivation behind group contributions is that results from a limited experimental data set can be applied to other systems with different molecule structures, but the same basic molecular groups. One major limitation of GC methods is that they cannot account for groups that are not present in the model-building set. GC methods assume that the number of a certain group present and the location of groups within a molecule do not affect the observed property of the molecule (Prausnitz, Lichtenthaler *et al.* 1999). This assumption is incorrect; improvement can come with the definition of more groups or higher-order groups, albeit with the need for more model parameters (Prausnitz, Lichtenthaler *et al.* 1999; Harper and Gani 2000). Predictions from GC methods offer a first approximation for properties (Prausnitz, Lichtenthaler *et al.* 1999) and are thus useful for property screening purposes (Gani, Nielsen *et al.* 1991).

4.1.2 Connectivity Indices

Topological descriptors are a class of molecular descriptors which identify individual atoms and their bonding configuration in a molecule. Connectivity indices are a type of topological descriptors first proposed by Randic (1975). Later work extended the use of connectivity indices to pharmaceutical product property prediction (Kier and Hall 1986) and polymer property prediction (Bicerano 2002). The use of connectivity indices have been proposed to describe missing groups for GC models (Gani, Harper *et al.* 2005; Satyanarayana, Abildskov *et al.* 2009).

Connectivity indices were chosen as the class of excipient descriptors to be used in model development. Connectivity indices were also used for some ionic liquid property models where group contribution did not perform with acceptable accuracy. Connectivity indices have utility due to the ability to calculate indices and to store bonding information for any molecular structure proposed, regardless of the molecular groups present. Additionally, connectivity indices have seen success in the prediction of properties for pharmaceutically relevant systems (Kier, Hall *et al.* 1975), including carbohydrate excipients (Roughton, Topp *et al.* 2012).

Connectivity indices (${}^{n}\chi$) describe the two-dimensional atomic and bonding features of a molecule while valence connectivity indices (${}^{n}\chi^{v}$) describe the electronic configuration. For calculation of connectivity indices, the molecule is represented as a hydrogen-suppressed graph where vertices represent non-hydrogen atoms and edges represent bonds. The vertex degree δ_i for any vertex *i* is equal to the number of vertices connected to the vertex by an edge and represents the number of non-hydrogen atoms that form bonds with the given non-hydrogen atom. The calculation of an *n-th* order connectivity index is giving by Equation 4.1.

$${}^{n}\chi = \sum_{k=1}^{N_s} \left(\prod_{i=1}^{n+1} \frac{1}{\delta_i} \right)_k^{1/2}$$

(Equation 4.1)

Where N_s is the number of subgraphs of size *n*. Vertices (atoms) are the subgraph considered for a zeroth-order connectivity index, edges (bonds) are the subgraph considered for a first-order connectivity index, paths of two edge-lengths (two bond paths) are the subgraph for a second-order connectivity index and so on. For a valence connectivity index, Equation 4.2 is used to determine the valence vertex degree δ_i^v and then Equation 3 is used for calculation, replacing δ_i with δ_i^v.

$$\delta_i^v = \frac{Z^v - N_H}{Z - Z^v - 1}$$

(Equation 4.2)

Where *Z* is the atomic number, Z^v is the number of valence electrons and N_H is the number of connected hydrogen atoms. Average simple or valence connectivity index values (ζ) for a given order are calculated by dividing the simple or valence connectivity index value by the number of subgraphs of the order being considered.

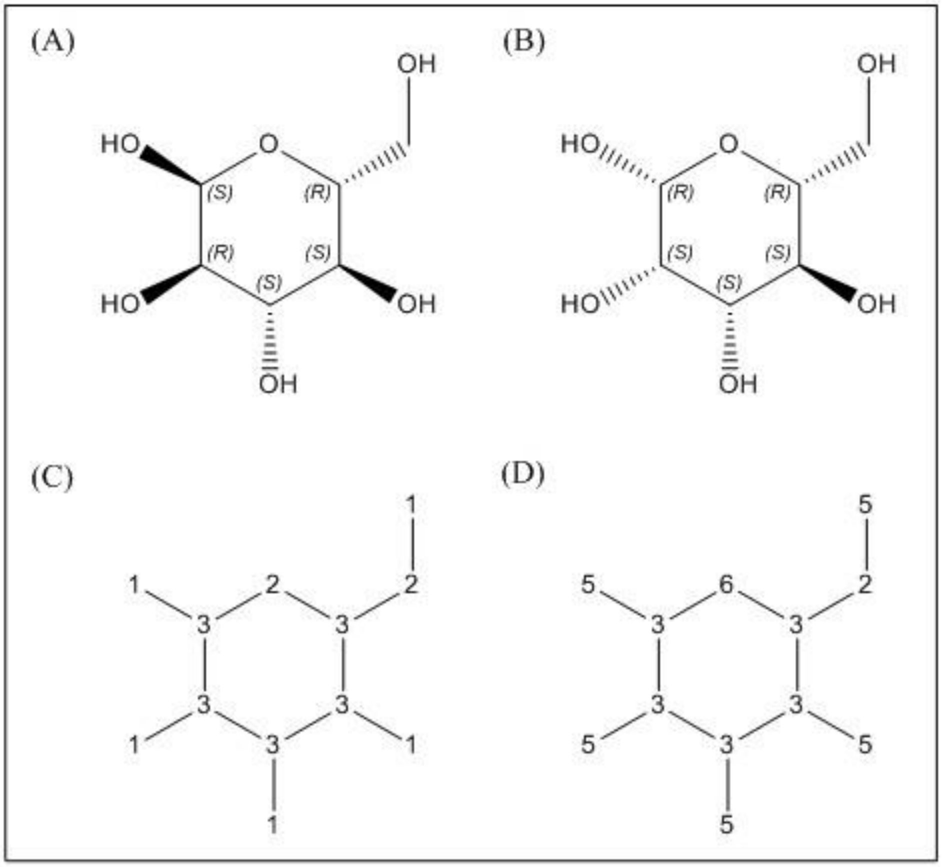

Figure 4.3 Comparison of the chiral structures of stereoisomers (A) glucose and (B) mannose The hydrogen suppressed graphs derived from glucose and mannose are given for (C) simple connectivity index calculations and (D) valence connectivity index calculations. (C) and (D) are representative of the topologies of both (A) and (B).

Due to the excipient molecules considered, three-dimensional structure is important. For example, glucose and mannose are stereoisomers which have the same two-dimensional representation but differ in three-dimensional configuration (see Figure 4.3). By using only simple connectivity indices, the two molecules are indistinguishable yet may contribute different to the stability of a given protein in a lyophilized formulation. To overcome these limitations, chiral-corrected connectivity indices were considered. For any chiral molecule, the vertex degree δ_i is replaced with either ($\delta_i + c$) for S-configuration or ($\delta_i - c$) for R-configuration, with *c* representing the chirality correction factor (Golbraikh, Bonchev *et al.* 2001). In this work, *c = 2* has been chosen. Connectivity indices are then calculated as described previously, using the chirality-corrected vertex degree values. By accounting for the differing chiral atoms, some three-dimensional or conformational information is captured without the need for three-dimensional structure determination.

4.1.3 Protein-Based Descriptors

Both biophysical properties and predictive descriptors of aggregation propensity were considered for protein descriptors. The biophysical descriptors capture basic structural information and innate stability information (via T_m) (Takahasi, Irie *et al.* 1969; Tani, Shirai *et al.* 1997; Arakawa and Kita 2000; Roychaudhuri, Sarath *et al.* 2003; Duy and Fitter 2005). The biophysical descriptors used along with values for each protein are given in Table 4.2.

Table 4.2 Biophysical descriptors for the proteins considered

Protein	PDB code	MW (kDa)	pI	ASA[a] (Å^2)	f_{ASA}[b]	% α helix	% β sheet	# SS bonds	# free thiols	T_m (°C)
Ovalbumin	1ova	44.3	5.19	34237	0.63	30.8	31.3	1	4	76[c]
RNAse A	5rsa	16.5	8.93	4052	0.60	21	33	4	0	62.5[d]
α-amylase	1bli	58	6.33	10480	0.60	26.2	25.6	0	0	102[e]
BSA	3v03	66	5.82	35921	0.68	67	0	17	1	59[f]
Trypsin inhibitor	1avu	20.1	4.95	4986	0.60	1.4	97.2	2	0	65[g]

a – ASA=apolar surface area
b – fASA = apolar surface area / total surface area
Melting temperature (T_m) values were obtained from literature: c (Tani, Shirai *et al.* 1997), d (TAKAHASHI, IRIE *et al.* 1969), e (Duy and Fitter 2005), f (Arakawa and Kita 2000), g (Roychaudhuri, Sarath *et al.* 2003)

Descriptors calculated from two primary sequence-based methods for the prediction of aggregation propensity were also considered: AGGRESCAN (Conchillo-Sole, de Groot et al. 2007) and PASTA (Trovato, Chiti et al. 2006; Trovato, Seno et al. 2007). Both methods require only the amino acid sequence and offer web-based servers for calculation of all relevant variables (AGGRESCAN: bioinf.uab.es/aggrescan/ and PASTA: http://biocomp.bio.unipd.it/pasta/). AGGRESCAN predicts aggregation propensity by determining "hot spots" or short amino acid sequences that are likely to be aggregation-prone. PASTA predicts aggregation propensity by determining sequences that are likely to induce aggregation through the formation of intermolecular β-strands. Both methods are primarily concerned with amyloid fibril formation. Explanation of the descriptors calculated or derived from these methods is given in Table 4.3.

Table 4.3 Descriptors obtained and derived from aggregation propensity prediction methods

AGGRESCAN Descriptor Name	**Definition**
a3vSA	Sequence average amino acid aggregation propensity
nHS	Number of aggregation hot spots
NnHS	nHS normalized by number of residues in protein
AAT	Area of aggregation profile above hot spot threshold
THSA	Total area of aggregation profile comprising hot spots
TA	Total area of aggregation profile
AATr	AAT normalized by number of residues in protein
THSAr	THSA normalized by number of residues in protein
Na4vSS	Sliding window average of amino acid propensity values divided by number of amino acids in protein
PASTA Descriptor Name	
Emin	Minimum energy of PASTA pairings
Eavg	Average energy of PASTA pairings
Lmax	Average amino acid pair length of PASTA pairings
Lavg	Maximum amino acid pair length of PASTA pairings
(E/L)min	Minimum ratio of energy to length of PASTA pairings
(E/L)avg	Average ratio of energy to length of PASTA pairings
# of Peaks	Number of peaks in PASTA aggregation profile

4.1.4 Principal Component Analysis

Principal component analysis (PCA) is a data-reduction technique which replaces an original set of variables with a smaller number of principal components, which are calculated through linear combinations of the original variables (Maindonald and Braun 2010). Through development of principal components, the majority of variance in the data set is captured with a minimal number of variables. In this work, PCA was used to visualize the excipient descriptor space. Such visualization is used for the discussion of results. PCA was performed using the DAAG package in R (Maindonald and Braun 2010).

4.2 Development of Linear QSPRs

Development of linear QSPRs is comprised of four steps:

1. Identification of key properties and procurement of experimental property values
2. Calculation of descriptors and descriptor selection
3. Linear regression
4. Cross-validation

The steps are further detailed in the following sections.

4.2.1 Glass Transition Properties

QSPRs were developed for the glass transition temperature of the anhydrous solute, glass transition temperature of the maximally concentrated solute, melting point of ice and Gordon-Taylor constant for carbohydrates. The experimental data were collected from published literature(Roos 1993). Discussion on glass transitions and their importance in lyophilized protein formulations is given in detail in Section 2.5.

4.2.2 Percent Monomer Remaining Following Lyophilization

The quantitative measure of aggregation used for property modeling was percent monomer remaining following lyophilization. Measurement and calculation of percent monomer is detailed in Section 3.3. Linear QSPRs for percent monomer were developed either as a function of protein structure (formulation-by-formulation basis) or as a function of excipient structure (protein-by-protein basis). Additionally, a non-linear QSPRs for percent monomer was developed as a function of both protein and excipient structure (see section 4.3). Protein-based descriptors were used to represent protein structure and chiral-corrected connectivity indices were used to represent excipient structure.

4.2.3 Properties for in situ NDHD recovery

The example case used for *in situ* product recovery during fermentation is the production of (1R,2S)-1,2-naphthalene dihydrodiol (NDHD) by *Escherichia coli*. NDHD is an important intermediate product that can be used in synthesis of pharmaceutical intermediates or in synthesis of polymers (Raschke, Meier *et al.* 2001). The reaction producing NDHD that is performed by *E. coli* is given in Figure 4.4 (Jerina, Daly *et al.* 1971).

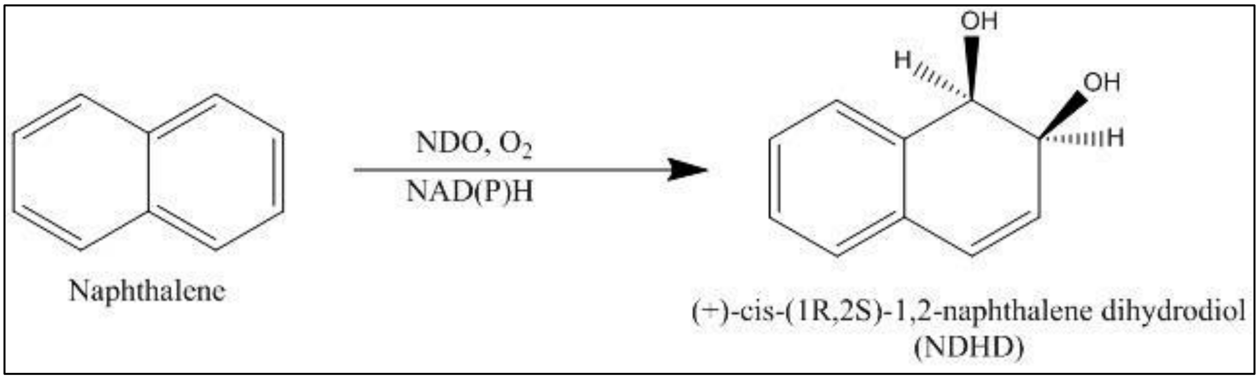

Figure 4.4 Oxidation of naphthalene to (1R,2S)-1,2-naphthalene dihydrodiol (NDHD) The reaction is catalyzed by the enzyme naphthalene dioxygenase (NDO), which is present in *E. coli*. The reaction requires oxygen (O_2) and nicotinamide adenine dinucleotide phosphate (NADPH). Adapted from (Jerina, Daly *et al.* 1971).

The key properties of interest when designing an ionic liquid to extract NDHD during fermentation are the partition coefficient of NDHD between ionic liquid and water (*K_x*) and the toxicity of the ionic liquid towards *E. coli* (*EC_{50}*). Group contribution models proved unable to successfully correlated the properties of interest to molecular structures; accordingly, connectivity index QSPRs were used. The partition coefficient of NDHD between ionic liquid and water is given by ratio between the mole fraction of NDHD in ionic liquid (*x_{IL}*) over the mole fraction of NDHD in water (*x_{aq}*), given by Equation 4.3.

$$K_x = \frac{x_{IL}}{x_{aq}}$$

(Equation 4.3)

Toxicity is measured by the half maximal effective concentration (*EC_{50}*) value, which represents the concentration that is effective in killing half of a given community of organisms. For the system considered here, *EC_{50}* represents the overall toxicity of the ionic liquid towards *E. coli*. Lower values of *EC_{50}* represent a more toxic ionic liquid. Experimental values were obtained for partition coefficient values of 10 ionic liquids and toxicity values of 12 ionic liquids (Scurto 2012).

4.2.4 Descriptor selection

Linear property models were developed relating percent monomer remaining after lyophilization to excipient structure on a protein-by-protein basis. Descriptor selection was performed to prevent over-fitting through use of Mallow's C_p statistic (see Equation 4.4). Conceptually, Mallow's C_p statistic is equal to the lack of fit plus a penalty for the number of descriptors chosen (Wasserman 2004).

$$C_p = \sum_{i=1}^{m} \left(Y_i - \widehat{Y}_i\right)^2 + 2p\sigma^2$$

(Equation 4.4)

Where Y_i is the observed or experimental value, $\widehat{Y}_i$ is the predicted value, *m* is the number of data points, *p* is the number of parameters or descriptors and σ^2 is the estimate of the residual variance. The value given by σ^2 is an unbiased estimate of the variance (Wasserman 2004), shown below:

$$\sigma^2 = \left(\frac{1}{m-p}\right)\sum_{j=1}^{m}\left(Y_i - \widehat{Y}_i\right)^2$$

(Equation 4.5)

When comparing models, the model with the minimal value of C_p represents the model that best correlates the data without over-fitting. For a given model size (number of descriptors), an exhaustive search was performed to select the descriptors that minimized C_p. All model sizes were then compared and the model size with the minimal C_p statistic was selected as the final model. Figure 4.5 gives a graphical example of the use of C_p in descriptor selection. For linear correlations, the selection results given by C_p are equivalent to AIC (Akakie Information Criterion) (Wasserman 2004). Accordingly, descriptor selection results may refer to either AIC or C_p, depending on the software package used for selection. Descriptor selection was performed using the Leaps package in R (Lumley 2004; Dalgaard 2008). The general procedure used in R for descriptor selection along with sample code is given in Appendix B.

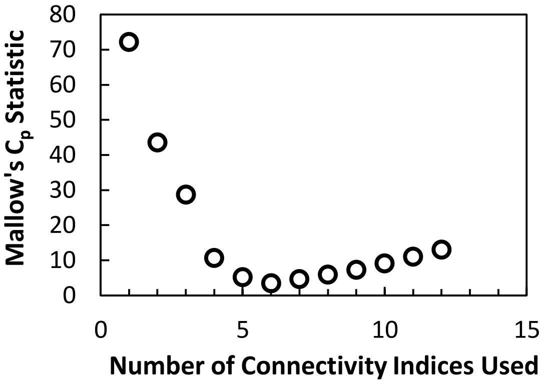

Figure 4.5 Values for Mallow's Cp statistic versus model size (number of connectivity indices used) The lowest value is observed when six connectivity indices are used, indicating the size of the model that should be used. Figure adapted from (Roughton, Topp et al. 2012).

4.2.5 Cross-Validation

Once a final model was selected, leave-one-out cross-validation (LOOCV) was performed to evaluate the predictive ability of the model. In LOOCV, one by one, each observation is left out of the data set and then the selected descriptors are again correlated to the data set. The resulting model is then used to predict the left-out data point. The process is repeated for each fold. Upon completion, the predictions are used to calculate the predicted residual sum of the square errors (*PRESS*) through use of Equation 4.6 (Quan 1988).

$$PRESS = \sum_{i=1}^{m} \left(Y_i - \hat{Y}_{\langle i \rangle}\right)^2$$

(Equation 4.6)

where $\hat{Y}_{\langle i \rangle}$ is the predicted value for the left-out observation and *m* is the total number of observations. The *PRESS* value is then used to calculate the cross-validation coefficient Q^2 (see Equation 4.7).

$$Q^2 = 1 - \frac{PRESS}{\sum_{i=1}^{m} (Y_i - \bar{Y})^2}$$

(Equation 4.7)

where $\bar{Y}$ is the average value for all data points. Q^2 has a maximal value of the model's R^2 value, which represents a perfect predictive ability (Quan 1988). When comparing models, smaller R^2-Q^2 values represent better predictive power. In general, Q^2 can be calculated for K-fold cross-validation by expanding upon Equation 4.6 to yield Equation 4.8. In K-fold cross-validation, K number of folds are generated from the original data set. The number of data left-out should be equal for each fold. As K decreases, the predictive power of the model is further strained as fewer observations are used to build the model.

$$PRESS = \sum_{j=1}^{k} \sum_{i=1}^{n} \left(Y_i - \hat{Y}_{\langle i \rangle}\right)^2$$

(Equation 4.8)

where *k* is the number of folds and *n* is the number of observations left-out in each fold. The general procedure used in R for cross-validation along with sample code is given in Appendix B.

4.3 Development of Non-Linear QSPRs

A non-linear QSPR was used to describe percent monomer remaining after lyophilization as a function of both protein and excipient choice. More details concerning percent monomer remaining after lyophilization can be found in Section 4.2.2. Development of non-linear QSPRs offer an added layer of complexity in comparison to linear QSPR development as a functional form must first be selected, where the functional form is assumed in linear QSPR development. Additionally, certain assumptions in the development of linear correlations do not hold for non-linear correlations.

4.3.1 Selection of Functional Forms

Several functional forms for a model describing protein stability following lyophilization as a function of excipient choice and protein choice were considered. Attempts to build a linear model of sufficient correlative quality were unsuccessful (results not shown). Non-linear models were considered to better correlate the descriptors to the %Monomer values. The final form used is given below:

$$\%Monomer = c\left(\sum a_i \chi_i\right)\left(\sum b_i\, \psi_i\right)$$

(Equation 4.9)

where χ represents excipient descriptors, ψ represents protein descriptors, and *a*, *b*, and *c* are adjustable parameters.

The form used for Equation 4.9 was motivated by the enthalpic contribution to the Flory-Huggins model, given by Equation 4.10. The Flory-Huggins model has been used previously to describe protein-sugar interactions in lyophilized solids (Katayama, Carpenter *et al.* 2009; Wang, Tchessalov *et al.* 2009). Equation 4.9 emulates the Flory-Huggins interaction parameter (χ_{12}) through the multiplication of excipient structural descriptors and protein structural descriptors. The success of the Flory-Huggins functional form of the universal model suggests that direct protein-excipient interactions play a significant role in stabilization of the protein during lyophilization for the formulations considered.

$$\Delta H_m = kTN_1\phi_1\chi_{12}$$

(Equation 4.10)

4.3.2 Parameter Fitting

A non-linear model was considered for the correlation between percent monomer remaining after lyophilization and both excipient and protein descriptors, referred to as the universal model. Parameter fitting was performed by minimization of the residual sum of the squares (*RSS*) between the model and experimental data. The minimization was performed as a mixed-integer non-linear program (MINLP), resulting in parameter values that were not guaranteed to be globally optimal. However, the formulation of the problem as a MINLP is necessary as a non-linear property model is used for the universal model. The Excel solver was utilized in solution of the MINLP.

4.3.3 Parameter Sensitivity

A parameter sensitivity analysis was used to select descriptors. Given the functional form, all descriptors were included. The parameters for each descriptor were determined such that the residual sum of the squares (*RSS*) between the model and experimental data was minimized (see Section 4.3.2). Sensitivity (S_x) was then calculated descriptor by descriptor through use of Equation 4.11.

$$S_x = \frac{RSS_{1.1*x}}{RSS}$$

(Equation 4.11)

Where $RSS_{1.1*x}$ represents the sum of the square errors after increasing the parameter value for a given descriptor (x) by a factor of 1.1. When S_x is equal to or near one, the descriptor in question had no discernible effect on the model outcome. Larger sensitivities suggest a stronger importance on model outcome for the descriptor of interest. Sensitivity values were used to guide two rounds of descriptor selection. In the first round of descriptor reduction, descriptors with sensitivities approximately equal to one were excluded. In the second round of descriptor reduction, the remaining descriptor with the lowest sensitivity was excluded from the model and parameter fitting through minimization of *RSS* was redone for the remaining descriptors. If the model performance statistics changed by less than an order of magnitude, the descriptor remained excluded; otherwise the descriptor was retained in the final model. The procedure was repeated for the descriptor with the next lowest sensitivity value until all descriptors had been considered.

4.3.4 Statistical Verification

The model performance statistics of interest were the percent average absolute deviation (*%AAD*) and the *reduced chi-squared* value. The statistics were used for the non-linear model over R^2 and Q^2 as R^2-based methods are poor indicators of non-linear model performance (Spiess and Neumeyer 2010). Furthermore, calculation of R^2 assumes that the total sum of squares is equal to the explained sum of squares plus the residual sum of squares (*TSS = ESS + RSS*). The assumption is valid for linear regression but does not hold for non-linear regression. The *%AAD* gives the average deviation between the experimental and the predicted values given by the model (see Equation 4.12). *%AAD* was used to evaluate the accuracy of the model.

$$\%AAD = 100\% * \frac{1}{m}\sum_{i=1}^{m}\left|Y_i - \hat{Y}_i\right|$$

(Equation 4.12)

The predictive power of the model was evaluated using *reduced chi-squared*. The *reduced chi-squared* statistic accounts for model variance as well as the number of parameters chosen (see Equation 4.13). For each data point, the difference between experimental and predicted is normalized by the uncertainty of the experimental measurement (σ). A value of one indicates that the model provides a good fit for the data, as the model variance is equal to the experimental variance (Spiess and Neumeyer 2010). Order of magnitude differences in *reduced chi-squared* value suggest that either measurement errors are over-estimated (*reduced chi-squared < 0.1*) or a combination of under-estimated measurement errors and incorrect choice of functional form for the model (*reduced chi-squared > 10*) (Spiess and Neumeyer 2010).

$$\textit{reduced chi-squared} = \frac{1}{m-p}\sum_{i=1}^{m}\frac{\left(Y_i-\hat{Y}_i\right)^2}{\sigma_i^2}$$

(Equation 4.13)

4.4 Group Contribution Methods

For design of IL-based separation processes, group contribution (GC) models for heat capacity (Gardas and Coutinho 2008) and density (Valderrama and Robles 2007) were required. A solubility parameter GC model was developed for use as a design target and ionic liquid selection criteria. Additionally, a thermal decomposition temperature GC model was developed for use in selection of ionic liquid candidates.

4.4.1 Hildebrand Solubility Parameter

The Hildebrand solubility parameter is used to predict whether compounds will be miscible (Barton 1991). Compounds with similar solubility parameter values are more likely to form a miscible solution. Solubility is a key parameter for selecting an entrainer, allowing the solubility parameter to be used as a tool for designing or selecting possible candidates. The cohesive energy density of a compound *i* (c_{ii}) is determined by its molar volume (v_i) and enthalpy of vaporization (Δh_{vap}). The Hildebrand solubility parameter (δ_i) is defined as the square root of the cohesive energy density, as shown in Equation 4.14.

$$\delta_i = c_{ii}^{1/2} = \left(\frac{\Delta h_{vap} - RT}{v_i}\right)^{1/2}$$

(Equation 4.14)

For mixtures, a geometric mean is used to determine the mixture cohesive energy density (Prausnitz, Lichtenthaler *et al.* 1999). The mixture cohesive energy density is then used to determine the volume average solubility parameter for the mixture ($\bar{\delta}$), as given by Equation 4.15.

$$\bar{\delta} = \sum_{i}^{n} \Phi_i \delta_i$$

(Equation 4.15)

Where the volume fraction for a component in the mixture (Φ_i) is determined from the mole fraction (x_i) and molar volume (v_i), as shown by Equation 4.16.

$$\Phi_i = \frac{x_i v_i}{\sum_j^n x_j v_j}$$

(Equation 4.16)

In the presented work, a GC model was developed for Hildebrand solubility parameter of ionic liquids. Several functional forms were considered (Roughton, White *et al.* 2011), but a linear GC model was determined to be appropriate given the small data set. Known solubility parameter values were used to calculate the volume average solubility parameter for azeotropic mixtures of interest.

4.4.2 Thermal Decomposition Temperature

An important consideration of the design or selection of an ionic liquid for a separations process is the thermal decomposition temperature. Temperatures under 500°C have been reported to lead to thermal decomposition of the alkyl chain substituents of the cation as well as the anion itself (Ohtani, Ishimura *et al.* 2008). Higher temperatures (>500°C) can result in thermal decomposition of the imidazolium ring in cations (Ohtani, Ishimura *et al.* 2008). Imidazolium-based cations generally exhibit higher thermal stability than other cation types, such as tetraalkyl ammonium-based cations (Ngo, LeCompte *et al.* 2000). Operating temperatures for any process utilizing ionic liquids must be well below the thermal degradation onset temperature of the ionic liquids.

4.4.3 Group Contribution Model Development

Group contribution models were developed to predict solubility parameters and thermal decomposition temperature for ionic liquids to provide a screening tool for selection of ionic liquids for use as entrainers. Additionally, group contributions form the basis of the activity coefficient predictions from the UNIFAC model (see Section 4.5). The ionic liquids were characterized as alkyl chain groups, cation groups, and anion groups. The groups used to develop ionic liquid GC models are given by Table 4.4.

Table 4.4 Ionic liquid groups used for GC model development Groups are classified either as alkyl chain groups, cation groups or anion groups. The X represents a point of connection with another group. δ = Hildebrand solubility parameter and T_d = thermal decomposition temperature.

Alkyl Chain Groups		
Name	*Structure*	*Models*
CH_3	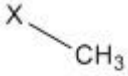	δ, T_d, UNIFAC
CH_2	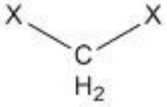	δ, T_d, UNIFAC
O (ether)	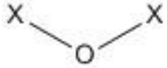	δ
Isobutyl	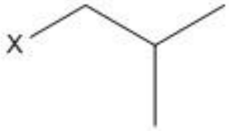	T_d
Ethylbenzyl	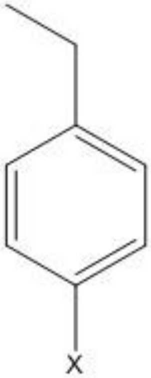	T_d

Cation Groups

Name	*Structure*	*Models*
Imidazolium [Im]	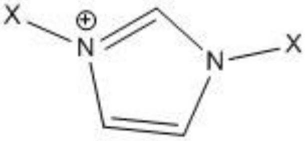	δ, T_d, UNIFAC
Pyridinium [Py]	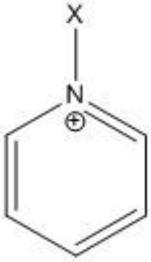	δ, UNIFAC
Pyrrolidinium [Pyr]	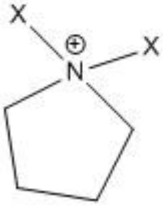	δ
Ammonium [N]	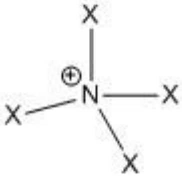	δ, T_d, UNIFAC
Phosphonium [P]	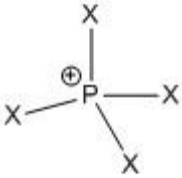	δ
Sulfonium [S]	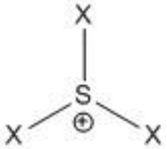	δ

Anion Groups

Name	*Structure*	*Models*
Dimethylphosphate [DMP]	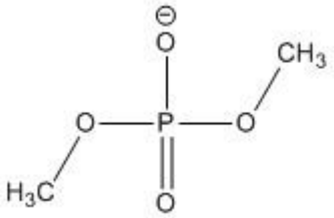	δ, UNIFAC
Diethylphosphate [DEP]	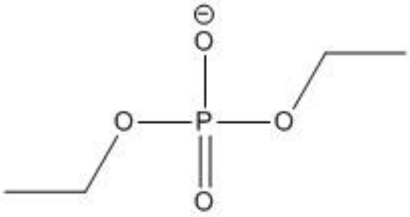	δ
Tetrafluoroborate [BF_4]	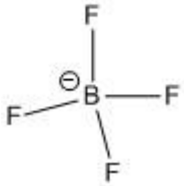	δ, T_d, UNIFAC
Hexafluorophosphate [PF_6]	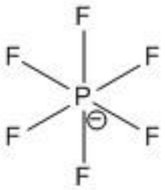	δ, T_d, UNIFAC
Trifluoroacetate [CF_3COO]	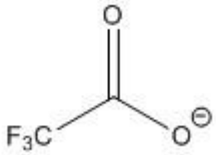	δ, T_d, UNIFAC
Trifluoromethanesulfonate [CF_3SO_3]	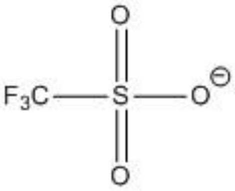	δ, T_d, UNIFAC

Bis(trifluoromethylsulfonyl) amide [Tf_2N]	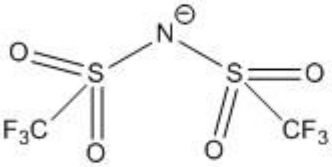	δ, T_d, UNIFAC
2-(2-methoxyethoxy)ethyl sulfate [$CH_3(OC_2H_4)_2SO_4$]	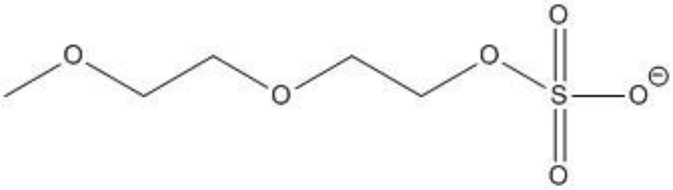	δ, UNIFAC
2-(methoxy)ethyl sulfate [$CH_3OC_2H_4SO_4$]	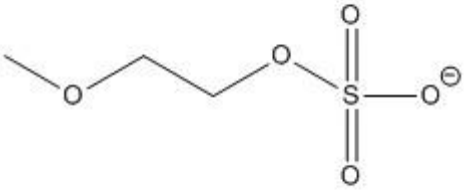	UNIFAC
2-(ethoxy)ethyl sulfate [$C_2H_5OC_2H_4SO_4$]	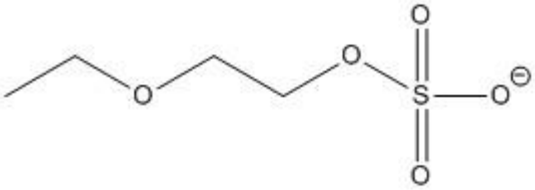	UNIFAC
Methyl sulfate [CH_3SO_4]	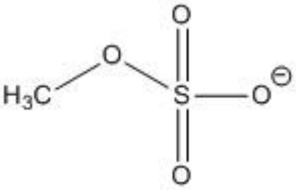	UNIFAC
Ethyl sulfate [$C_2H_5SO_4$]	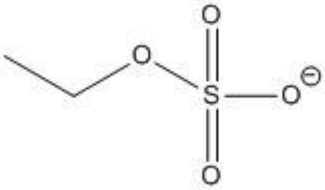	UNIFAC
Octyl sulfate [$C_8H_{17}SO_4$]	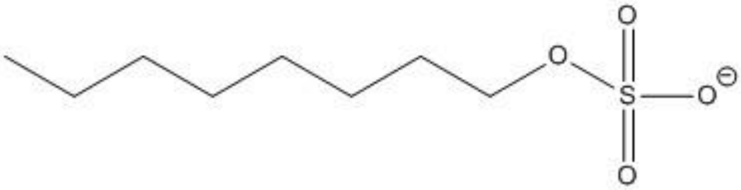	δ
Thiocyanate [SCN]	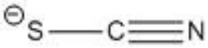	δ, UNIFAC

Tosylate [TOS]	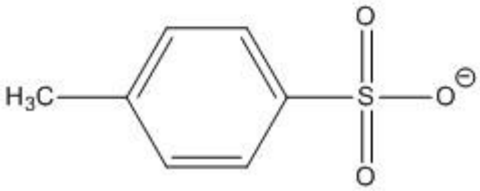	δ
Chloride [Cl]	$Cl^{\ominus}$	δ, T_d, UNIFAC
Bromide [Br]	$Br^{\ominus}$	T_d, UNIFAC
Iodide [I]	$I^{\ominus}$	UNIFAC

Linear models were proposed to predict the solubility parameter and thermal decomposition temperature. The function form for prediction of property *P* is given by Equation 4.17, where n_i describes the number of groups of type *i*, C_i is the contribution of group *i* to the overall property value, and *b* is a constant. The contributions from the alkyl chain groups, cation groups, and anion groups are summed to give the predicted property value. The function forms used in the UNIFAC model differ and are explained in Section 4.5.

$$P = P^{c}_{Alkyl\ Chain} + P^{c}_{Cation} + P^{c}_{Anion}$$

$$= \sum_{Alkyl\ Chain} n_i C_i + \sum_{Cation} n_j C_j + \sum_{Anion} n_k C_k + b$$

(Equation 4.17)

Experimental values of ionic liquid solubility parameters were obtained from literature (Marciniak 2010). The solubility parameter value can change with temperature, so the model was developed to predict the solubility parameter at 298.15 K. Even though a temperature dependence exists, solubility parameter often scales linearly for all compounds (Barton 1991). Thus, the GC model developed can be utilized to design or select an ionic liquid for a given azeotrope at any given temperature assuming that the difference between the solubility parameter values will be similar at different temperatures. Experimental values of thermal decomposition temperature were also obtained from literature (D. Holbrey and R. Seddon 1999; Ngo, LeCompte *et al.* 2000; Visser Ann, Reichert *et al.* 2002; Awad, Gilman *et al.* 2004; Fredlake, Crosthwaite *et al.* 2004; Wooster, Johanson *et al.* 2006; Luo, Huang *et al.* 2008).

For both property models, the contributions for each group were determined such that the %AARD (percent average absolute relative deviation) between experimental and predicted solubility parameters was minimized. The problem was formulated as a linear program (LP) and solved using the CPLEX solver in the GAMS optimization software package. The objective function is given by Equation 4.18.

$$\min z = \left(\frac{100}{n}\right)\sum_{i=1}^{n}\frac{\left|P_i^{pred} - P_i^{exp}\right|}{P_i^{exp}}$$

(Equation 4.18)

To make the problem formulation linear, the absolute value term was transformed into the sum of two error terms for each data point $(\in_i^+, \in_i^-)$ and additional constraints were added. The resulting formulation is given by Equation 4.19.

$$\min z = \left(\frac{100}{n}\right)\sum_{i=1}^{n}\frac{\in_i^+ + \in_i^-}{P_i^{exp}}$$

s.t

$$\in_i^+ + \in_i^- = P_i^{exp} - P_i^{pred}$$

$$\in_i^+, \in_i^- \geq 0$$

(Equation 4.19)

4.5 UNIFAC-IL Model Development

Design of separations requires the determination of thermodynamic parameters for all components involved in the separation. For the design of extractive distillation processes, the activity coefficient is needed for the light components, heavy components and the entrainers. A UNIFAC model was developed to predict ionic liquid activity coefficients (UNIFAC-IL). Known UNIFAC parameters were used for light and heavy components.

4.5.1 Theory

Modeling or prediction of VLE is a key tool needed for the design of separation processes. For the examples considered, the pressure was near or at atmosphere and the vapor phase was considered ideal. The Poynting correction was neglected and the saturated fugacity coefficients were assumed to be unity, also due to low pressure. Due to the extremely low vapor pressure exhibited by ionic liquids, the saturation pressure (P_i^{sat}) for the ionic liquids was assumed to be zero. As a result, no ionic liquid was assumed to be present in the vapor phase. Factoring in the assumptions, total pressure for a ternary system containing an ionic liquid is given by Equation 4.20, where components (1) and (2) are not ionic liquids.

$$P = x_1\gamma_1 P_1^{sat} + x_2\gamma_2 P_2^{sat}$$

(Equation 4.20)

Given a known total pressure, the vapor compositions for component (1) or (2) are given by Equation 4.21.

$$y_i = \frac{x_i\gamma_i P_i^{sat}}{P}$$

(Equation 4.21)

The UNIFAC model is a method used to predict activity coefficient values (γ_i). The original UNIFAC model has been used in this work, as data was insufficient to use the modified UNIFAC model. The original model uses a group contribution concept to calculate activity coefficients of a mixture, which are then used to predict VLE (Fredenslund, Gmehling *et al.* 1977; Lei, Zhang *et al.* 2009). The activity coefficients are calculated from a combinatorial and a residual contribution, as shown by Equation 4.22.

$$ln\gamma_i = ln\gamma_i^c + ln\gamma_i^R$$

(Equation 4.22)

The combinatorial contribution, shown in Equation 4.23, is due to the size and shape of the molecule – that is the entropic features.

$$ln\gamma_i^c = 1 - V_i + lnV_i - 5q_i\left(1 - \frac{V_i}{F_i} + ln\left(\frac{V_i}{F_i}\right)\right)$$

(Equation 4.23)

V_i and *F_i* are parameters that are calculated from pure component parameters *r_i* and *q_i*, which represent the van der Waals volume and molecular surface area respectively. The molar composition of species *i* is given by *x_i*. The calculation for *V_i* and *F_i* are given by Equation 4.24.

$$F_i = \frac{q_i}{\sum_j q_j x_j}$$

$$V_i = \frac{r_i}{\sum_j r_j x_j}$$

(Equation 4.24)

The pure component parameters r_i and q_i are the sum of group volume and surface area parameters R_k and Q_k. R_k and Q_k are UNIFAC model parameters and are usually derived from the rules of Bondi (Bondi

1964). Calculation of the parameters is given by Equation 4.25, with $v_k^{(i)}$ representing the number of groups of type *k* present in molecule *i*.

$$r_i = \sum_k v_k^{(i)} R_k$$

$$q_i = \sum_k v_k^{(i)} Q_k$$

(Equation 4.25)

The residual contribution, shown in Equation 4.26, accounts for the interactions between groups – that is the enthalpic contribution.

$$ln\gamma_i^R = \sum_k v_k^{(i)} \left[ln\Gamma_k - ln\Gamma_k^{(i)}\right]$$

(Equation 4.26)

The group residual activity coefficient is given by Γ_k (see Equation 4.27), where $\Gamma_k{}^{(i)}$ represents residual activity coefficient of group *k* in a reference solution containing only molecules of type *i*.

$$ln\Gamma_k = Q_k \left[1 - ln\left(\sum_m \theta_m \psi_{mk}\right) - \sum_m \left(\frac{\theta_m \psi_{km}}{\sum_n \theta_n \psi_{nm}}\right)\right]$$

(Equation 4.27)

θ_m is a volume contribution parameter and is dependent on X_m, which is the fraction of group *m* in the given mixture. Calculation of θ_m and X_m is given by Equation 4.28.

$$\theta_m = \frac{Q_m X_m}{\sum_n Q_n X_n}$$

$$X_m = \frac{\sum_i v_m^{(i)} x_i}{\sum_i \sum_k v_k^{(i)} x_i}$$

(Equation 4.28)

The interaction parameter ψ_{nm} (see Equation 4.29) is a function of the group interaction parameter a_{nm} and temperature (T). The group interaction parameter a_{nm} is a fitted UNIFAC model parameter with the property that $a_{nm} \neq a_{mn}$.

$$\psi_{nm} = exp\left(-\frac{a_{nm}}{T}\right)$$

(Equation 4.29)

4.5.2 Determination of Groups and Group Parameters

The ionic liquids were characterized by the same groups as used for the solubility parameter: alkyl chain groups, cation groups, and anion groups. Previous attempts to develop a UNIFAC model for ionic liquids characterized a cation and anion pair as one group (Lei, Zhang *et al.* 2009). The UNIFAC-IL model presented here treats cations and anion as separate groups, increasing the number of ionic liquid combinations and allowing for prediction of thermodynamic behavior with ionic liquids not used in the model development data set (Roughton, Christian *et al.* 2012). The UNIFAC-IL model proposed can predict VLE for systems containing ionic liquids that have yet to be synthesized.

The combinatorial contribution is based on entropic effects and is calculated from group volume and surface area parameters. Parameters were determined for the new ionic groups using the following procedure:

1. The rules of Bondi for estimation of molecular volume and surface area were used (Bondi 1964).
2. For groups that were undefined by the rules of Bondi, values from previous UNIFAC groups were used. For example, the volume and surface area parameters for a di-substituted pyridine group were assumed to be roughly equal to the volume and surface area parameters for a di-substituted pyridinium group.
3. Values for groups still undefined were found in literature using correlations or molecular simulation to determine volume and surface area parameters (Lei, Zhang *et al.* 2009).

4.5.3 Determination of Interaction Parameters

A wide range of experimental data on activity coefficients of various solutes at infinite dilution in ionic liquids was collected from previously published work (Heintz, Kulikov et al. 2001; Heintz, Kulikov et al. 2002; Krummen, Wasserscheid et al. 2002; Letcher, Soko et al. 2003; Letcher, Soko et al. 2003; Eike, Brennecke et al. 2004; Kato and Gmehling 2004; Vasiltsova, Verevkin et al. 2004; Heintz, Casás et al. 2005; Heintz and Verevkin 2005; Kato and Gmehling 2005; Kato and Gmehling 2005; Letcher, Domanska et al. 2005; Letcher, Marciniak et al. 2005; Vasiltsova, Verevkin et al. 2005; Heintz, Vasiltsova et al. 2006; Heintz, Verevkin et al. 2006; Domańska and Marciniak 2007; Ge, Wang et al. 2007; Domanska and Marciniak 2008; Domańska and Marciniak 2008; Ge and Wang 2008; Ge, Wang et al. 2008; Shimoyama, Hirayama et al. 2008; Yang, Wu et al. 2008). The experimental values were used to obtain UNIFAC group binary interaction parameters between the ionic liquid groups and solute groups through regression, using the Thermodynamic Modeling Library (TML) within the ICAS software suite (Gani, Hytoft *et al.* 1997). The objective function, given by Equation 4.30, was minimized using the VA05AD solver method. The method is a compromise between the Newton-Raphson, Steepest Descent and Marquardt algorithms for minimizing a sum of squares (HSL 2011).

$$\min z = \sum_{i=1}^{n} \left(\frac{\gamma_i^{pred} - \gamma_i^{exp}}{\gamma_i^{exp}} \right)^2$$

(Equation 4.30)

Only the unknown interaction parameters between the new ionic liquid groups and existing UNIFAC groups were determined. For interactions between existing UNIFAC groups, the current revised UNIFAC interaction parameters were used (Wittig, Lohmann *et al.* 2002). The interaction parameters between ionic liquid groups were assumed to be zero, due to the strong interaction and weak dissociation between ion pairs (Lei, Zhang *et al.* 2009) and also to allow more flexibility in the design of the ionic liquid.

5.0 MOLECULAR DESIGN METHODS: THE REVERSE PROBLEM

Two main approaches were taken to address the reverse problem of CAMD: deterministic and stochastic. Deterministic design was applied to solution of ionic liquid entrainers and is detailed in Section 5.1. Tabu search, a stochastic method, was utilized for the design of ionic liquid extractants and carbohydrate glass-formers, as described in Section 5.2. Additionally, two stochastic methods (tabu search and genetic algorithms) were developed, tuned and compared for the design of carbohydrate excipients in lyophilized protein formulations. Development is detailed in Section 5.3, tuning is explained in Section 5.4 and the methods of solution comparison are given in Section 5.5.

5.1 DETERMINISTIC DESIGN OF IONIC LIQUID ENTRAINERS

Given an azeotropic mixture of interest, a CAMD problem was formulated to design an ionic liquid entrainer. The solubility parameter is used as the target property. First, the design stage in the CAMD problem selects all ionic liquids that have solubility parameters in a range between the azeotrope mixture's solubility parameter and the entrained component's solubility parameter. From the initial design step, several ionic liquid candidates can be generated. Next, the candidates are screened based on other desirable properties such as melting temperature, thermal decomposition temperature, and toxicity. The candidates remaining are then screened using the UNIFAC-IL model to determine how much IL is needed to break the desired azeotrope. The candidates requiring minimal ionic liquid concentrations are then finally screened based on distillation column energy requirements as determined by simulation (see Section 6.0).

For the examples provided in this work, the property models for the screening of secondary properties are not yet available. To provide an illustrative example of the proposed methodology, the initial number of design candidates was limited. Only two candidates for each azeotropic mixture were selected based on the extremes of the range of solubility parameters that are considered. One ionic liquid was selected based on its match to the azeotropic mixture's solubility parameter and another was selected based on its match to the component that is desired to be entrained. Then, the candidates are screened by comparing the amount of ionic liquid needed to break the azeotrope. For the examples given, the best possible ionic liquid is not guaranteed to be selected as the entire range of design candidates was not considered.

The optimization problem was formulated as a mixed-integer linear program (MILP) and solved using the CPLEX solver in GAMS (CPLEX solution manual, http://www.gams.com/dd/docs/solvers/cplex.pdf). Due to the simplicity of the design problem, use of a deterministic method was feasible and chosen to ensure global optimality of the solution. The objective function was used to minimize the difference between the target solubility parameter (δ_{target}) and the predicted solubility parameter of the designed ionic liquid (δ_{pred}). For the examples given, the target is either set to the volume average solubility parameter of the mixture at the azeotrope or the solubility parameter of the entrained component. To make the problem formulation linear, the absolute value term was transformed into the sum of two error terms for each data point ($\in_i^+, \in_i^-$) and additional constraints were added (Ferguson). The resulting objective function and constraints are given by Equation 5.1.

$$\min \mathrm{z} = \in^+ + \in^-$$

s.t.

$$\delta^{pred} - \delta^{target} \leq \in^+$$

$$-\delta^{pred} + \delta^{target} \leq \in^-$$

$$\in_i^+, \in_i^- \geq 0$$

(Equation 5.1)

To ensure a feasible ionic liquid was designed, several structural constraints were added. Many common ionic liquids have methyl, ethyl, butyl, hexyl, and octyl alkyl groups on the cation. To determine the number of CH_2 groups and ensure that the number matched with common ionic liquids, the following constraints were introduced:

$$\text{Chain Length} = 0 * \mathrm{a}(\mathrm{j} = 1) + 1 * \mathrm{a}(\mathrm{j} = 2) + 3 * \mathrm{a}(\mathrm{j} = 3) + 5 * \mathrm{a}(\mathrm{j} = 4) + 7 * \mathrm{a}(\mathrm{j} = 5)$$

(Equation 5.2)

$$\sum_{\mathrm{j}=1}^{5} \mathrm{a}(\mathrm{j}) = 1$$

(Equation 5.3)

where $\mathrm{a}(\mathrm{j})$ is a binary variable declaring the existence of an alkyl chain. Due to the limited property models, only ionic liquids with one alkyl chain on the cation were designed. If desired, Equation 5.3 could be edited to allow for more than one alkyl chain. To ensure that only one cation and one anion were used in the design of the ionic liquid, constraints are given by Equation 5.4.

$$\sum_{\mathrm{i}=1}^{\mathrm{n}} \mathrm{y}_{\mathrm{cation}}(\mathrm{i}) = 1$$

$$\sum_{\mathrm{k}=1}^{\mathrm{m}} \mathrm{y}_{\mathrm{anion}}(\mathrm{k}) = 1$$

(Equation 5.4)

where $\mathrm{y}_{\mathrm{cation}}(\mathrm{i})$ and $\mathrm{y}_{\mathrm{anion}}(\mathrm{k})$ are binary variables declaring the existence of cation i and anion k, respectively. The variables *n* and *m* represent the number of cation groups and anion groups available for design. Once an ionic liquid candidate was chosen, the UNIFAC-IL model was used to verify that the azeotrope was broken by the ionic liquid and to ensure that only one liquid phase was present.

5.2 Use of Tabu Search in Design of Ionic Liquid Extractants and Carbohydrate Glass-Formers

An existing molecular design framework was utilized for the design of ionic liquid extractants and carbohydrate glass-formers (Eslick 2009; Eslick, Ye et al. 2009; McLeese, Eslick et al. 2010). Tabu search was used to provide locally optimal solutions. The design targets for the two design problems are given in Table 5.1.

Table 5.1 Property targets for molecular design using tabu search The tabu search was performed via a modified version of Polymer Designer Pro (Eslick, Ye et al. 2009).

Ionic Liquid Extractant	
Property	*Target*
Partition coefficient (K_x)	50
Toxicity ($lnEC_{50}$)	4.0
Carbohydrate Glass-Former	
Property	*Target*
Glass Transition Temperature of the Anhydrous Solute (T_g)	100°C
Glass Transition Temperature of the Maximally Freeze-Concentrated Solute (T_g')	-30°C
Melting Temperature of Ice (T_m')	-25°C
Concentration of the Maximally Freeze-Concentrated Solute (C_g')	0.85

The existing molecular design framework was contained in a software package named Polymer Designer (PD), written in C++ (Eslick 2009). For each design case, groups were changed to represent groups that existed in the data set used to develop the corresponding property models. Design was limited to the cation for the ionic liquid extactant case, with the anion set at tris(perfluoroalkyl)trifluorophosphate (FAP). The groups used for both design problems are catalogued in Appendix C, along with general guidelines for the use of PD. Additionally, the necessary property models were added to the program. The tabu Search algorithm used in PD follows a procedure similar to the tabu Search algorithm described in Section 5.3.3.

While useful for optimal structure determination, several factors necessitated the development of a separate software package for design of carbohydrate excipients for lyophilized protein formulations. The primary reason was the desire for comparison between tabu Search and genetic algorithms for use in CAMD. A molecular representation that would be useful for both stochastic methods was necessary for fair comparison. PD was developed with concern for cross-linked polymer systems and thus some elements of the code were unnecessary for the design problems considered and added time to solution. Additionally, tuning required easily editable parameter values. Any editing done to the source code or group database for PD requires the program to be deleted and the code to be recompiled. The steps needed for editing and recompiling the PD code are detailed in Appendix C. As the solution methods needed to be ran many times for tuning purposes with different parameter values, ultimately the existing framework proved too cumbersome. Development of a framework more suited to the desired tasks is given in the following section.

5.3 Development of Stochastic Design Methods for Carbohydrate Excipients in Lyophilized Protein Formulations

A CAMD framework for the design of carbohydrate excipients was developed for use with either tabu search or a genetic algorithm. The framework was implemented in Visual Basic for Applications (VBA), with Microsoft Excel used as the database for groups used in design. The overall framework is diagramed in Figure 5.1.

5.3.1 Molecular Representation

For implementation of the design phase, a representation is needed for the molecular structure that allows calculation of relevant descriptors and properties. The molecular representation also needs to allow for easy structural modifications to determine new solutions. For the work detailed here, the lowest level of molecular representation is given by an array of group numbers. Each number corresponds to a database entry which contains the group adjacency matrix, the vertex degree δ_i for each non-hydrogen atom in the group, the valence vertex degree δ_i^v for each non-hydrogen atom in the group and the number of hydrogens bonded to each non-hydrogen atom in the group. For the design of carbohydrate excipients, 9 building block groups were identified from the set of molecules used to generate the experimental *%Monomer* values. From the building blocks groups selected, chiral sub-groups were identified with 89 total groups available for use (see Table 5.2). Terminal groups were fixed as hydroxyl groups.

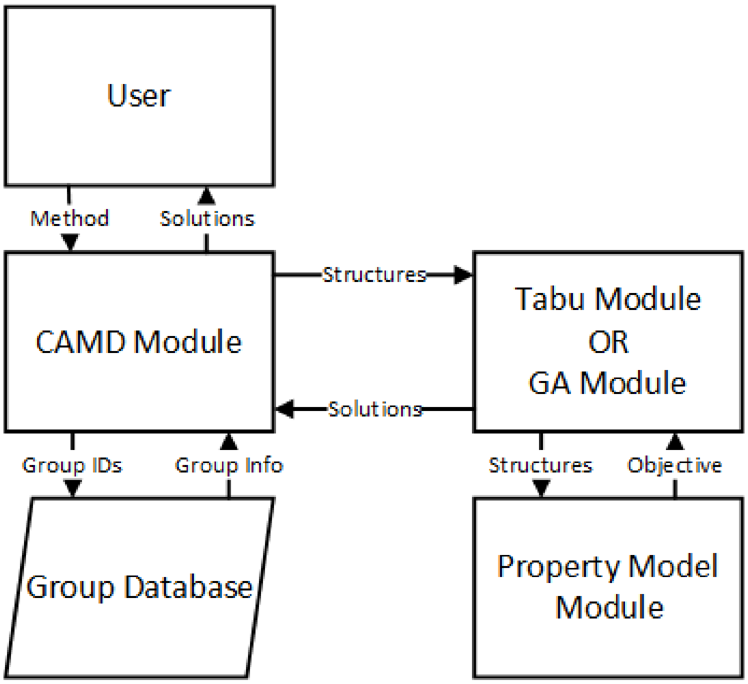

Figure 5.1 CAMD framework developed to design carbohydrate excipients using either tabu search or a genetic algorithm The CAMD module contains the functions needed to build the adjacency matrix from the array of groups present in the molecule. See Table 5.3 for more details.

Table 5.2 Building block groups and chiral subgroups available for design of new excipient candidates Chiral carbons are identified with "*". Connections to the next group are identified by "X".

Building Block Group	Chemical Formula	Group Structure	Number of Chiral Sub-Groups
1	CH_2	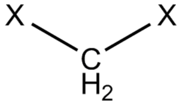	N/A
2	CH_2O	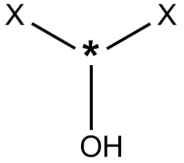	2
3	O	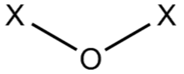	N/A
4	CO	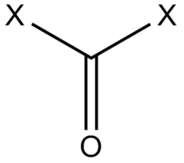	N/A
5	$C_3H_6O_2$	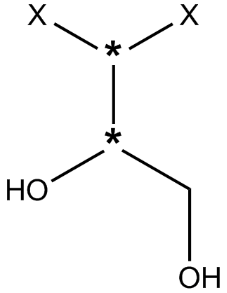	4
6	$C_4H_6O_3$	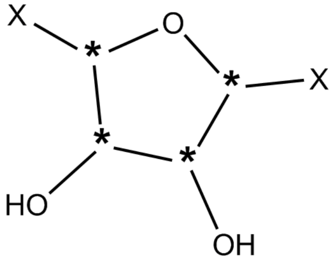	16

7	$C_5H_8O_4$	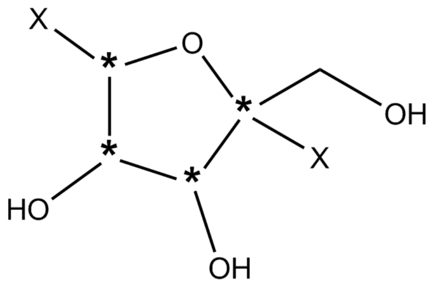	16
8	$C_5H_8O_3$	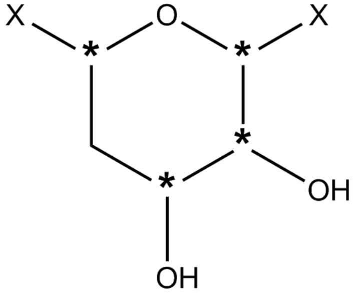	16
9	$C_5H_8O_4$	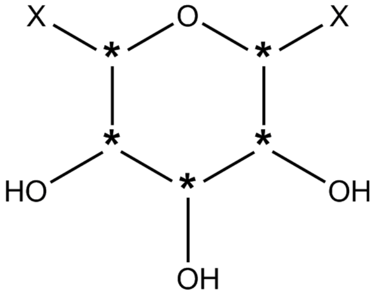	32

By factoring in chirality, there is an order of magnitude increase in the number of groups available for selection during the generation of new candidate structures. The increase in the number of groups available for selection has a marked impact on the number of possible molecular structure combinations, resulting in a combinatorial problem. Figure 5.2 demonstrates how the number of possible combinations increases exponentially as the number of groups available for selection increases. For the design problem considered, the maximum number of groups selected is set at six as all molecules used in the data set can be described by six or fewer of the groups given in Table 5.2. With a maximum molecule size of six groups and 89 groups available for selection, 8.66×10^8 combinations and

$5.03x10^{11}$ permutations exist. Given the number of possible solutions, a rational and effective method is needed to quickly identify only the most promising candidates. The stochastic methods utilized in the CAMD framework proposed offer a means to eliminate the combinatorial contribution to the design problem.

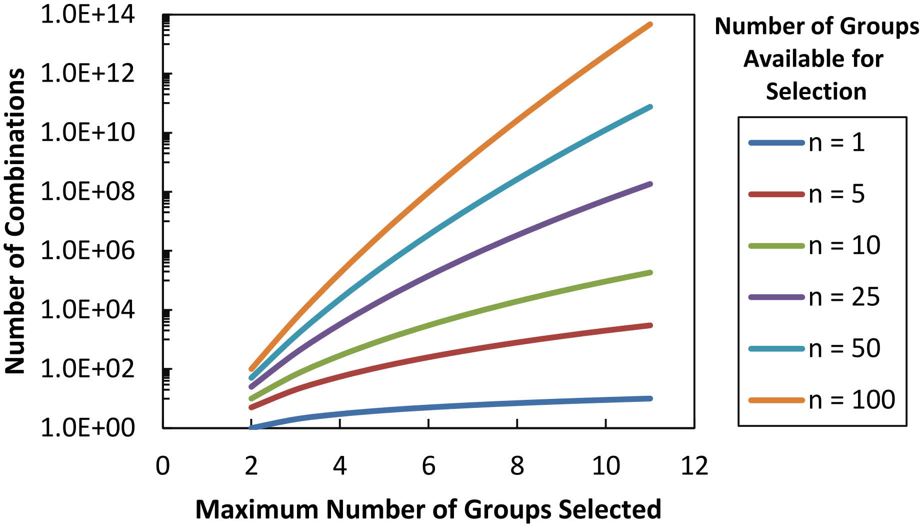

Figure 5.2 Number of possible combinations of groups that would provide solutions to a CAMD problem The number of combinations are a function of the maximum number of groups selected and the number of distinct groups available for selection The vertical axis uses a logarithmic scale.

The low-level group representation is used in the stochastic methods, where groups are changed according to the rules for each algorithm (see Sections 5.3.3 and 5.3.4 for more details). For property calculation, a higher level of detail is needed. The groups are used to construct an adjacency matrix for the molecule. Lists containing the vertex degree (δ_i) for each non-hydrogen atom in the molecule, the valence vertex degree (δ_i^v) for each non-hydrogen atom in the molecule and the number of hydrogens bonded to each non-hydrogen atom in the molecule are also generated. The functions and subroutines used to build the molecular representations are detailed in Table 5.3. The source code for the functions and subroutines is given in Appendix D. From the adjacency matrix and the lists, connectivity indices can be calculated.

Table 5.3 Description of VBA functions and subroutines used for molecular representation Source code can be found in Appendix D.

Function Name	**Argument(s)**	**Resulting Value**
atoms	Number of group	Number of atoms in group
name	Number of group	String containing name of worksheet in excel database containing group structural information
terminus	Number of group, number of atom in molecule that represents the left-hand terminal atom in group	Number of the atom in the molecule that represents the right-hand terminal atom in group
Subroutine Name	**Argument(s)**	**Result of Procedure**
BuildMolecule	Array containing groups in molecule, array containing the vertex degree (δ_i) for each non-hydrogen atom in the molecule, array containing the valence vertex degree (δ_i^v) for each non-hydrogen atom in the molecule, array containing the number of hydrogens bonded to each non-hydrogen atom in the molecule, array containing adjacency matrix	Adds hydroxyl terminals to both the first and last group in the molecule. Updates adjacency matrix and lists of other structural values for molecule represented by the array containing the groups in the molecule
GetConnectivity	Array containing the vertex degree (δ_i) for each non-hydrogen atom in the molecule, array containing the valence vertex degree (δ_i^v) for each non-hydrogen atom in the molecule, array containing the number of hydrogens bonded to each non-hydrogen atom in the molecule, array containing adjacency matrix, number of non-hydrogen atoms in the molecule, array containing simple connectivity indices (χ),array containing valence connectivity indices (χ^v), array containing average simple connectivity indices (ξ),array containing average valence connectivity indices (ξ^v)	Updates chiral connectivity index values for molecule represented by the adjacency matrix and lists of other structural values

5.3.2 Calculation of Chiral Connectivity Indices and Objective Function

A depth-first search algorithm is used to determine the existence of paths in the adjacency matrix ranging from lengths of zero to five (West 2001). The path length information is then used calculate the chiral connectivity indices. Both the path search and connectivity index calculation are performed in the *GetConnectivity* subroutine (see Table 5.3 and Appendix D). The calculated chiral connectivity indices are used for property prediction, which is in turn used to calculate the objective function value. The objective function is a characteristic CAMD type which describes the sum of the normalized absolute differences between target properties and predicted properties (See Section 2.12 and Equation 2.8). The objective function used has been modified by the inclusion of a penalty score and is given by Equation 5.5. The penalty score is used to disallow final solutions from containing certain group combinations that are unfavorable. In particular, the formation of peroxide bonds (O-O) and bonding of two ring groups together are prevented through use of the penalty scores. Peroxides are undesired as the bond is unstable. A bond between two rings in not wanted as such a bond is not observed in carbohydrates. The penalty score is large enough to make objective function values for solutions containing such structural features to be much larger in comparison to solutions without said features. The penalty function along with the rules for adding and removing groups in each of the stochastic design methods (explained further in Sections 5.3.3 and 5.3.4) eliminates the need for explicit structural constraints. Additionally, the definition of groups eliminates the need to store the presence of double or triple bonds in the adjacency matrix.

$$\min z = \left(\sum\nolimits_{M} \frac{1}{P_m^{scale}} \left|P_m - P_m^{target}\right|\right) + Penalty$$

s.t.

$$Penalty = \begin{cases} 1000 \ \mathit{If\ molecule\ contains\ peroxide\ bond\ or\ two\ rings\ bonded\ together} \\ 0 \ \mathit{Otherwise} \end{cases}$$

$$P_m = f_m(y)$$

$$y = g(a_{ij}, w_i)$$

(Equation 5.5)

5.3.3 Tabu Search Algorithm

The tabu search algorithm utilizes solution history to generate locally optimal solutions to the molecular design problem. In the following implementation, solutions are given as arrays of groups representing the molecular structure. The tabu search algorithm developed is given in Figure 5.3. The tabu search begins with a random initial solution which is generated by calling the *InitialSolution* subroutine (see Table 5.4 and Appendix D). The connectivity indices are calculated for the initial solution and used to determine the objective function. The solution is set as the current solution and then stored as the initial entry in the tabu list. The information stored in the tabu list is comprised of the array of groups comprising the molecule and the ${}^{0}\chi$ value for checking to see if a solution is tabu.

The first iteration then begins by determining the number of neighbors to the current solution. The number chosen is a random integer with a value between one and the set maximum number of members to evaluate. A neighboring structure is generated through use of the *Make_Neighbor* function, which takes the current solution's array of groups as an argument and returns a neighboring solution's array of groups (see Appendix D). The *Make_Neighbor* function randomly selects one of four types of local moves to be made to generate the neighboring solution. The types of moves are explained with examples in Table 5.4.

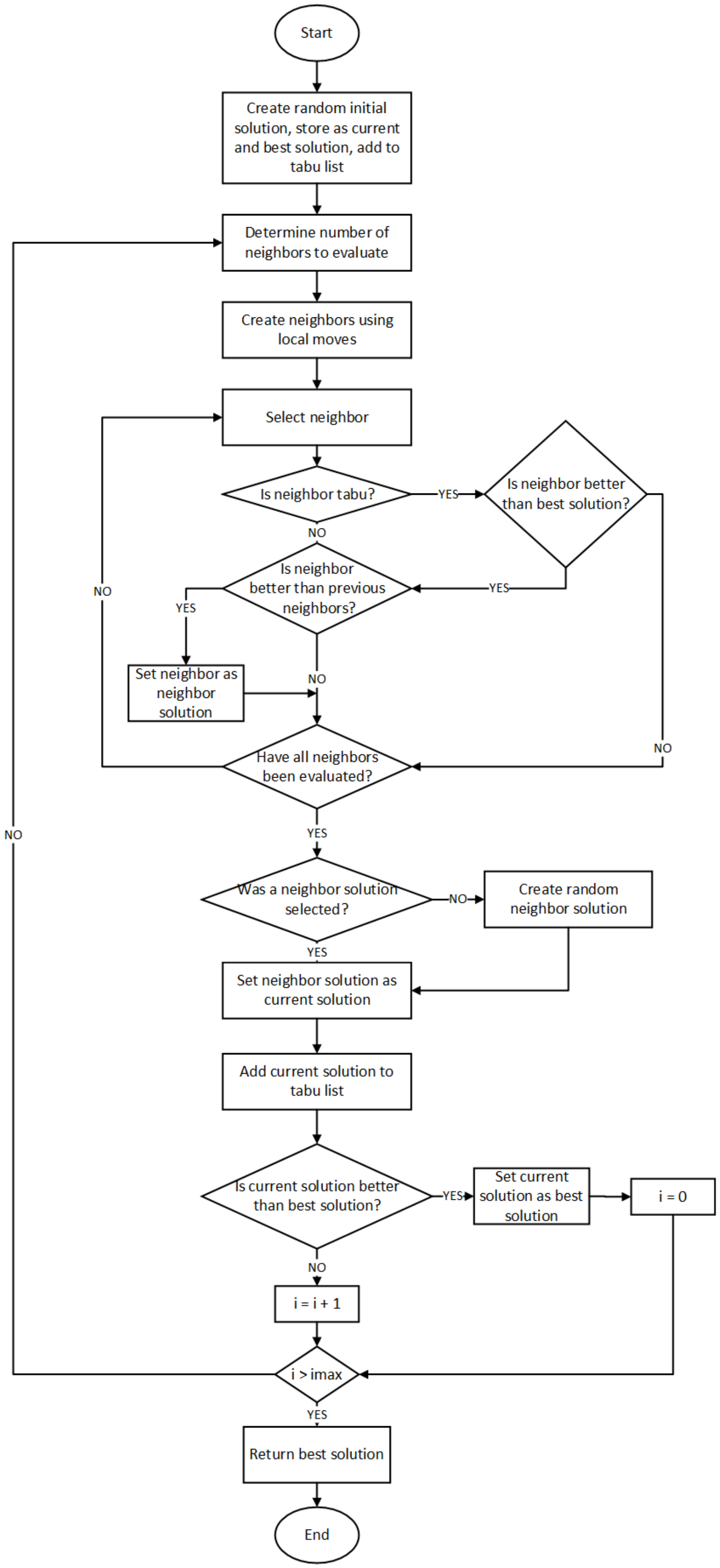
Start
Create random initial solution, store as current and best solution, add to tabu list
Determine number of neighbors to evaluate
Create neighbors using local moves
Select neighbor
Is neighbor tabu?
YES
Is neighbor better than best solution?
NO
Is neighbor better than previous neighbors?
YES
YES
NO
Set neighbor as neighbor solution
NO
NO
Have all neighbors been evaluated?
NO
YES
Was a neighbor solution selected?
NO
Create random neighbor solution
YES
Set neighbor solution as current solution
Add current solution to tabu list
Is current solution better than best solution?
YES
Set current solution as best solution
i = 0
NO
i = i + 1
i > imax
YES
Return best solution
End

Figure 5.3 Tabu search algorithm as implemented in the CAMD framework

Table 5.4 Moves used to generate neighbors to current solution in tabu search Moves are classified either as local or global. Letters are analogous to the group numbers used to represent the molecule in the algorithm. The highlighted letter(s) represents the group(s) selected by the move operation.

Local Moves		
Name	*Description*	*Example*
Swap	Selects two random groups and switches their position in the molecule.	A-B-C-D → A-D-C-B
Insert	Selects two random groups and inserts a random group between their positions in the molecule.	A-B-C-D → A-B-A-C-D
Delete	Selects one random group and removes the group from the molecule.	A-B-C-D → A-B-D
Replace	Selects one random group and replaces the group with a new, randomly generated group.	A-B-C-D → A-B-A-D
Global Moves		
Name	*Description*	*Example*
InitialSolution	Completely rebuilds a new solution, selecting random groups to comprise the molecule.	A-B-C-D → C-A-A

Following the generation of neighbors, each is checked against the tabu list. A solution is considered tabu if it violates the tabu criterion, which is given by Equation 5.6. A solution must pass tabu testing for all members on the tabu list to be accepted. If the solution is accepted, the solution becomes the first entry in the tabu list and the indices for all other entries in the tabu list are increased by one. Once the index of an entry exceeds the maximum size of the tabu list, the entry is removed from the tabu list. Therefore stored solutions leave memory on a first-in-first-out basis. The tabu list provides short-term solution memory.

$$\left| {}^{0}\chi_{current\ solution} - {}^{0}\chi_{previous\ solution} \right| > Tabu\ Criterion$$

(Equation 5.6)

If the solution violates the tabu criterion, the solution's objective function is checked against the best known solution. If the new tabu solution has a superior objective function to the best solution found so far, the new solution is retained despite its tabu status. The process of allowing violation of tabu criteria for good solutions is referred to as *aspiration* (Glover 1989). If all of the neighbors are deemed tabu, then a global move is used to direct the local search to new region of the solution space. The global move used is creation of a new random solution (see Table 5.4). The best non-tabu solution or best solution allowed by aspiration is chosen as the current solution. If the new current solution is better than any previously encountered solution, the solution is stored as the best solution. Storage of the best solution yet encountered provides long-term solution memory. The procedure continues until the maximum number of non-improving iterations is reached, where a solution obtained by a non-improving iteration does not have a better objective function value than the best obtained solution. Upon completion, the solution encountered with the best objective function value is returned.

5.3.4 Genetic Algorithm

The genetic algorithm mimics evolution to provided locally optimal solutions to the CAMD problem. The data structure used for molecular structure is identical to the representation used in the tabu search. For the genetic algorithm, the groups are analogous to genes. Each molecule, or member of the *population*, is comprised of a set of genes. Genetic operations (*i.e.*, moves) are used to alter the genes of members of the population. Through succession iterations, or *generations*, optimal genomes are determined. The procedure used by the genetic algorithm is detailed in Figure 5.4, with source code provided in Appendix D.

The search for solutions begins with random generation of members of the population through use of the *InitialSolution* subroutine (see Table 5.4 and Appendix D). The size of the population determines the number of solutions that are evaluated and generated during each generation. The fitness is determined for each member of the population, where the fitness is given as the inverse of the objective function (*e.g.*, when the objective function is minimized, the fitness is maximized). The fitness is used to calculate the probability (as a %) that a member will become a *parent* for the next generation through use of Equation 5.7. A parent is a member which undergoes a move to create a new member.

$$Probability(j) = 100\% * \left(\frac{Fit(j)}{\sum_{i=1}^{n} Fit(i)}\right)$$

(Equation 5.7)

Where *Fit(j)* represents the fitness of the *j-th* member of the population of size *n*. Once the probability is determined for a member, a roulette selection is used to determine whether the member will be a parent. A random integer between zero and the maximum allowable probability is chosen. If the integer is less than the probability calculated for the member, the member is chosen as a parent. Due to the semi-random selection, any number of members may become parents but members with higher fitness values are more likely to become parents. If no parents are chosen, then two parents are randomly selected from the population. The fitness of the selected parents is checked against the fitness of the best encountered solution. If the fitness exceeds the best known, the parent is retained in the next generation through a rule known as *elitist policy* (Venkatasubramanian, Chan et al. 1995).

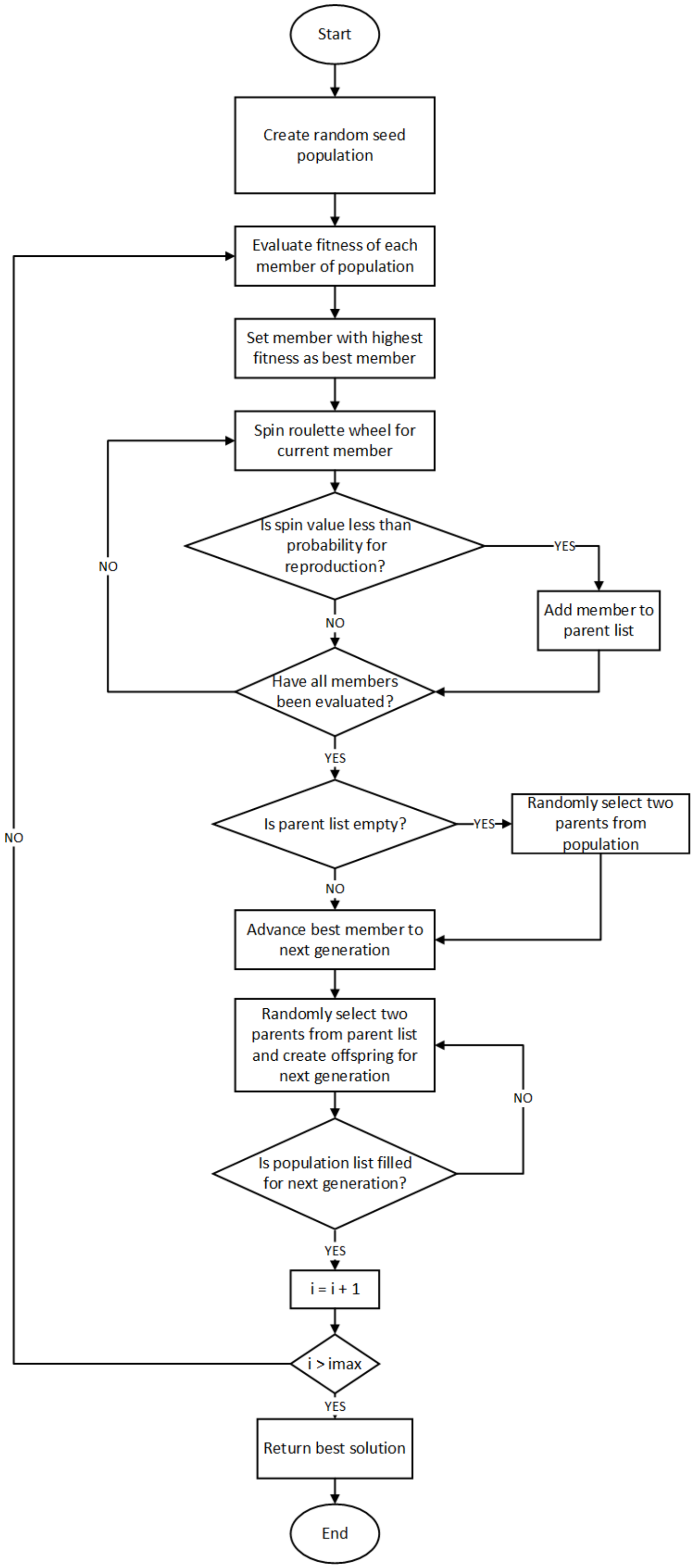
Start
Create random seed population
Evaluate fitness of each member of population
Set member with highest fitness as best member
Spin roulette wheel for current member
Is spin value less than probability for reproduction?
YES
Add member to parent list
NO
NO
Have all members been evaluated?
YES
Is parent list empty?
YES
Randomly select two parents from population
NO
NO
Advance best member to next generation
Randomly select two parents from parent list and create offspring for next generation
NO
Is population list filled for next generation?
YES
i = i + 1
i > imax
YES
Return best solution
End

Figure 5.4 Genetic algorithm as implemented in the CAMD framework

Table 5.5 Moves used to generate offspring to selected parents in the genetic algorithm Moves require either one parent or two parents. Letters are analogous to the genes or group numbers used to represent the molecule in the algorithm. The highlighted letter(s) represents the gene(s) selected by the move operation. Bold font is used in the two parent moves to distinguish groups belonging to the second parent.

One Parent Moves

Name	*Description*	*Example*
Hop	Selects two random genes and switches their position in the molecule.	A-B-C-D → A-D-C-B
Insert	Selects two random genes and inserts a random gene between their positions in the molecule.	A-B-C-D → A-B-A-C-D
Delete	Selects one random gene and removes the gene from the molecule.	A-B-C-D → A-B-D
Mutate	Selects one random gene and replaces the gene with a new, randomly generated gene.	A-B-C-D → A-B-A-D

Two Parent Moves

Name	*Description*	*Example*
Blend	Combines two parent molecules end to end to create one offspring molecule.	A-B + **C-D** → A-B-**C-D**
Crossover	Selects a random gene in each parent molecule to use as a crossover point, generating two offspring molecules.	A-B-C-D + **A-B-C-D** → A-**C-D** + **A-B**-B-C-D

New members for the next generation are produced by randomly selecting two parents from the list of parents generated through the roulette selection. The parents' structures (given as group arrays) are used as arguments in the *Make_Offspring* function (see Appendix D). The *Make_Offspring* randomly selects either a one parent move or a two parent move to generate a new member for the next generation (see Table 5.5). Each move is analogous to known genetic operations that occur in genomes of organisms. Comparison shows that all one parent moves have matching local moves in the tabu search algorithm (see Table 5.4). Following the generation of all new members of the population, the next generation begins. The genetic algorithm proceeds for a set number of maximum generations, returning the member with the highest fitness from the last generation.

5.4 Tuning of Stochastic Design Methods for Carbohydrate Excipients in Lyophilized Protein Formulations

The objective of tuning is to produce a stochastic design method that efficiently produces high quality solutions. Efficiency is measured by the time to solution and quality is measured by the solution's objective function value. Each design method contains several key parameters whose values affect the solution search. Tuning provided the rationale behind the values used for the parameter values in each design method. During tuning, a parameter was changed while all other values were kept constant. For each adjusted parameter value, 100 runs were performed with the objective values and times to solution captured for each run. The process was repeated for each parameter of interest.

From the observations, parameter values were chosen to yield a high percentage of high quality solutions (designed molecules with property values within 5% of the target property values) while minimizing the time to solution. The parameters tuned for each method are detailed in the following subsections. The parameters are not exhaustive for the two stochastic methods considered, but do represent the key parameters for the methods as developed here. Different implementations of tabu search and genetic algorithms may use slightly different parameters to guide the search for new solutions than the parameters presented here. The parameters used here were chosen to allow the best comparison possible between the two methods for CAMD applications.

A simple test case with a known global optimum was used as the test case for tuning. Each algorithm was used to generate solutions with a target molecular weight of 342 g/mol. For tuning, penalty functions were not employed in the objective function. The only other difference between the tuning and final design runs is the property model that is used, which does not affect the search process and only affects the objective function calculated for a given molecular structure. Thus it is expected that the tuning results would hold for any other CAMD design case where only the property model is altered.

5.4.1 Tabu Search Algorithm

For the tabu search algorithm, four parameters were used for tuning:

- *Maximum number of non-improving iterations* – determines how long the search will be performed.
- *Maximum number of neighbors evaluated per iteration* – determines how many new solutions to consider at each iteration.
- *Size of tabu list* – determines how many previous solutions are stored in memory. Also effects the time spent checking to see if a solution is tabu.
- *Tabu criterion* – determines how likely a solution is to be considered tabu.

The base parameter values are presented in Table 5.6.

Table 5.6 Parameter values used for the base case during tuning of the tabu search Parameters were altered on at a time to observe the effects of the parameter value on solution quality and time to solution.

Parameter	**Base Value**
Maximum number of non-improving iterations	10
Maximum number of neighbors evaluated per iteration	2
Size of tabu list	10
Tabu criterion	0.5

5.4.2 Genetic Algorithm

For the genetic algorithm, three parameters were used for tuning. The base parameter values are presented in Table 5.7:

- *Maximum number of generations* – determines how long the search will be performed.
- *Population size* – determines how many solutions are considered at each iteration/generation.
- *Maximum allowable probability that member is chosen as parent* – determines how likely a solution is to be used as a parent to generate new solutions for the next iteration/generation. As the value decreases, it becomes more likely that any given solution will be selected as a parent.

Table 5.7 Parameter values used for the base case during tuning of the genetic algorithm Parameters were altered on at a time to observe the effects of the parameter value on solution quality and time to solution.

Parameter	**Base Value**
Maximum number of generations	10
Population size	10
Maximum allowable probability	100

5.5 Comparison of Stochastic Design Methods for Carbohydrate Excipients in Lyophilized Protein Formulations

From the design methods, many excipient candidates are designed. The value of the objective function represents the indicator of solution quality, with the minimal value representing the optimal solution. Comparison of objective function values between the candidates generated by tabu Search and the genetic algorithm allows for identification of the method that provides the best overall solution as well as the method that most consistently provides good solutions (as defined by the percentage of designed molecules with property values within 5% of the target property values). However, solely relying on the objective function value may be misleading as many candidates could have statistically similar property values to best solution and thus be solutions of equal quality.

A QSPR's use lies in predicting a property for a new molecule of interest, represented by the molecular descriptors. The resulting predicted value has some error term involved. A novel approach to design solution comparison using prediction intervals was utilized. Prediction intervals allow for the error from the fitted model as well as any error in a future observation to be quantified (Wasserman 2004). A confidence interval only accounts for error in the correlation, so a prediction interval is always larger than a confidence interval. A 1 - α prediction interval for a predicted property of interest $P_*$is given by Equation 5.8.

$$P_* \pm t_{\alpha/2}\sqrt{\hat{\sigma}^2(x_*^T(X^TX)^{-1}x_* + 1)}$$

Equation 5.8

where $t_{\alpha/2}$ is the student's t-test value for the given degrees of freedom, x_* is the vector of descriptors used in the prediction, x_*^T is the transposed vector of descriptors used in the prediction, X is the matrix of descriptors used to build the correlation, X^T is the transposed matrix of descriptors used to build the correlation, and $\hat{\sigma}^2$ is the unbiased estimator of the model variance.

Given the connectivity indices for a designed carbohydrate excipient, new property values were predicted. Using the connectivity index values, R was used to calculate prediction intervals at a 95% level (The R Project for Statistical Computing, www.r-project.org). The procedure used in R for calculation of prediction intervals along with sample code is given in Appendix B. The prediction intervals were included to provide a reasonable range for the expected properties of the designed excipient molecule. The prediction intervals were also used to determine if two solutions from the optimal design phase were statistically different once the solutions were found using either tabu search or a genetic algorithm. When comparing the predicted properties of two designed molecules, overlapping prediction intervals indicate that the solutions are not statistically different. The use of prediction intervals to compare solutions represents a novel approach to evaluating solutions generated in computer-aided molecular design.

6.0 Simultaneous Product and Process Design

CAMD was linked with separation process design for the simultaneous design of an ionic liquid entrainer and azeotropic separation process. Key to the IL-based separation process is the extractive distillation column, where the azeotrope is broken. Once a candidate was designed and confirmed to break an azeotrope of interest using the UNIFAC-IL model, design of the separation process was performed. The extractive distillation column was designed using the driving force method, as detailed in Section 6.1. After design of the column, simulations were used to design the ionic liquid recovery unit and to determine overall heat duty for the process. The simulation procedure is given in Section 6.2. The overall feedback between product and process design is outlined in Figure 6.1. Details concerning the molecular design component can be found in Section 5.1.

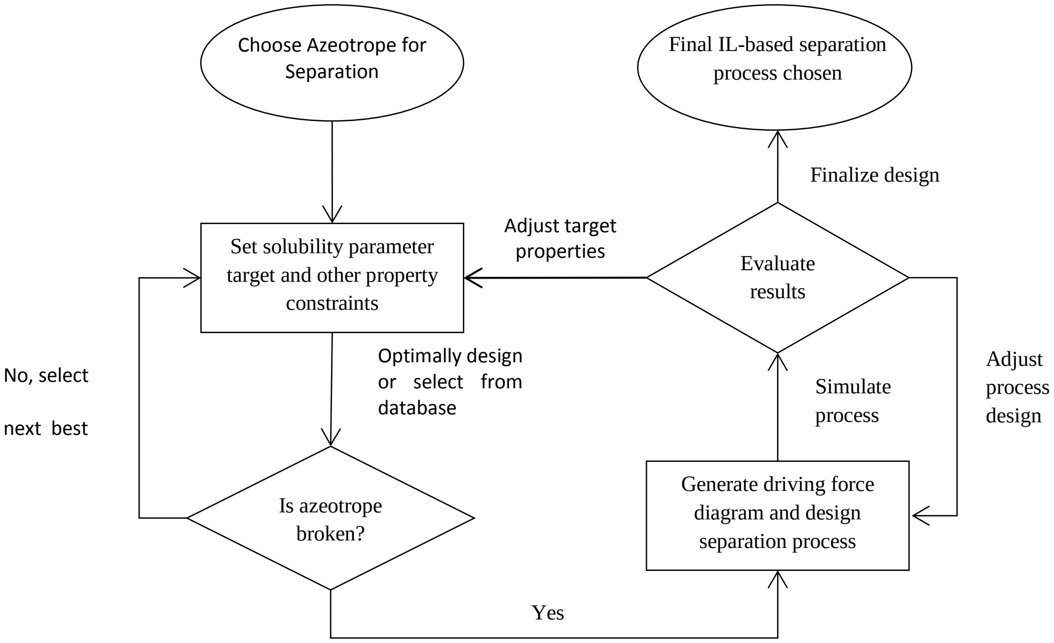
Choose Azeotrope for Separation
Final IL-based separation process chosen
Finalize design
Adjust target properties
Set solubility parameter target and other property constraints
Evaluate results
No, select next best
Optimally design or select from database
Simulate process
Adjust process design
Is azeotrope broken?
Generate driving force diagram and design separation process
Yes

Figure 6.1 Overall methodology for simultaneous design of ionic liquid entrainers and IL-based separation processes Figure is adapted from (Roughton, Christian *et al.* 2012).

6.1 Driving Force Based Design

For separation of a given azeotrope, an extractive distillation column was designed using the driving force method. The driving force is defined as the difference between the vapor and liquid composition of the light key component (Bek-Pedersen, Gani *et al.* 2000). The driving force is used to evaluate the feasibility of a proposed separation process, ensuring that the driving force is never zero (Bek-Pedersen, Gani *et al.* 2000). By designing the separation process based upon the maximum driving force, near optimal distillation columns can be designed with respect to energy requirements (Gani and Bek-Pedersen 2000).

The UNIFAC-IL model was used to generate the driving force for each ternary system consisting of the binary azeotrope plus an ionic liquid. The two components comprising the azeotropic mixture were defined as the key binary mixture. Product purities of the azeotrope components (on an ionic liquid free basis) were specified at ASTM purity standards. The driving force was plotted against the light key component mole fraction and the location (D_x) and value (D_y) of the maximum driving force was determined for varying ionic liquid compositions. The number of stages (N) were determined by finding the minimum number of stages necessary to achieve the desired product specifications, as determined by rigorous simulation (detailed in section 2.3.2). As the location of the maximum driving force was determined on an ionic liquid free basis, the location was modified using Equation 6.1. The driving force profile is only an estimate for the systems considered, as the ionic liquid concentration may vary throughout the column. The feed stage location (NF) was determined using Equation 6.2 (Gani and Bek-Pedersen 2000) with a modification due to one stage being used as the entrainer feed stage.

$$D_x = (1 - x_{IL})D_{x,IL-Free\ Basis}$$

(Equation 6.1)

$$NF = (1 - D_x)(N - 1)$$

(Equation 6.2)

The original driving force method was proposed for systems with one feed. The proposed distillation column consists of a main feed for the azeotropic mixture and an ionic liquid feed at the top of the tower. For moderate to high ionic liquid concentrations, scaling of the feed tray location may be necessary. The scaling factor (*SF*) is given by Equation 6.3, where $x_{LK,D}$ is the specification for the light key distillate mole fraction and $x_{HK,B}$ is the specification for the heavy key bottoms mole fraction (Bek-Pedersen, Gani *et al.* 2000). Calculation of $x_{LK,D}$ and $x_{HK,B}$ is performed taking into account the ionic liquid present in the column. When *SF* ≤ 0.01 and D_x < 0.7, scaling is necessary and Equation 6.4 is used to determine the site where the feed stage should be relocated in the column. In the initial implementation of driving force based design, the feed stage will always move up the column between a minimum of 10% of the total number of trays when scaling is required. By scaling the feed tray location through use of Equation 6.4, a more accurate location is determined then by relocating either by 5% or 10% as proposed by Bek-Pedersen *et al.* (Bek-Pedersen, Gani *et al.* 2000). By using the scaled feed tray location when the stated conditions are met, a near-optimal column design is achieved with respect to overall energy consumption for a column with a main feed and a separate ionic liquid feed.

$$SF = \frac{1 - x_{LK,D}}{1 - x_{HK,B}}$$

(Equation 6.3)

$$NF_{scaled} = NF - [-0.1Nlog(SF)]$$

(Equation 6.4)

6.2 Azeotrope Separation Process Simulation

ChemCAD (www.chemstations.com) was used for rigorous simulation of the extractive distillation processes. The overall process selected for separation of the azeotropic mixtures and regeneration of the ionic liquid has been used successfully in design and simulation of ionic liquid-based separation processes (Seiler, Jork *et al.* 2004). The process, shown in Figure 6.2, consists of a distillation column, flash drum, and stripper. The distillation column is used to separate the light key component (1) from the heavy key component (2) and the ionic liquid (3). The flash drum and stripper are used to separate component (2) and any remaining component (1) from the ionic liquid. The proposed process is desirable as it minimizes energy inputs and the stripper uses only air to regenerate the ionic liquid entrainer.

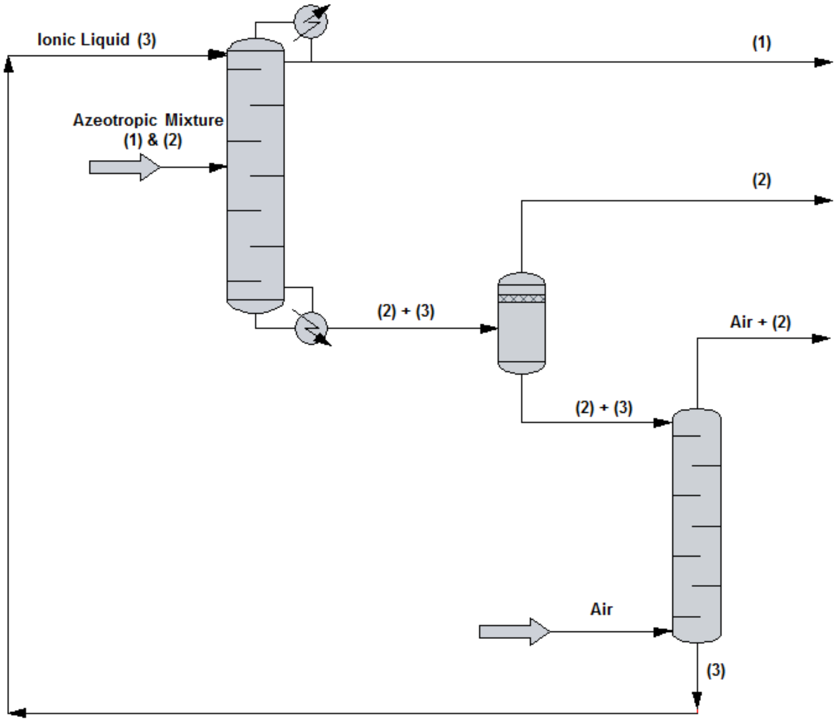

Figure 6.2 Proposed ionic liquid-based azeotropic separation process A distillation column is used to separate the light (1) and heavy (2) components, which the ionic liquid (3) entraining the heavy component. The heavy component is then separated from the ionic liquid by flash distillation and stripping.

Fixed parameters for the process were chosen to match previous simulation work (Seiler *et al.*, 2004) for comparison of results. For both the acetone-methanol and ethanol-water azeotropes, a total feed rate of 200 kmol per hour was used. Ionic liquid feed rate, column size, and feed tray location were altered to minimize energy consumption of the column. The distillate specifications were set to ASTM standards for purity. The azeotropic mixture was fed as a saturated liquid. The ionic liquid was fed at the same temperature as the feed. First approximation of the feed stage location was obtained using the driving force method as outlined in the previous section. The location was then moved above and below the initial stage to ensure that energy use was minimized. The procedure was repeated for varying flow rates of ionic liquid until a column configuration and entrainer flow rate that minimized overall energy consumption was identified. The values of the free variables for the entire distillation and entrainer regeneration process were determined by the ChemCAD solver such that overall energy requirements were minimized, while also satisfying constraints on column size, air flow rate and final product purity of the ionic liquid entrainer leaving the column (specified as 99.9% pure on a molar basis). The fixed parameters and free process variables are outlined in Table 6.1 for both azeotropic systems.

Prediction of heat capacity was needed for the ionic liquids in order to accurately calculate the energy requirements of the proposed separation processes. Group contribution models from literature were used to predict the isobaric heat capacities of the ionic liquids used in the simulations (Gardas and Coutinho 2008; Ren, Zhao *et al.* 2011). Column simulation was performed for both the optimal and non-optimal ionic liquid entrainers (selected for comparison purposes). The entire process, including entrainer regeneration, was performed only for the best ionic liquid candidates. Energy requirements for the ethanol-water separation were compared to results found for an ionic liquid known to experimentally break the given azeotropes but not designed with CAMD methods (henceforth referred to as an experimentally-selected ionic liquid) and also for a conventional entrainer (Seiler, Jork *et al.* 2004).

Table 6.1 Fixed parameters and free variables for ionic liquid-based extractive distillation processes

Fixed Parameters			
		Acetone-Methanol	*Ethanol -Water*
Distillation Column			
	Operating pressure [atm]	1.00	1.00
Column Feed			
	Flow rate [kmol/hr]	200	200
	x_1	0.5	0.7
	x_2	0.5	0.3
Distillate			
	Flow rate [kmol/hr]	100	140
	x_1	0.995	0.998
Flash Tank			
	Operating pressure [atm]	0.10	0.10
Stripper			
	x_{IL} *(bottom)*	0.999	0.999
	Air temperature [K]	298.15	298.15
Free Variables			
Distillation Column			
	Number of stages		
	Feed stage		
	Reflux ratio		
Flash Tank			
	Temperature		
Stripper			
	Number of stages		
	Air flow rate		

7.0 MOLECULAR SIMULATION FOR DESIGN AND POST-DESIGN STAGES

Stabilizing additives, or excipients, are often included in lyophilized formulations to reduce aggregation. Nonionic surfactants have been shown to bind with weak affinity to proteins (McNally and Hastedt 2008). Such binding could interact with hydrophobic regions on the protein and limit access to aggregation prone “hot spots”. Nonionic surfactants such as Tween 80 have been shown to decrease aggregation in lyophilized protein formulations (Kerwin 2008). However, difficulties can arrise during the lyophilization process due to the low glass transition temperatures exhibited by surfactants (McNally and Hastedt 2008). A successful formulation using surfactants requires the presence of glass formers, such as sugars or polymers.

Sugar molecules have also been shown to exhibit site-specific effects on proteins during lyophilization through use of hydrogen-deuterium exchange mass spectroscopy (Li, Williams *et al.* 2008), indicating that interaction between sugars and proteins occur in the lyophilized state. Such interactions can be exploited to provide better coverage of aggregation prone “hot spots” on the protein. By selecting excipients that interact preferably with aggregation prone regions, a lyophilized formulation can be developed to reduce aggregation.

In following section, a simulation-guided design approach is utilized to select a sugar and surfactant pair that optimally provides the most interaction with an aggregation prone region on the protein calmodulin (*Protein ID #1CLL,* Protein Data Bank via http://www.rcsb.org/pdb/home/home.do). By choosing a formulation with maximal protein-excipient interactions, the potential for aggregation is reduced. While surfactants may interact more than sugars on a per molecule basis, a sugar was included to ensure that a stable glass could be formed. The use of molecular docking simulations to aid in post-design screening is also proposed.

7.1 Use of AutoDock for Blind Docking Simulations

Molecular simulation results were generated for use in guiding formulation design. The tool used for molecular simulation was AutoDock (http://autodock.scripps.edu/), which utilizes blind docking to determine regions of protein-ligand interaction with no *a priori* knowledge of binding site (Huey, Morris *et al.* 2007). AutoDock employs a grid-based approach along with a semiempirical free energy force field to identify interaction sites with minimal free energy (Huey, Morris *et al.* 2007). AutoDock leaves the protein as a rigid molecule and only adjusts the ligand conformation. The ligand conformation is described by rotation, translation and torsional degrees of freedom (Goodsell, Morris *et al.* 1996). Search for conformations is guided by one of three stochastic optimization methods chosen by the user: Monte Carlo simulated annealing, traditional genetic algorithm and Lamarkian genetic algorithm (Morris, Goodsell *et al.* 1998). As all solution methods are stochastic, the conformations returned are local optima. The work presented here employs the simulated annealing method. Blind docking has proved successful in detecting binding sites on proteins for small molecule drug-like compounds (Hetényi and van der Spoel 2006) and peptides (Hetényi and van der Spoel 2002), which encompass the size of descriptors considered here.

7.2 Determination of Protein-Excipient Interactions

To predict the amino acids of calmodulin most likely to interact with a given excipient, blind docking simulations were performed using AutoDock. Each simulation provided ten docking conformations that provided the lowest free energy of the conformations encountered. Five simulations were done for each excipient with calmodulin, providing fifty docking conformations total for each excipient. Each conformation was analyzed to determine which resides were in contact, through hydrogen bonding, with the excipient molecule. An important limitation to note is that the blind docking simulations do not consider that the protein is lyophilized but rather employ an implicit solvation model. It follows that the approach used for estimating protein-excipient interactions does not take into account any dynamics that may result from the lyophilization process. The approach only provides a first-approximation of protein-excipeint interactions that may be present. Docking free energy calculations are therefore not instructive to the approach taken and are not utilized.

The computational results from Autodock were qualitatively compared to experimental hydrogen-deuterium exchange (HDX) mass spectroscopy experiments using lyophilized formulations of calmodulin and either trehalose, sucrose, raffinose, or mannitol (Li, Williams *et al.* 2008). Regions of the protein that are able to freely exchange hydrogen for deuterium are exposed and are not protected by protein-excipient interactions. Experimentally, the extent of protein-excipient interactions is inversely related to deuterium uptake. For comparison between experimental and simulation results, it is expected that regions of high protein-excipient interaction identified by simulation should correspond with regions of low deuterium uptake experimentally.

7.3 Optimal Selection of Excipients

Contact information provided by the docking simulations was used to optimally select excipients that have the highest number of interactions with aggregation prone "hot spots". The hot spots were predicted using Aggrescan (Conchillo-Sole, de Groot et al. 2007). For each hot spot, a sugar and a surfactant molecule were chosen to maximize protein-excipient interactions. For selection purposes, whichever excipient had the most interactions with a particular residue was chosen as the best candidate. It was assumed that the molecule with the most interactions with a residue would have the dominant effect and thus contribute the most to the protection of the residue of interest. At each residue in the hot spot, the best sugar candidate and the best surfactant candidate were compared. Whichever excipient had the most interactions was selected and the process was repeated for the entire hot spot sequence. The sugar-surfactant pair that provided the maximum number of interactions was selected as the optimal drug formulation. The formulation of the optimization problem is given in

Equation 7.1. The problem is formulated as a MINLP and was solved using the DICOPT solver in GAMS (GAMS documentation, http://www.gams.com/).

$$\max \sum_{i}^{n} \text{interaction score}\,(i)$$

$$\begin{aligned}
&\text{s.t.}\\
&\text{interaction score}\,(i) = y_{sugar}(i) \cdot \text{sugar score}(i) + y_{surfactant}(i) \cdot \text{surfactant score}(i)\\
&\text{sugar score}(i) = \sum_{j=1}^{4} y_j \cdot score_j(i)\\
&\text{surfactant score}(i) = \sum_{k=1}^{3} y_k \cdot score_k(i)\\
&y_{sugar}(i) \le \frac{\text{sugar score}(i)}{\text{surfactant score}(i)}\\
&y_{surfactant}(i) \le \frac{\text{surfactant score}(i)}{\text{sugar score}(i)}\\
&y_{sugar}(i) + y_{surfactant}(i) = 1\\
&\sum_{j=1}^{4} y_j = 1\\
&\sum_{k=1}^{3} y_k = 1\\
&y_{sugar}, y_{surfactant}, y_j, y_k = \{0,1\}
\end{aligned}$$

(Equation 7.1)

where *i* is a residue location, *n* is the number of residues in the hot spot of interest, *j* is a specific sugar, and *k* is a specific surfactant. The score$_j$(i) and score$_k$(i) are input as parameters based on the results from molecular docking. The scores are integer values, but are not explicitly defined as such in GAMS. The constraints ensure that the highest interaction score between a sugar and a surfactant is chosen for each residue. The constraints provide an interaction score that is summarized below, without the need for disjunctive programming:

$$\text{interaction score}\,(i) = \begin{cases} \text{sugar score}\,(i) & \text{if sugar score}\,(i) \ge \text{surfactant score}\,(i) \\ \text{surfactant score}\,(i) & \text{if surfactant score}\,(i) > \text{sugar score}\,(i) \end{cases}$$

(Equation 7.2)

7.4 Docking Simulation Results

Docking simulations providing fifty conformations were performed individually for mannitol, trehalose, sucrose, raffinose, octyl glucoside, tween 40, and tween 80 with the protein calmodulin. The results for the sugars were compared to experimental HDX results. Overall, the docking results compared favorably with the HDX results. Regions of high interactions in the docking simulations corresponded to regions that were protected from hydrogen/deuterium exchange. The histogram of interactions versus residue location is provided in Figure 7.1 for trehalose. Residues that interacted frequently with trehalose match well with the shaded regions indicating protection from hydrogen/deuterium exchange.

Figure 7.2 provides a visual comparison of the regions with high interaction and the regions protected from exchange for the trehalose-calmodulin system. From the comparison of the computational and experimental results, the docking simulations provide a reasonable prediction of the residues involved in protein-excipient interactions and provide a useful tool for selecting excipients for lyophilized protein formulations.

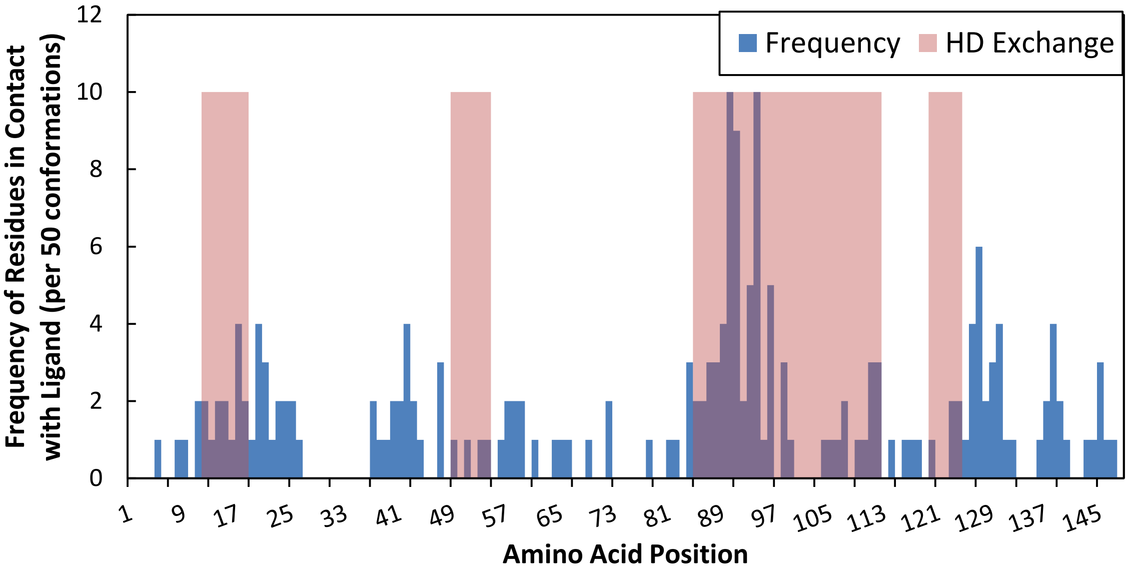

Figure 7.1 Frequency of amino acid residues of calmodulin in contact with trehalose Results are given for 50 docking conformations. The shaded regions indicate amino acids that were protected by trehalose in the lyophilized state, as determined by HDX experiments (Li, Williams *et al.* 2008). Figure adapted from (Roughton, Pokphanh *et al.* 2012).

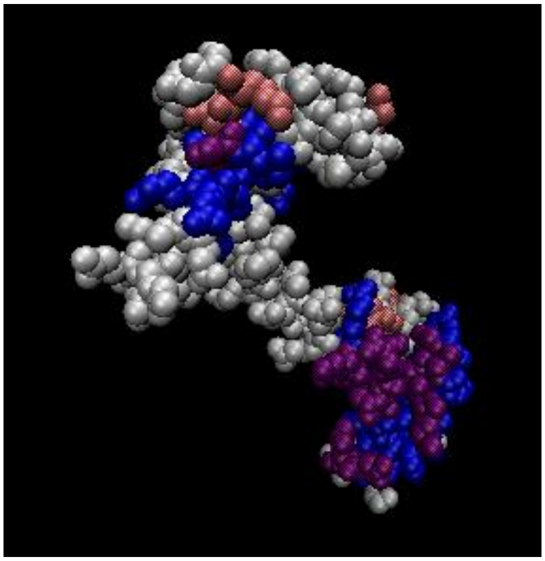

Figure 7.2 Trehalose interaction regions mapped to the surface of calmodulin Blue regions indicate residues that interacted with trehalose in more than three conformations. Red regions indicate regions that were protected by trehalose in the lyophilized state, as determined by HDX experiments. Purple regions are theintersect of the computationally predicted high interaction regions and the experimentally determined protected regions. Figure adapted from (Roughton, Pokphanh *et al.* 2012).

7.5 Formulation Selection for Maximizing Protein-Excipient Interactions

Using the docking simulation results and the previously described optimization problem formulation, sugar-surfactant pairs were selected for each hot spot region on calmodulin. The hot spots were predicted using Aggrescan (Conchillo-Sole, de Groot et al. 2007). Due to the proximity of hot spots 4 and 5, a formulation was also selected for the combined region. The results are given in Table 7.1. The interaction scores provided correspond to the number of interactions exhibited in the docking simulations.

Table 7.1 Sugar-surfactant formulations selected for maximum interaction with hot spot regions Table adapted from (Roughton, Pokphanh *et al.* 2012).

Hot Spot	*Amino Acids*	*Sugar*	*Surfactant*	*Combined Interaction Score*	*Sugar Interaction Score*	*Surfactant Interaction Score*
1	15-19	Trehalose	Tween 40	24	10	24
2	33-38	Mannitol	Tween 40	13	10	7
3	67-73	Sucrose	Tween 40	17	9	15
4	99-103	Raffinose	Octyl Glucoside	10	7	8
5	106-111	Raffinose	Tween 80	17	11	13
6	141-145	Raffinose	Octyl Glucoside	26	15	26
4 & 5	99-111	Raffinose	Octyl Glucoside	29	18	22

The results show that the excipients providing maximal interactions vary from hot spot to hot spot. All available excipients were selected at least once. The addition of a sugar provided no additional interactions for the formulations selected for hot spots 1 and 6 and thus was not beneficial from a protein-excipient interaction standpoint. A sugar would be necessary to ensure a stable glass was formed during the lyophilization.

The procedure outlined above could be used for any number of excipients and proteins to predict formulations with maximal protein-excipient interactions. By maximizing protein-excipient interactions, the aggregation propensity is reduced and a safer, more effective drug product is produced. The fact that the sugar-surfactant pair providing maximal interactions differed between hotspots highlights the complexity of selecting beneficial excipients for a lyophilized protein formulation.

While the proposed approach may have some application in the design phase of CAMD (as outlined above), a potentially more useful application is for post-design review. Following design, promising candidates could be further screened using a molecular docking approach to identify candidates with benficial protein-excipient interactions. Molecular docking provides a faster screening procedure than HDX experiments, which would be especially useful for large candidate lists. Following screening by molecular docking, HDX experiments can provide final verification and selection of design candidates. It is noted that additional protein-excipient systems have been explored using the molecular simulation approach outlined by Anthony I. Pokphanh and Haider S. Tarar at the University of Kansas. The data they have collected is not included in the presented work, but also provides good comparison to corresponding experimental HDX studies.

8.0 RESULTS FOR IONIC LIQUID DESIGN

The following section contains the modeling and molecular design results for the two ionic liquid design examples considered: sections 8.1-8.3 are concerned with entrainer design and sections 8.4-8.5 are concerned with extractant design for *in situ* fermentation.

The group contribution model for ionic liquid solubility parameter is presented in Section 8.1. The acetone-methanol and ethanol-water azeotropes were chosen for evaluation of the CAMD methodology for design of ionic liquid entrainers. In addition, the 1-propanol-water, 2-propanol-water, and ethyl acetate-ethanol azeotropes were used for evaluation of the UNIFAC-IL predictions in Section 8.2. The molecular design results for the ionic liquid entrainer case are presented in Section 8.3 and the separation process design results are given in Section 8.4.

The connectivity index models for both the partition coefficient of NDHD in ionic liquid and ionic liquid toxicity are presented in Section 8.5. Design results for ionic liquid extractant design obtained through tabu search are discussed in Section 8.6.

8.1 HILDEBRAND SOLUBILITY PARAMETER GROUP CONTRIBUTION MODEL

Experimental values for 24 different ionic liquids was used for the development of the Hildebrand solubility parameter GC model (Marciniak 2010). In addition to 3 terms for the alkyl chain groups, 5 cation and 12 anion groups were used to describe the ionic liquids in the data set. The total number of independent variables in the model are 21 (including a constant term), giving 3 degrees of freedom. The degrees of freedom are relatively low, which is a consequence of the use of group contribution models with small data sets. The developed model (see Equation 4.17) provides a good fit of experimental data with a value of 0.34 %AARD between the predicted and experimental solubility parameter values. The maximum relative deviation observed was 0.305. The results are shown in Figure 8.1.

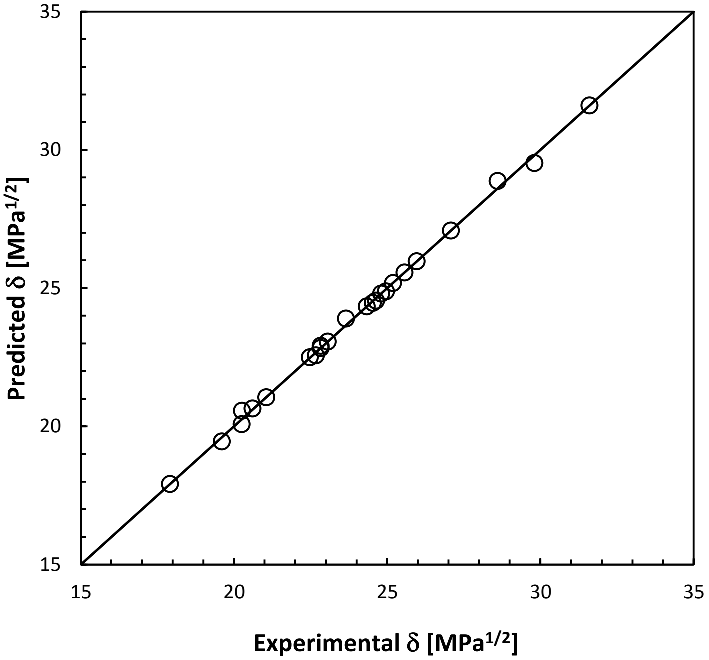

Figure 8.1 Comparison between experimental and predicted solubility parameter values Predictions were made using the group contribution model shown in Table 8.1. Experimental ionic liquid solubility values are obtained from (Marciniak 2010). Figure adapted from (Roughton, Christian *et al.* 2012).

The contributions for each group are given in Table 8.1 Increasing the alkyl chain length decreases the overall solubility parameter value, as the value for CH_2 groups is negative. Ionic liquids with pyridinium cations are usually more hydrophobic than those with imidazolium cations (Papaiconomou, Salminen *et al.* 2007), reflected in the model by the smaller contribution for the pyridinium cation compared to the imidazolium cation. In general, the many of the anion contributions are larger in magnitude than the commonly encountered imidazolium, pyridinium, and pyrrolidonium cation contributions. For the design examples, only imidazolium and pyridinium cations were used as cation choices to ensure that the UNIFAC-IL model could be used to predict VLE. The minimum solubility parameter value predicted by the model using the design problem's cation restrictions was 17.8 MPa$^{1/2}$ for 1-octyl-4-methylpyridinium chloride. The maximum solubility parameter value predicted was 32.6 MPa$^{1/2}$ for 1,3-dimethylimidazolium tetrafluoroborate.

Table 8.1 Group contribution values for ionic liquid Hildebrand solubility parameter model See Table 4.4 for descriptions of groups. Table is adapted from (Roughton, Christian *et al.* 2012).

	Ionic Liquid Group	Contribution ($MPa^{1/2}$)
Cation groups		
	Imidazolium (Im)	1.427
	Pyridinium (Py)	1.355
	Pyrrolidonium (Pyr)	1.765
	Phosphonium (P)	-13.633
	Sulfonium (S)	-16.101
Anion groups		
	Trifluoroacetate (CF_3COO)	1.720
	Thiocyanide (SCN)	1.342
	Trifluormethane sulfonate (CF_3SO_3)	-0.629
	2-(2-methoxyethoxy)ethyl sulfate ($MDEGSO_4$)	1.603
	Octyl sulfate ($OcSO_4$)	-0.367
	Tosylate (TOS)	-0.065
	Bis(trifluoromethylsulfonyl)imide (Tf_2N)	-2.485
	Dimethyl phosphate (DMP)	2.918
	Diethyl phosphate (DEP)	2.120
	Tetrafluoroborate (BF_4)	8.403
	Hexafluorophosphate (PF_6)	6.319
	Chloride (Cl)	-4.000
Alkyl chain groups		
	CH_3	9.094
	CH_2	-0.322
	CH_2O	0.496
Intercept (constant)		4.547

8.2 UNIFAC-IL Model

8.2.1 UNIFAC-IL Parameters

Using the previous described procedure, group volume and surface area parameters were defined for all ionic liquid groups used in the UNIFAC-IL model. The results are given in Table 8.2. The subgroups for the cation are chosen based on the smallest alkyl group present in the cation. For example, 1,3-dimethylimidazolium is represented by a [MIm] and a CH_3 group. 1-octyl-4-methylpyridinium is represented by a [MPy] group, a CH_3 group, and seven CH_2 groups. Group parameters for existing UNIFAC groups were not changed.

Table 8.2 Volume (R_k) and surface area (Q_k) parameters for the UNIFAC-IL model The [MIm] and [MPy] subgroups are for the imidazolium and pyridinium cations that contain a methyl group. Table adapted from (Roughton, Christian *et al.* 2012).

Group	Subgroup	R_k	Q_k
[Im]	[Im]	1.9471	0.8660
	[MIm]	2.8482	1.7140
[Py]	[Py]	2.6670	1.5530
	[MPy]	3.5681	2.4010
[N]	[CH_3N]	1.1865	0.9400
(quad-	[C_2H_5N]	1.8609	1.4800
substituted)	[C_3H_7N]	2.5353	2.0200
	[C_4H_9N]	3.2097	2.5600
[DMP]	[DMP]	3.4127	3.2820
[BF_4]	[BF_4]	1.7856	1.4940
[PF_6]	[PF_6]	7.0615	6.5787
[Tf_2N]	[Tf_2N]	5.7738	4.9320
[CF_3COO]	[CF_3COO]	3.1773	3.2200
[CF_3SO_4]	[CF_3SO_4]	4.0870	3.9160
[CH_3SO_4]	[CH_3SO_4]	3.4832	3.7280
[$CH_3CH_2SO_4$]	[$CH_3CH_2SO_4$]	4.1576	4.1760
[$CH_3OC_2H_4SO_4$]	[$CH_3OC_2H_4SO_4$]	5.0759	5.3560
[$C_2H_5OC_2H_4SO_4$]	[$C_2H_5OC_2H_4SO_4$]	5.7503	5.8040
[$CH_3(OC_2H_4)_2SO_4$]	[$CH_3(OC_2H_4)_2SO_4$]	6.6686	6.9840
[Br]	[Br]	0.9492	0.8320
[Cl]	[Cl]	0.7660	0.7200
[I]	[I]	1.2640	0.9920
[SCN]	[SCN]	1.9446	1.1752

Binary interaction parameters were determined for all ionic groups for which data was available. The parameters used to describe the final design candidates in examples provided are given in Table 8.3. The entire UNIFAC-IL interaction parameter matrix is available (see Appendix E). Due to lack of measured data, not all groups used in the solubility parameter GC model are present in the UNIFAC-IL model and the converse is also true.

Table 8.3 UNIFAC-IL binary interaction parameters for the groups used for the final design candidates in the acetone-methanol and ethanol-water examples The lightly shaded region corresponds to UNIFAC groups with previously determined interaction parameters, which are not included here (Fredenslund, Gmehling *et al.* 1977). The full list of UNIFAC-IL binary interaction parameters is provided in Appendix E. Table is adapted from (Roughton, Christian *et al.* 2012).

	CH_2	OH	CH_3OH	H_2O	CH_2CO	[Im]	[Py]	[CF_3SO_3]	[DMP]
CH_2	Previous UNIFAC Groups					65.08	-24.94	694.19	879.73
OH						-199.99	-147.61	91.85	-33.36
CH_3OH						380.03	841.54	-335.72	-182.43
H_2O						-914.38	-666.90	-211.41	-650.60
CH_2CO						-266.87	-143.22	443.95	320.25
[Im]	134.11	737.69	0.05	0.00	438.53	0.00	0.00	0.00	0.00
[Py]	1269.62	1789.95	-224.11	-0.01	507.94	0.00	0.00	0.00	0.00
[CF_3SO_3]	-285.94	220.70	350.14	0.00	-191.88	0.00	0.00	0.00	0.00
[DMP]	-326.80	64.06	-211.21	1209.55	-42.56	0.00	0.00	0.00	0.00

8.2.2 UNIFAC-IL Performance for Azeotropic Systems

To determine the performance of the UNIFAC-IL model for predicting the VLE of ternary systems with binary azeotropic mixtures and ionic liquids, UNIFAC-IL predictions were compared to experimental data for several systems. While the UNIFAC-IL model could be used for other applications, due to the scope of the work only the performance of the model for several common azeotropes was evaluated: acetone-methanol, 1-propanol-water, 2-propanol-water, ethyl acetate-ethanol, and ethanol-water. Experimental ternary VLE data of the listed binary azeotropes with the ionic liquids 1-ethyl-3-methyl trifluoromethane sulfonate ([emim][triflate]) and/or 1,3-dimethylimidazolium dimethylphosphate ([mmim][dmp]) were used for comparison to UNIFAC-IL predictions (Orchillés, Miguel *et al.* 2006; Orchillés, Miguel *et al.* 2007;

Orchillés, Miguel *et al.* 2008; Orchillés, Miguel *et al.* 2010; Wang, Wang *et al.* 2010). Figures 8.2-8.7 show the comparison between the UNIFAC-IL predictions and experimental data, where component (1) is the light component and is listed first in the figure caption.

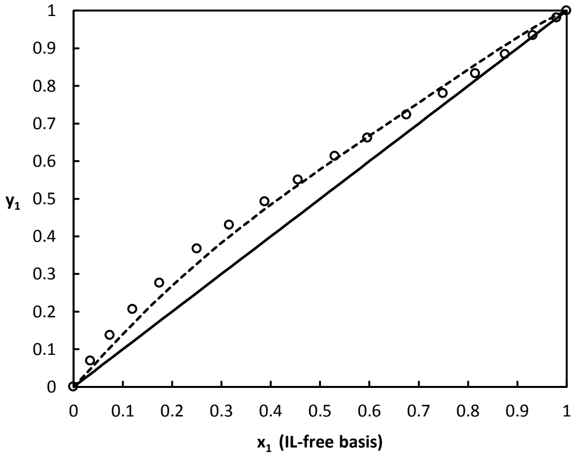

Figure 8.2 Acetone-methanol-[emim][triflate] x-y diagram at 100 kPa 6.0 mol% ionic liquid is present. The dashed line indicates the UNIFAC-IL prediction and the open circles represent experimental data (Orchillés, Miguel *et al.* 2006). 6.84 %AARD was observed between the experimental and predicted vapor fractions. Figure adapted from (Roughton, Christian *et al.* 2012).

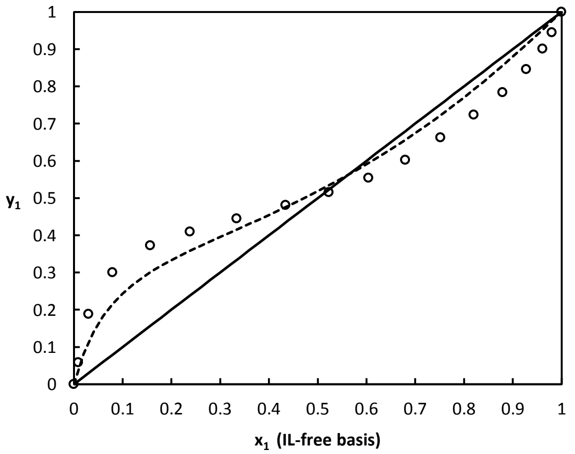

Figure 8.3 1-propanol-water-[emim][triflate] x-y diagram at 100 kPa 6.0 mol% ionic liquid is present. The dashed line indicates the UNIFAC-IL prediction and the open circles represent experimental data (Orchillés, Miguel *et al.* 2008). 10.84 %AARD was observed between the experimental and predicted vapor fractions. Figure adapted from (Roughton, Christian *et al.* 2012).

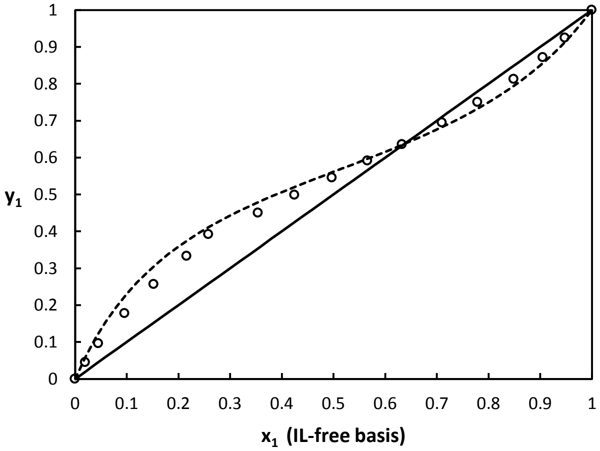

Figure 8.4 Ethyl acetate-ethanol-[emim][triflate] x-y diagram at 100 kPa 6.0 mol% ionic liquid is present. The dashed line indicates the UNIFAC-IL prediction and the open circles represent experimental data (Orchillés, Miguel *et al.* 2007). 7.93 %AARD was observed between the experimental and predicted vapor fractions. Figure adapted from (Roughton, Christian *et al.* 2012).

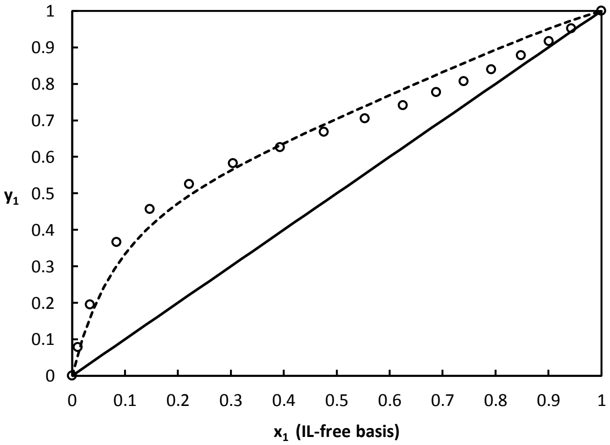

Figure 8.5 Ethanol-water-[emim][triflate] x-y diagram at 100 kPa 6.0 mol% ionic liquid is present. The dashed line indicates the UNIFAC-IL prediction and the open circles represent experimental data (Orchillés, Miguel *et al.* 2010). 6.45 %AARD was observed between the experimental and predicted vapor fractions. Figure adapted from (Roughton, Christian *et al.* 2012).

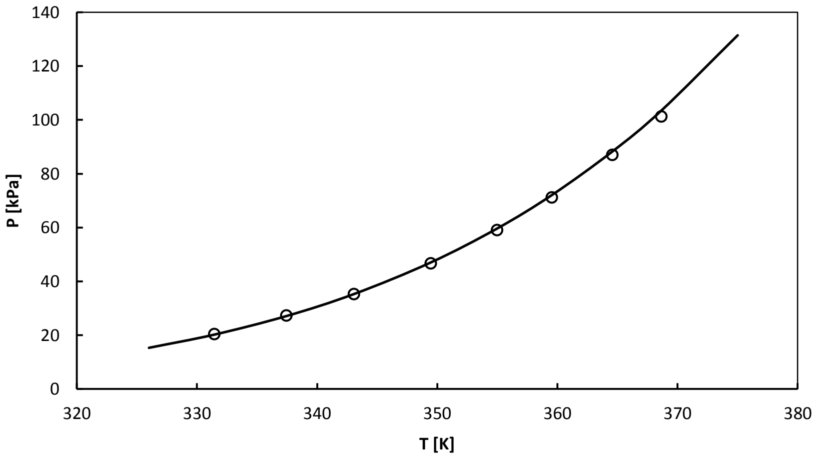

Figure 8.6 1-propanol-water-[mmim][dmp] P-T diagram x_1 = 0.6669 and x_2 = 0.2472. The solid line indicates the UNIFAC-IL prediction and the open circles represent experimental data (Wang, Wang *et al.* 2010). 1.10 %AARD was observed between the experimental and predicted total pressures. Figure adapted from (Roughton, Christian *et al.* 2012).

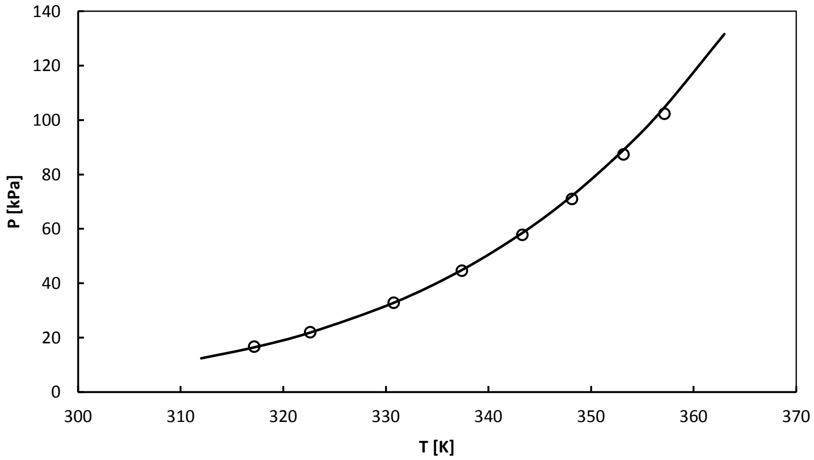

Figure 8.7 2-propanol- water-[mmim][dmp] P-T diagram x_1 = 0.6669 and x_2 = 0.2472. The solid line indicates the UNIFAC-IL prediction and the open circles represent experimental data (Wang, Wang *et al.* 2010). 1.34 %AARD was observed between the experimental and predicted total pressures. Figure adapted from (Roughton, Christian *et al.* 2012).

Overall, the UNIFAC-IL model shows good prediction of the experimentally observed VLE. As the experimental data used for model evaluation was not used to regress the UNIFAC-IL parameters, agreement between the model and experiments was not assured. The largest AARD between the experimental and predicted vapor composition values is observed for the 1-propanol-water-[emim][triflate] system with a value of 10.84%. The UNIFAC-IL predictions of azeotrope existence and location agree very well with the experimental data. Qualitatively, the shapes of the x-y curves are similar when comparing the UNIFAC-IL predictions and the experimental data. The P-T predictions showed very good agreement with experimental data, with the largest AARD value of 1.34% observed for the 2-propanol- water-[mmim][dmp] system. While the comparison to experimental data is limited, the results indicate that the UNIFAC-IL model will provide reasonable predictions for the azeotropes considered for simultaneous ionic liquid and separation process design. The two ionic liquids present in the experimental data are similar (or the same for [mmim][dmp]) to the designed ionic liquids for both azeotrope examples, suggesting that the UNIFAC-IL predictions for the designed ionic liquids will be reasonably accurate.

8.3 CAMD Results for Ionic Liquid Entrainers

Ionic liquid entrainers were designed for use with both the acetone-methanol and ethanol-water azeotropes. Candidates were found that either best matched the volume average solubility parameter value of each azeotropic mixture or the solubility parameter of the desired entrained component. The cation choices were limited to imidazolium and pyridinium to ensure that the designed ionic liquid could be used with the UNFAC-IL model. With the groups determined by CAMD, the groups were then constructed to make a feasible ionic liquid. The design candidates for the acetone-methanol azeotrope were 1-octyl-4-methylpyridinium trifluoromethane sulfonate ([ompy][triflate]) with a solubility parameter value of 21.2 MPa$^{1/2}$ and 1-butyl-3-methylimidazolium hexafluorophosphate ([bmim][PF$_6$]) with a solubility parameter value of 29.5 MPa$^{1/2}$. 1,3-dimethylimidazolium dimethylphosphate ([mmim][dmp]) with a solubility parameter value of 27.1 MPa$^{1/2}$ and 1,3-dimethylimidazolium tetrafluoroborate ([mmim][BF_4]) with a solubility parameter value of 32.6 MPa$^{1/2}$ were the design candidates for the ethanol-water azeotrope.

The UNIFAC-IL model was used to ensure that the azeotropes were broken by the designed ionic liquids and that the correct component was entrained by the ionic liquid. Existence of only one liquid phase was confirmed by the UNIFAC-IL model. The UNIFAC-IL model was also used to predict the minimum amount of ionic liquid needed to break the azeotrope at 101.325 kPa. The ionic liquid 1-ethyl-3-methyl trifluoromethane sulfonate ([emim][triflate]) has been shown experimentally to break both the acetone-methanol and ethanol-water azeotropes (Orchillés, Miguel *et al.* 2006; Orchillés, Miguel *et al.* 2010). Based on the predicted solubility parameter, [emim][triflate] would not be designed using the CAMD procedure for both azeotropes. The UNIFAC-IL model was used to predict the minimum amount of [emim][triflate] needed to break both azeotropes at 101.325 kPa. VLE calculations were used to calculate vapor compositions of components for each liquid composition for increasing ionic liquid concentrations from no ionic liquid present to the concentration where the azeotrope is just broken, defined as the minimum ionic liquid concentration needed to break the azeotrope. The ionic liquid composition was increased by 0.01 mol% and calculations were performed at each composition. The minimum ionic liquid concentrations required were used to screen the design candidates. For acetone-methanol, slightly more [emim][triflate] on a mole fraction basis was needed to break the azeotropes when compared to the designed ionic liquid [ompy][triflate]. The designed ionic liquid [bmim][PF_6] required a much higher concentration to break the acetone-methanol azeotrope when compared to the other design candidate and was eliminated from further consideration. Approximately the same amount of the design candidates [mmim][dmp] and [mmim][BF_4] were needed to break the ethanol-water azeotrope, so both ionic liquids were keep as entrainer candidates. The experimentally selected ionic liquid [emim][triflate] broke the ethanol-water azeotrope at a similar concentration to that of the design candidates. The results are summarized in Table 5. To illustrate the performance of the designed ionic liquid candidates and the experimentally selected ionic liquid, Figures 8.8 and 8.9 show the x-y diagrams for the acetone-methanol and ethanol-water systems with 10 mol% of each considered ionic liquid added. The candidate [ompy][triflate] shows much higher vapor mole fractions than the candidate [bmim][PF_6] at any given liquid mole fraction, indicating that [ompy][triflate] generates noticeably higher driving forces ($y_1 - x_1$) for separation. The driving forces generated by [ompy][triflate] are also slightly higher than the driving forces generated by the experimentally selected ionic liquid [emim][triflate]. For the ethanol-water system, both the candidate ionic liquids and the experimentally selected ionic liquid showed similar driving forces.

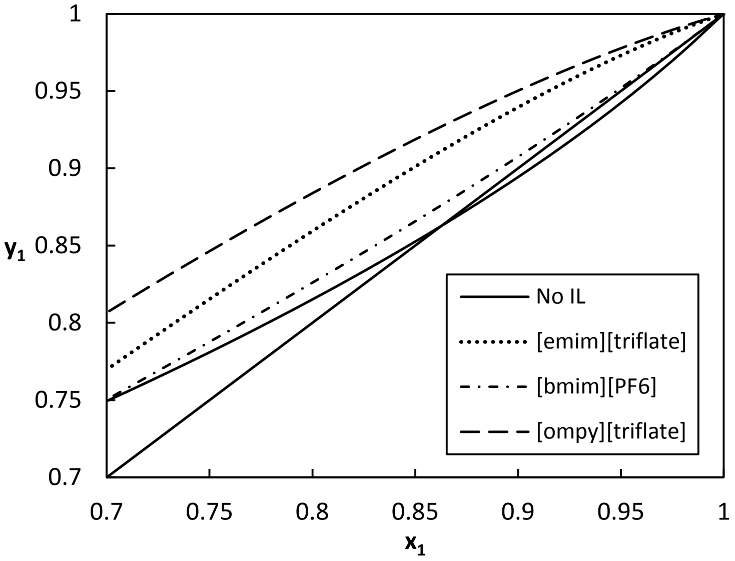

Figure 8.8 x-y diagram showing the performance of several ionic liquid entrainers on the acetone-methanol azeotrope at 101.325 kPa The concentration of all ionic liquid entrainers is set a 10 mol%. The 45 degree line is included to indicate where $y_1 = x_1$. Figure adapted from (Roughton, Christian *et al.* 2012).

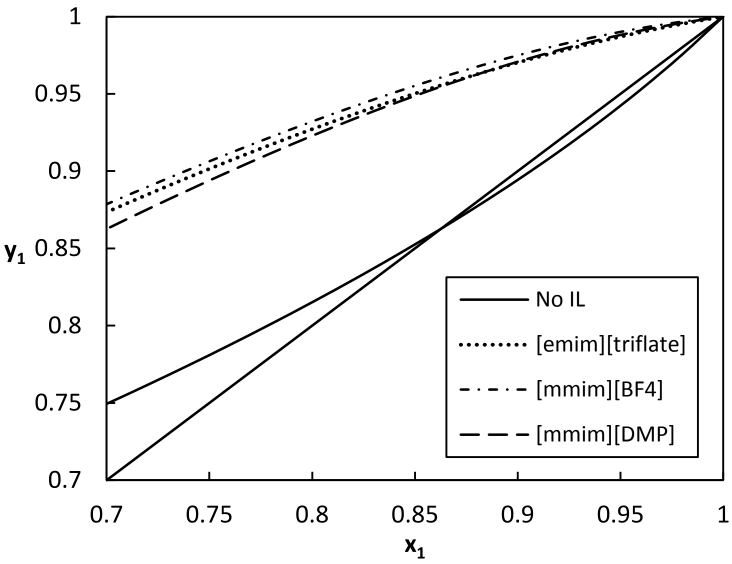

Figure 8.9 x-y diagram showing the performance of several ionic liquid entrainers on the ethanol-water azeotrope at 101.325 kPa The concentration of all ionic liquid entrainers is set a 10 mol%. The 45 degree line is included to indicate where $y_1 = x_1$. Figure adapted from (Roughton, Christian *et al.* 2012).

By designing the ionic liquid entrainer based on solubility parameter targets and screening based on the amount needed to break the azeotrope, ionic liquid candidates were identified that required minimal concentrations to break a given azeotrope. By requiring less ionic liquid, material inputs are reduced and energy requirements are reduced as less ionic liquid needs to be recovered. The ionic liquid [emim][triflate] appears to be a good candidate for breaking the ethanol-water azeotrope but does not have a predicted solubility parameter value that lies within the range of solubility parameter values that would be considered for the initial design step in the CAMD procedure. Although [emim][triflate] would not be chosen through the design process, the designed candidates both break the ethanol-water azeotrope with the same or similar minimum concentration. Design of ionic liquids for the example systems provided ionic liquid candidates that could break the azeotropes with concentrations less than or equal to the concentration of the experimentally selected ionic liquid [emim][triflate].

Table 8.4 Comparison of minimum amount of designed and experimentally selected ionic liquids required to break the acetone-methanol and ethanol-water azeotropes at 101.325 kPa Predictions were made using UNIFAC-IL model. Table adapted from (Roughton, Christian *et al.* 2012).

Azeotrope	Azeotropic Mixture Target	Entrained Component Target	Experimentally selected Ionic Liquid
Acetone-Methanol			
Target δ (MPa$^{1/2}$)	21.1	29.6	-
IL used	[ompy][triflate]	[bmim][PF$_6$]	[emim][triflate]
Predicted δ (MPa$^{1/2}$)	21.2	29.5	23.1
Minimum concentration to break azeotrope (mol%)	1.10	9.30	1.30
Ethanol-Water			
Target δ (MPa$^{1/2}$)	27.3	47.9	-
IL used	[mmim][dmp]	[mmim][BF$_4$]	[emim][triflate]
Predicted δ (MPa$^{1/2}$)	27.1	32.6	23.1
Minimum concentration to break azeotrope (mol%)	0.95	1.00	0.95

8.4 Design of Ionic Liquid-Based Azeotropic Separation Processes

Using the outlined procedure and specifications, distillation columns for the azeotrope mixtures were designed using both designed ionic liquid candidates and an experimentally selected ionic liquid. At a given ionic liquid flow rate, the minimum amount of stages needed to achieve the specified separation was determined. The driving force method with the proposed modified scaling was used an initial guess for the feed stage. The feed stage was then moved up and down to find the optimal feed stage in terms of energy requirements. In all cases, the optimal feed stage was at or near the feed stage proposed by the driving force method. The results for the ethanol-water-[mmim][dmp] system are given by Figure 8.10. The results indicate that use of the driving force method with the new proposed scaling can be used to design optimal or near-optimal distillation columns with a main feed and separate ionic liquid feed. The driving force method was originally proposed for a distillation column with only one feed. By comparing the columns with optimal feed stages at different ionic liquid flow rates, the flow rate and column configuration yielding the minimum stages and energy requirements was obtained for each system. The results for the ethanol-water-[mmim][dmp] system are given by Figure 8.11.

From the simulation results, optimal distillation columns in regards to minimal stages required and energy inputs were obtained for the methanol-acetone and ethanol-water systems using either designed entrainer candidates or an experimentally selected ionic liquid entrainer. The results are summarized in Table 8.5.

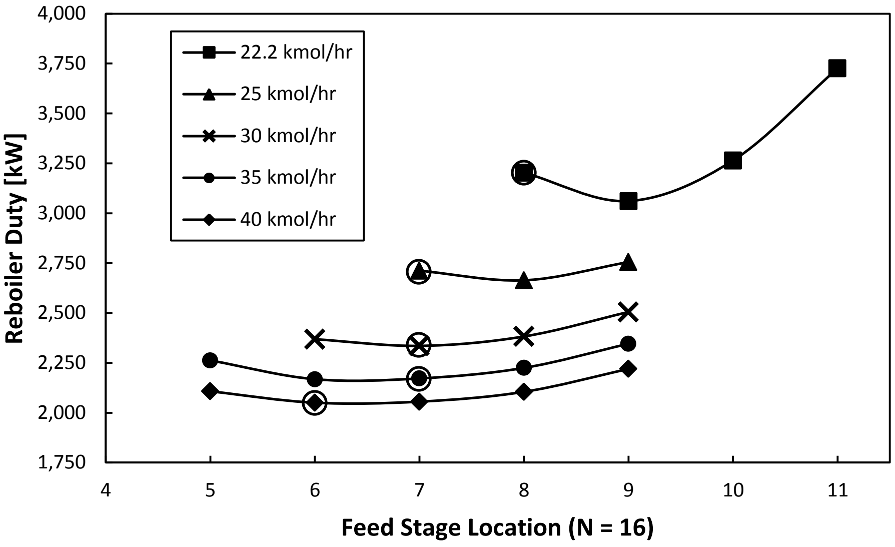

Figure 8.10 Reboiler heat duty as a function of feed stage location for separation of the ethanol-water azeotrope using various amounts of [mmim][dmp] as an entrainer The scaled feed stage location calculated by the driving force method is circled in the figure for each ionic liquid feed rate. The lines are drawn to guide the eyes. Figure adapted from (Roughton, Christian *et al.* 2012).

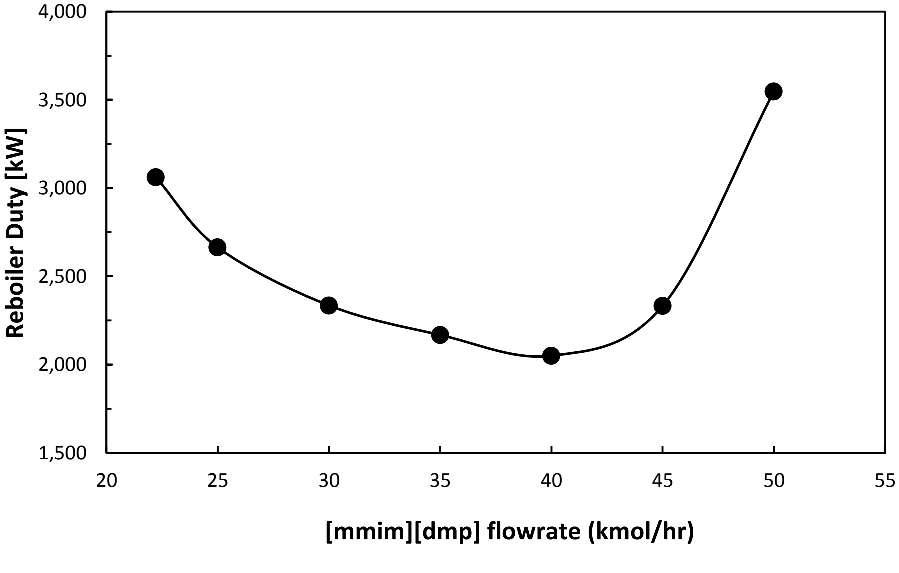

Figure 8.11 Reboiler heat duty as a function of ionic liquid flow rate for separation of the ethanol-water azeotrope using [mmim][dmp] as an entrainer Each point indicates the optimal column configuration in terms of energy requirements for the specified ionic liquid flow rate. The line is drawn to guide the eyes. Figure adapted from (Roughton, Christian *et al.* 2012).

Table 8.5 Simulation results for ionic liquid-based azeotropic separation processes Simulations were performed in ChemCAD. Table adapted from (Roughton, Christian *et al.* 2012).

	Acetone-Methanol-[emim][triflate]	*Acetone-Methanol-[ompy][triflate]**	*Ethanol-Water-[emim][triflate]*	*Ethanol-Water-[mmim][dmp]**	*Ethanol-Water-[mmim][BF_4]^*	*Ethanol-Water-[emim][BF_4]$^+$*
Distillation Column						
Entrainer flow rate [kmol/hr]	55.0	60.0	22.2	40.0	40.0	100/120
Number of stages	50	35	15	16	15	28/28
Feed stage	28	14	9	6	6	22/21
Reflux ratio	8.346	5.941	0.740	0.007	3.160	0.41/0.25
Reboiler Duty [kW]	8000	6039	2785	2046	3383	2994/2958
Flash Tank						
Temperature [K]		373.0		435.0		383.15/383.15
Heat duty [kW]		971		744		177/5
Stripper						
Number of stages		10		35		8
Air flow rate [kmol/hr]		500		375		479/579
Bottom temperature [K]		313.5		341.3		342.1/341.9
Total Energy Requirements [kW]		7010		2790		3171/2963

*Using azeotrope solubility parameter value as design target

^Using solubility parameter of entrained component as design target

$^+$Results from (Seiler, Jork *et al.* 2004)

For both systems, a designed ionic liquid was found to have significant energy savings in comparison to the experimentally selected ionic liquid. Based on the column simulation results, the ionic liquid candidates with the lowest energy requirements were kept and the other candidates were eliminated. The ionic liquid flow rates used in the simulation were selected based on minimizing energy requirements, resulting in different flow rates for the different ionic liquids. While the experimentally selected ionic liquid used lower flow rates, the energy requirements were higher for both azeotropic systems when compared to the final design candidates. For acetone-methanol, use of [ompy][triflate] provided the lowest energy requirements and reduced energy consumption by 24.5% (1961 kW) compared to the experimentally selected ionic liquid [emim][triflate]. As no other design candidate remained, [ompy][triflate] was selected as the final design candidate for the acetone-methanol system. Energy requirements for the ethanol-water system were lowest when using [mmim][dmp], reducing heat duty by 26.5% (739 kW) when compared to the experimentally selected ionic liquid [emim][triflate]. As the column using [mmim][dmp] required less energy than the other design candidate [mmim][BF_4], [mmim][dmp] was chosen as the final design candidate and [mmim][BF_4] was eliminated from consideration. Both [ompy][triflate] (Papaiconomou, Salminen *et al.* 2007) and [mmim][dmp] (Wang, Wang *et al.* 2010) have been previously synthesized and studied. The structures of [ompy][triflate] and [mmim][dmp] are shown in Figure 8.12 and Figure 8.13.

The column energy requirements were closer in value for the ethanol-water system than the acetone-methanol system, likely influenced by the fact that [mmim][dmp], [mmim][BF_4], and [emim][triflate] have similar maximum driving force values at the ionic liquid concentrations used. The minimum number of stages needed for the separation was found to be less for the methanol-acetone system using the designed ionic liquid than found when using the experimentally selected ionic liquid. The experimentally selected ionic liquid was able to achieve separation in one less stage than the final ionic liquid design candidate for the ethanol-water system, but the reduced capital cost would not offset the larger energy requirement. Due to the energy savings, the entire process including entrainer regeneration was simulated only for the systems using the final design candidate entrainers. The energy required for air flow into the stripper was neglected in calculation of the total energy requirements for the processes.

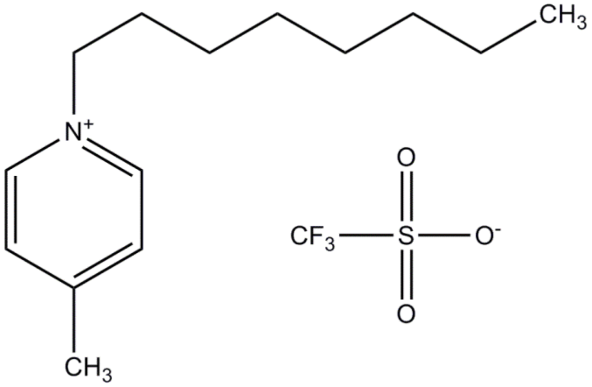

Figure 8.12 1-octyl-4-methylpyridinium trifluoromethane sulfonate ([ompy][triflate]) With a solubility parameter value of 21.2 MPa$^{1/2}$, the ionic liquid is the final design candidate for the acetone-methanol azeotrope.

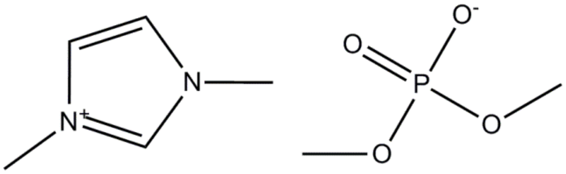

Figure 8.13 1,3-dimethylimidazolium dimethylphosphate ([mmim][dmp]) With a solubility parameter value of 27.1 MPa$^{1/2}$, the ionic liquid is the final design candidate for the ethanol-water azeotrope.

The results for the ethanol-water-[mmim][dmp] system were compared to previously published simulation results for ethanol-water separation using a conventional entrainer (1,2-ethanediol) and a experimentally selected ionic liquid entrainer (1-ethyl-3-methylimidazolium tetrafluoroborate [emim][BF_4]) (Seiler, Jork *et al.* 2004). The results for the experimentally selected ionic liquid are compared to the results for the designed ionic liquid candidates in Table 8.5. The separation process was the same as used in the current work and the number of stages in the distillation column was set at 28 for both the conventional and ionic liquid entrainers. Simulations were performed to calculate energy requirements at various entrainer concentrations. The optimal energy requirements were 3917 kW for the conventional entrainer and 2963 kW for the ionic liquid (Seiler, Jork *et al.* 2004). Comparison of the separation processes shows an energy savings of 28.8% (1127 kW) when using [mmim][dmp] instead of the conventional entrainer and an energy savings of 5.8% (173 kW) when using [mmim][dmp] over an experimentally selected ionic liquid. Due to inherent error in the UNIFAC-IL model, the calculated excess enthalpies may result in some error in the calculated energy requirements. Use of ionic liquids offers an alternative to conventional entrainers which may reduce energy requirements when separating azeotropic mixtures. By designing the ionic liquid structure to match a solubility parameter target range and further screening candidates by minimum concentration needed to break the azeotrope and column energy requirements, energy requirements in the resulting separation and entrainer regeneration processes are reduced compared to processes using ionic liquids that were not designed or selected using a CAMD procedure.

8.5 Prediction of Relevant Properties for in situ Extractive Fermentation

The data sets used to generate the models for partition coefficient of NDHD in ionic liquid (K_x) and toxicity of ionic liquid towards *E. coli* ($lnEC_{50}$) were too small to allow descriptor selection through use of Mallow's C_p. Alternatively, models were compared using the based on R^2-Q^2 value, with the model showing the minimum value being selected. R^2-Q^2 provides a measure of the difference between the fit and the predictive capability. Minimal differences are desired.

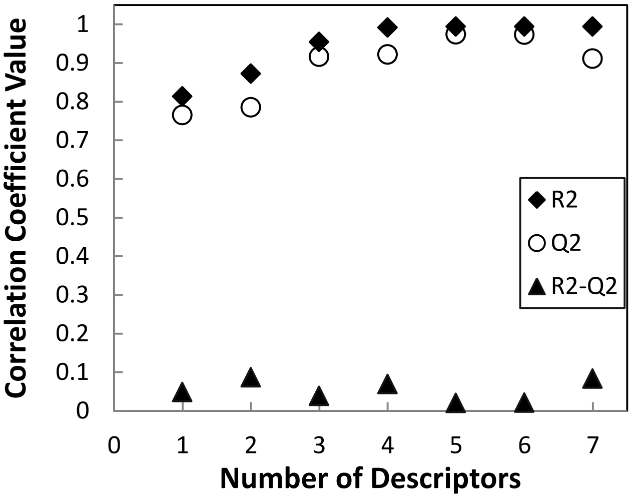

Figure 8.14 Comparison of correlation coefficient values belong to different model sizes for the partition coefficient model (K_x)

For the partition coefficient model, a model size of five showed the smallest R^2-Q^2 value (0.02) and was selected as the final model. The equation for the model is given by Equation 8.1. Four of the five descriptors selected describe the cation. All descriptors pass significance testing at a 99% confidence level. The model provides an excellent fit to the data and good predictive quality, with R^2 = 0.994 and Q^2 = 0.974.

$$K_x = 129.6\ {}^1\chi - 4631.5\ {}^1\xi - 139.7\ {}^1\chi^v + 2960.0\ {}^3\xi^v + 748.7\ {}^4\xi^{anion} + 1709.3$$

(Equation 8.1)

A model size of five was also selected for the toxicity model. Again, four of the five descriptors selected describe the cation structure. In comparison to the partition coefficient model, the toxicity model shows a much poorer fit (R^2 = 0.805). The predictive capability of the model is poor (Q^2 = 0.090) and thus use of the model for molecular design is questionable. The model is given by Equation 8.2. The use of different molecular descriptors and/or a non-linear model form are possible directions to pursue for improvement of the toxicity model.

$$lnEC_{50} = -180.5\ {}^{2}\xi + 2.01\ {}^{1}\chi^{v} + 129.2\ {}^{1}\xi^{v} - 192.6129.2\ {}^{4}\xi^{v} + 748.7\ {}^{1}\xi^{anion} + 16.8$$

(Equation 8.2)

8.6 CAMD RESULTS FOR IN SITU EXTRACTANTS

Design was limited to the cation and the anion was fixed to tris(perfluoroalkyl)trifluorophosphate (FAP). Furthermore, the cation class was limited to imidazolium based ionic liquids. Due to the questionable quality of the toxicity correlation, two different design cases were considered: (A) design with only a partition coefficient target and (B) design with both a partition coefficient target and a toxicity target. Tabu search was used to generate multiple candidates for both design cases. The top candidates for both cases A and B are compared in Figure 8.15.

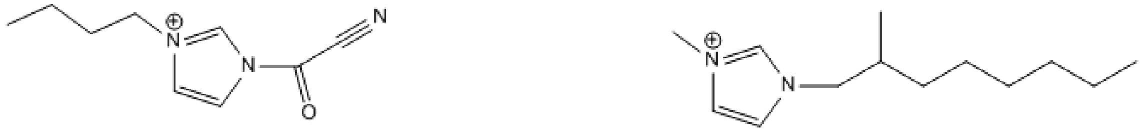

Design Case (A)

Objective function = 5.48x10^{-6}
MW = 206.3 g/mol
$lnEC_{50}$ = 2.67 ± 4.09
K_x = 50.1 ± 22.1

Design Case (B)

Objective function = 0.0022
MW = 209.6 g/mol
$lnEC_{50}$ = 3.82 ± 3.84
K_x = 50.7 ± 23.2

Figure 8.15 The best cation candidates for the design cases (A) and (B) For (A) and (B) the target was K_x = 50. Additionally, (B) had a target for $lnEC_{50}$ = 4. Prediction intervals are given for K_x and $lnEC_{50}$ values. The anion was set to FAP.

As seen from the prediction intervals in Figure 8.15, both design cases yield solutions with statistically similar property values and of similar size (*i.e.*, molecular weight). However, the large prediction intervals for the $lnEC_{50}$ values further exemplify the poor predictive quality of the model and the corresponding predictions are likely to be unreliable. Of interest is the observation that the inclusion of toxicity as a target prevented any polar groups from being included in the alkyl chain of the cation, where polar groups are present when only partition coefficient was used as a target.

9.0 RESULTS FOR LYOPHILIZED EXCIPIENT DESIGN

The following section presents the results for property models developed for CAMD of lyophilized excipients. Also included are the tuning and design results for the CAMD methods considered. Two main approaches were used to design excipients for lyophilized protein formulations: a vitrification approach with optimal glass transition temperatures and an overall reduction of aggregation approach to maintain *%Monomer* at 100% following lyophilization.

Section 9.1 presents the model results for various glass transition correlations. The molecular design results using tabu search are presented in Section 9.2. The experimental measurements observed for protein loss following lyophilization are detailed in Section 9.3. Sections 9.4-9.6 present and discuss the results for various post-lyophilization protein loss models. The tuning results for both tabu search and a genetic algorithm are given in Section 9.7. Finally, Section 9.8 contains the molecular design results using the post-lyophilization protein loss models with the tuned stochastic algorithms. Results are compared between optimization methods and also between the proteins included in the formulation.

9.1 GLASS TRANSITION TEMPERATURE PROPERTY MODELS

The R statistical program (R-Development-Core-Team 2010) was used for linear regression of the desired properties to the connectivity indices of the excipients in the training set. The model data was obtained from literature (Roos 1993). The carbohydrate excipients used in the model data set were monosaccharides (ribose, xylose, fructose, fucose, glucose, and sorbose), disaccharides (lactose, lactulose, melibiose, sucrose, and trehalose), oligosaccharides (raffinose), and sugar alcohols (maltitol, sorbitol, and xylitol). The leaps package in R (Lumley 2004) was used to conduct an exhaustive search to determine which combination of descriptors provided the lowest C_p value for each number of possible descriptors that could be used for the QSPR (ranging from one to twelve). A summary of the QSPRs developed in this work is provided in Table 9.1. The individual QSPRs are further detailed in the following subsections.

Table 9.1 Summary of glass transition-related QSPRs developed Figure adapted from (Roughton, Topp *et al.* 2012).

QSPR	Number of Descriptors Selected	R^2
T_g	9	0.998
T_g’	6	0.994
T_m’	7	0.997
k	9	0.998

9.1.1 QSPR for Glass Transition Temperature of Anhydrous Solute

The glass transition temperature of the anhydrous solute provides an indication of the stability of the carbohydrate excipient during storage conditions. In addition to being used as a criterion for storage stability, T_g is used in the calculation of the excipient concentration in a maximally freeze-concentrated matrix.

The correlation developed for the T_g of carbohydrate excipients is:

$$T_g(°C) = -243.13\ {}^0\chi + 1314.26\ {}^1\chi + 184.37\ {}^2\chi - 1444.52\ {}^1\chi^v - 270.82\ {}^2\chi^v + 6028.51\ {}^0\xi - 12674.4\ {}^1\xi - 6833.65\ {}^2\xi + 29314.02\ {}^2\xi^v - 1539.27$$

(Equation 9.1)

Equation 9.1 provides a good fit for the experimental measurements, providing a coefficient of determination (R^2) value of 0.998. The predicted T_g values are compared to the experimental values using a parity plot in Figure 9.1.

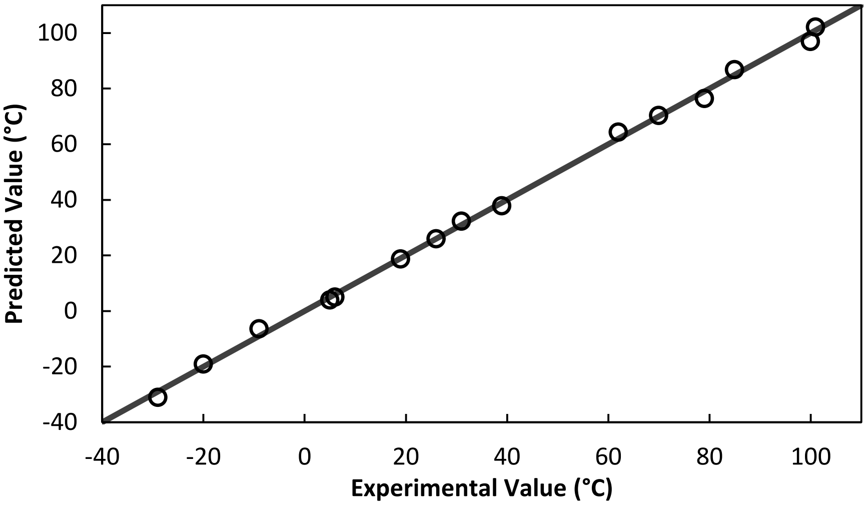

Figure 9.1 Comparison of measured experimental values to QSPR predicted values for the glass transition temperature of the anhydrous solute (T_g) The y=x line indicates were predicted = experimental. Figure adapted from (Roughton, Topp et al. 2012).

9.1.2 QSPR for Glass Transition Temperature of Maximally Concentrated Solute

In addition to being used as a criterion for ensuring formation of a maximally freeze-concentrated glass matrix, the glass transition temperature of the maximally concentrated solute (T_g’) is used in the calculation of the excipient concentration in the glass matrix.

The correlation developed for the T_g’ of carbohydrate excipients is:

$$T_g'(°C) = 40.79\ {}^0\chi + 16.63\ {}^2\chi - 70.27\ {}^0\chi^v - 373.79\ {}^1\xi - 815.24\ {}^2\xi + 2028.90\ {}^2\xi^v + 7.12 \qquad \text{(Equation 9.2)}$$

Equation 9.2 provides a good fit for the experimental measurements, providing an R^2 value of 0.994. The predicted T_g’ values are compared to the experimental values using a parity plot in Figure 9.2.

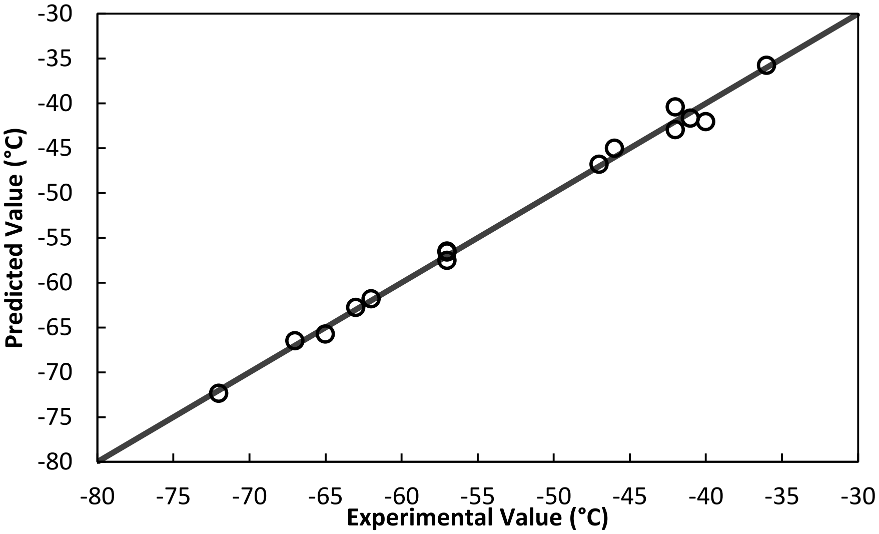

Figure 9.2 Comparison of measured experimental values to QSPR predicted values for the glass transition temperature of the maximally freeze-concentrated solute (T_g') The y=x line indicates were predicted = experimental. Figure adapted from (Roughton, Topp et al. 2012).

9.1.3 QSPR for the Melting Point of Ice

The melting point of ice represents the onset of ice formation during the freezing part of the lyophilization process. The concentrated solution must be annealed between T_g' and T_m' to ensure that the resulting freeze-concentrated glass matrix is maximally concentrated.

The correlation developed for the T_m' of carbohydrate excipients is given below:

$$T_m'(°C) = 65.63\ {}^0\chi + 79.76\ {}^1\chi + 14.73\ {}^2\chi - 175.32\ {}^0\chi^v - 607.09\ {}^1\xi + 1591.25\ {}^0\xi^v + 442.48\ {}^1\xi^v - 759.39$$

(Equation 9.3)

Equation 9.3 provides a good fit for the experimental measurements, providing an R^2 value of 0.997. The predicted T_m' values are compared to the experimental values using a parity plot in Figure 9.3.

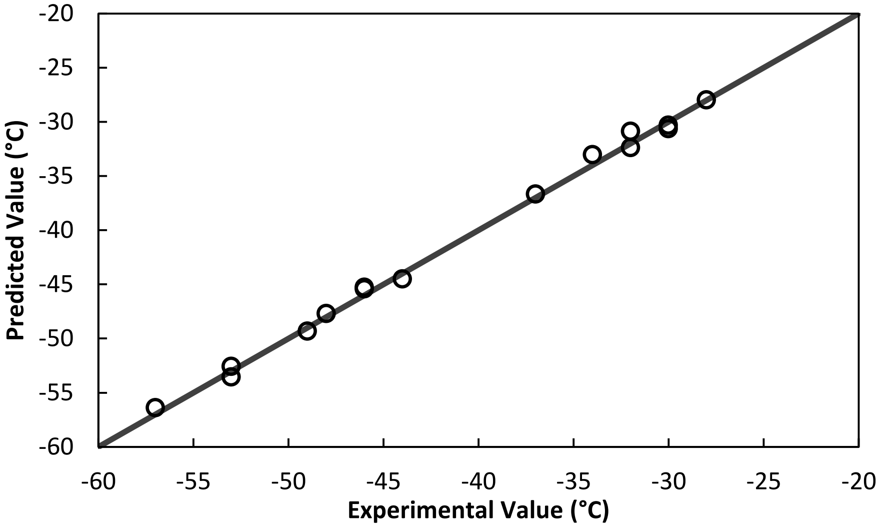

Figure 9.3 Comparison of measured experimental values to QSPR predicted values for the melting point of ice (T_m') The y=x line indicates were predicted = experimental. Figure adapted from (Roughton, Topp et al. 2012).

9.1.4 QSPR for Gordon-Taylor Constant

The Gordon-Taylor constant is used in the calculation of the solute concentration from the Gordon-Taylor equation. The Gordon-Taylor constant for a compound is usually derived from glass transition measurements (Roos 1993). It should be noted that through the descriptor selection method, the same connectivity indices were found to provide the best model as those used in the model for glass transition temperature of the anhydrous solute.

The developed correlation for the Gordon-Taylor constant of carbohydrate excipients is given below:

$$k = -7.13\ {}^{0}\chi + 38.50\ {}^{1}\chi + 5.45\ {}^{2}\chi - 42.26\ {}^{1}\chi^{v} - 8.03\ {}^{2}\chi^{v} + 177.64\ {}^{0}\xi - 371.72\ {}^{1}\xi - 200.43\ {}^{2}\xi + 858.52\ {}^{2}\xi^{v} - 42.00$$

(Equation 9.4)

Equation 9.4 provides a good fit for the experimental measurements, providing an R^2 value of 0.998. The predicted k values are compared to the experimental values using a parity plot in Figure 9.4.

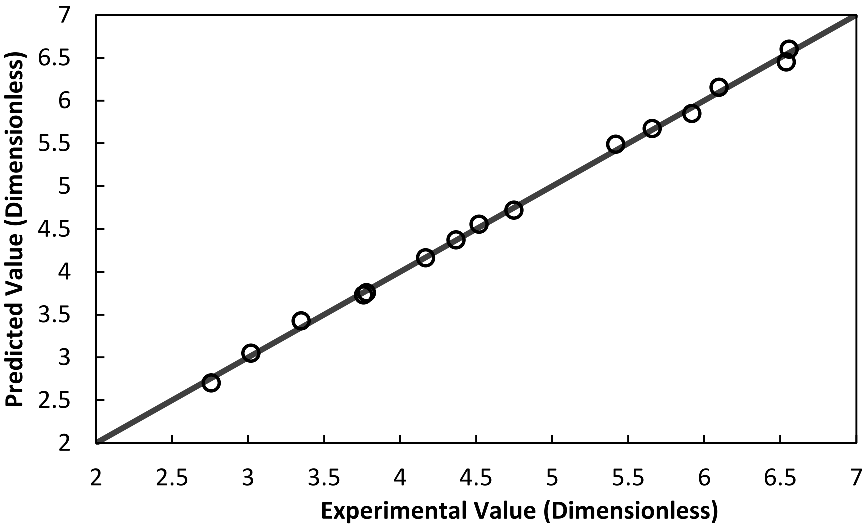

Figure 9.4 Comparison of measured experimental values to QSPR predicted values for the Gordon-Taylor constant (k) The y=x line indicates were predicted = experimental. Figure adapted from (Roughton, Topp et al. 2012).

9.2 Results for Optimal Glass Former Design

According to vitrification theory, a protein stabilizing excipient should be able to form a glass during lyophilization and subsequent storage of the therapeutic product. The glass transition temperature of the maximally freeze-concentrated solute and the melting point of ice for a carbohydrate excipient must be high enough to be feasibly reached during the lyophilization process. The protein drug product must first be annealed at a temperature between T_g' and T_m and then reduced below T_g' to yield a maximally freeze-concentrated matrix (Roos 1997). The melting temperature of ice is higher than the glass transition temperature of the maximally concentrated solute. The glass transition temperature of the anhydrous solute must be sufficiently high such that the carbohydrate remains a glass during storage of the protein drug product. A common heuristic is that the storage temperature of an amorphous drug formulation should be 50°C below the anhydrous glass transition temperature (Costantino and Pikal 2004). For a formulation to be stored at room temperature, a T_g of at least 80°C is desired. This criterion is very important, as more than 70% of commercial lyophilized products cannot be stored at room temperature and must be refrigerated to maintain stability, complicating the use of the drugs (Costantino and Pikal 2004). All three phase transition temperatures are used along with the Gordon-Taylor constant to determine the excipient concentration (weight fraction) of a maximally freeze-concentrated matrix, without protein present. A higher excipient concentration corresponds to lower residual water in the matrix, which lowers the mobility of the protein and thus reduces the potential for aggregation. No target is placed on the actual value of the Gordon-Taylor constant. The Gordon-Taylor constant is calculated only for use in subsequent calculation of the excipient concentration in a maximally freeze-concentrated matrix.

Table 9.2 Property values of candidate carbohydrate excipients designed using tabu search Prediction intervals for the properties predicted by the QSPR models were calculated at a 95% level. A lower objective function score indicates a better match for the target property values. Table is adapted from (Roughton, Topp *et al.* 2012).

Property	Candidate 1	Candidate 2	Candidate 3
T_g	100.9±12.7°C	99.8±15.0°C	90.3 ± 20.6°C
T_g’	-32.6±6.5°C	-33.1±6.7°C	-31.7± 5.0°C
T_m’	-24.8±3.2°C	-23.7±3.5°C	-24.1 ± 4.1°C
k	6.76± 0.37	6.73 ± 0.44	6.46 ± 0.61
C_g’	0.838	0.838	0.845
MW	373.3 g/mol	373.3 g/mol	373.3 g/mol
Obj function	0.00800	0.01367	0.01373

The described molecular design framework was employed using the PD program previously used to design various molecules, including dental polymers (Eslick, Ye et al. 2009) and ionic liquids (McLeese, Eslick *et al.* 2010).The results for the three best excipient candidates are given in Table 9.2, determined by the solutions with the lowest objective function scores. Seven total candidates were generated. Error was calculated using prediction integrals at a 95% level for the property values predicted using the QSPR models. The structures of the proposed carbohydrate excipients are given in Figures 9.5-9.7.

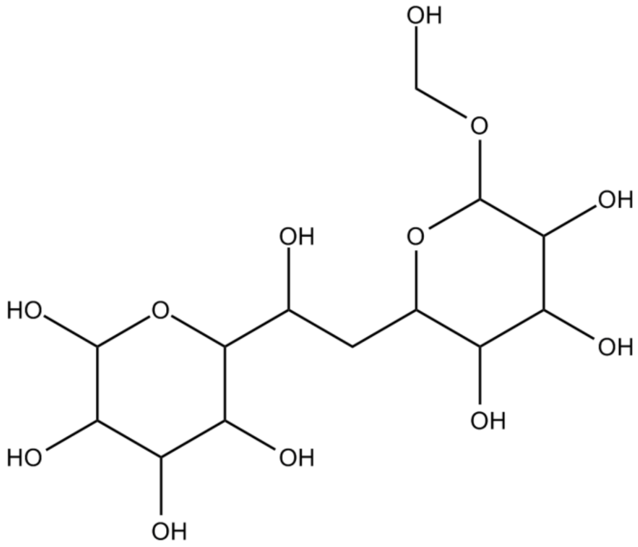

Figure 9.5 Optimal carbohydrate excipient candidate 1 proposed by CAMD using tabu search The objective function score is 0.00800. Figure adapted from (Roughton, Topp et al. 2012).

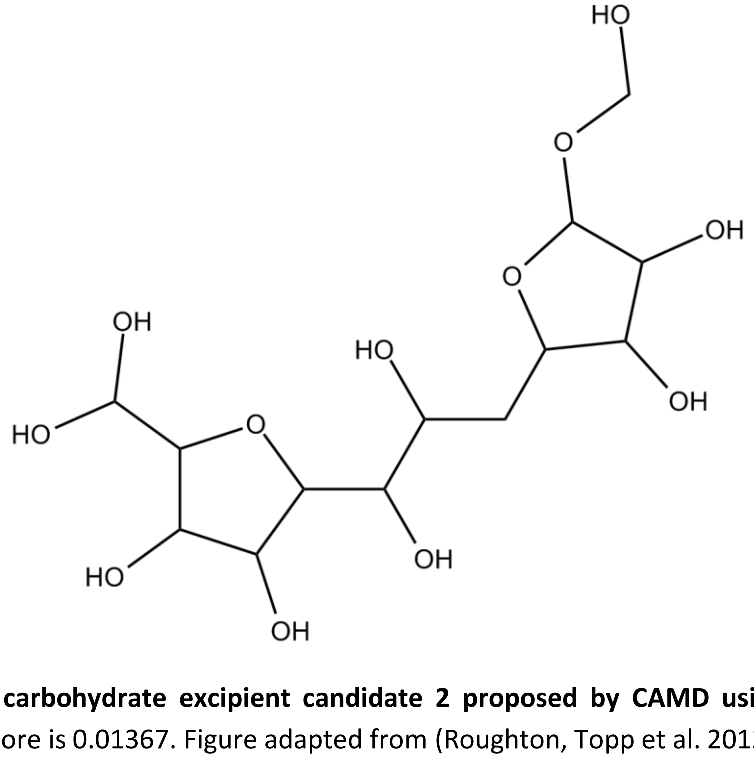

Figure 9.6 Optimal carbohydrate excipient candidate 2 proposed by CAMD using tabu search The objective function score is 0.01367. Figure adapted from (Roughton, Topp et al. 2012).

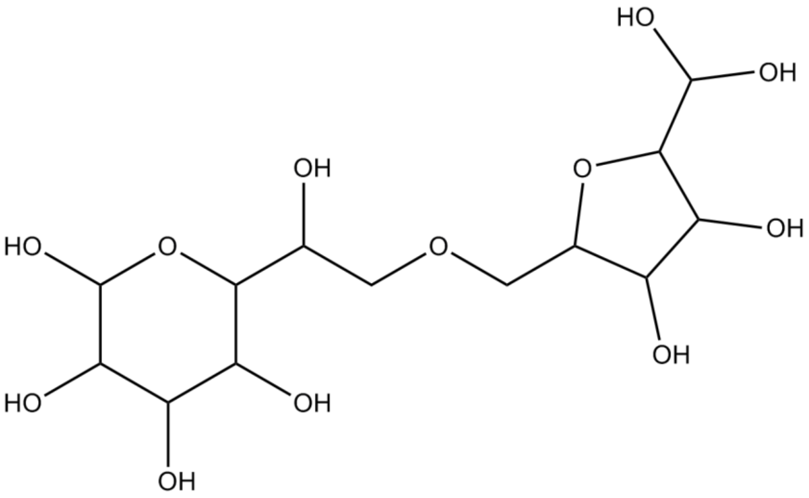

Figure 9.7 Optimal carbohydrate excipient candidate 3 proposed by CAMD using tabu serach The objective function score is 0.01373. Figure adapted from (Roughton, Topp et al. 2012).

The proposed excipients are similar to disaccharide and oligosaccharide molecular topologies. Candidates 1, 2, and 3 are isomers. The property values of the proposed excipients show that the computationally designed excipient molecules should stabilize protein formulations. Protein mobility should be limited due to the high solute concentration of the maximally freeze-concentrated matrix. The values for the glass transition temperature of the maximally freeze-concentrated solute and the melting point of ice are high enough that they can be reached during lyophilization. Additionally, the gap in the two temperatures is large enough to allow for annealing between the two temperatures, ensuring that the maximum solute concentration is reached in the freeze-concentrated matrix. The high glass transition temperatures of the anhydrous solute are high enough that drying and long term storage conditions will not change the desired glass structure of the protein formulation.

The prediction intervals show that for all three candidates, all four properties predicted by the QSPR models have overlapping prediction intervals. Due to the overlapping prediction intervals, the predicted property values of all the candidates are not statistically different; all three candidates are valid solutions for the optimization problem. Use of tabu search was able to provide several optimal excipient candidates with statistically similar property values, where a deterministic method would have only provided one candidate. The prediction intervals for the glass transition temperature of the anhydrous solute were large for all three candidates. The large magnitude of the prediction interval is likely due to the target value being close to the upper limit of the property data used to build the correlation.

One should note that since not all possible properties of importance for an excipient have been included, these structures should be considered candidates for protein drug excipients, and not finalized designs to be immediately utilized. Since all of the structures designed in this work are similar to disaccharides, it is likely that they can be synthesized. However, further studies would be required to ensure that the excipients themselves exhibit sufficient properties to be used in protein drug formulations.

9.3 Experimental Results for Post-Lyophilization Protein Loss

Experimental studies were performed in two rounds. The first round was focused on creating a dataset for modeling *%Monomer* as a function of protein structure. Accordingly, a large amount of proteins were considered and fewer excipients. The second round was focused on creating a dataset for correlation of *%Monomer* to excipient structure. Therefore, a large amount of excipients were considered with a small set of proteins.

It is noted here that the experiments for the first round were not performed by the author and were instead conducted by Lavanya K. Iyer at Purdue University. The methods and procedures used were the same as those used by the author and described in Section 3.0. The results and discussion arising from the experiments is included as the data was used to build the corresponding models for *%Monomer* as a function of protein structure.

9.3.1 Experimental Results for Data Set Concerning Protein Structure

For the fifteen proteins and five lyophilized formulations studied here, aggregation varied with protein, with formulation and with the analytical method used to assess aggregation (see Table F.1, Appendix F). The proteins can be grouped according to aggregation tendency. Five proteins (lysozyme, ovalbumin, cytochrome C, α-amylase, BSA) showed high aggregation tendency across the formulation types as indicated by low (< 80%) recovery of monomeric protein (*%Monomer*) by SEC, high aggregation index (> 100) and/or the presence of high molecular weight bands on SDS-PAGE. Six proteins (RNAse A, α-chymotrypsinogen, ConA, α-lactoglobulin, SOD, trypsin inhibitor) showed low aggregation tendency using these metrics, while the remaining four proteins (myoglobin, DNAse I, catalase, b-lactoglobulin) showed intermediate aggregation tendency. Greater than 100% recovery of monomeric protein by SEC was observed for some samples and could reflect incomplete separation of aggregate from monomeric protein or protein unfolding. While the assignment of proteins to these groups is somewhat arbitrary, it is clear that the proteins selected show a range of aggregation propensities on lyophilization. The data set is therefore suitable for assessing the effects of protein structure on lyophilization-induced aggregation within the parameter space defined by their structural descriptors. Note that, since the largest protein in the data set (BSA, 66 kD) is considerably smaller than monoclonal antibodies, these and other large proteins are not expected to be well-described by the correlations developed here.

With regard to formulation, those containing buffer, sucrose or glycine all produced aggregates following lyophilization for some of the proteins studied (see Table F.1, Appendix F). Compared to these excipients, urea formulations produced a greater extent of aggregation for a greater number of proteins, as expected for this denaturant (see Table F.1, Appendix F). Formulations containing Gdn HCl showed no retention of monomeric protein by SEC for 11 of the 15 proteins, and pellets and/or high molecular weight bands on SDS-PAGE for 8 of 15. Because the observed extent of aggregation was very high and relatively insensitive to protein structure in Gdn HCl formulations, this formulation was omitted in developing correlations. The correlations thus were developed using the four remaining excipients (i.e., buffer, sucrose, glycine or urea).

Of the three methods used to assess aggregation (SDS-PAGE, AI, SEC), only AI and SEC were used quantitatively; therefore, only results from these two methods can be used to develop quantitative correlations with protein structural descriptors. AI values were not considered quantitatively reliable. For example, some formulations for proteins such as concanavalin A, cytochrome-c, β-lactoglobulin and trypsin inhibitor showed large AI values but had large errors. In other cases, proteins with low AI values showed loss of monomeric protein by SEC and formation of a pellet on SDS-PAGE (*e.g.*, catalase in urea, Table F.1, Appendix F). This may be due to the formation of insoluble precipitates that settle out of solution and are not detected on UV. Furthermore, RNase, lysozyme α–chymotrypsinogen and many other proteins did not show significant differences in AI values across formulations. As a result, correlations were developed based on the *%Monomer* as measured by SEC and AI values were not used further.

9.3.2 Experimental Results for Data Set Concerning Excipient Structure

SEC chromatographs were collected for BSA and RNAse A with all excipients considered and for α-amylase, ovalbumin and trypsin inhibitor for a subset of carbohydrate excipients. Peak areas were used to calculate percent monomer remaining after lyophilization (%Monomer). Values ranged from 88.2 – 99.8% for α-amylase, 82.6 – 95.9% for BSA, 92.5 – 99.6% for ovalbumin, 81.0 – 102.4% for RNAse A and 86.5 – 101.2% for trypsin inhibitor. All values that exceeded 100% had standard errors of mean (SEM) values that indicated the value was not statistically different than 100%, with the exception of rhamnose with trypsin inhibitor (111.1 ± 0.8%). Due to the lack of physical meaning and the extreme difference (9.9%) between the value for rhamnose and the next highest formulation, the rhamnose-trypsin inhibitor data point was considered an outlier and excluded from the universal model building data set. SEC results are summarized in Table F.2 (see Appendix F).

The excipients showing the best stabilization were glucose with α-amylase (99.8 ± 2.5%), α-methylglucopyranoside with BSA (95.9 ± 0.6%), sorbitol with ovalbumin (99.6 ± 0.4%) and with trypsin inhibitor (101.2 ± 2.1%) and psicose with RNAse A (102.4 ± 2.6%). Maltitol, a sugar alcohol, had low stability values for all proteins when compared to other excipient choices: 93.5 ± 0.5% for α-amylase, 85.9 ± 2.3% for BSA, 92.5 ± 0.9% for ovalbumin, 86.6 ± 1.0% for RNAse A and 91.2 ± 0.3% for trypsin inhibitor. Raffinose provided poor protection for α-amylase (91.3 ± 4.1%) and trypsin inhibitor (86.5 ± 2.2%). The sugar alcohol mannitol provided poor protection for BSA (82.6 ± 1.1%), RNAse A (85.3 ± 1.7%) and trypsin inhibitor (88.9 ± 3.5%). There was no consensus best or worst excipient choice.

SDS-PAGE results provided qualitative verification of the presence of aggregates following lyophilization (see Table F.3, Appendix F). As noted in the previous subsection, use of AI as a quantitative tool was not pursued.. The presence of aggregates was halted under reducing conditions for ovalbumin with all formulations, suggesting that aggregate formation is due at least in part to formation of disulfide bridges. All lyophilized formulations evaluated by pxrd showed that the resulting solid was largely amorphous (See Figure F.1, Appendix F).

9.4 Post-Lyophilization Protein Loss Models: As a Function of Protein Structure

Two methods were used to develop correlations relating protein descriptors to percent monomer retained following lyophilization: exhaustive search and forward selection. For both methods, the descriptor set used to generate correlations for each formulation was comprised of physical descriptors, AGGRESCAN descriptors and PASTA descriptors. The following subsections detail and compare the results for each method.

9.4.1 Exhaustive Search Method

The exhaustive search method was performed using all available descriptors for each formulation. Good fits, as determined by minimum C_p scores, were obtained with model sizes between eight and twelve descriptors (see Table 9.3). The descriptors selected for each formulation are listed in Table 9.3, together with statistical measures of goodness-of-fit (R^2) and predictive power (Q^2 and R^2-Q^2).

Table 9.3 Descriptors selected using an exhaustive search method with model size selected by minimizing C_p score Table adapted from (Roughton, Iyer *et al.* 2013).

	Model	**Descriptors Selected**					
Formulation	**Size**	**Physical**	**AGGRESCAN**	**PASTA**	R^2	Q^2	R^2 - Q^2
Buffer[a]	12	%α-helix, %β-sheet, MW, # S-S, # free SH, T_m	a3vSA, THSA	E_{min}, E_{avg}, $(E/L)_{min}$, Peaks	1.000	0.999	0.001
Urea	10	apolar, pI, # S-S, T_m	TA, Na4vSS	E_{avg}, L_{avg}, $(E/L)_{min}$, $(E/L)_{avg}$	0.998	0.976	0.022
Sucrose	9	%β-sheet, MW, pI, T_m	a3vSA, NnHS, THSA, TA	Peaks	0.999	0.987	0.012
Glycine	8	%α-helix, %β-sheet	NnHS, AATr, THSAr, Na4vSS	E_{avg}, Peaks	0.982	0.805	0.176

[a] Buffer used in the formulation was potassium phosphate buffer (20 mM, pH 7.4)

In general, the descriptors selected differed from formulation to formulation. Across all formulations, each descriptor type was selected with similar frequencies: physical descriptors were selected 16 times, AGGRESCAN descriptors were selected 12 times and PASTA descriptors were selected 11 times. No single descriptor was selected for all formulations. The most commonly selected descriptors were *% ⍰-*

sheet, T_m, E_{avg}, and *Peaks*, which were all selected for three of the four formulations. At least one descriptor of each type was selected for each formulation.

The correlations for all four formulations had (R^2-Q^2) < 0.20 and R^2 values close to 1, indicating that they provide a reasonable tool for predicting the percent retained monomeric protein after lyophilization within each formulation type. The correlation for the buffer formulation had the best fit and best predictive power, having the highest R^2 and Q^2 values and the lowest (R^2-Q^2) values. The correlation for the glycine formulation provided the poorest fit and lowest Q^2 value, and also provided the poorest predictive power as indicated by the largest (R^2-Q^2) value. A summary of the regression for the four formulations, together with values of the regression coefficients, is presented in Table 9.4.

Table 9.4 Correlation results for all four formulations Descriptors were selected via exhaustive search with C_p evaluation. Table adapted from (Roughton, Iyer *et al.* 2013).

Formulation	Descriptor	Coefficient Value	Standard Error (p-value[a]
Buffer[b]	(Intercept)	-0.25	0.48 $^{(0.65)}$
	% α-helix	-0.37	0.01 ***
	% β-sheet	-0.17	0.01 **
	MW	-0.53	0.01 ***
	# S-S	-0.88	0.02 ***
	# free SH	-13.68	0.11 ***
	T_m	-0.50	0.01 ***
	a3vSA	155.36	2.70 ***
	THSA	-0.07	0.03 $^{(0.13)}$
	E_{min}	-16.25	0.30 ***
	E_{avg}	3.27	0.31 **
	$(E/L)_{min}$	-53.63	0.34 ***
	Peaks	11.23	0.05 ***
Urea	(Intercept)	164.10	13.07 ***
	apolar	4.66E-03	1.57E-04 ***
	pI	-7.16	0.80 ***
	# S-S	5.85	0.38 ***
	T_m	-2.17	0.09 ***
	TA	-0.32	0.08 *
	Na4vSS	5.13	0.47 ***
	E_{avg}	12.53	1.64 **
	L_{avg}	6.37	0.59 ***
	$(E/L)_{min}$	-338.10	17.14 ***
	$(E/L)_{avg}$	260.90	20.63 ***
Sucrose	(Intercept)	159.17	2.77 ***
	% β-sheet	0.69	0.03 ***
	MW	-2.84	0.08 ***
	pI	-0.84	0.25 *
	T_m	0.62	0.03 ***
	a3vSA	686.56	17.31 ***
	NnHS	-19.03	0.49 ***
	THSA	1.69	0.09 ***
	TA	-2.44	0.06 ***
	Peaks	3.89	0.20 ***
Glycine	(Intercept)	387.91	19.91 ***
	% α-helix	-0.65	0.11 ***
	% β-sheet	-0.53	0.17 *
	NnHS	-23.98	1.88 ***
	AATr	-2326.82	162.79 ***
	THSAr	2247.68	155.16 ***
	Na4vSS	3.04	0.31 ***
	AvgE	13.64	1.33 ***
	Peaks	-3.73	0.60 ***

[a] Significance codes for the p-values are: *** for < 0.001, ** for < 0.01, * for < 0.05

[b] Buffer used in the formulation was potassium phosphate buffer (20 mM, pH 7.4)

9.4.2 Forward Selection Method

Forward selection was also used to build correlations using all available descriptors. The computational package used for forward selection used AIC for descriptor selection; however, AIC yields equivalent models to C_p for linear correlations (Wasserman 2004), resulting in no discrepancy between descriptor selection between the forward search and exhaustive search methods. Due to the nature of the selection method, the final correlations differ in the number of descriptors selected (see Table 9.5). Physical descriptors were selected most frequently with this method, accounting for 9 out of the 11 descriptors selected (see Table 9.5). Only physical descriptors were selected for urea and sucrose formulations and four out of the five descriptors selected for the buffer formulation were physical descriptors. The most commonly selected descriptor was *pI*, which was selected first for the buffer and sucrose formulations and second for the urea formulation. The early selection of *pI* indicates that this descriptor provides a superior fit to the experimental data for the buffer and sucrose formulations and a very good fit for the urea formulation when compared to the other descriptors.

Table 9.5 Descriptors selected using a forward search method with AIC evaluation Numbering indicates order in which descriptors were selected. No emphasis indicates physical descriptors and bold text indicates AGGRESCAN descriptors. No PASTA descriptors were selected. Table adapted from (Roughton, Iyer *et al.* 2013).

	Descriptors Selected					**Regression Performance**		
Formulation	**1**	**2**	**3**	**4**	**5**	**R^2**	**Q^2**	**R^2 - Q^2**
Buffer[a]	pI	T_m	%β-sheet	%α-helix	**THSA**	0.74	0.16	0.58
Urea	# free SH	pI	T_m	-	-	0.54	0.11	0.43
Sucrose	pI	%β-sheet	-	-	-	0.57	0.19	0.38
Glycine	**a3vSA**	-	-	-	-	0.14	-0.28	0.42

[a]Buffer used in the formulation was potassium phosphate buffer (20 mM, pH 7.4)

With forward selection, all of the (R^2-Q^2) values were large and no correlation provided a good fit to the data, as indicated by the low R^2 values. The correlation for the buffer formulation had the highest number of descriptors and yielded the highest R^2 value. However, the predictive power of the correlation was unsatisfactory and provided the largest (R^2-Q^2) value among the four formulations. The sucrose formulation provided a slightly higher R^2 value than the urea formulation, despite using one less descriptor. The correlation for the sucrose formulation had the lowest (R^2-Q^2) value among the correlations generated by forward selection.

9.4.3 Comparison of methods

Models generated by exhaustive search were superior to those generated by forward selection, having better fits and greater predictive power as indicated by the higher R^2, higher Q^2 and lower (R^2-Q^2) values (compare Tables 9.3 and 9.5). Forward selection is less computationally expensive when compared to exhaustive search. For development with models that involve large sets of possible descriptors, use of exhaustive search may be infeasible due to computation requirements. However, the time needed for descriptor selection was comparable for both methods using the descriptor set in this model. Additionally, the results indicate that use of a forward search is insufficient in developing a predictive model with sufficient accuracy. As a result, the forward selection method was not pursued and models generated by exhaustive search are emphasized in the results and discussion that follow for th*e %Monomer* model as a function of protein structure. Only exhaustive search was used for development of the %Monomer model as a function of excipient structure (see Section 9.5).

9.4.4 Predictive Power of Correlations

Within a formulation, correlations showed good fits (R^2>0.98) and satisfactory predictive power (R^2-Q^2<0.2) using the exhaustive search method (see Table 9.3). Parity plots comparing the predicted percentage of monomeric protein to the experimental value are shown in Figure 9.8. Good agreement between predicted and actual values is observed for all four formulations, with the greatest deviation observed for the glycine formulation. The data for the urea formulation is spread fairly evenly and validation resulted in a high Q^2 value. For the other formulations, one protein had a substantially lower observed and predicted percent monomer values than the other proteins. However, this outlying observation resulted in lower Q^2 values only for the glycine formulations, as high prediction error was found for the outlier when the point was left out during cross-validation. High Q^2 values were obtained for both the buffer and sucrose formulations, despite the outlier. The results suggest that the descriptors selected for the buffer and sucrose formulation are able to account for the structural differences in the outlying protein sufficiently, yielding a low prediction error when the protein was left-out during cross-validation.

9.4.5 Performance of Individual Descriptor Sets

The models presented in Tables 9.3-9.5 were generated by pooling all of the available descriptors from three descriptor sets: (i) physical descriptors, (ii) AGGRESCAN descriptors, (iii) PASTA descriptors. Correlations were also developed for each individual descriptor set in isolation, using the exhaustive search method (data not shown). At small model sizes, physical descriptors provided the best fit for the buffer, urea and sucrose formulations. The glycine formulation showed similar fits for model sizes of one descriptor, regardless of the descriptor set used. At larger model sizes, no single descriptor set could provide a fit comparable to that given by pooling all available descriptors.

Overall, physical descriptors performed better across all model sizes than the other individual descriptor sets. Thus, while reasonable fits could be obtained using only one descriptor set in isolation ($R^2 \approx 0.7$-0.8; data not shown), pooling the descriptors provided better fits ($R^2 \geq 0.98$; Table 9.3).

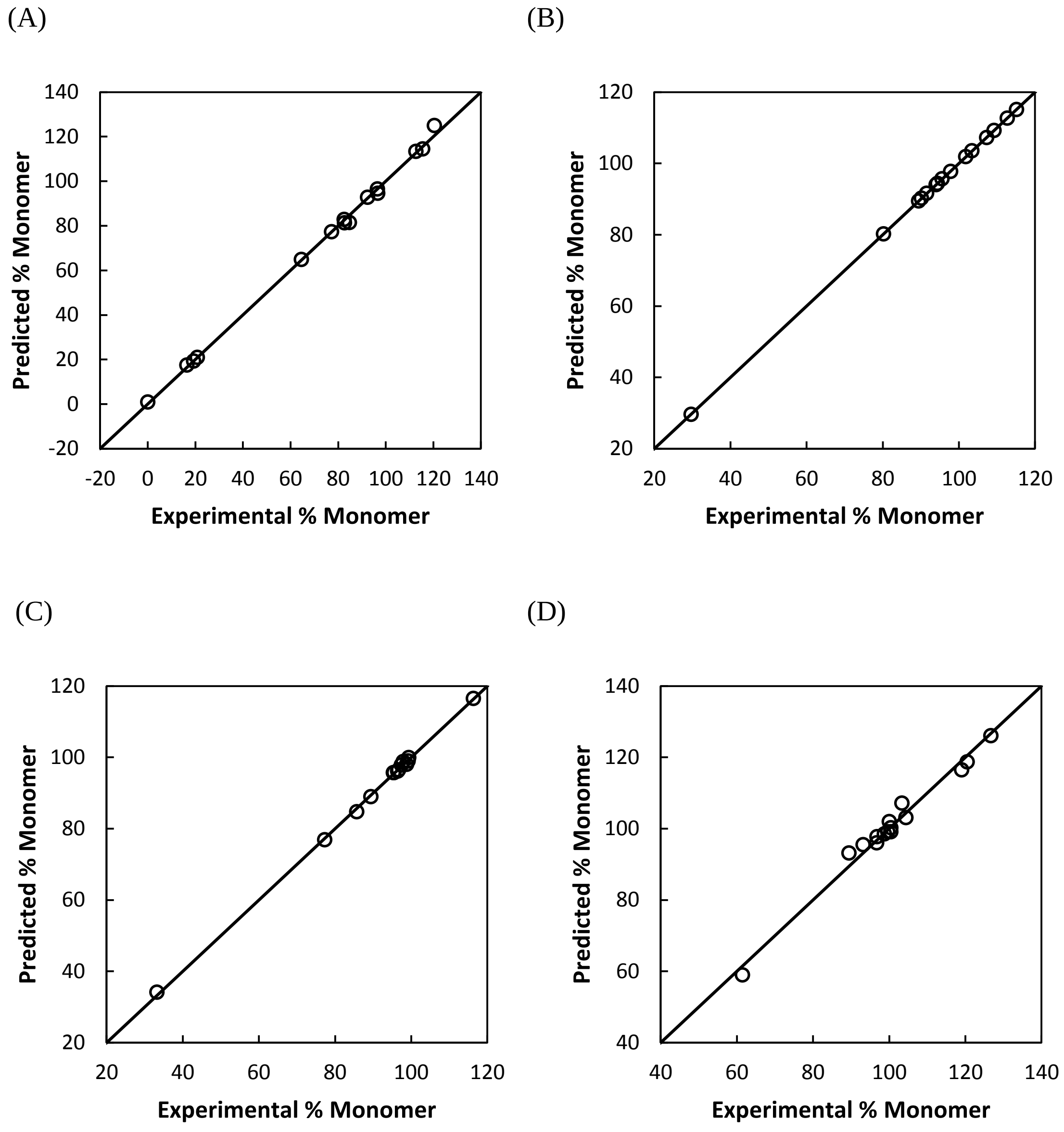

Figure 9.8 Parity plots of experimental percent monomeric protein values (%Monomer) from SEC versus predicted %Monomer values Correlations were developed for (A) urea, (B) buffer (potassium phosphate 20 mM, pH 7.4), (C) sucrose, and (D) glycine formulations. Figure adapted from (Roughton, Iyer *et al.* 2013).

9.4.6 Protein Descriptor Covariance

The descriptors used in developing the correlations were taken from several different sources without regard to possible covariance, either within a given descriptor set or among the pooled descriptors. Analysis of covariance was performed to determine which descriptors were correlated strongly with one another. Moderate to high covariance (≥|0.7|) was observed for some descriptor pairs taken from different descriptor sets, as expected (see Table 9.6). Within a given descriptor set, AGGRESCAN descriptors showed moderate to high covariance (≥|0.7|), as did PASTA descriptors. Some pairs of physical descriptors also showed high covariance (e.g., *% α-helix* vs *% β-sheet*). For any given correlation developed through multiple linear regression (Tables 9.3 and 9.5), few or no descriptors were selected that show moderate to high covariance (≥|0.7|).

9.4.7 Discussion of Model Development Results

The results presented here demonstrate that, for a given type of formulation, the extent of protein aggregation on lyophilization is strongly correlated with both physical and heuristic-based computational descriptors of protein structure. The best correlations (see Tables 9.3 and 9.4) were achieved using an exhaustive search method and descriptors pooled from the AGGRESCAN and PASTA algorithms along with selected physical descriptors (see Tables 4.2 and 4.3, Section 4.1.3). LOOCV demonstrated that the resulting correlations were able to provide good predictions of aggregation propensity. The results suggest that protein structure determines aggregation propensity during lyophilization and can be used for prediction purposes when the formulation components are held constant.

Table 9.6 Summary of covariance analysis Variable pairs with high degrees of covariance are given. Note that |Covariance (X,Y)| = |Covariance(Y,X)|. Table adapted from (Roughton, Iyer *et al.* 2013).

$\lvert\mathbf{Covariance(X,Y)}\rvert \geq \mathbf{0.7}$	$\lvert\mathbf{Covariance(X,Y)}\rvert \geq \mathbf{0.8}$	$\lvert\mathbf{Covariance(X,Y)}\rvert \geq \mathbf{0.9}$
$(apolar, MW)$ $(L_{max}, (E/L)_{avg})$ $((E/L)_{min}, (E/L)_{avg})$ $(a3vSA, E_{min})$ $(a3vSA, E_{avg})$ (MW, AAT) (AAT, E_{min}) (AAT, E_{avg}) $(THSA, E_{min})$ $(THSA, E_{avg})$ $(a3vSA, THSA)$ $(a3vSA, TA)$ $(a3vSA, AATr)$ $(TA, AATr)$ $(a3vSA, THSAr)$ $(NnHS, THSAr)$ $(Na4vSS, E_{min})$ $(Na4vSS, E_{avg})$ $(Na4vSS, THSA)$ $(Na4vSS, TA)$ $(Na4vSS, AATr)$ $(Na4vSS, THSAr)$	$(\%\ \alpha\text{-}helix, \%\ \beta\text{-}sheet)$ $(apolar, \#\ free\ SH)$ (MW, nHS) (AAT, nHS) $(THSA, nHS)$	(E_{avg}, E_{min}) (L_{avg}, L_{max}) $(Na4vSS, a3vSA)$

Independently, each of the heuristic-based algorithms provided considerably poorer correlations with lower predictive power than those built from pooled set of descriptors. The descriptors from both the AGGRESCAN and PASTA sets showed high covariance (see Table 9.6). As a result, the amount of structural information captured by either method is limited despite the large number of descriptors obtained from both methods. The addition of physical descriptors in the pooled set allows more structural features of the protein to be represented and thus provides better fits.

Descriptors selected varied between formulations and no single protein descriptor could account for the extent of aggregation across all formulations. This indicates that, for lyophilized formulations, the excipient and its interactions with the protein are important contributors to aggregation. The heuristic-based algorithms used here do not explicitly include excipient or medium effects. However, the heuristic-based algorithms were developed using data from proteins in solution. As both AGGRESCAN and PASTA descriptors were frequently selected, the algorithms are shown to be useful in prediction of aggregation under lyophilized conditions.

The most commonly selected descriptors provide insight into the factors contributing to lyophilization-induced aggregation. In the eight correlations presented in Tables 9.3 and 9.5, *pI*, *% β-sheet*, and T_m were selected five times and were the most commonly selected descriptors. All three have been implicated in aggregation induced by colloidal interactions or protein unfolding. The PASTA descriptors *Peaks* and E_{avg} were selected for three of the four correlations generated by exhaustive search (see Table 9.3). Interestingly, the percent monomer *increased* with increasing *Peaks* values for the buffer and sucrose formulations. While the reason for this is not clear, it may reflect a decrease in the size of each aggregation prone region as the number of regions increases. The PASTA descriptor E_{avg} describes the average interaction energies between residue pairings for a given protein, with lower energies indicating stronger interactions. As the average energies across all pairings for a protein (E_{avg}) were more highly selected than the pairing resulting in the minimum energy (E_{min}), the presence of several moderately aggregation-prone regions may increase the propensity towards aggregation more than the presence of one highly aggregation-prone region. Also, the two descriptors showed a high covariance (0.99), which may explain why only one was selected. The descriptors *# of free SH* and # S-S combined to be selected in four of the eight correlations. The frequent selection of thiol/disulfide related descriptors is not surprising, since free thiol groups are reactive and can lead to the formation of disulfide-linked covalent aggregates. SDS-PAGE results confirmed that reducible aggregates were observed for proteins containing four or more free thiol groups (Table F.1, Appendix F).

Examination of the descriptors that were *not* selected is also instructive. Apolar surface area (*apolar*) and fractional apolar surface area (f_{apolar}) were not highly selected. The lack of selection of *apolar* suggests that aggregation during lyophilization is not strongly correlated to total apolar surface area. Furthermore, larger percentages of apolar surface area do not appear to affect aggregation as f_{apolar} was not chosen for any of the correlations.

The predictive ability of the correlations is expected to be greatest for proteins whose properties fall within the structural space defined by the 15 proteins studied here. Perhaps more importantly, the correlations are limited in that the effects of excipients on aggregation are not included quantitatively, since the number of excipients tested was small.

9.5 Post-Lyophilization Protein Loss Models: As a Function of Excipient Structure

Models were developed to describe %Monomer as a function of excipient structure. During model development, several techniques were introduced to further gain insight into the models developed. Principle component analysis (PCA) was used to investigate the descriptor space. The impact of using chiral connectivity indices versus simple connectivity indices was determined. Finally, K-fold cross-validation was used in addition to LOOCV to further probe the predictive power of the models presented here.

9.5.1 Principal Component Analysis and Descriptor Comparison

Both simple connectivity indices and chiral connectivity indices up to the fifth order were considered for use as descriptors for development of the protein-by-protein linear models. PCA was performed using the chiral connectivity indices to visualize the descriptor space for the molecules considered (see Figure 9.9). Two principal components were sufficient to account for 99% of the variance observed in the data set, allowing a two dimensional representation of the descriptor space to be sufficient. PCA revealed three main clusters of excipient structures roughly correlating with monosaccharides, disaccharides and trisaccharides.

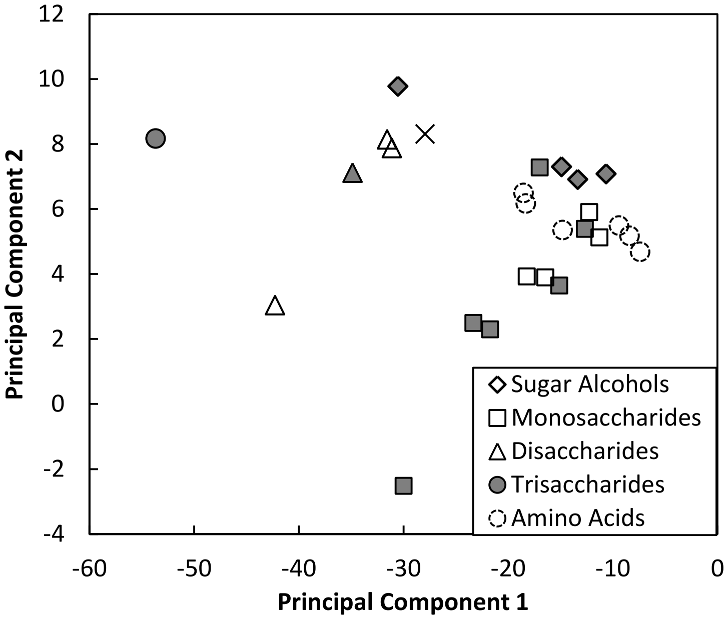

Figure 9.9 Principal component analysis of descriptor space for excipients used in study The "X" marker represents N-acetyl-neuraminic acid. Filled in markers represent excipients used for all proteins while un-filled markers represent excipients used only with BSA and RNAse A. Descriptors used to construct the principal components are connectivity indices up to the fifth order with a chirality correction factor of two.

Chirality connectivity indices were able to provide fits with good accuracy ($R^2 > 0.9$) for α-amylase, ovalbumin and trypsin inhibitor. Simple connectivity indices were unable to provide fits with sufficient accuracy. For BSA and RNAse A, neither class of descriptors was able to yield a model with acceptable accuracy. Excipients derived from amino acids were considered for BSA and RNAse A formulations, but were not considered for the other proteins. PCA results suggested that the amino acid based excipients were structurally similar to the monosaccharides considered (see Figure 9.9). However, the molecular descriptors used do not explicitly account for charge. Amino acids are either charged or zwitterionic at the solution conditions used in the study. Separation of the data into two sets (a carbohydrate set and amino acid set) provided correlations with increased accuracy when using chiral connectivity indices for the carbohydrate data set and when using either type of connectivity indices for the amino acid set (see Figure 9.10). Chiral connectivity indices were used for model development for all carbohydrate data sets. As no molecule belonging to the amino acid class contains more than one chiral center and all chiral centers are S-configuration, simple connectivity indices were used instead of chiral connectivity indices for model development for all amino acid data sets.

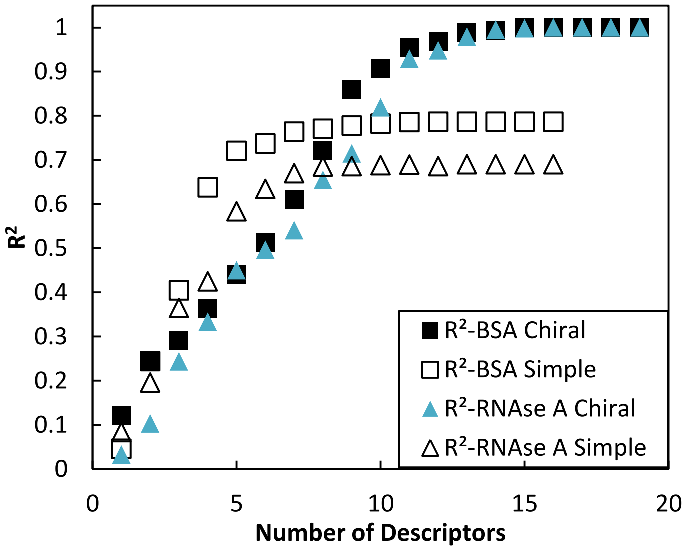

Figure 9.10 Comparison of chiral and simple connectivity indices for BSA and RNAse carbohydrate models Each point represents the model with the maximum R^2 for the given number of descriptors. Each model building set contained 20 data points.

9.5.2 Correlation and K-Fold Cross-Validation

With data sets finalized, descriptor selection was used to build linear correlations relating %Monomer to excipient structure on a protein-by-protein basis. Correlations of high accuracy (R^2 ≈ 0.99) were obtained for all models, indicating that the descriptors considered were able to sufficiently model the %Monomer data without over-fitting (See Figures 9.11 and 9.12, Table 9.7). In general, the number of descriptors was large compared to the number of data points. Model size is equal to the number of descriptors selected plus one as an intercept was used for all models. A model size of 14 was selected for the BSA carbohydrate model while a larger model size of 17 was selected for the RNAse A carbohydrate model (both datasets contain 20 data points). For the proteins with carbohydrate data sets of 12 points, a model size of 8-9 was selected. For the amino acid models, a model size of 4 was selected for both BSA and RNAse A (both data sets contain 6 points). A summary of model parameters is given in Table 9.8.

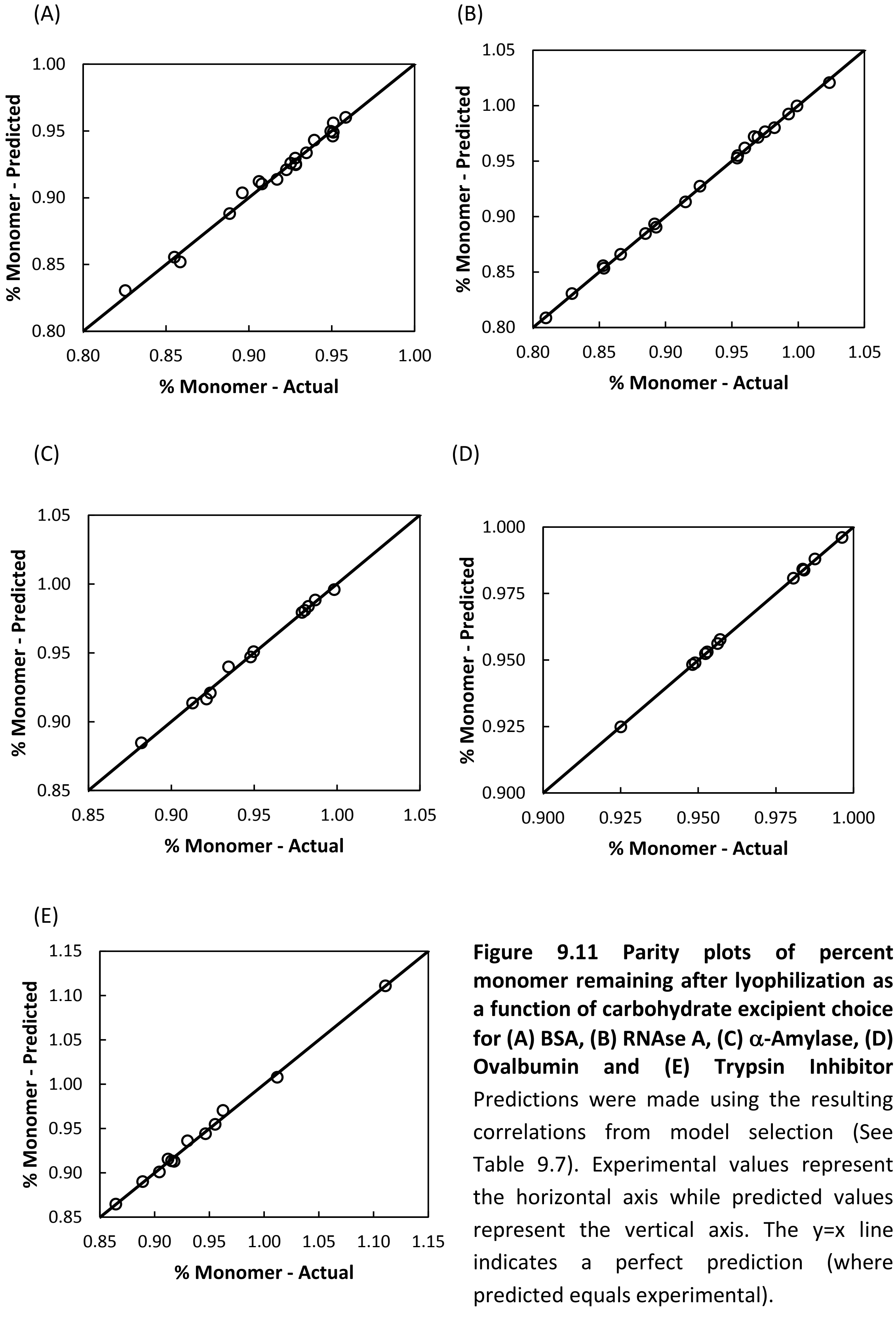

Figure 9.11 Parity plots of percent monomer remaining after lyophilization as a function of carbohydrate excipient choice for (A) BSA, (B) RNAse A, (C) α-Amylase, (D) Ovalbumin and (E) Trypsin Inhibitor Predictions were made using the resulting correlations from model selection (See Table 9.7). Experimental values represent the horizontal axis while predicted values represent the vertical axis. The y=x line indicates a perfect prediction (where predicted equals experimental).

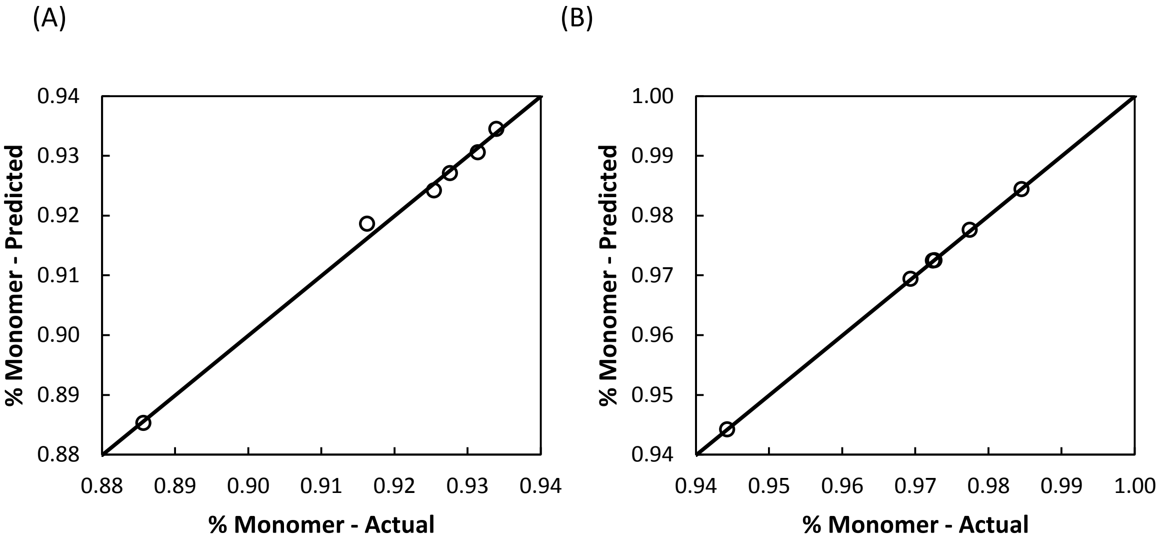

Figure 9.12 Parity plots of percent monomer remaining after lyophilization as a function of amino acid excipient choice for (A) BSA and (B) RNAse A Predictions were made using the resulting correlations from model selection (See Table 9.7). Experimental values represent the horizontal axis while predicted values represent the vertical axis. The y=x line indicates a perfect prediction (where predicted equals experimental).

K-fold cross-validation was performed to test the predictive power of the models. As more data is left out in each fold, the number of folds (K) generated from the data set decreases and the resulting Q^2 is expected to decrease. As a rule, a $Q^2 \geq 0.6$ is desired (Golbraikh, Shen *et al.* 2003). Folds were increased in size and Q^2 was evaluated until a value was obtained below 0.6 (see Table 9.7). The size of the fold obtained at the lowest K value where $Q^2 \geq 0.6$ gives an indication of how much data can be left-out while retaining reliable prediction accuracy. Thus the results give an estimation of the minimum number of points in a given set of molecules that are required to be known experimentally. Ideally, the number would be low so that a small number of data points are sufficient to build a widely applicable predictive model.

For the BSA carbohydrate model, the minimum acceptable number of folds was K=5 (corresponding to a fold size of 4 or 20% of the data). The RNAse A model however showed an unacceptable Q^2 value for the minimum fold size of 1 (K=20). Inspection of the PRESS scores for each left-out point showed that the prediction for N-acetylneuraminic acid was much poorer than all other predictions and was skewing the data towards a lower Q^2. The point was excluded from the data set and the data set was again correlated to %Monomer values. The resulting model provides a similar R^2 value to the original (0.999) while reducing the number of descriptors needed by two (see Table 9.7). Prediction ability is improved by increasing the minimum fold size from 1 to 2. The amino acids models had minimum fold sizes of 2, accounting for 33% of the data. The carbohydrate models for the proteins with smaller data sets had minimum fold sizes between 3 – 4, accounting for 25 – 33% of the data.

Table 9.7 Comparison of model size (including intercept), R2 and Q2 values for final protein-specific models selected Q^2 values are given for varying sizes of k-fold cross-validation. The number of folds (*K*) indicates how many sets of left-out data were used for the cross-validation. The size of the fold is the value in parenthesis. For example, the BSA and RNAse A datasets with K=20 represents leave-one-out cross validation.

					Q^2		
Protein	**Data Set**	**Model Size**	**R^2**	*K=20*	*K=10*	*K=5*	*K=4*
				(Fold =1)	*(2)*	*(4)*	*(5)*
BSA	*Carbohydrates*	14	0.989	0.841	0.715	0.712	<0
RNAse A	*Carbohydrates*	17	0.999	0.591	<0	-	-
RNAse A	*Carbohydrates**	15	0.999	0.926	0.826	<0	-
				K=6	*K=3*		*K=2*
				(1)	*(2)*		*(3)*
BSA	*Amino Acids*	4	0.995	0.731	0.812		<0
RNAse A	*Amino Acids*	4	1.000	0.999	0.995		<0
				K=12	*K=6*	*K=4*	*K=3*
				(1)	*(2)*	*(3)*	*(4)*
α-Amylase	*Carbohydrates*	8	0.995	0.934	0.949	0.752	<0
Ovalbumin	*Carbohydrates*	9	1.000	0.998	0.932	0.904	<0
Trypsin Inhibitor	*Carbohydrates*	8	0.996	0.961	0.912	0.708	0.874

*Data set does not include N-acetyl-neuraminic acid

9.5.3 Discussion of Model Development Results

Development of the protein-by-protein models illustrates that protein stability following lyophilization is strongly correlated to excipient choice. The need to separate amino acids from carbohydrates indicates that while structurally similar to monosaccharaides on the basis of molecular connectivity (see Figure 9.9), the structural features of the two molecular classes act in different ways to stabilize the protein. Additionally, cross-validation revealed that N-acetyl neuraminic acid was the carbohydrate molecule with the largest prediction errors. Structural comparisons show that N-acetyl neuraminic acid is similar to disaccharides (see Figure 9.9). The descriptors used do not account for charge, which is present in amino acids and N-acetylneuraminic acid at the solution conditions considered. Accounting for charge may offer a means to unify the carbohydrate and amino acid models into one model and improve prediction for carbohydrate molecules containing charges. The improvement of the carbohydrate models through use of chiral connectivity indices (see Figure 9.10) indicates that the three-dimensional conformation is an important feature of the excipient in the stabilization of the protein.

The cross-validation analysis suggests that the maximum amount of data acceptable to leave out was 33%, which suggests the need to take at least 2/3 of the data experimentally in order to build a reliable and predictive model. However, the analysis does not suggest a hard and fast rule when developing similar models. Indeed, these numbers could likely be improved by rationally designing the test and training set (Golbraikh, Shen *et al.* 2003) and/or focusing the data set to a more restrictive molecular class, such as monosaccharides rather than carbohydrates.

Table 9.8 Protein-by-protein model parameters determined by multiple linear regression following descriptor selection Carbohydrate models use connectivity indices with a chirality correction of 2. Amino acid models use connectivity indices with no chirality correction. All parameter values pass confidence testing at a 99% level.

BSA Carbohydrate Model			RNAse A Carbohydrate Model			α-Amylase Carbohydrate Model			Ovalbumin Carbohydrate Model			Trypsin Inhibitor Carbohydrate Model		
Descript.	*Value*	*Std Error*	*Descript.*	*Value*	*Std Error*	*Descript.*	*Value*	*Std Error*	*Descript.*	*Value*	*Std Error*	*Descript.*	*Value*	*Std Error*
Int.	5.9445	0.2841	Int.	12.2710	0.2310	Int.	0.6937	0.1019	Int.	1.1102	0.0064	Int.	-6.7860	0.3828
χ^3	-0.2790	0.0197	χ^1	0.0637	0.0222	χ^3	-0.3134	0.0148	χ^2	-0.0514	0.0006	χ^4	0.1362	0.0149
χ^5	-0.3754	0.0256	χ^3	0.5761	0.0101	χ^5	-0.1256	0.0064	χ^4	0.5165	0.0054	ζ^0	13.9898	0.6602
ζ^0	-10.0317	0.5350	χ^5	-0.1392	0.0153	ζ^0	1.6912	0.1649	ζ^2	1.0148	0.0222	ζ^1	-11.5258	0.4757
ζ^1	7.5983	0.4227	ζ^0	-18.2244	0.3654	ζ^2	5.1274	0.2628	ζ^5	-7.1490	0.0752	$^v\chi^1$	0.0346	0.0114
ζ^4	-16.2788	1.4259	ζ^2	3.9332	0.4304	$^v\chi^3$	0.8448	0.0400	$^v\chi^4$	-1.0949	0.0128	$^v\chi^3$	-0.2911	0.0373
ζ^5	23.4753	1.7903	ζ^5	6.0029	0.2366	$^v\zeta^0$	-2.3518	0.1226	$^v\zeta^0$	-0.4271	0.0156	$^v\zeta^2$	16.7938	0.6344
$^v\chi^0$	0.2149	0.0125	$^v\chi^1$	0.6086	0.0468	$^v\zeta^2$	-7.9700	0.4276	$^v\zeta^4$	-1.4052	0.0876	$^v\zeta^5$	-19.2179	0.8031
$^v\chi^1$	-0.7594	0.0451	$^v\chi^2$	-2.5101	0.0454				$^v\zeta^5$	16.5243	0.2006			
$^v\chi^2$	-0.1974	0.0294	$^v\chi^4$	3.5378	0.0674									
$^v\chi^3$	2.2207	0.1486	$^v\chi^5$	-3.1432	0.0793									
$^v\chi^5$	-0.7265	0.0727	$^v\zeta^2$	36.8323	1.4771									
$^v\zeta^2$	8.4658	0.7505	$^v\zeta^3$	-44.3452	1.8540									
$^v\zeta^3$	-21.0254	1.3801	$^v\zeta^4$	-19.6284	1.8236									
			$^v\zeta^5$	13.1564	1.3862									

BSA Amino Acid Model			RNAse A Amino Acid Model		
Descript.	*Value*	*Std Error*	*Descript.*	*Value*	*Std Error*
Int.	1.3323	0.0245	Int.	0.6688	0.0033
χ^2	-0.1835	0.0107	χ^0	0.0184	0.0002
χ^5	0.4396	0.0266	ζ^2	0.5119	0.0060
$^v\zeta^4$	-1.5401	0.1277	$^v\chi^5$	-0.1900	0.0013

9.6 Post-Lyophilization Protein Loss Models: As a Function of Both Protein and Excipient Structure

Chiral connectivity indices and all discussed protein descriptors were used as potential descriptors for the universal model. Only data for formulations containing carbohydrate excipients were considered, resulting in a data set of 73 *%Monomer* values. The resulting model required a non-linear form, which required differences in model development as compared to the linear models described previously.

9.6.1 Non-Linear Model Development

Attempts to build a linear model of sufficient correlative quality were unsuccessful (results not shown). Non-linear models were considered to better correlate the descriptors to the %Monomer values. Several functional forms were considered, with the best form given by Equation 9.5.

$$\%Monomer = c\left(\sum a_i \chi_i\right)\left(\sum b_i\,\psi_i\right)$$

(Equation 9.5)

where χ represents excipient descriptors, ψ represents protein descriptors, and *a*, *b*, and *c* are adjustable parameters. All descriptors considered were used initially for model development, with 24 descriptors accounting for excipient structure and 25 descriptors accounting for protein structure. Given the parameters determined for each descriptor, a parameter sensitivity analysis was performed to identify the parameters that had no impact on the model prediction. In total 13 descriptors were identified as having no impact on the model prediction, with two descriptors accounting for excipient structure and 11 descriptors accounting for protein structure (see Table 9.9). The descriptors were removed and the model parameters were again determined for the scaling constant (*c*) and the remaining 20 excipient and 6 protein descriptors. After one round of descriptor reduction, the model *%AAD* = 2.58% and *reduced chi-squared* = 3.23 (see Table 9.10 and Figure 9.13).

Table 9.9 List of descriptors considered for non-linear model development Descriptors with no impact on model performance (sensitivity ≈ 1) are shaded. Descriptors remaining after two rounds of parameter reduction are bolded.

Excipient Descriptors				Protein Descriptors			
Chiral Connectivity Indices		*Chiral Valence Connectivity Indices*		*Biophysical Descriptors*		*Aggrescan Descriptors*	*PASTA Descriptors*
$\boldsymbol{\chi^0}$ $\boldsymbol{\chi^1}$ $\boldsymbol{\chi^2}$ χ^3 χ^4 χ^5	ξ^0 $\boldsymbol{\xi^1}$ $\boldsymbol{\xi^2}$ ξ^3 ξ^4 ξ^5	${}^v\chi^0$ ${}^v\chi^1$ ${}^v\chi^2$ ${}^v\chi^3$ ${}^v\chi^4$ ${}^v\chi^5$	${}^v\xi^0$ ${}^v\xi^1$ ${}^v\xi^2$ ${}^v\xi^3$ ${}^v\xi^4$ ${}^v\xi^5$	**ASA** f_{ASA} **% α-helix** **% β-sheet** **MW** pI	# S-S # free SH $\mathbf{T_m}$	a3vSA nHS NnHS AAT THSA TA AATr THSAr Na4vSS	Emin Eavg Lmax Lavg (E/L)min (E/L)avg Peaks

Subsequent descriptor reduction guided by sensitivity analysis reduced the number of descriptors to 10, with 5 descriptors accounting for the excipient structure and 5 descriptors accounting for the protein structure (see Table 9.9). The resulting model is given by Equation 9.6.

$$\%Monomer = 2.51\times10^{-5}\ (-2.43\chi^0 + 6.52\chi^1 - 3.12\chi^2 - 94.32\xi^1 + 74.04\xi^2)\ (0.029ASA + 19.35\%\alpha helix - 60.34\%\beta sheet - 71.54MW + 66.38T_m)$$

(Equation 9.6)

Table 9.10 Summary statistics of non-protein specific model Model uses the form given by Equation 9.6. *AAD* is average absolute deviation and *Max AD* is the maximum absolute deviation noted.

Statistics	**After First Parameter Reduction**	**After Second Parameter Reduction**
Size of data set	73	73
Number of parameters	27	11
Parameters relating to excipient	20	5
Parameters relating to protien	6	5
Reduced Chi-squared	3.23	4.45
AAD	2.58%	3.38%
Max AD	8.53%	11.83%
Number of points outside AAD	33 (45%)	33 (45%)
*Number of points outside 2*AAD*	8 (11%)	7 (10%)

The model performs similarly to the results after the first parameter reduction, with *%AAD* = 3.38% and *reduced chi-squared* = 4.45 (see Table 9.10 and Figure 9.13). The further reduced model is more desirable as there are fewer descriptors needed for calculation, reducing the risk of over-fittting. When comparing the models after the first and second rounds of parameter reduction, both models have the same number of predicted points that exceed the model *%AAD* (33 or 45% of the data set). The second parameter reduction reduced the number of points that exceeded twice the model *%AAD* from 8 to 7. Predictions that exceeded three times the model *%AAD* increased from 1 to 2 after the second parameter reduction. The resulting model presents sufficient accuracy with reduced risk of over-fitting, as evidenced by reduced chi-squared value. The *%AAD* value of 3.38% observed is of similar value to the average experimental standard deviation value of 2.20% observed in *%Monomer* calculations. Therefore the error in the model prediction does not greatly exceed the error that would be encountered in experimental measurements.

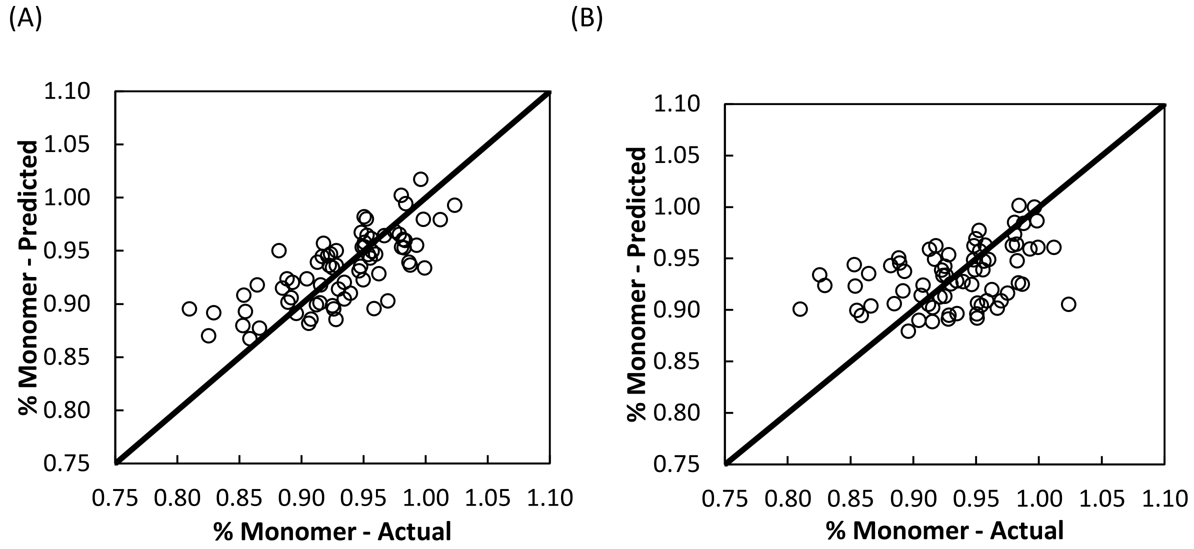

Figure 9.13 Parity plots of percent monomer remaining after lyophilization as a function of both protein and excipient structure Predictions were made using results for non-linear model development. **(A)** represents model after first parameter reduction and **(B)** represents model after second parameter reduction. Experimental values represent the horizontal axis while predicted values represent the vertical axis. The y=x line indicates a perfect prediction (where predicted equals experimental).

9.6.2 Discussion of Results from Model Development

Several functional forms for a model describing protein stability following lyophilization as a function of excipient choice and protein choice were considered. The final form used is given by Equation 9.6, which was motivated by the enthalpic contribution of the Flory-Huggins model, given by Equation 9.7. The Flory-Huggins model has been used previously to describe protein-sugar interactions in lyophilized solids (Katayama, Carpenter *et al.* 2009; Wang, Tchessalov *et al.* 2009). Equation 9.6 emulates the Flory-Huggins interaction parameter (χ_{12}) through the multiplication of excipient structural descriptors and protein structural descriptors. The success of the Flory-Huggins functional form of the universal model suggests that direct protein-excipient interactions may play a significant role in stabilization of the protein during lyophilization for the formulations considered.

$$\Delta H_m = kTN_1\phi_1\chi_{12}$$

(Equation 9.7)

Parameter sensitivity analysis revealed that all of the descriptors obtained or derived from aggregation prediction methods had no significant impact on the model prediction (see Table 9.9). The results suggest that AGGRESCAN and PASTA may not be applicable to aggregation induced by the lyophilization process or at least are not the strongest predictors of aggregation in lyophilized systems. Both the number of disulfide bridges and the number of free thiols had sensitivity values near unity, indicating that intermolecular disulfide bond formation was not a primary cause of aggregation for the proteins considered. The SDS-PAGE results support this conclusion as only ovalbumin showed reduction of aggregate formation under reducing conditions (see Table F.3, Appendix F). The isoelectric point had a sensitivity value of one, suggesting that charge-based associations were not driving forces for aggregation in the proteins considered. Both %α-helix and %β-sheet were descriptors that were retained in the final model, indicating that secondary structure was an important factor in protein stability following lyophilization. The amount of α-helix content increased protein stability while the amount of β-sheet content reduced protein stability. All excipient descriptors retained in the final model were chiral connectivity indices of second order or less, suggesting that the short range connectivity (bond paths of 2, bonds, and atoms present) was the most important excipient structural feature in regards to protein stability.

The model presented provides predictions for protein stability following lyophilization as a function of excipient choice and protein choice. Limitations on the model exist due to the data set used for correlation. Only carbohydrates were considered, so extension to other classes of excipients is not expected to provide accurate predictions. Additionally, predictions for proteins with structural features that do not lie within the range of the proteins considered are not expected to be accurate. The success of the model illustrates that such a model development procedure can be applied to other classes of proteins and/or excipients for determination of predictive models for a given data set.

9.7 Stochastic Optimization Tuning Results

Tuning of both a tabu search and genetic algorithm was performed to determine their suitability for CAMD applications. For fair comparison, both methods used the same molecular representation. For each parameter considered, 100 runs were performed for varying parameter values while all other parameters were kept constant. Average value of the objective function, average time to solution, percentage of runs that matched the target property (hit%) and percentage of runs that were within 5% of the target property (close%) were the four measures used to guide tuning. Tuning was performed through VBA on a PC with Windows 7 32-bit OS, Intel Core i5-2400 CPU @ 3.10 GHz, and 4.00 GB RAM. Results for each stochastic optimization method follow.

9.7.1 Tabu search tuning results

For tabu search, four parameters were considered for tuning: the maximum number of non-improving iterations, the maximum number of neighbors evaluated per iteration, the size of tabu list and the value of tabu criterion (see Section 5.4 for more information on parameters). For each parameter value used in tuning, 100 trials were conducted. Figures 9.14-9.17 display the tuning results for each of the parameters considered.

The parameter with the most influence on objective function value and percentage of correct or nearly correct solutions was the maximum number of non-improving iterations (see Figure 9.14). The result is intuitive, as the longer the search is allowed to be performed the more likely that a very good result will be found. As the maximum number of non-improving iterations is increased, the time to solution increases linearly (R^2 = 0.99, Figure 9.14). Consequently, a trade-off exists between solution quality and solution efficiency. From tuning, a value of 100 maximum non-improving iterations was chosen as longer searches had minimal effects on solution quality while greatly extending time to solution.

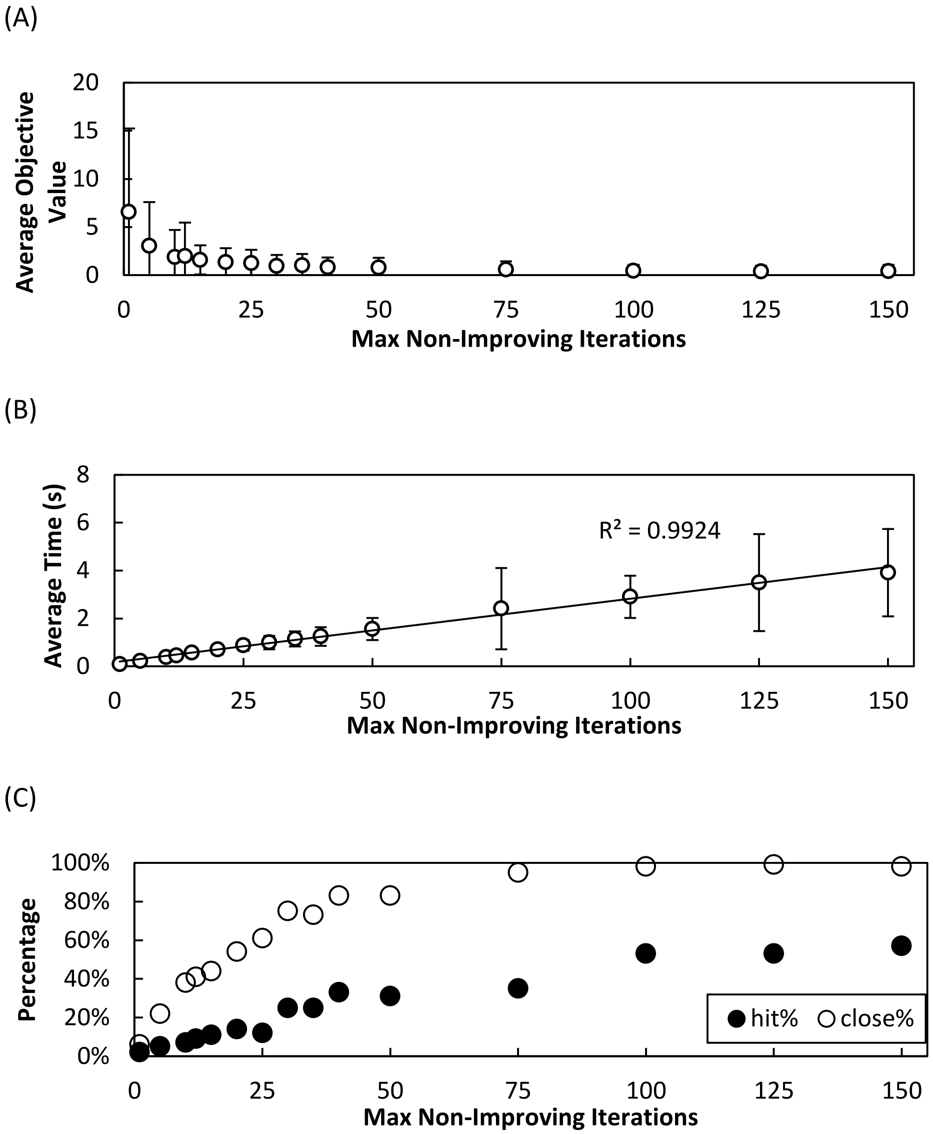

Figure 9.14 Tuning results for tabu search with varying maximum number of non-improving iterations (A) presents the effect of the parameter on average objective value, with error bars representing standard deviation from 100 trials. (B) presents the effect of the parameter on average time to solution (seconds), with error bars representing standard deviation from 100 trials. (C) displays the percentage of 100 trial solutions that hit the desired property target (hit%) or were within 5% of the desired property value (close%) for varying parameter values.

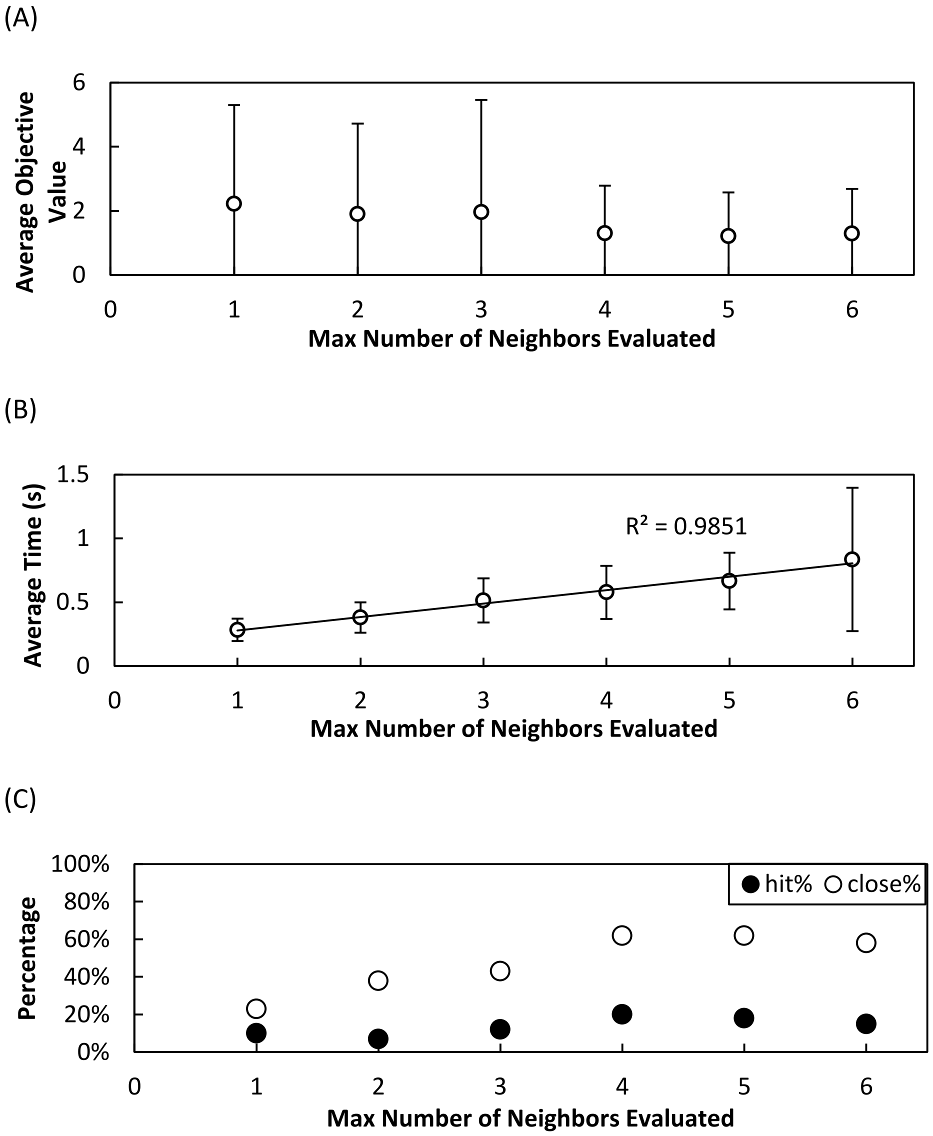

Figure 9.15 Tuning results for tabu search with varying maximum number of neighbors considered at each iteration (A) presents the effect of the parameter on average objective value, with error bars representing standard deviation from 100 trials. (B) presents the effect of the parameter on average time to solution (seconds), with error bars representing standard deviation from 100 trials. (C) displays the percentage of 100 trial solutions that hit the desired property target (hit%) or were within 5% of the desired property value (close%) for varying parameter values.

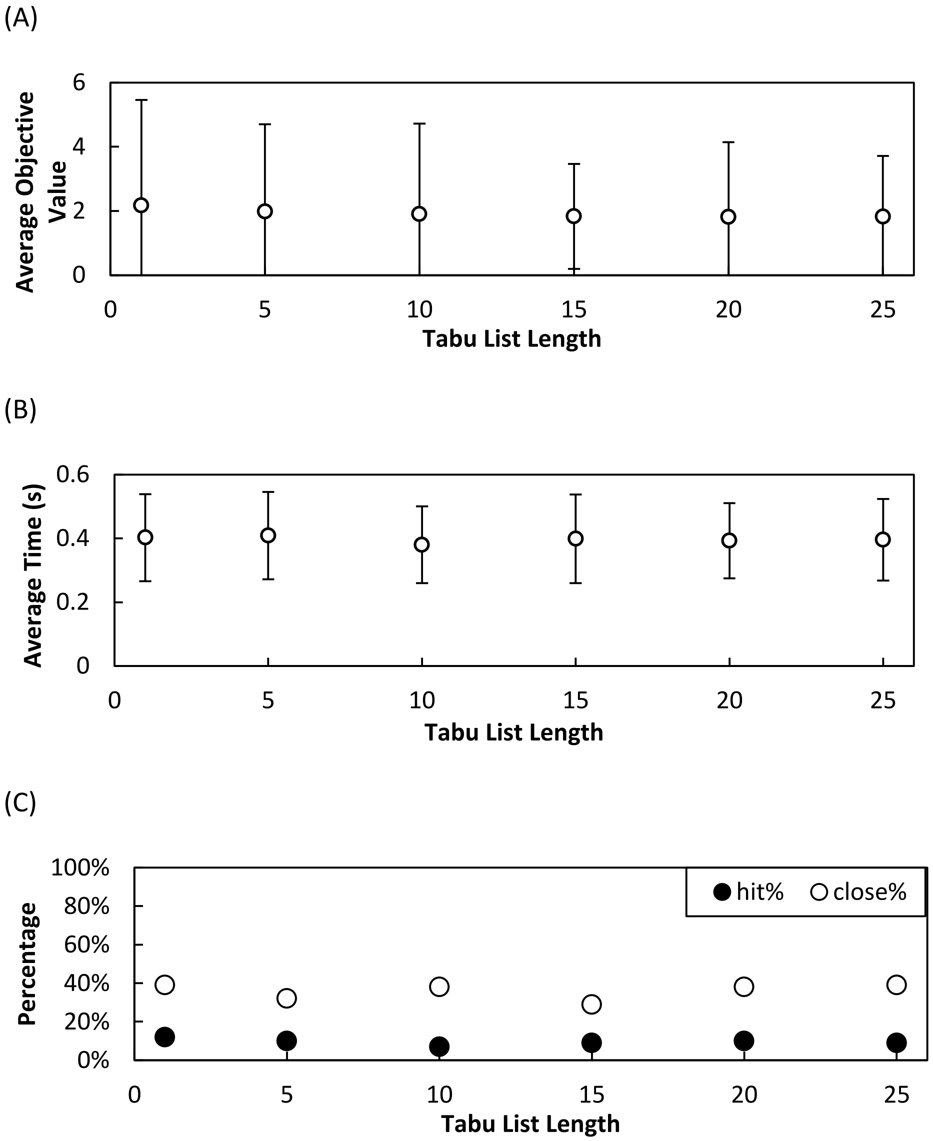

Figure 9.16 Tuning results for tabu search with varying tabu list length of stored solution (A) presents the effect of the parameter on average objective value, with error bars representing standard deviation from 100 trials. (B) presents the effect of the parameter on average time to solution (seconds), with error bars representing standard deviation from 100 trials. (C) displays the percentage of 100 trial solutions that hit the desired property target (hit%) or were within 5% of the desired property value (close%) for varying parameter values.

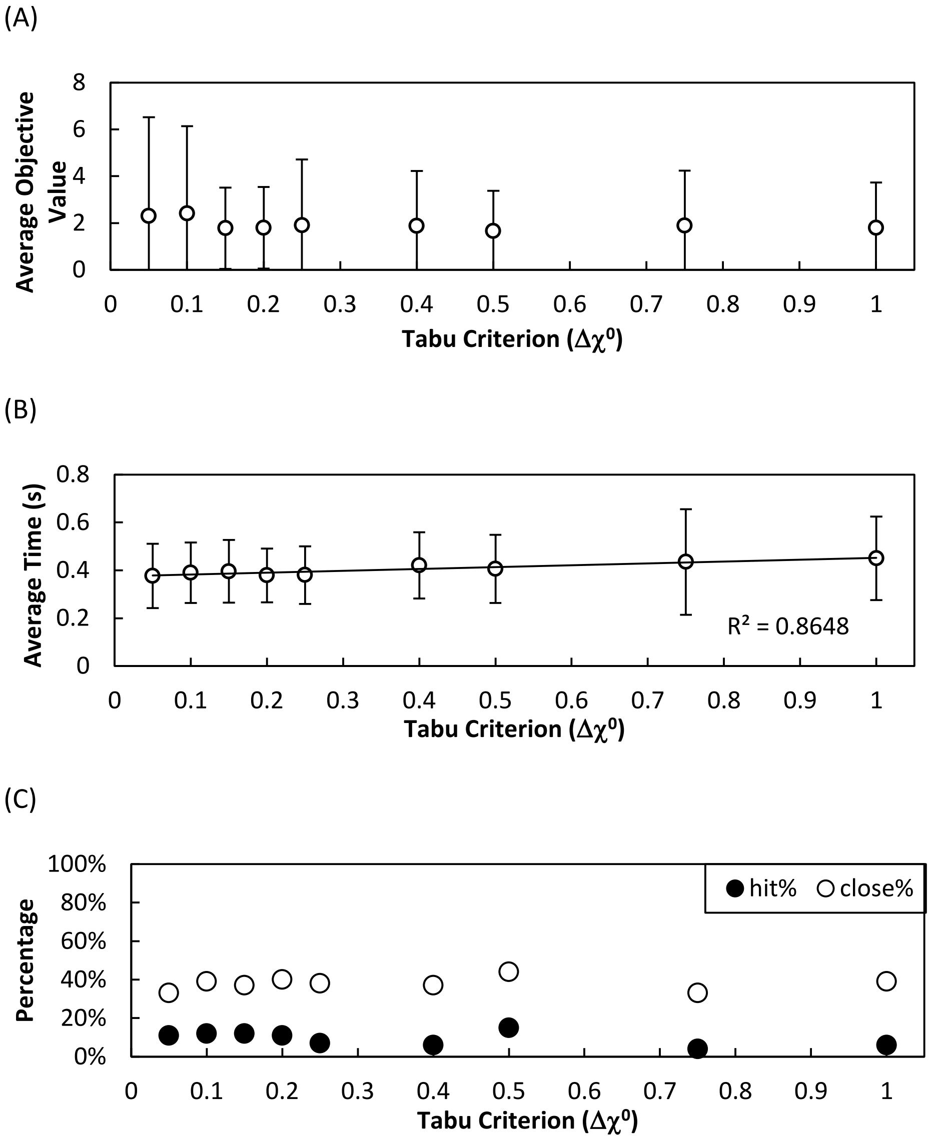

Figure 9.17 Tuning results for tabu search with varying tabu criteria (A) presents the effect of the parameter on average objective value, with error bars representing standard deviation from 100 trials. (B) presents the effect of the parameter on average time to solution (seconds), with error bars representing standard deviation from 100 trials. (C) displays the percentage of 100 trial solutions that hit the desired property target (hit%) or were within 5% of the desired property value (close%) for varying parameter values.

Increasing the maximum number of neighbors evaluated at each iteration and the tabu criterion also lead to linear increases in time to solution (see Figure 9.15b and 9.17b). The time effect from increasing the number of neighbors considered follows logically as more time is needed for evaluation and tabu checks. The effect of increasing the tabu criterion is caused by placing too much restriction on the search. As the tabu criterion becomes larger, it is more likely that a neighboring solution will be deemed tabu. If too many solutions are declared tabu, the search will require more global moves and become more time-consuming. The maximum number of neighbors was chosen to be four, as a discernible increase in correct or nearly correct solutions is noted as the parameter changes from three to four (see Figure 9.15c). The variability in average objective function value also noticeably decreases as the maximum number of neighbors increase from three to four (see Figure 9.15a). Past four neighbors considered, no benefit is gained in solution quality. Tabu criterion had no distinguishable effect on solution quality and the base value of 0.5 was retained. The length of the tabu list had minimal effect on solution quality and no effect on time to solution. The length of the tabu list was set at 15 as that parameter value showed reduced variability in average objective function value (see Figure 9.16).

9.7.2 Genetic Algorithm Tuning Results

For the genetic algorithm, three parameters were considered for tuning: the maximum number of generations, the size of population in each generation and the maximum probability that a member of the population will be chosen as a parent (see Section 5.4 for more information on parameters). For each parameter value investigate, 100 trials were performed. Figures 9.18-9.20 display the tuning results for each of the parameters considered.

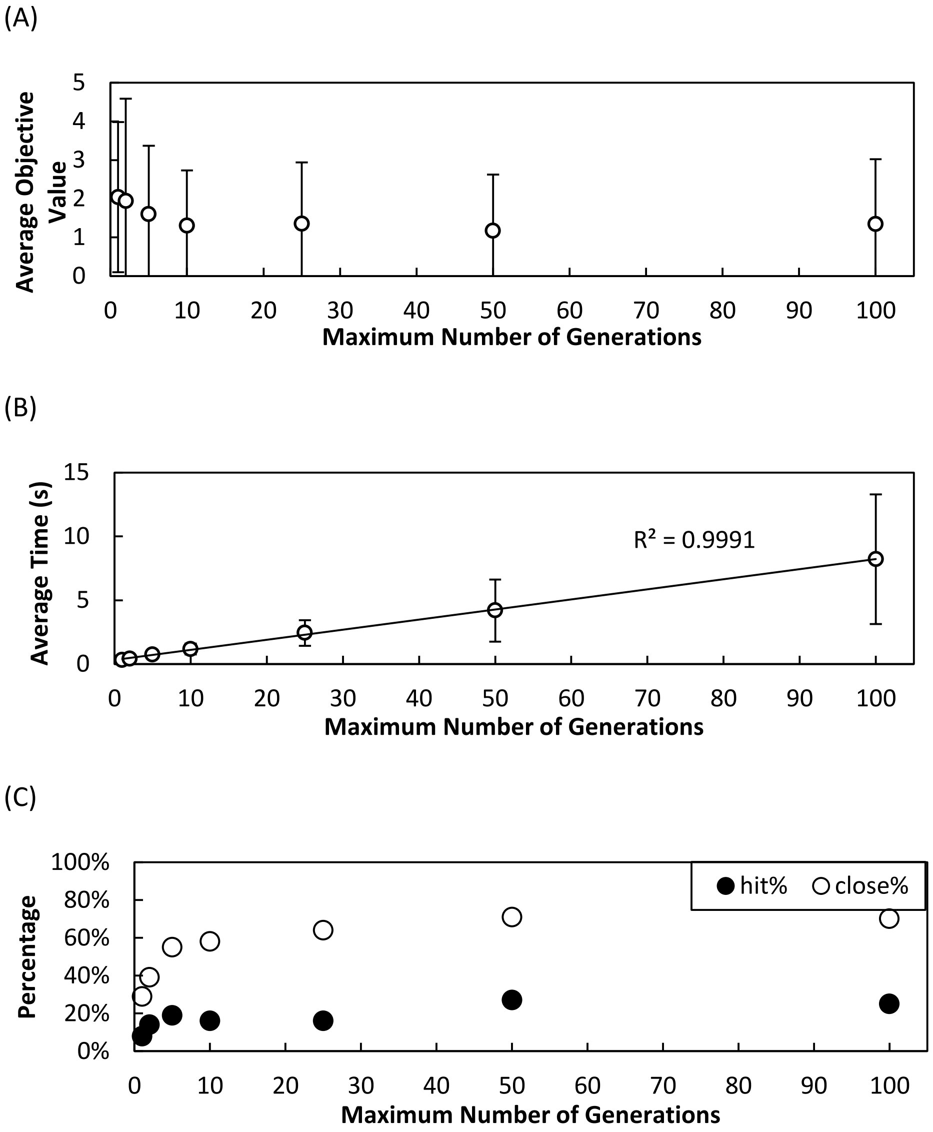

Figure 9.18 Tuning results for genetic algorithm with varying maximum number of generations (A) presents the effect of the parameter on average objective value, with error bars representing standard deviation from 100 trials. (B) presents the effect of the parameter on average time to solution (seconds), with error bars representing standard deviation from 100 trials. (C) displays the percentage of 100 trial solutions that hit the desired property target (hit%) or were within 5% of the desired property value (close%) for varying parameter values.

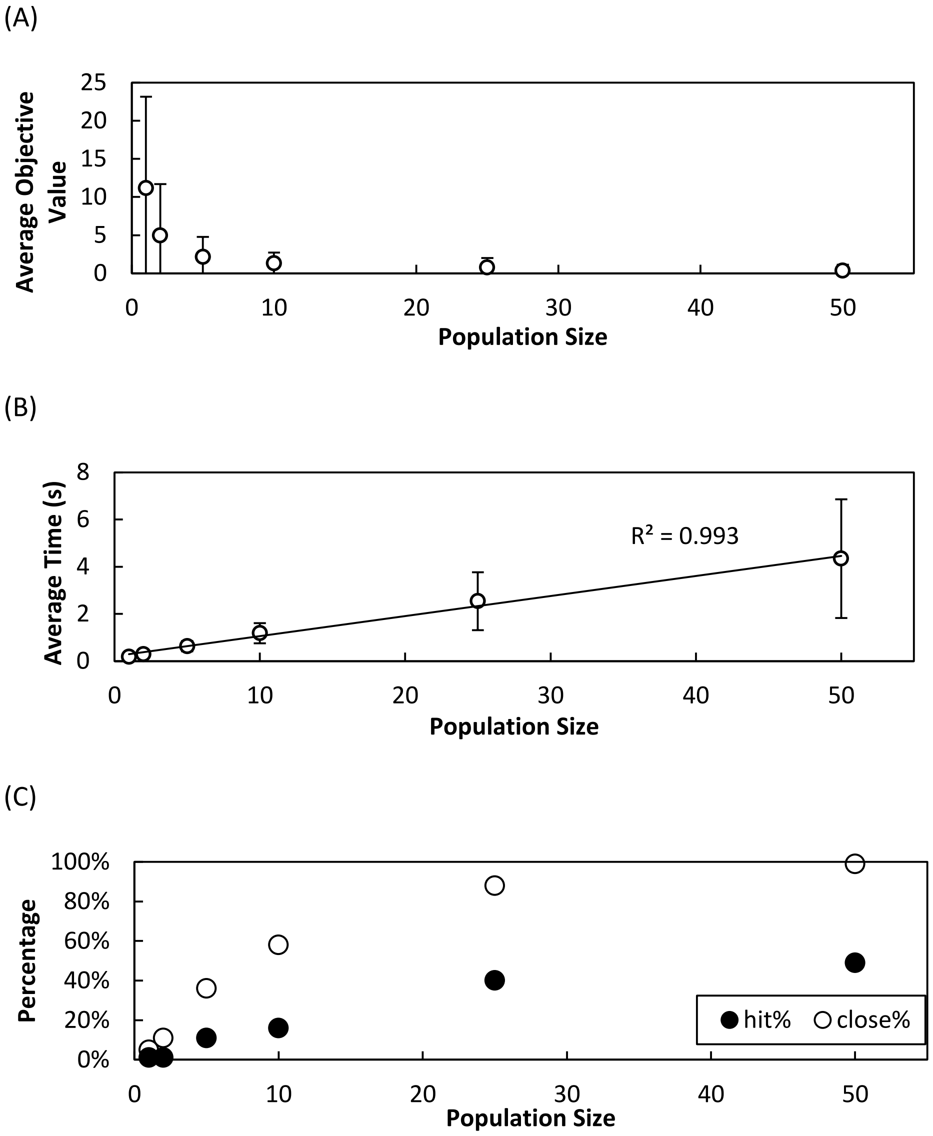

Figure 9.19 Tuning results for genetic algorithm with population size per generation (A) presents the effect of the parameter on average objective value, with error bars representing standard deviation from 100 trials. (B) presents the effect of the parameter on average time to solution (seconds), with error bars representing standard deviation from 100 trials. (C) displays the percentage of 100 trial solutions that hit the desired property target (hit%) or were within 5% of the desired property value (close%) for varying parameter values.

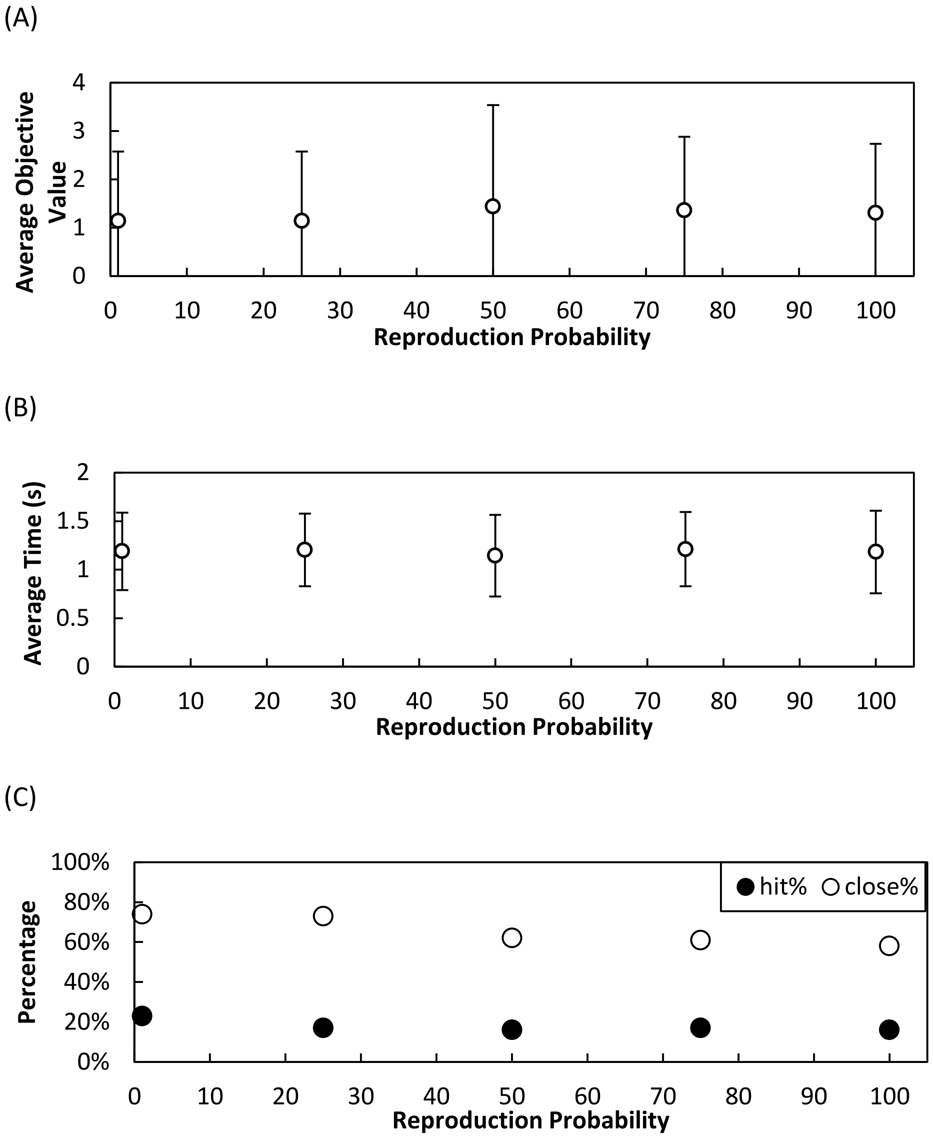

Figure 9.20 Tuning results for genetic algorithm with varying maximum probability that a member will be selected as a parent (A) presents the effect of the parameter on average objective value, with error bars representing standard deviation from 100 trials. (B) presents the effect of the parameter on average time to solution (seconds), with error bars representing standard deviation from 100 trials. (C) displays the percentage of 100 trial solutions that hit the desired property target (hit%) or were within 5% of the desired property value (close%) for varying parameter values.

The maximum number of generations and the population size in each generation were the parameters that had the most effect on the solution quality (see Figures 9.18 and 9.19). Increasing both parameters led to a linear increase in time to solution, as increases in both parameters correspond to increases in the number of solution evaluations that must be performed. The maximum number of generations was set at 25 as further increases result in minimal improvements in solution quality (see Figure 9.18a,c). The population size was set at 50 to ensure highest solution quality (see Figure 9.19a,c). Varying maximum probability that a member will be selected as a parent had no effect on solution quality or time to solution (see Figure 20). The base case value of 100 was retained for the probability value. Overall, the effectiveness of the genetic algorithm seems to be most dependent on the seed population. A large seed population allows for many local minima to be probed, increasing the probability that a good solution will be found. The time spent searching (*i.e.*, number of generations) has an effect, but past a certain point the search yields no further improvement.

9.7.3 Comparison of Solution Methods for Test Case

Following tuning, the final parameter values were determined and are available in Table 9.11. The parameter values were used to evaluate 100 trials of the test case (*MW* = 342 g/mol) for each solution method. The objective function values and times to solution over the trials were compared across methods.

Table 9.11 Final tuned values for tabu search and the genetic algorithm The parameter values shown were used for the test case comparison and design cases in Section 9.8.

Tabu Search		**Genetic Algorithm**	
Parameter	*Tuned Value*	*Parameter*	*Tuned Value*
Maximum non-improving iterations	100	Maximum number of generations	25
Maximum neighbors evaluated per iteration	4	Population Size	50
Tabu list length	15	Maximum reproduction probability	100
Tabu criterion	0.5		

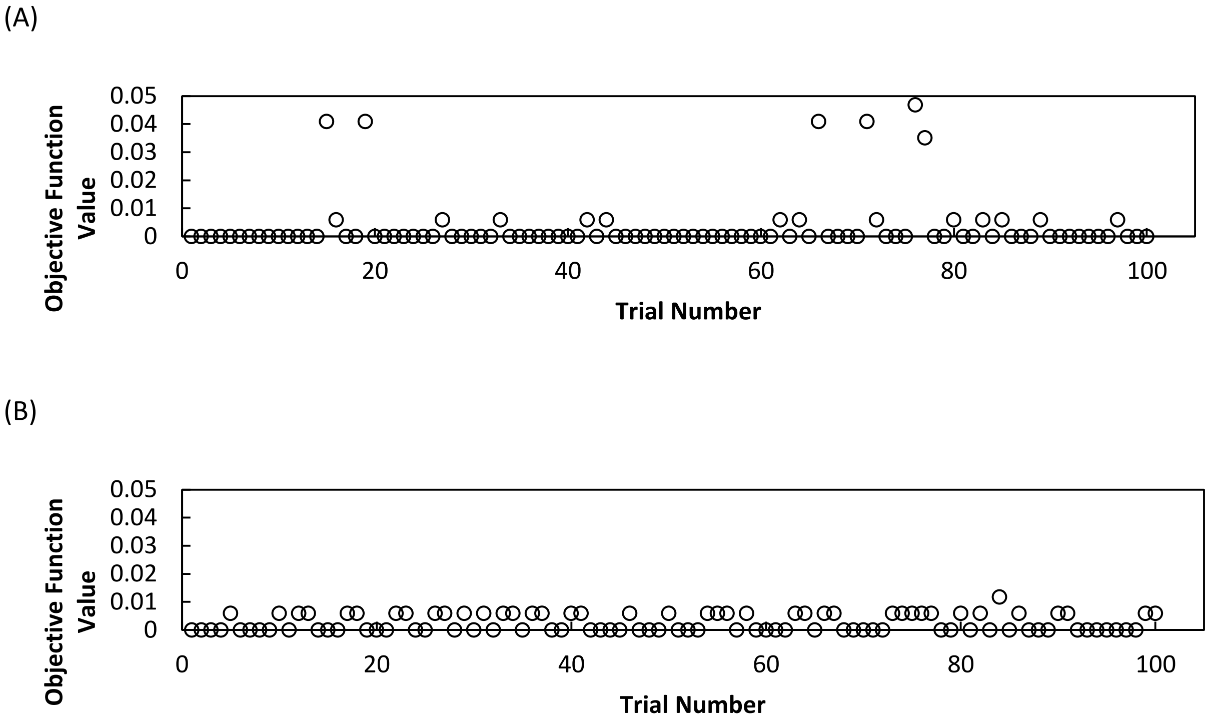

Figure 9.21 Comparison between objective function values obtained for all 100 trial solutions of the test case by (A) tabu search and (B) the genetic algorithm

In Figure 9.21, the objective function values for all 100 trials are compared between the tabu search and genetic algorithm. It should be noted that the test case had many possible combinations exist which satisfy the target value and thus had many opportunities to find a global optimum. The tabu search returned a molecule with the target value 81% of the time and returned a molecule within 5% of the target value in all trials. The genetic algorithm had somewhat lower success, returning a molecule with the target value 59% of the time. Yet the genetic algorithm still returned a molecule within 5% of the target value in all trials. Additionally, the tabu search had several trials that returned much higher objective function values when compared to the all of the trials for the genetic algorithm. So while the tabu search has a higher probability of returning a correct solution, it also appears to have a higher probability of returning a relatively poor solution when compared to the genetic algorithm.

The times to solution for all 100 trials are compared between the tabu search and genetic algorithm in Figure 9.22. The genetic algorithm had much less variability in time to solution as compared to tabu search. The time to solution is also faster on average for the genetic algorithm. Neither observation is surprising as the search effectively restarts during tabu search when a new best solution is identified. The amount of restarts is random, leading to variability in time to solution. The tuning results suggest that tabu search can return results with better objective function values while the genetic algorithm returns results with significantly lower time to solution. To further compare the stochastic methods, several design cases are considered in the following section.

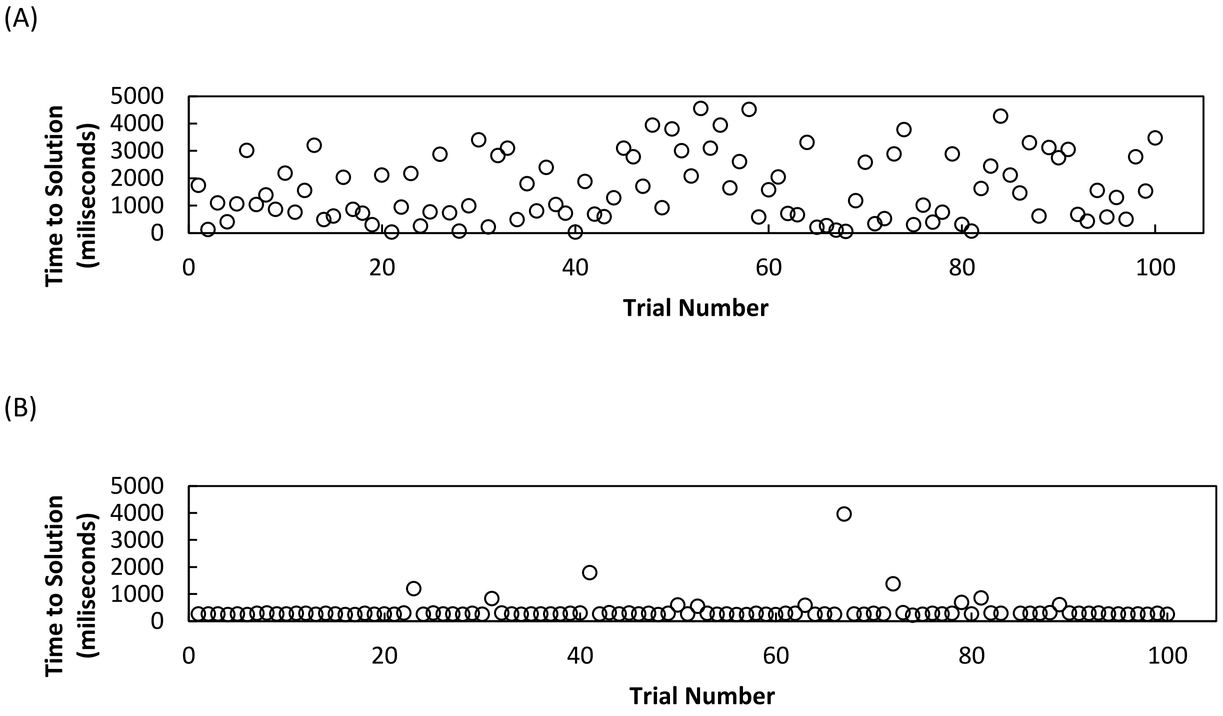

Figure 9.22 Comparison between times to solution observed for all 100 trial solutions of the test case during (A) tabu search and (B) the genetic algorithm

9.8 Results for Optimal Design of Stabilizers for Lyophilized Protein Formulations

The tuned stochastic optimization methods presented in Section 9.7 were used in CAMD to obtain optimal stabilizing excipient candidates for the property models outline in Section 9.5. The models for individual proteins were chosen over the universal model given in Section 9.6 as the *%Monomer* models dependent on excipient show superior fit and predictive capability. Therefore the models are good examples to illustrate the ability of the CAMD methods to design excipients that optimally match the given target value with low prediction error, as evaluated by prediction intervals. Design was limited to carbohydrate excipients. Every design case was subjected to 100 trials. Results are compared across stochastic optimization methods and also across proteins.

9.8.1 Comparison of CAMD Results Obtained by Tabu Search and a Genetic Algorithm

CAMD was used to generate optimal carbohydrate stabilizers for BSA, RNAse A, α-amylase, ovalbumin and trypsin inhibitor design cases. Solutions were obtained through use of the tuned stochastic optimization methods presented in Section 9.7. The best solutions out of 100 runs of both solution methods are displayed for each protein in Figures 9.23-9.27. The use of chirality connectivity indices in the models allows chiral information to be determined for the solutions, giving an indication of three-dimensional structure. A summary of the average objective function values and average times to solution for all 100 runs is also presented in the figures.

For all design cases, the best results obtained from tabu search and the genetic algorithm had prediction intervals that overlapped the target property value. Therefore, all of the best candidates returned displayed predicted property values that were statistically similar to the desired target property value of 100% monomer remaining after lyophilization. Additionally, for each design case, the prediction intervals for the best tabu search solution overlapped with the prediction intervals for the best genetic algorithm solution. Despite returning solutions with objective function values that differed up to two orders of magnitudes, both methods returned statistically similar solutions for all design cases. From the basis of target property value returned by the best solution, both stochastic methods perform at a similarly high level (*i.e.*, both models return solutions that match the target property).

From case to case, the magnitude of prediction intervals varied. As the size of prediction intervals is related to the expected error in the observed property value, solutions with small prediction intervals are desired. Considering the best solutions only, tabu search returned solutions with smaller prediction intervals for 3 cases (RNAse A, a-amylase and trypsin inhibitor) and the genetic algorithm returned solutions with smaller prediction intervals for 2 cases (BSA and ovalbumin). The magnitude also varied from case to case. In particular, the ovalbumin design case had solutions with extremely small prediction intervals (see Figure 9.26). The magnitude of prediction intervals increases as the descriptors used in the prediction diverge from the descriptor values used to build the predictive model. A quick look at the best solutions reveals that many of the structures are quite different from the monosaccharaide, disaccharaide, trisaccharaide and sugar alcohol structures used in model development. An exception occurs in the ovalbumin design case. The tabu solution is very similar to maltitol and the genetic algorithm solution is very similar to galactitol. Maltitol was used in model development and galactitol is a stereoisomer of sorbitol and mannitol, both of which were used in model development. As a result, the prediction intervals for both ovalbumin solutions are very small. In general, the prediction intervals for all design cases are comparable to the average experimental standard deviation of 2.20%.

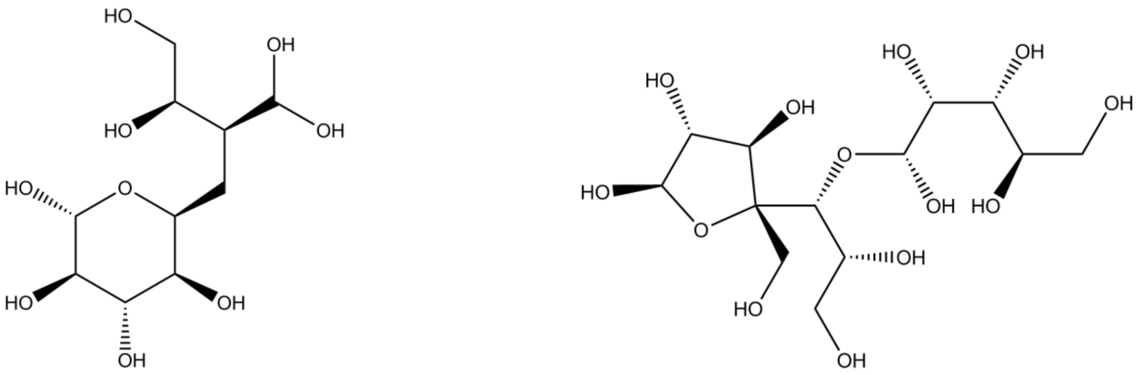

Tabu Search (A)

Objective function = $1.29\text{x}10^{-6}$
t = 4.571 sec
%Monomer = 100.00% ± 4.31%
MW = 284 g/mol
HBD = 8
HBA = 9
Rings = 1
Average Obj = 0.00461 ± 0.00534
Average t = 4.753 ± 1.878 sec
Close% = 100%

Genetic Algorithm (B)

Objective function = $1.25\text{x}10^{-4}$
t = 0.265 sec
%Monomer = 100.01% ± 3.98%
MW = 390 g/mol
HBD = 11
HBA = 13
Rings = 1
Average Obj =0.0245 ± 0.1317
Average t =1.495 ± 1.954 sec
Close% = 96%

Figure 9.23 Optimal carbohydrate stabilizer candidates for BSA, as determined by (A) tabu search and (B) genetic algorithm The objective function value (*obj*), time to solution in seconds (*t*), predicted target property value (*%Monomer*), molecular weight (*MW*), number of hydrogen-bond donors (*HBD*), number of hydrogen-bond acceptors (*HBA*) and number of rings present (*rings*) are listed for the top solution. Also listed are the average objective function values, average time to solution values and percentage of trials with 5% (*close%*) of target property for 100 trials. Prediction intervals provide the ± interval for the objective function value of the best solution. The standard deviation of 100 trials represents the ± interval for the average values over 100 trials.

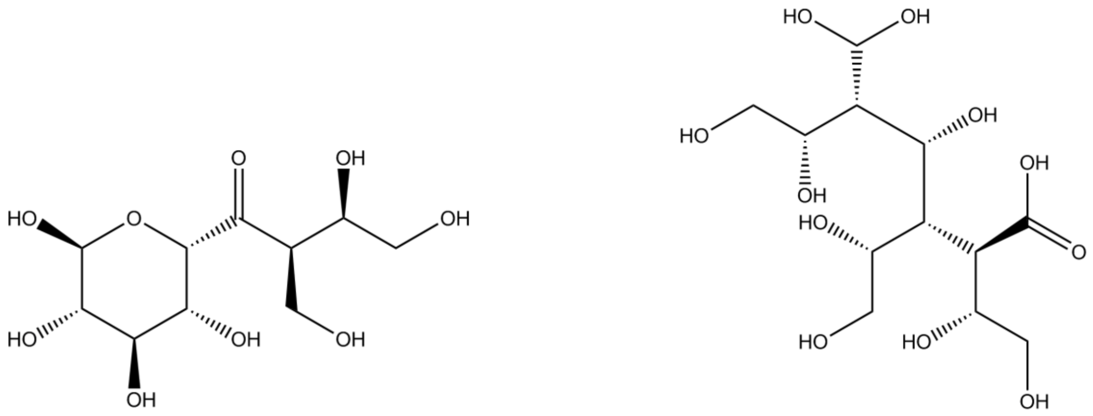

Tabu Search (A)

Objective function = 1.19x10^{-4}
t = 5.929 sec
%Monomer = 99.99% ± 3.08%
MW = 282 g/mol
HBD = 7
HBA = 9
Rings = 1
Average Obj = 0.00669 ± 0.00917
Average t = 4.786 ± 1.590 sec
Close% = 100%

Genetic Algorithm (B)

Objective function = 3.63x10^{-5}
t = 0.265 sec
%Monomer = 100.00% ± 5.19%
MW = 344 g/mol
HBD = 10
HBA = 11
Rings = 0
Average Obj = 0.203 ± 1.005
Average t = 2.684 ± 3.683 sec
Close% = 90%

Figure 9.24 Optimal carbohydrate stabilizer candidates for RNAse A, as determined by (A) tabu search and (B) genetic algorithm Description of figure values is given in caption for Figure 9.23.

When looking at the quality of solutions over all 100 trials, the tabu search has a better average objection function value when compared to the genetic algorithm for all design cases. The objective function value has lower variability for the tabu search results compared to the genetic algorithm for all design cases, as indicated by the standard deviation values. In addition, the percentage of solutions that are within 5% of the target value is 100% for tabu search runs in all design cases while the percentage ranges from 90-99% for the genetic algorithm runs. On average, the tabu search can be expected to return a solution of higher quality than the genetic algorithm. The results from tuning the test case suggest the same conclusion.

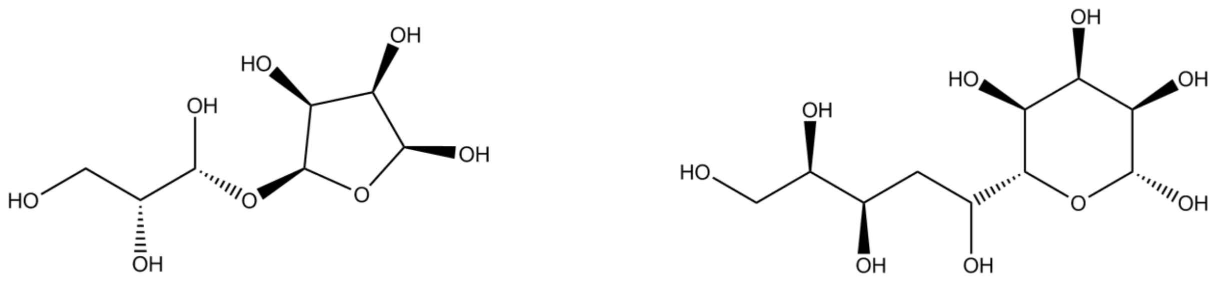

Tabu Search (A)

Objective function = 1.83x10^{-5}
t = 10.187 sec
%Monomer = 100.00 ± 1.50%
MW = 240 g/mol
HBD = 7
HBA = 8
Rings = 1
Average Obj = 0.00153 ± 0.00162
Average t = 5.240 ± 1.985 sec
Close% = 100%

Genetic Algorithm (B)

Objective function = 3.65x10^{-5}
t = 0.265 sec
%Monomer = 100.00% ± 1.66%
MW = 284 g/mol
HBD = 8
HBA = 9
Rings = 1
Average Obj =0.00536 ± 0.02107
Average t = 0.384 ± 0.397 sec
Close% = 99%

Figure 9.25 Optimal carbohydrate stabilizer candidates for α-amylase, as determined by (A) tabu search and (B) genetic algorithm Description of figure values is given in caption for Figure 9.23.

By method, the times to solution for the best solutions and the average times to solution were comparable. Comparing methods, the genetic algorithm is an order of magnitude faster than tabu search in determining a solution. The tabu search displays a higher variability in time to solution, as indicated by the larger standard deviation values. As noted in the tuning results (see Section 9.7), the tabu search effectively restarts when a new best solution is encountered. The number of times this occurs is directly proportional to the time to solution. Average time to solution does vary somewhat as the design case is varied, which likely indicates that more good solutions exist in the solution space for some models as compared to others. If there are higher numbers of good solutions, the probability of encountered a good solution is higher and the expected time to solution would be faster. Overall, the results from the design cases agree with the results from the test case that time to solution is faster and experiences lower variability with the genetic algorithm as compared to the tabu search.

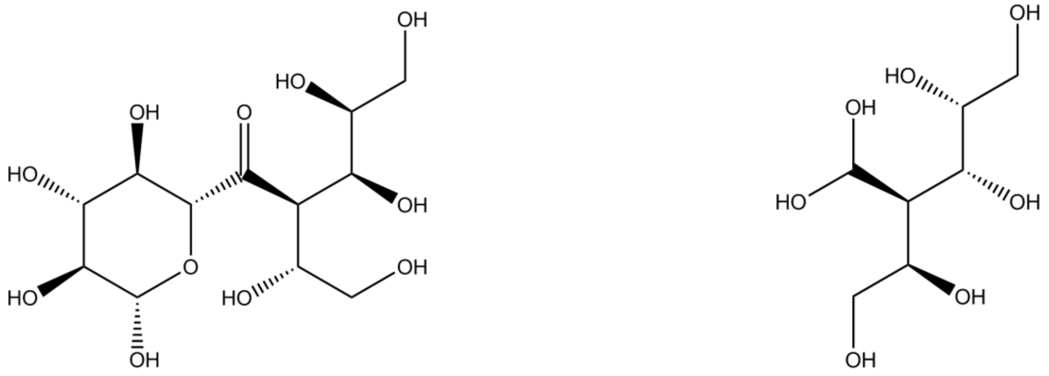

Tabu Search (A)

Objective function = $4.60\text{x}10^{-5}$
t = 4.982 sec
%Monomer = 100.00% ± 0.29%
MW = 342 g/mol
HBD = 9
HBA = 11
Rings = 1
Average Obj = 0.00186 ± 0.00171
Average t = 4.930 ± 1.746 sec
Close% = 100%

Genetic Algorithm (B)

Objective function = $3.49\text{x}10^{-5}$
t = 0.281 sec
%Monomer = 100.00% ± 0.21%
MW = 212 g/mol
HBD = 7
HBA = 7
Rings = 0
Average Obj = 0.0402 ± 0.2923
Average t = 0.516 ± 0.946 sec
Close% = 97%

Figure 9.26 Optimal carbohydrate stabilizer candidates for ovalbumin, as determined by (A) tabu search and (B) genetic algorithm Description of figure values is given in caption for Figure 9.23.

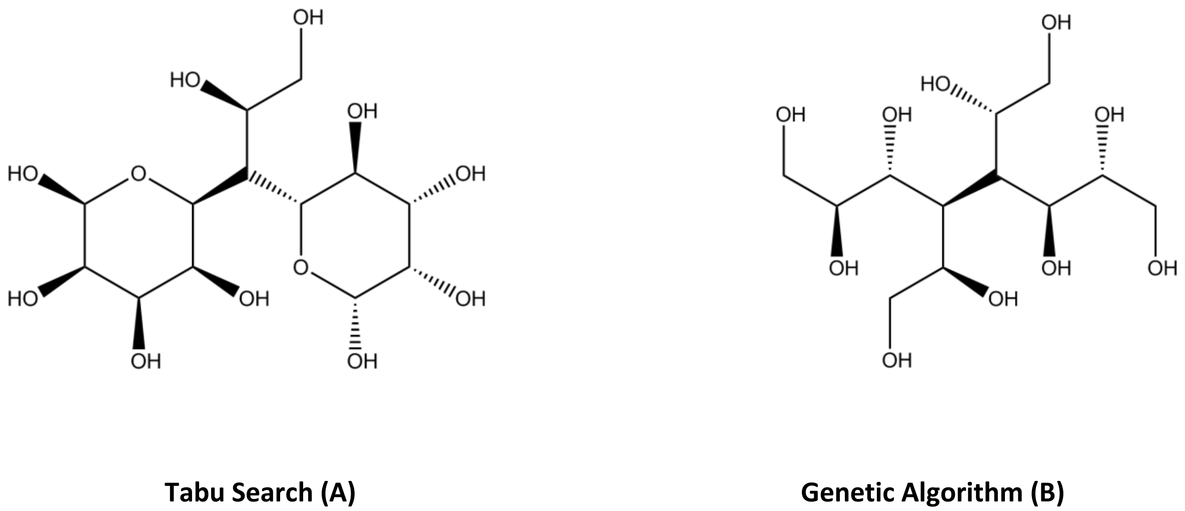

Tabu Search (A)

Objective function = 9.98x10^{-6}
t = 5.054 sec
%Monomer = 100.00 ± 3.42%
MW = 372 g/mol
HBD = 10
HBA = 12
Rings = 2
Average Obj = 0.00145 ± 0.00159
Average t = 5.652 ± 1.924 sec
Close% = 100%

Genetic Algorithm (B)

Objective function = 1.01x10^{-4}
t = 0.390 sec
%Monomer = 100.00% ± 5.75%
MW = 330 g/mol
HBD = 10
HBA = 10
Rings = 0
Average Obj = 0.0231 ± 0.1913
Average t = 0.430 ± 0.477 sec
Close% = 99%

Figure 9.27 Optimal carbohydrate stabilizer candidates for trypsin inhibitor, as determined by (A) tabu search and (B) genetic algorithm Description of figure values is given in caption for Figure 9.23.

Comparison of the methods demonstrates that tabu search provides solution with higher quality (as indicated by the objective function) and the genetic algorithm provides solutions with less computation effort (as indicated by the time to solution). It is tempting to select the tabu search method as the better stochastic method for CAMD due to higher solution quality, yet the best genetic algorithm solutions are statistically comparable to the best tabu search solutions. Additionally, the genetic algorithm on average can roughly produce a list of 100 candidates in the time it would take the tabu search to produce a list of 10 candidates. Therefore, the genetic algorithm is more efficient than the tabu search and equally capable of producing high quality results for all design cases.

9.8.2 Comparison of CAMD Results as a Function of Protein Included in the Formulation

A comparison of solutions between each design case (*i.e.*, protein) was performed to determine if certain chemical characteristics were preferred by one protein over another. The chemical properties used for comparison were molecular weight (*MW*), number of hydrogen bond donors (*HBD*), number of hydrogen bond acceptors (*HBA*) and number of rings present (*rings*). The comparison of average CAMD solution properties by protein is given in Figure 9.28.

Comparison of results indicates that no significant difference in the properties considered exist across proteins. The solutions for both stochastic methods average to a monosaccharide (1 ring) with six to seven hydrogen bond donors, eight to nine hydrogen bond acceptors and a molecular weight less than 300 g/mol. The disaccharides sucrose and trehalose are often cited as effective lyoprotectants (Schwegman, Hardwick *et al.* 2005). The average solution property values are lower than the property values observed for sucrose and trehalose, which are isomers and have molecular weights of 342 g/mol, eight hydrogen bond donors and eleven hydrogen bond donors. Of the best solutions presented in Section 9.8.1, only one solution contained two rings (see Figure 9.27a). All other solutions contained either one ring or no rings.

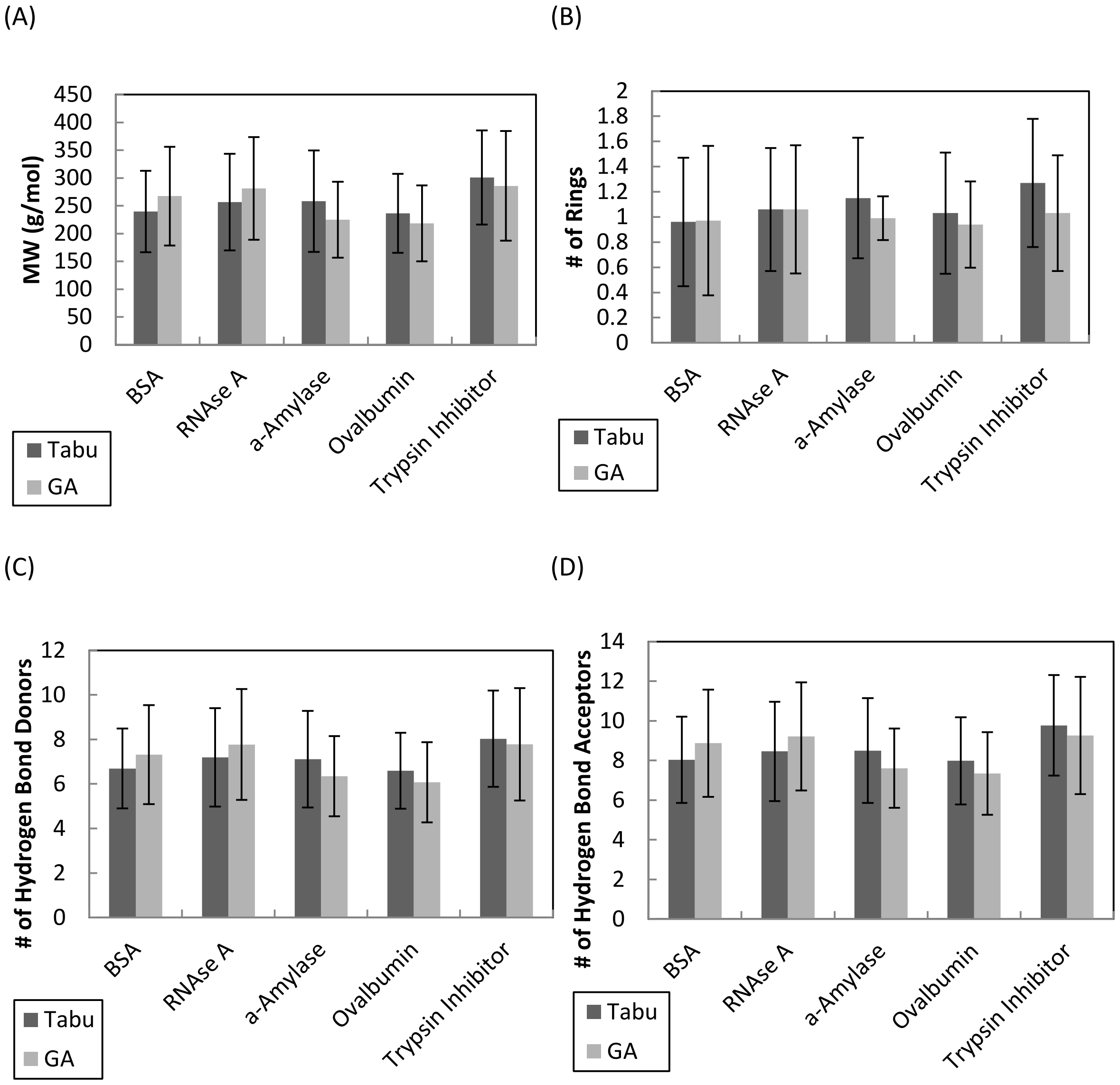

Figure 9.28 Comparison across protein models of average chemical information for solutions derived by both tabu search and genetic algorithm The information used for comparison are **(A)** molecular weight (g/mol), **(B)** number of rings, **(C)** number of hydrogen bond donors, and **(D)** number of hydrogen bond acceptors. Error bars represent the standard deviation of 100 trials for each case.

The three-dimensional conformation appears to be more important than the chemical properties considered for obtaining 100% monomer remaining after lyophilization. By incorporating chiral connectivity indices in the *%Monomer* property models, three-dimensional information is captured. Only nine building block groups are used in the determination of all the solutions presented. Yet, the inclusion of chirality information vastly increases the number of possible solutions and is the overriding factor in the design of optimal solutions. The models and CAMD results here present the first use of chiral connectivity indices in CAMD and the first use of topological descriptors to provide CAMD solutions with three-dimensional structural information. It is important to note that the solutions provided were not designed using all relevant excipient properties and should therefore not be considered final candidates for immediate inclusion in lyophilized protein formulations. However, both stochastic methods are able to quickly generate a large list of optimal candidates that can be further screened in a post-design phase, which may include any combination of additional property models, molecular simulations and experiments that are deemed necessary. The work here provides a starting point for the CAMD of excipients with three-dimensional structural information for stabilization of lyophilized proteins.

10.0 Conclusions and Future Recommendations

The work presented here describes the comprehensive development of CAMD methods with applications towards bioengineering, namely the design of ionic liquid media for bioseparations and the design of excipients for lyophilized protein formulations. The pre-design approach to CAMD is concerned with the determination of systems of interest and the acquisition of data for property of interests. Where available, data was collected from literature to build the models developed here. For prediction of monomeric protein remaining after lyophilization, the collection of experimental data was required.

The design phase of CAMD is comprised of two sub-problems. The forward problem is concerned with property model development, linking structure to properties of interest. Several approaches novel to CAMD were employed to better provide models of sufficient fit and predictive power. Descriptor selection was used when applicable to provide models with sufficient fit while avoiding overfitting. Exhaustive selection was found to be superior to forward selection when developing models describing *%Monomer* as a function of protein structure. The use of cross-validation has been used previously in CAMD (Eslick, Ye et al. 2009), but the approach was furthered here with the use of K-fold validation to more significantly probe predictive capability of models describing *%Monomer* as a function of excipient structure. Additionally, the use of Q^2 as an indicator of predictive power was illustrated with poor Q^2 values leading to predicted ionic liquid toxicity values with large prediction intervals. Molecular descriptors novel to CAMD were used for the models describing *%Monomer* as a function of excipient structure, which provided chirality information to help distinguish between molecules. By using chiral connectivity indices, some three-dimensional structural information was captured using only a two-dimensional molecular representation.

The reverse problem of the CAMD aims to propose molecular structures that optimally match given target property values. Molecular candidates to the ionic liquid and excipient design problems were proposed using a variety of solution approaches. Deterministic methods were used to solve for ionic liquid entrainers for separation of azeotropic mixtures. Tabu search, a stochastic method, was used to design ionic liquid extractants and excipients with optimal glass forming properties. Novel to the work presented here, two stochastic optimization methods (*i.e.*, tabu search and genetic algorithm) were tuned for CAMD applications. The stochastic methods were then used to design carbohydrate stabilizers for lyophilized protein formulations. Evaluation of the two methods showed that tabu search had longer time to solutions but higher solution quality and consistency when compared to the genetic algorithm. However when comparing the best solutions from each method, the predicted target values were similar as indicated by overlapping prediction intervals. Use of prediction intervals are original to the CAMD approaches used here and help to provide a statistical means of comparison between solutions. By incorporating chiral connectivity indices in the design of stabilizing excipients, three-dimensional structural information for design solutions was provided for the first time in CAMD approaches through use of only two-dimensional structural information.

The post-design of CAMD aims to further screen and establish good candidates for a given application. The coupling of product and process design allowed for the design of ionic liquid entrainers and azeotropic separation processes with near-optimal performance in terms of energy requirements. Final ionic liquid separation process results were shown to require less energy to perform separations than systems using entrainers that were not rationally designed. Molecular simulation was investigated as a tool to approximate hydrogen-deuterium exchange experiments and gleam information on possible protein-excipient interactions. Use of simulation results are likely insufficient to guide design at the current state of implementation. A better use of molecular simulation is likely to be as a post-design screening tool to further narrow down an excipient candidate list for a given lyophilized protein formulation.

Moving forward, more property models are needed for the examples considered to better generate a list of candidates that would be expected to perform successfully. For example, human toxicity would be important for the design of excipients for protein drug formulations. Additionally, several of the design solutions are reducing sugars, which would not be acceptable for protein formulations. Rules for group addition or improved penalty functions could be employed to prevent reducing sugars from being selected as solutions. In several of the design examples, the error in property prediction of *%Monomer* exceeds what would be acceptable from the viewpoint of the biopharmaceutical industry. A multi-objective optimization problem could be formulated to minimize both differences between target and predicted properties along with prediction intervals of predicted properties. Such a problem formulation would insure that solutions are returned where confidence in the predicted property values is high. For prediction of glass transitions, multiple transitions may occur in a sugar. Improvement to glass transition properties could include the prediction of polymorphic systems where multiple transitions would be expected to occur. The shift from one-dimensional (*e.g.*, group contribution) and two-dimensional descriptors towards three-dimensional or quantum descriptors will likely provide better property prediction and more accurate design results in future CAMD applications.

Tuning of the tabu search and genetic algorithm was performed on a basic level. Future work in tuning and increased levels of sophistication in the design algorithms will be useful in improving algorithm efficiency and solution quality. For example, mutation rate and crossover rate were randomly selected in the genetic algorithm. Further tuning could identify rates that were more useful for CAMD. Additionally, the tuning results presented are dependent on the base values of parameters used for tuning. It is possible that the base value for a parameter could have such a value that the parameter overwhelmed the effects of other parameters. Further investigation into the base parameter values and their effect on the final chosen tuned values would be of interest. An especially promising area of algorithm development is the parallelization of stochastic optimization methods, which is expected to provide substantial improvements to the computational costs of performing CAMD. As molecular complexity increases, the resulting combinatorial search space could warrant the need for vastly reduce search times that would be proffered by parallelization. The parallelization of both stochastic solution methods would also be of interest from the point of view of a pure scientific curiosity. Combination of the design process with a database search offers a promising avenue of future post-design methods. For example, a molecule that is design could be used to identify similar molecules in online structure databases, such as PubChem. Similarity searches would provide a way to experimentally validate CAMD design results without the time and complexity that would result from chemical synthesis of the design solutions. Information from experimental validation could be used to further improve property models and design methods. Such an integrated experimental-computational CAMD approach would be instrumental in the identification of molecule candidates for use in a variety of bioengineering applications, including the lyophilized protein formulation design and ionic liquid solvent design cases considered here.

REFERENCES

Akamatsu, M. (2002). "Current State and Perspectives of 3D-QSAR." Current Topics in Medicinal Chemistry **2**(12): 1381-1394.

Anfinsen, C. B. (1972). "The formation and stabilization of protein structure." Biochem. J. **128**(4): 737-749.

Ann, E. V., J. B. Nicholas and D. R. Robin (2012). Preface. Ionic Liquids: Science and Applications, American Chemical Society. **1117:** ix-x.

Arakawa, T., D. Ejima, T. Li and J. S. Philo (2010). "The critical role of mobile phase composition in size exclusion chromatography of protein pharmaceuticals." Journal of Pharmaceutical Sciences **99**(4): 1674-1692.

Arakawa, T. and Y. Kita (2000). "Stabilizing effects of caprylate and acetyltryptophanate on heat-induced aggregation of bovine serum albumin." Biochimica et Biophysica Acta (BBA) - Protein Structure and Molecular Enzymology **1479**(1–2): 32-36.

Arakawa, T. and S. N. Timasheff (1982). "Stabilization of protein structure by sugars." Biochemistry **21**(25): 6536-6544.

Awad, W. H., J. W. Gilman, M. Nyden, R. H. Harris Jr, T. E. Sutto, J. Callahan, P. C. Trulove, H. C. DeLong and D. M. Fox (2004). "Thermal degradation studies of alkyl-imidazolium salts and their application in nanocomposites." Thermochimica Acta **409**(1): 3-11.

Bäck, T. (1996). Evolutionary algorithms in theory and practice : evolution strategies, evolutionary programming, genetic algorithms. New York, Oxford University Press.

Barton, A. F. M. (1991). CRC handbook of solubility parameters and other cohesion parameters. Boca Raton, Fla., CRC Press.

Barton, P. (2000). "Solvent recovery opportunities in the pharmaceutical industry." Current Opinion in Drug Discovery & Development **3**(6): 707 - 713.

Bek-Pedersen, E., R. Gani and O. Levaux (2000). "Determination of optimal energy efficient separation schemes based on driving forces." Computers & Chemical Engineering **24**(2-7): 253-259.

Bicerano, J. (2002). Prediction of polymer properties. New York, Marcel Dekker.

Bondi, A. (1964). "van der Waals Volumes and Radii." The Journal of Physical Chemistry **68**(3): 441-451.

Camarda, K. V. and C. D. Maranas (1999). "Optimization in Polymer Design Using Connectivity Indices." Industrial & Engineering Chemistry Research **38**(5): 1884-1892.

Camarda, K. V. and P. Sunderesan (2005). "An Optimization Approach to the Design of Value-Added Soybean Oil Products." Industrial & Engineering Chemistry Research **44**(12): 4361-4367.

Carpenter, J. F. and J. H. Crowe (1989). "An infrared spectroscopic study of the interactions of carbohydrates with dried proteins." Biochemistry **28**(9): 3916-3922.

Carpenter, J. F., T. W. Randolph, W. Jiskoot, D. J. A. Crommelin, C. R. Middaugh and G. Winter (2010). "Potential inaccurate quantitation and sizing of protein aggregates by size exclusion chromatography: Essential need to use orthogonal methods to assure the quality of therapeutic protein products." Journal of Pharmaceutical Sciences **99**(5): 2200-2208.

Carpenter, J. F., T. W. Randolph, W. Jiskoot, D. J. A. Crommelin, C. R. Middaugh, G. Winter, Y.-X. Fan, S. Kirshner, D. Verthelyi, S. Kozlowski, K. A. Clouse, P. G. Swann, A. Rosenberg and B. Cherney (2009). "Overlooking subvisible particles in therapeutic protein products: Gaps that may compromise product quality." Journal of Pharmaceutical Sciences **98**(4): 1201-1205.

Chang, B. S., B. S. Kendrick and J. F. Carpenter (1996). "Surface-induced denaturation of proteins during freezing and its inhibition by surfactants." Journal of Pharmaceutical Sciences **85**(12): 1325-1330.

Cheng, F., J. Shen, X. Luo, W. Zhu, J. Gu, R. Ji, H. Jiang and K. Chen (2002). "Molecular docking and 3-D-QSAR studies on the possible antimalarial mechanism of artemisinin analogues." Bioorganic & Medicinal Chemistry **10**(9): 2883-2891.

Chennamsetty, N., V. Voynov, V. Kayser, B. Helk and B. L. Trout (2009). "Design of therapeutic proteins with enhanced stability." Proceedings of the National Academy of Sciences **106**(29): 11937-11942.

Chi, E., S. Krishnan, T. Randolph and J. Carpenter (2003). "Physical Stability of Proteins in Aqueous Solution: Mechanism and Driving Forces in Nonnative Protein Aggregation." Pharmaceutical Research **20**(9): 1325-1336.

Chi, E. Y., S. Krishnan, T. W. Randolph and J. F. Carpenter (2003). "Physical stability of proteins in aqueous solution: Mechanism and driving forces in nonnative protein aggregation." Pharmaceutical Research **20**(9): 1325-1336.

Chowdhury, S. K., V. Katta and B. T. Chait (1990). "Probing conformational changes in proteins by mass spectrometry." Journal of the American Chemical Society **112**(24): 9012-9013.

Clas, S. D., R. Faizer, R. E. O'Connor and E. B. Vadas (1995). "Quantification of crystallinity in blends of lyophilized and crystalline MK-0591 using x-ray powder diffraction." International Journal of Pharmaceutics **121**(1): 73-79.

Cleland, J. L., R. S. Langer and American Chemical Society. Division of Biochemical Technology. (1994). Formulation and delivery of proteins and peptides. Washington, DC, American Chemical Society.

Conchillo-Sole, O., N. de Groot, F. Aviles, J. Vendrell, X. Daura and S. Ventura (2007). "AGGRESCAN: a server for the prediction and evaluation of "hot spots" of aggregation in polypeptides." BMC Bioinformatics **8**(1): 65.

Conchillo-Sole, O., N. S. de Groot, F. X. Aviles, J. Vendrell, X. Daura and S. Ventura (2007). "AGGRESCAN: a server for the prediction and evaluation of "hot spots" of aggregation in polypeptides." BMC Bioinformatics **8**: 65.

Consonni, V. and R. Todeschini (2000). Handbook of molecular descriptors. Weinheim ; Chichester, Wiley-VCH.

Conte, E., R. Gani, Y. S. Cheng and K. M. Ng (2012). "Design of formulated products: Experimental component." AIChE Journal **58**(1): 173-189.

Conte, E., R. Gani and K. M. Ng (2011). "Design of formulated products: A systematic methodology." AIChE Journal **57**(9): 2431-2449.

Costantino, H. R. and M. J. Pikal (2004). Lyophilization of biopharmaceuticals. Arlington, VA, AAPS Press.

Cottone, G., G. Ciccotti and L. Cordone (2002). "Protein--trehalose--water structures in trehalose coated carboxy-myoglobin." The Journal of Chemical Physics **117**(21): 9862-9866.

Crowe, J. H., J. F. Carpenter and L. M. Crowe (1998). "The role of vitrification in anhydrobiosis." Annual Review of Physiology **60**(1): 73-103.

Cussler, E. L. and G. D. Moggridge (2011). Chemical product design. Cambridge ; New York, Cambridge University Press.

D. Holbrey, J. and K. R. Seddon (1999). "The phase behaviour of 1-alkyl-3-methylimidazolium tetrafluoroborates; ionic liquids and ionic liquid crystals." Journal of the Chemical Society, Dalton Transactions(13): 2133-2140.

Dalgaard, P. (2008). Introductory Statistics with R. New York, NY, Springer Science+Business Media, LLC.

Domanska, U. and A. Marciniak (2008). "Measurements of activity coefficients at infinite dilution of aromatic and aliphatic hydrocarbons, alcohols, and water in the new ionic liquid [EMIM][SCN] using GLC." The Journal of Chemical Thermodynamics **40**(5): 860-866.

Domańska, U. and A. Marciniak (2007). "Activity Coefficients at Infinite Dilution Measurements for Organic Solutes and Water in the Ionic Liquid 1-Ethyl-3-methylimidazolium Trifluoroacetate." The Journal of Physical Chemistry B **111**(41): 11984-11988.

Domańska, U. and A. Marciniak (2008). "Activity Coefficients at Infinite Dilution Measurements for Organic Solutes and Water in the Ionic Liquid 1-Butyl-3-methylimidazolium Trifluoromethanesulfonate." The Journal of Physical Chemistry B **112**(35): 11100-11105.

Duran, M. and I. Grossmann (1986). "An outer-approximation algorithm for a class of mixed-integer nonlinear programs." Mathematical Programming **36**(3): 307-339.

Duy, C. and J. Fitter (2005). "Thermostability of Irreversible Unfolding α-Amylases Analyzed by Unfolding Kinetics." Journal of Biological Chemistry **280**(45): 37360-37365.

Eden, M. R., S. B. Jørgensen, R. Gani and M. M. El-Halwagi (2004). "A novel framework for simultaneous separation process and product design." Chemical Engineering and Processing: Process Intensification **43**(5): 595-608.

Edgar, T. F., D. M. Himmelblau and L. S. Lasdon (2001). Optimization of chemical processes. New York, McGraw-Hill.

Eike, D. M., J. F. Brennecke and E. J. Maginn (2004). "Predicting Infinite-Dilution Activity Coefficients of Organic Solutes in Ionic Liquids." Industrial & Engineering Chemistry Research **43**(4): 1039-1048.

Eljack, F. T. and M. R. Eden (2008). "A systematic visual approach to molecular design via property clusters and group contribution methods." Computers & Chemical Engineering **32**(12): 3002-3010.

Engelsman, J., P. Garidel, R. Smulders, H. Koll, B. Smith, S. Bassarab, A. Seidl, O. Hainzl and W. Jiskoot (2011). "Strategies for the Assessment of Protein Aggregates in Pharmaceutical Biotech Product Development." Pharmaceutical Research **28**(4): 920-933.

Eslick, J. (2009). Molecular Design of Crosslinked Copolymers. Department of Chemical and Petroleum Engineering, University of Kansas. **PhD in Chemical Engineering**.

Eslick, J. C., Q. Ye, J. Park, E. M. Topp, P. Spencer and K. V. Camarda (2009). "A computational molecular design framework for crosslinked polymer networks." Computers & Chemical Engineering **33**(5): 954-963.

Eslick, J. C., Q. Ye, J. Park, E. M. Topp, P. Spencer and K. V. Camarda (2009). "A computational molecular design framework for crosslinked polymer networks." Computers and Chemical Engineering **33**(5): 954-963.

Ferguson, T. Linear Programming: A Concise Introduction.

Floudas, C. A. (1995). Nonlinear and mixed-integer optimization: fundamentals and applications, Oxford University Press.

Fredenslund, A., J. Gmehling and P. Rasmussen (1977). Vapor-liquid equilibria using UNIFAC: a group contribution method, Elsevier Scientific Pub. Co.

Fredlake, C. P., J. M. Crosthwaite, D. G. Hert, S. N. V. K. Aki and J. F. Brennecke (2004). "Thermophysical Properties of Imidazolium-Based Ionic Liquids." Journal of Chemical & Engineering Data **49**(4): 954-964.

Fung, J., A. A. Darabie and J. McLaurin (2005). "Contribution of simple saccharides to the stabilization of amyloid structure." Biochemical and Biophysical Research Communications **328**(4): 1067-1072.

Gangasharan and S. S. N. Murthy (1995). "Nature of the Relaxation Processes in the Supercooled Liquid and Glassy States of Some Carbohydrates." The Journal of Physical Chemistry **99**(32): 12349-12354.

Gangu, S. A., L. R. Weatherley and A. M. Scurto (2009). "Whole-Cell Biocatalysis with Ionic Liquids." Current Organic Chemistry **13**(13): 1242-1258.

Gani, R. (2004). "Chemical product design: challenges and opportunities." Computers & Chemical Engineering **28**(12): 2441-2457.

Gani, R. and E. Bek-Pedersen (2000). "Simple new algorithm for distillation column design." AIChE Journal **46**(6): 1271-1274.

Gani, R. and E. A. Brignole (1983). "Molecular design of solvents for liquid extraction based on UNIFAC." Fluid Phase Equilibria **13**(0): 331-340.

Gani, R., P. M. Harper and M. Hostrup (2005). "Automatic Creation of Missing Groups through Connectivity Index for Pure-Component Property Prediction." Industrial & Engineering Chemistry Research **44**(18): 7262-7269.

Gani, R., G. Hytoft, C. Jaksland and A. K. Jensen (1997). "An integrated computer aided system for integrated design of chemical processes." Computers & Chemical Engineering **21**(10): 1135-1146.

Gani, R., B. Nielsen and A. Fredenslund (1991). "A group contribution approach to computer-aided molecular design." AIChE Journal **37**(9): 1318-1332.

Gani, R., N. Tzouvaras, P. Rasmussen and A. Fredenslund (1989). "Prediction of gas solubility and vapor-liquid equilibria by group contribution." Fluid Phase Equilibria **47**(2-3): 133-152.

Gardas, R. L. and J. o. A. P. Coutinho (2008). "A Group Contribution Method for Heat Capacity Estimation of Ionic Liquids." Industrial & Engineering Chemistry Research **47**(15): 5751-5757.

Ge, M.-L. and L.-S. Wang (2008). "Activity Coefficients at Infinite Dilution of Polar Solutes in 1-Butyl-3-methylimidazolium Trifluoromethanesulfonate Using Gas–Liquid Chromatography." Journal of Chemical & Engineering Data **53**(3): 846-849.

Ge, M.-L., L.-S. Wang, M.-Y. Li and J.-S. Wu (2007). "Activity Coefficients at Infinite Dilution of Alkanes, Alkenes, and Alkyl Benzenes in 1-Butyl-3-methylimidazolium Trifluoromethanesulfonate Using Gas−Liquid Chromatography." Journal of Chemical & Engineering Data **52**(6): 2257-2260.

Ge, M.-L., L.-S. Wang, J.-S. Wu and Q. Zhou (2008). "Activity Coefficients at Infinite Dilution of Organic Solutes in 1-Ethyl-3-methylimidazolium Tetrafluoroborate Using Gas−Liquid Chromatography." Journal of Chemical & Engineering Data **53**(8): 1970-1974.

Glover, F. (1989). "Tabu search—part I." ORSA Journal on computing **1**(3): 190-206.

Gmehling, J., Menke, J., Krafczyk, J., Fischer, K. (1994). Azeotropic Data. Weinheim, Germany, VCH.

Golbraikh, A., D. Bonchev and A. Tropsha (2001). "Novel Chirality Descriptors Derived from Molecular Topology." Journal of Chemical Information and Computer Sciences **41**(1): 147-158.

Golbraikh, A., M. Shen, Z. Xiao, Y.-D. Xiao, K.-H. Lee and A. Tropsha (2003). "Rational selection of training and test sets for the development of validated QSAR models." Journal of Computer-Aided Molecular Design **17**(2-4): 241-253.

Goodsell, D. S., G. M. Morris and A. J. Olson (1996). "Automated docking of flexible ligands: Applications of autodock." Journal of Molecular Recognition **9**(1): 1-5.

Gsponer, J. and M. Vendruscolo (2006). "Theoretical approaches to protein aggregation." Protein and peptide letters **13**(3): 287-293.

Hackel, C., T. Zinkevich, P. Belton, A. Achilles, D. Reichert and A. Krushelnitsky (2012). "The trehalose coating effect on the internal protein dynamics." Physical Chemistry Chemical Physics **14**(8): 2727-2734.

Harper, P. M. and R. Gani (2000). "A multi-step and multi-level approach for computer aided molecular design." Computers & Chemical Engineering **24**(2–7): 677-683.

Harper, P. M., R. Gani, P. Kolar and T. Ishikawa (1999). "Computer-aided molecular design with combined molecular modeling and group contribution." Fluid Phase Equilibria **158–160**(0): 337-347.

Heintz, A., L. M. Casás, I. A. Nesterov, V. N. Emel'yanenko and S. P. Verevkin (2005). "Thermodynamic Properties of Mixtures Containing Ionic Liquids. 5. Activity Coefficients at Infinite Dilution of Hydrocarbons, Alcohols, Esters, and Aldehydes in 1-Methyl-3-butyl-imidazolium Bis(trifluoromethyl-sulfonyl) Imide Using Gas−Liquid Chromatography." Journal of Chemical & Engineering Data **50**(5): 1510-1514.

Heintz, A., D. V. Kulikov and S. P. Verevkin (2001). "Thermodynamic Properties of Mixtures Containing Ionic Liquids. 1. Activity Coefficients at Infinite Dilution of Alkanes, Alkenes, and Alkylbenzenes in 4-Methyl-n-butylpyridinium Tetrafluoroborate Using Gas−Liquid Chromatography." Journal of Chemical & Engineering Data **46**(6): 1526-1529.

Heintz, A., D. V. Kulikov and S. P. Verevkin (2002). "Thermodynamic properties of mixtures containing ionic liquids. Activity coefficients at infinite dilution of polar solutes in 4-methyl- N-butyl-pyridinium tetrafluoroborate using gas-liquid chromatography." The Journal of Chemical Thermodynamics **34**(8): 1341-1347.

Heintz, A., T. V. Vasiltsova, J. Safarov, E. Bich and S. P. Verevkin (2006). "Thermodynamic Properties of Mixtures Containing Ionic Liquids. 9. Activity Coefficients at Infinite Dilution of Hydrocarbons, Alcohols, Esters, and Aldehydes in Trimethyl-butylammonium Bis(trifluoromethylsulfonyl) Imide Using Gas−Liquid Chromatography and Static Method." Journal of Chemical & Engineering Data **51**(2): 648-655.

Heintz, A. and S. P. Verevkin (2005). "Thermodynamic Properties of Mixtures Containing Ionic Liquids. 6. Activity Coefficients at Infinite Dilution of Hydrocarbons, Alcohols, Esters, and Aldehydes in 1-Methyl-3-octyl-imidazolium Tetrafluoroborate Using Gas−Liquid Chromatography." Journal of Chemical & Engineering Data **50**(5): 1515-1519.

Heintz, A., S. P. Verevkin and D. Ondo (2006). "Thermodynamic Properties of Mixtures Containing Ionic Liquids. 8. Activity Coefficients at Infinite Dilution of Hydrocarbons, Alcohols, Esters, and Aldehydes in 1-Hexyl-3-methylimidazolium Bis(trifluoromethylsulfonyl) Imide Using Gas−Liquid Chromatography." Journal of Chemical & Engineering Data **51**(2): 434-437.

Hetényi, C. and D. van der Spoel (2002). "Efficient docking of peptides to proteins without prior knowledge of the binding site." Protein Science **11**(7): 1729-1737.

Hetényi, C. and D. van der Spoel (2006). "Blind docking of drug-sized compounds to proteins with up to a thousand residues." FEBS Letters **580**(5): 1447-1450.

Holland, J. H. (1975). Adaptation in natural and artificial systems : an introductory analysis with applications to biology, control, and artificial intelligence. Ann Arbor, University of Michigan Press.

HSL. (2011). "A collection of Fortran codes for large scale scientific computation." from http://www.hsl.rl.ac.uk.

Huang, H.-J., S. Ramaswamy, U. W. Tschirner and B. V. Ramarao (2008). "A review of separation technologies in current and future biorefineries." Separation and Purification Technology **62**(1): 1-21.

Huey, R., G. M. Morris, A. J. Olson and D. S. Goodsell (2007). "A semiempirical free energy force field with charge-based desolvation." Journal of Computational Chemistry **28**(6): 1145-1152.

Irbäck, A. and S. Mohanty (2006). "PROFASI: A Monte Carlo simulation package for protein folding and aggregation." Journal of Computational Chemistry **27**(13): 1548-1555.

Jerina, D. M., J. W. Daly, A. M. Jeffrey and D. T. Gibson (1971). "Cis-1,2-dihydroxy-1,2-dihydronaphthalene: A bacterial metabolite from naphthalene." Archives of Biochemistry and Biophysics **142**(1): 394-396.

Joback, K. G. and R. C. Reid (1987). "Estimation of pure-component properties from group-contribution." Chemical Engineering Communications **57**(1): 233 - 243.

Karunanithi, A. T., L. E. K. Achenie and R. Gani (2006). "A computer-aided molecular design framework for crystallization solvent design." Chemical Engineering Science **61**(4): 1247-1260.

Katayama, D. S., J. F. Carpenter, K. P. Menard, M. C. Manning and T. W. Randolph (2009). "Mixing properties of lyophilized protein systems: A spectroscopic and calorimetric study." Journal of Pharmaceutical Sciences **98**(9): 2954-2969.

Katayama, D. S., R. Nayar, D. K. Chou, J. Campos, J. Cooper, D. G. Vander Velde, L. Villarete, C. P. Liu and M. Cornell Manning (2005). "Solution behavior of a novel type 1 interferon, interferon-τ." Journal of Pharmaceutical Sciences **94**(12): 2703-2715.

Kato, R. and J. Gmehling (2004). "Activity coefficients at infinite dilution of various solutes in the ionic liquids [MMIM]+[CH3SO4]-, [MMIM]+[CH3OC2H4SO4]-, [MMIM]+[(CH3)2PO4]-, [C5H5NC2H5]+[(CF3SO2)2N]- and [C5H5NH]+[C2H5OC2H4OSO3]." Fluid Phase Equilibria **226**: 37-44.

Kato, R. and J. Gmehling (2005). "Measurement and correlation of vapor-liquid equilibria of binary systems containing the ionic liquids [EMIM][(CF3SO2)2N], [BMIM][(CF3SO2)2N], [MMIM][(CH3)2PO4] and oxygenated organic compounds respectively water." Fluid Phase Equilibria **231**(1): 38-43.

Kato, R. and J. Gmehling (2005). "Systems with ionic liquids: Measurement of VLE and [gamma][infinity] data and prediction of their thermodynamic behavior using original UNIFAC, mod. UNIFAC(Do) and COSMO-RS(Ol)." The Journal of Chemical Thermodynamics **37**(6): 603-619.

Katta, V., B. T. Chait and S. Carr (1991). "Conformational changes in proteins probed by hydrogen-exchange electrospray-ionization mass spectrometry." Rapid Communications in Mass Spectrometry **5**(4): 214-217.

Kerton, F. M. (2009). Alternative solvents for green chemistry. Cambridge, UK, RSC Pub.

Kerwin, B. A. (2008). "Polysorbates 20 and 80 used in the formulation of protein biotherapeutics: Structure and degradation pathways." Journal of Pharmaceutical Sciences **97**(8): 2924-2935.

Kier, L. B. and L. H. Hall (1986). Molecular connectivity in structure-activity analysis. New York, Research Studies Press ;

Wiley.

Kier, L. B., L. H. Hall, W. J. Murray and M. Randi (1975). "Molecular connectivity I: Relationship to nonspecific local anesthesia." Journal of Pharmaceutical Sciences **64**(12): 1971-1974.

Krummen, M., P. Wasserscheid and J. Gmehling (2002). "Measurement of Activity Coefficients at Infinite Dilution in Ionic Liquids Using the Dilutor Technique." Journal of Chemical & Engineering Data **47**(6): 1411-1417.

Kuntz Jr, I. D. and W. Kauzmann (1974). Hydration of Proteins and Polypeptides. Advances in Protein Chemistry. J. T. E. C.B. Anfinsen and M. R. Frederic, Academic Press. **Volume 28:** 239-345.

Lauer, T. M., N. J. Agrawal, N. Chennamsetty, K. Egodage, B. Helk and B. L. Trout (2012). "Developability index: a rapid in silico tool for the screening of antibody aggregation propensity." J Pharm Sci **101**(1): 102-115.

Lauer, T. M., N. J. Agrawal, N. Chennamsetty, K. Egodage, B. Helk and B. L. Trout (2012). "Developability index: A rapid in silico tool for the screening of antibody aggregation propensity." Journal of Pharmaceutical Sciences **101**(1): 102-115.

Leader, B., Q. J. Baca and D. E. Golan (2008). "Protein therapeutics: a summary and pharmacological classification." Nat Rev Drug Discov **7**(1): 21-39.

Lei, Z., J. Zhang, Q. Li and B. Chen (2009). "UNIFAC Model for Ionic Liquids." Industrial & Engineering Chemistry Research **48**(5): 2697-2704.

Letcher, T. M., U. Domanska, M. Marciniak and A. Marciniak (2005). "Activity coefficients at infinite dilution measurements for organic solutes in the ionic liquid 1-butyl-3-methyl-imidazolium 2-(2-methoxyethoxy) ethyl sulfate using g.l.c. at T = (298.15, 303.15, and 308.15) K." The Journal of Chemical Thermodynamics **37**(6): 587-593.

Letcher, T. M., A. Marciniak, M. Marciniak and U. Domanska (2005). "Activity coefficients at infinite dilution measurements for organic solutes in the ionic liquid 1-hexyl-3-methyl-imidazolium bis(trifluoromethylsulfonyl)-imide using g.l.c. at T = (298.15, 313.15, and 333.15) K." The Journal of Chemical Thermodynamics **37**(12): 1327-1331.

Letcher, T. M., B. Soko, D. Ramjugernath, N. Deenadayalu, A. Nevines and P. K. Naicker (2003). "Activity Coefficients at Infinite Dilution of Organic Solutes in 1-Hexyl-3-methylimidazolium Hexafluorophosphate from Gas−Liquid Chromatography." Journal of Chemical & Engineering Data **48**(3): 708-711.

Letcher, T. M., B. Soko, P. Reddy and N. Deenadayalu (2003). "Determination of Activity Coefficients at Infinite Dilution of Solutes in the Ionic Liquid 1-Hexyl-3-methylimidazolium Tetrafluoroborate Using Gas−Liquid Chromatography at the Temperatures 298.15 K and 323.15 K." Journal of Chemical & Engineering Data **48**(6): 1587-1590.

Li, Y., T. Williams and E. Topp (2008). "Effects of Excipients on Protein Conformation in Lyophilized Solids by Hydrogen/Deuterium Exchange Mass Spectrometry." Pharmaceutical Research **25**(2): 259-267.

Li, Y., T. D. Williams, R. L. Schowen and E. M. Topp (2007). "Characterizing protein structure in amorphous solids using hydrogen/deuterium exchange with mass spectrometry." Analytical Biochemistry **366**(1): 18-28.

Li, Y., T. D. Williams, R. L. Schowen and E. M. Topp (2007). "Trehalose and calcium exert site-specific effects on calmodulin conformation in amorphous solids." Biotechnology and Bioengineering **97**(6): 1650-1653.

Lin, B., S. Chavali, K. Camarda and D. C. Miller (2005). "Computer-aided molecular design using Tabu search." Computers & Chemical Engineering **29**(2): 337-347.

Liu, J., J. Andya and S. Shire (2006). "A critical review of analytical ultracentrifugation and field flow fractionation methods for measuring protein aggregation." The AAPS Journal **8**(3): E580-E589.

Lumley, T. (2004). "The LEAPS package." from cran.r-project.org/doc/packages/leaps.pdf.

Lumley, T. (2004). "The leaps package." cran.r-project.org/doc/packages/leaps.pdf.

Luo, H., J.-F. Huang and S. Dai (2008). "Studies on Thermal Properties of Selected Aprotic and Protic Ionic Liquids." Separation Science and Technology **43**(9-10): 2473-2488.

Ma, B. and R. Nussinov (2006). "Simulations as analytical tools to understand protein aggregation and predict amyloid conformation." Current Opinion in Chemical Biology **10**(5): 445-452.

Maindonald, J. H. and J. Braun (2010). Data analysis and graphics using R : an example-based approach. Cambridge ; New York, Cambridge University Press.

Manning, M., D. Chou, B. Murphy, R. Payne and D. Katayama (2010). "Stability of Protein Pharmaceuticals: An Update." Pharmaceutical Research **27**(4): 544-575.

Marciniak, A. (2010). "The Solubility Parameters of Ionic Liquids." International Journal of Molecular Sciences **11**(5): 1973-1990.

Marsh, K. N., J. A. Boxall and R. Lichtenthaler (2004). "Room temperature ionic liquids and their mixtures--a review." Fluid Phase Equilibria **219**(1): 93-98.

Marshall, S. A., G. A. Lazar, A. J. Chirino and J. R. Desjarlais (2003). "Rational design and engineering of therapeutic proteins." Drug Discovery Today **8**(5): 212-221.

Martin, A. N., P. J. Sinko and Y. Singh (2011). Martin's physical pharmacy and pharmaceutical sciences : physical chemical and biopharmaceutical principles in the pharmaceutical sciences. Baltimore, MD, Lippincott Williams & Wilkins.

Matsumoto, M., K. Mochiduki, K. Fukunishi and K. Kondo (2004). "Extraction of organic acids using imidazolium-based ionic liquids and their toxicity to Lactobacillus rhamnosus." Separation and Purification Technology **40**(1): 97-101.

McLeese, S. E., J. C. Eslick, N. J. Hoffmann, A. M. Scurto and K. V. Camarda (2010). "Design of ionic liquids via computational molecular design." Computers & Chemical Engineering **34**(9): 1476-1480.

McNally, E. J. and J. E. Hastedt (2008). Protein formulation and delivery. New York, Informa Healthcare.

Meste, M. L., D. Champion, G. Roudaut, G. Blond and D. Simatos (2002). "Glass Transition and Food Technology: A Critical Appraisal." Journal of Food Science **67**(7): 2444-2458.

Morris, G. M., D. S. Goodsell, R. S. Halliday, R. Huey, W. E. Hart, R. K. Belew and A. J. Olson (1998). "Automated docking using a Lamarckian genetic algorithm and an empirical binding free energy function." Journal of Computational Chemistry **19**(14): 1639-1662.

Münch, C. and A. Bertolotti (2010). "Exposure of Hydrophobic Surfaces Initiates Aggregation of Diverse ALS-Causing Superoxide Dismutase-1 Mutants." Journal of Molecular Biology **399**(3): 512-525.

Ngo, H. L., K. LeCompte, L. Hargens and A. B. McEwen (2000). "Thermal properties of imidazolium ionic liquids." Thermochimica Acta **357–358**(0): 97-102.

Ohtani, H., S. Ishimura and M. Kumai (2008). "Thermal Decomposition Behaviors of Imidazolium-type Ionic Liquids Studied by Pyrolysis-Gas Chromatography." Analytical Sciences **24**(10): 1335-1340.

Orchillés, A. V., P. J. Miguel, E. Vercher and A. Martínez-Andreu (2006). "Ionic Liquids as Entrainers in Extractive Distillation: Isobaric Vapor−Liquid Equilibria for Acetone + Methanol + 1-Ethyl-3-methylimidazolium Trifluoromethanesulfonate." Journal of Chemical & Engineering Data **52**(1): 141-147.

Orchillés, A. V., P. J. Miguel, E. Vercher and A. Martínez-Andreu (2007). "Isobaric Vapor−Liquid Equilibria for Ethyl Acetate + Ethanol + 1-Ethyl-3-methylimidazolium Trifluoromethanesulfonate at 100 kPa." Journal of Chemical & Engineering Data **52**(6): 2325-2330.

Orchillés, A. V., P. J. Miguel, E. Vercher and A. Martínez-Andreu (2008). "Isobaric Vapor−Liquid Equilibria for 1-Propanol + Water + 1-Ethyl-3-methylimidazolium Trifluoromethanesulfonate at 100 kPa." Journal of Chemical & Engineering Data **53**(10): 2426-2431.

Orchillés, A. V., P. J. Miguel, E. Vercher and A. Martínez-Andreu (2010). "Using 1-Ethyl-3-methylimidazolium Trifluoromethanesulfonate as an Entrainer for the Extractive Distillation of Ethanol + Water Mixtures." Journal of Chemical & Engineering Data **55**(4): 1669-1674.

Ourique, J. E. and A. Silva Telles (1998). "Computer-aided molecular design with simulated annealing and molecular graphs." Computers & Chemical Engineering **22, Supplement 1**(0): S615-S618.

Pace, C. N., B. A. Shirley, M. McNutt and K. Gajiwala (1996). "Forces contributing to the conformational stability of proteins." The FASEB Journal **10**(1): 75-83.

Papaiconomou, N., J. Salminen, J.-M. Lee and J. M. Prausnitz (2007). "Physicochemical Properties of Hydrophobic Ionic Liquids Containing 1-Octylpyridinium, 1-Octyl-2-methylpyridinium, or 1-Octyl-4-methylpyridinium Cations." Journal of Chemical & Engineering Data **52**(3): 833-840.

Patel, S. J., D. Ng and M. S. Mannan (2009). "QSPR Flash Point Prediction of Solvents Using Topological Indices for Application in Computer Aided Molecular Design." Industrial & Engineering Chemistry Research **48**(15): 7378-7387.

Prausnitz, J. M., R. N. Lichtenthaler and E. G. d. Azevedo (1999). Molecular thermodynamics of fluid-phase equilibria. Upper Saddle River, N.J., Prentice Hall PTR.

Prestrelski, S. J., N. Tedeschi, T. Arakawa and J. F. Carpenter (1993). "Dehydration-induced conformational transitions in proteins and their inhibition by stabilizers." Biophysical Journal **65**(2): 661-671.

Printz, M., D. S. Kalonia and W. Friess (2012). "Individual second virial coefficient determination of monomer and oligomers in heat-stressed protein samples using size-exclusion chromatography-light scattering." Journal of Pharmaceutical Sciences **101**(1): 363-372.

Quan, N. T. (1988). "The Prediction Sum of Squares as a General Measure for Regression Diagnostics." Journal of Business & Economic Statistics **6**(4): 501-504.

R-Development-Core-Team. (2010). "R: A language and environment for statistical computing." http://www.R-project.org.

Rahman, M. S., I. M. Al-Marhubi and A. Al-Mahrouqi (2007). "Measurement of glass transition temperature by mechanical (DMTA), thermal (DSC and MDSC), water diffusion and density methods: A comparison study." Chemical Physics Letters **440**(4–6): 372-377.

Raman, V. S. and C. D. Maranas (1998). "Optimization in product design with properties correlated with topological indices." Computers & Chemical Engineering **22**(6): 747-763.

Raschke, H., M. Meier, J. G. Burken, R. Hany, M. D. Müller, J. R. Van Der Meer and H.-P. E. Kohler (2001). "Biotransformation of Various Substituted Aromatic Compounds to Chiral Dihydrodihydroxy Derivatives." Applied and Environmental Microbiology **67**(8): 3333-3339.

Ren, J., Z. Zhao and X. Zhang (2011). "Vapor pressures, excess enthalpies, and specific heat capacities of the binary working pairs containing the ionic liquid 1-ethyl-3-methylimidazolium dimethylphosphate." The Journal of Chemical Thermodynamics **43**(4): 576-583.

Roos, Y. (1993). "Melting and glass transitions of low molecular weight carbohydrates." Carbohydrate Research **238**: 39-48.

Roos, Y. H. (1997). "Frozen state transitions in relation to freeze drying." Journal of Thermal Analysis and Calorimetry **48**(3): 535-544.

Rose, G. D., P. J. Fleming, J. R. Banavar and A. Maritan (2006). "A backbone-based theory of protein folding." Proceedings of the National Academy of Sciences **103**(45): 16623-16633.

Rosenberg, A. S. (2006). "Effects of protein aggregates: an immunologic perspective." AAPS J **8**(3): E501-507.

Rosenberg, I. M. (2005). Protein analysis and purification : benchtop techniques. Boston, Birkhäuser.

Roughton, B. C., B. Christian, J. White, K. V. Camarda and R. Gani (2012). "Simultaneous design of ionic liquid entrainers and energy efficient azeotropic separation processes." Computers & Chemical Engineering **42**(0): 248-262.

Roughton, B. C., L. K. Iyer, E. Bertelsen, E. M. Topp and K. V. Camarda (2013). "Protein aggregation and lyophilization: Protein structural descriptors as predictors of aggregation propensity." Computers & Chemical Engineering **58**(0): 369-377.

Roughton, B. C., A. I. Pokphanh, E. M. Topp and K. V. Camarda (2012). Optimizing Protein-Excipient Interactions for the Development of Aggregation-Reducing Lyophilized Formulations. Computer Aided Chemical Engineering. A. K. Iftekhar and S. Rajagopalan, Elsevier. **Volume 31:** 1351-1355.

Roughton, B. C., E. M. Topp and K. V. Camarda (2012). "Use of glass transitions in carbohydrate excipient design for lyophilized protein formulations." Computers & Chemical Engineering **36**(0): 208-216.

Roughton, B. C., J. White, K. V. Camarda and R. Gani (2011). Simultaneous Design of Ionic Liquids and Azeotropic Separation Processes. Computer Aided Chemical Engineering. M. C. G. E.N. Pistikopoulos and A. C. Kokossis, Elsevier. **Volume 29:** 1578-1582.

Roychaudhuri, R., G. Sarath, M. Zeece and J. Markwell (2003). "Reversible denaturation of the soybean Kunitz trypsin inhibitor." Archives of Biochemistry and Biophysics **412**(1): 20-26.

Sahinidis, N. V. and M. Tawarmalani (2000). "Applications of global optimization to process and molecular design." Computers & Chemical Engineering **24**(9–10): 2157-2169.

Satyanarayana, K. C., J. Abildskov and R. Gani (2009). "Computer-aided polymer design using group contribution plus property models." Computers & Chemical Engineering **33**(5): 1004-1013.

Schwegman, J. J., L. M. Hardwick and M. J. Akers (2005). "Practical Formulation and Process Development of Freeze-Dried Products." Pharmaceutical Development and Technology **10**(2): 151-173.

Scurto, A. M. (2012). Personal Communication.

Seiler, M., C. Jork, A. Kavarnou, W. Arlt and R. Hirsch (2004). "Separation of azeotropic mixtures using hyperbranched polymers or ionic liquids." AIChE Journal **50**(10): 2439-2454.

Shackelford, J. F. (2009). Introduction to materials science for engineers. Upper Saddle River, N.J., Pearson Prentice Hall.

Shimoyama, Y., T. Hirayama and Y. Iwai (2008). "Measurement of Infinite Dilution Activity Coefficients of Alcohols, Ketones, and Aromatic Hydrocarbons in 4-Methyl-N-butylpyridinium Tetrafluoroborate and 1-Butyl-3-methylimidazolium Hexafluorophosphate by Gas−Liquid Chromatography." Journal of Chemical & Engineering Data **53**(9): 2106-2111.

Siddhaye, S., K. V. Camarda, E. Topp and M. Southard (2000). "Design of novel pharmaceutical products via combinatorial optimization." Computers & Chemical Engineering **24**(2–7): 701-704.

Simoni, L. D., A. Chapeaux, J. F. Brennecke and M. A. Stadtherr (2010). "Extraction of biofuels and biofeedstocks from aqueous solutions using ionic liquids." Computers & Chemical Engineering **34**(9): 1406-1412.

Sinha, S., Y. Li, T. D. Williams and E. M. Topp (2008). "Protein Conformation in Amorphous Solids by FTIR and by Hydrogen/Deuterium Exchange with Mass Spectrometry." Biophysical journal **95**(12): 5951-5961.

Slade, L. and H. Levine (1995). "Water and the glass transition -- Dependence of the glass transition on composition and chemical structure: Special implications for flour functionality in cookie baking." Journal of Food Engineering **24**(4): 431-509.

Sophocleous, A. M., J. Zhang and E. M. Topp (2012). "Localized Hydration in Lyophilized Myoglobin by Hydrogen–Deuterium Exchange Mass Spectrometry. 1. Exchange Mapping." Molecular Pharmaceutics **9**(4): 718-726.

Speakman, S. A. "Basics of X-Ray Powder Diffraction." Retrieved June 12, 2013, from http://prism.mit.edu/xray/Basics%20of%20X-Ray%20Powder%20Diffraction.pdf.

Spiess, A.-N. and N. Neumeyer (2010). "An evaluation of R2 as an inadequate measure for nonlinear models in pharmacological and biochemical research: a Monte Carlo approach." BMC Pharmacology **10**(1): 6.

Strickley, R. (2004). "Solubilizing Excipients in Oral and Injectable Formulations." Pharmaceutical Research **21**(2): 201-230.

TAKAHASHI, T., M. IRIE and T. UKITA (1969). "A Comparative Study on Enzymatic Activity of Bovine Pancreatic Ribonuclease A, Ribonuclease S and Ribonuclease S." Journal of Biochemistry **65**(1): 55-62.

Takahasi, T., M. Irie and T. Ukita (1969). "A Comparative Study on Enzymatic Activity of Bovine Pancreatic Ribonuclease A, Ribonuclease S and Ribonuclease S." Journal of Biochemistry **65**(1): 55-62.

Tani, F., N. Shirai, F. Venelle, K. Yasumoto, T. Onishi and E. Doi (1997). "Temperature control for kinetic refolding of heat-denatured ovalbumin." Protein Science **6**(7): 1491-1502.

Tartaglia, G. G. and M. Vendruscolo (2008). "The Zyggregator method for predicting protein aggregation propensities." Chem Soc Rev **37**(7): 1395-1401.

Timasheff, S. N. (1998). Control of Protein Stability and Reactions by Weakly Interacting Cosolvents: The Simplicity of the Complicated. Advances in Protein Chemistry. D. S. E. Frederic M. Richards and S. K. Peter, Academic Press. **Volume 51:** 355-432.

Trotta, R. and I. Miracca (1997). "Approach to the industrial process." Catalysis Today **34**(3-4): 429-446.

Trovato, A., F. Chiti, A. Maritan and F. Seno (2006). "Insight into the Structure of Amyloid Fibrils from the Analysis of Globular Proteins." PLoS Comput Biol **2**(12): e170.

Trovato, A., F. Seno and S. C. Tosatto (2007). "The PASTA server for protein aggregation prediction." Protein Eng Des Sel **20**(10): 521-523.

Trovato, A., F. Seno and S. C. E. Tosatto (2007). "The PASTA server for protein aggregation prediction." Protein Engineering Design and Selection **20**(10): 521-523.

Tsutsui, Y. and P. L. Wintrode (2007). "Hydrogen/Deuterium Exchange-Mass Spectrometry: A Powerful Tool for Probing Protein Structure, Dynamics and Interactions." Current Medicinal Chemistry **14**(22): 2344-2358.

U.S. Dept. of Energy, O. o. E. E. a. R. E. (2001) "Distillation Column Modeling Tools." DOE.

Valderrama, J. O. and P. A. Robles (2007). "Critical Properties, Normal Boiling Temperatures, and Acentric Factors of Fifty Ionic Liquids." Industrial & Engineering Chemistry Research **46**(4): 1338-1344.

Van Holde, K. E., W. C. Johnson and P. S. Ho (2006). Principles of physical biochemistry. Upper Saddle River, N.J., Pearson/Prentice Hall.

Vasiltsova, T. V., S. P. Verevkin, E. Bich, A. Heintz, R. Bogel-Lukasik and U. Domanska (2004). "Thermodynamic Properties of Mixtures Containing Ionic Liquids. Activity Coefficients of Ethers and Alcohols in 1-Methyl-3-Ethyl-Imidazolium Bis(Trifluoromethyl-sulfonyl) Imide Using the Transpiration Method." Journal of Chemical & Engineering Data **50**(1): 142-148.

Vasiltsova, T. V., S. P. Verevkin, E. Bich, A. Heintz, R. Bogel-Lukasik and U. Domańska (2005). "Thermodynamic Properties of Mixtures Containing Ionic Liquids. 7. Activity Coefficients of Aliphatic and Aromatic Esters and Benzylamine in 1-Methyl-3-ethylimidazolium Bis(trifluoromethylsulfonyl) Imide Using the Transpiration Method." Journal of Chemical & Engineering Data **51**(1): 213-218.

Venkatasubramanian, V., K. Chan and J. M. Caruthers (1994). "Computer-aided molecular design using genetic algorithms." Computers & Chemical Engineering **18**(9): 833-844.

Venkatasubramanian, V., K. Chan and J. M. Caruthers (1995). "Evolutionary Design of Molecules with Desired Properties Using the Genetic Algorithm." Journal of Chemical Information and Computer Sciences **35**(2): 188-195.

Visser Ann, E., W. M. Reichert, P. Swatloski Richard, D. Willauer Heather, G. Huddleston Jonathan and D. Rogers Robin (2002). Characterization of Hydrophilic and Hydrophobic Ionic Liquids: Alternatives to Volatile Organic Compounds for Liquid-Liquid Separations. Ionic Liquids, American Chemical Society. **818:** 289-308.

Wang, B., S. Tchessalov, N. W. Warne and M. J. Pikal (2009). "Impact of sucrose level on storage stability of proteins in freeze-dried solids: I. correlation of protein–sugar interaction with native structure preservation." Journal of Pharmaceutical Sciences **98**(9): 3131-3144.

Wang, J., D. Wang, Z. Li and F. Zhang (2010). "Vapor Pressure Measurement and Correlation or Prediction for Water, 1-Propanol, 2-Propanol, and Their Binary Mixtures with [MMIM][DMP] Ionic Liquid." Journal of Chemical & Engineering Data **55**(11): 4872-4877.

Wang, W. (2005). "Protein aggregation and its inhibition in biopharmaceutics." International Journal of Pharmaceutics **289**(1–2): 1-30.

Wang, W., S. Nema and D. Teagarden (2010). "Protein aggregation--Pathways and influencing factors." International Journal of Pharmaceutics **390**(2): 89-99.

Wasserman, L. (2004). All of statistics : a concise course in statistical inference. New York, Springer.

West, D. B. (2001). Introduction to graph theory. Upper Saddle River, N.J., Prentice Hall.

Wittig, R., J. Lohmann and J. Gmehling (2002). "Vapor−Liquid Equilibria by UNIFAC Group Contribution. 6. Revision and Extension." Industrial & Engineering Chemistry Research **42**(1): 183-188.

Wooster, T. J., K. M. Johanson, K. J. Fraser, D. R. MacFarlane and J. L. Scott (2006). "Thermal degradation of cyano containing ionic liquids." Green Chemistry **8**(8): 691-696.

Yang, X.-J., J.-S. Wu, M.-L. Ge, L.-S. Wang and M.-Y. Li (2008). "Activity Coefficients at Infinite Dilution of Alkanes, Alkenes, and Alkyl Benzenes in 1-Hexyl-3-methylimidazolium Trifluoromethanesulfonate Using Gas−Liquid Chromatography." Journal of Chemical & Engineering Data **53**(5): 1220-1222.

Zhao, H., S. Xia and P. Ma (2005). "Use of ionic liquids as 'green' solvents for extractions." Journal of Chemical Technology & Biotechnology **80**: 1089-1096.

A. NOMENCLATURE

The meanings of abbreviations and symbols are provided below. Definitions are giving in the order of appearance. As much as possible, clarification is also given in the text.

m, n	Size of a set
i, j ,k	Index of a set
CAMD	Computer-aided molecular design
SAP	Spatial aggregation propensity algorithm
T_g	Glass transition temperature, specifically for an anhydrous solute
k	Gordon-Taylor constant
m_1 , m_2	Weight fractions
T_g'	Glass transition temperature of the maximally freeze-concentrated solute
T_m'	Melting point of ice in the freeze-concentrated solution
C_g'	Maximal freeze concentration of solute
NMR	Nuclear magnetic resonance
GC	Group contribution
Y	Response variable
X, x	Dependent variable matrix or array
β	Coefficient vector
RSS	Residual sum of the squares
μ	Chemical potential
φ_i	Fugacity coefficient
γ_i	Activity coefficient
f_i^0	Fugacity at standard conditions
y_i	Vapor mole fraction
x_i	Liquid mole fraction
P	Pressure
z	Objective function
P_m	Property value
y	Representation of molecular structure
a_{ijk}	Adjacency matrix
w_i	Chemical group

h_c	Structural constraint
A	Absorbance
ε	Extinction coefficient
c	Concentration
l	Path length
AI	Aggregation index
OD	Optical density
$\%Monomer$	Percent of protein monomer remaining after lyophilization
SEC	Size exclusion chromatography
SDS-PAGE	Sodium-dodecyl-sulfate polyacrylamide gel electrophoresis
pxrd	Powder X-ray diffraction
θ	Incident angle
λ	Wavelength
d_{hkl}	Characteristic vector defined by crystal geometry
<I>	Intensity
k_i	Rate constant
HX-MS	Hydrogen-deuterium exchange mass spectroscopy
δ	Hildebrand solubility parameter
T_d	Thermal decomposition temperature
K_x	Partition Coefficient, specificly for NDHD
EC_{50}	Half maximal effective concentration
$^{n}\chi$	Simple connectivity index of n-th order
$^{n}\chi^{v}$	Valence connectivity index of n-th order
N_s	Number of subgraphs
δ_i	Vertex degree
δ_i^v	Valence vertex degree
Z	Atomic number
Z^v	Number of valence electrons
N_H	Number of connected hydrogen atoms
$^{n}\zeta$	Average simple connectivity index of n-th order
$^{n}\zeta^{v}$	Average valence connectivity index of n-th order
a3vSA	Sequence average amino acid aggregation propensity
nHS	Number of aggregation hot spots

NnHS	nHS normalized by number of residues in protein
AAT	Area of aggregation profile above hot spot threshold
THSA	Total area of aggregation profile comprising hot spots
TA	Total area of aggregation profile
AATr	AAT normalized by number of residues in protein
THSAr	THSA normalized by number of residues in protein
Na4vSS	Sliding window average of amino acid propensity values divided by number of amino acids in protein
Emin	Minimum energy of PASTA pairings
Eavg	Average energy of PASTA pairings
Lmax	Average amino acid pair length of PASTA pairings
Lavg	Maximum amino acid pair length of PASTA pairings
(E/L)min	Minimum ratio of energy to length of PASTA pairings
(E/L)avg	Average ratio of energy to length of PASTA pairings
# of Peaks	Number of peaks in PASTA aggregation profile
C_p	Mallow's C_p statistic
p	Number of parameters
σ^2	Variance
LOOCV	Leave-one-out cross-validation
$PRESS$	Predicted residual sum of the square errors
Q^2	Cross-validation coefficient
R^2	Correlation coefficient
S_x	Sensitivity
$\%AAD$	Percent average absolute deviation
c_{ii}	Cohesive energy density
v_i	Molar volume
Δh_{vap}	Enthalpy of vaporization
Φ_i	Volume fraction
C_i	Contribution of group
R_k	Group volume parameters
Q_k	Surface area parameters
Γ_k	Group residual activity coefficient
θ_m	Volume contribution parameter

X_m	Group fraction parameter
ψ_{nm}	Interaction parameter
a_{nm}	Group interaction parameter
$\in_i^+, \in_i^-$	Error terms
$\mathrm{a(j)}$	Binary variable declaring the existence of an alkyl chain
$\mathrm{y_{cation}(i)}$, $\mathrm{y_{anion}(k)}$	Binary variables declaring the existence of cation and anion
$Fit(j)$	Fitness of j-th member
$t_{\alpha/2}$	Student’s t-test value
D_x	Location of maximum driving force
D_y	Value of maximum driving force
N	Number of stages
NF	Feed stage location
SF	Scaling factor

B. R Procedure For Model Development

The following procedure describes the steps used in R to develop linear QSPRs, including descriptor selection and cross-validation. The steps needed for calculation of prediction intervals are also given. At the end follows an example of code written in R to perform the described tasks.

1. Open R program
2. The first time you run the program, you will need to install the leaps package, which is used for descriptor selection. Click on Packages>Install package(s) …

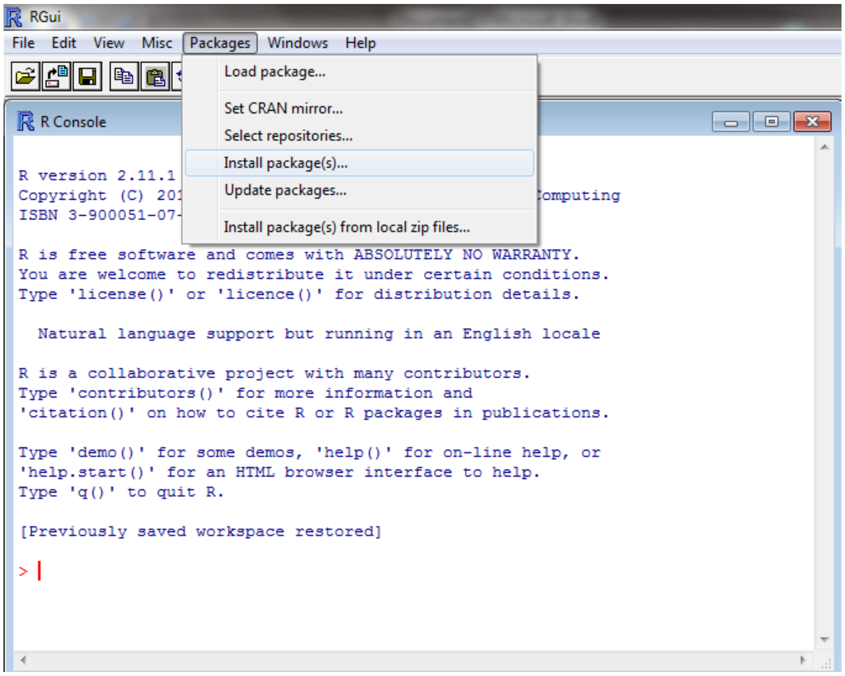

```
R version 2.11.1
Copyright (C) 201                                     omputing
ISBN 3-900051-07-

R is free software and comes with ABSOLUTELY NO WARRANTY.
You are welcome to redistribute it under certain conditions.
Type 'license()' or 'licence()' for distribution details.

  Natural language support but running in an English locale

R is a collaborative project with many contributors.
Type 'contributors()' for more information and
'citation()' on how to cite R or R packages in publications.

Type 'demo()' for some demos, 'help()' for on-line help, or
'help.start()' for an HTML browser interface to help.
Type 'q()' to quit R.

[Previously saved workspace restored]

> 
```

3. Select the CRAN mirror for the download. Choose whichever site you would like and click OK.

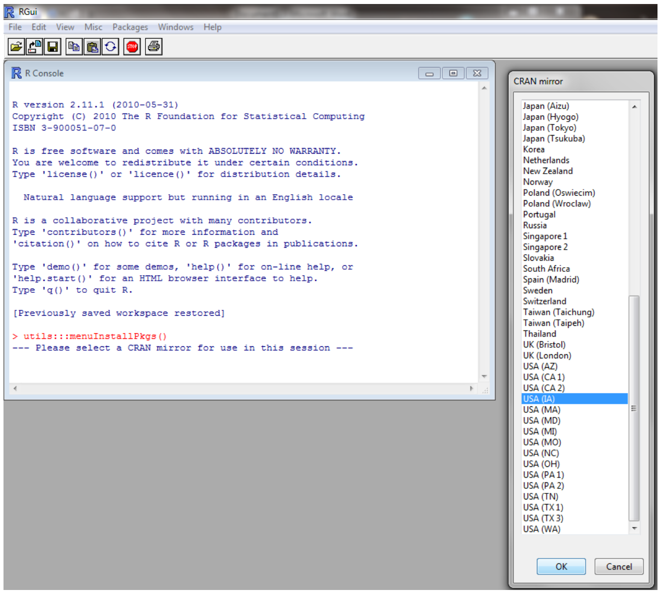

```
R version 2.11.1 (2010-05-31)
Copyright (C) 2010 The R Foundation for Statistical Computing
ISBN 3-900051-07-0

R is free software and comes with ABSOLUTELY NO WARRANTY.
You are welcome to redistribute it under certain conditions.
Type 'license()' or 'licence()' for distribution details.

  Natural language support but running in an English locale

R is a collaborative project with many contributors.
Type 'contributors()' for more information and
'citation()' on how to cite R or R packages in publications.

Type 'demo()' for some demos, 'help()' for on-line help, or
'help.start()' for an HTML browser interface to help.
Type 'q()' to quit R.

[Previously saved workspace restored]

> utils:::menuInstallPkgs()
--- Please select a CRAN mirror for use in this session ---
```

4. From the Packages selection screen, select leaps and click OK

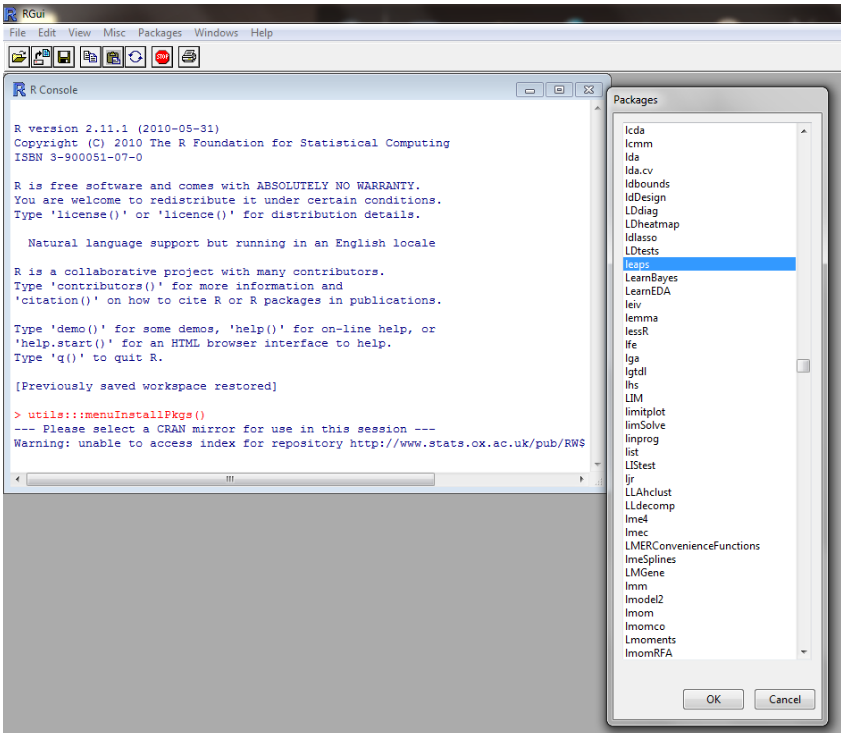

```
R version 2.11.1 (2010-05-31)
Copyright (C) 2010 The R Foundation for Statistical Computing
ISBN 3-900051-07-0

R is free software and comes with ABSOLUTELY NO WARRANTY.
You are welcome to redistribute it under certain conditions.
Type 'license()' or 'licence()' for distribution details.

  Natural language support but running in an English locale

R is a collaborative project with many contributors.
Type 'contributors()' for more information and
'citation()' on how to cite R or R packages in publications.

Type 'demo()' for some demos, 'help()' for on-line help, or
'help.start()' for an HTML browser interface to help.
Type 'q()' to quit R.

[Previously saved workspace restored]

> utils:::menuInstallPkgs()
--- Please select a CRAN mirror for use in this session ---
Warning: unable to access index for repository http://www.stats.ox.ac.uk/pub/RW$
```

5. After the installation, the leaps package can be used. The package only needs to be installed once. To load the leaps package, click on Packages>Load package… and then select the leaps package

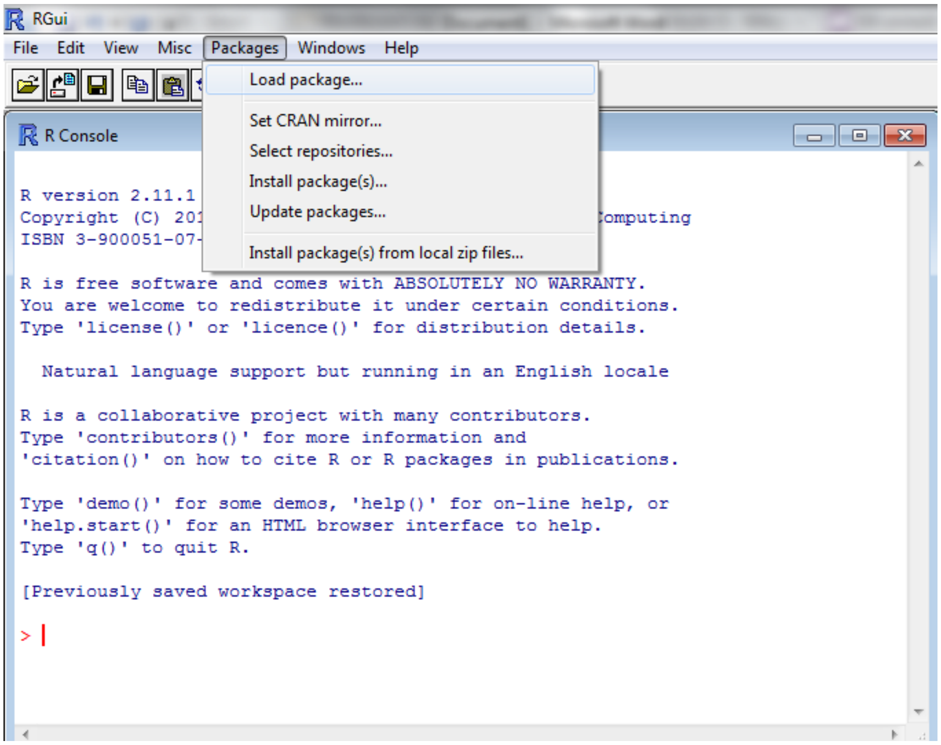

```
R version 2.11.1
Copyright (C) 201                                      omputing
ISBN 3-900051-07-

R is free software and comes with ABSOLUTELY NO WARRANTY.
You are welcome to redistribute it under certain conditions.
Type 'license()' or 'licence()' for distribution details.

  Natural language support but running in an English locale

R is a collaborative project with many contributors.
Type 'contributors()' for more information and
'citation()' on how to cite R or R packages in publications.

Type 'demo()' for some demos, 'help()' for on-line help, or
'help.start()' for an HTML browser interface to help.
Type 'q()' to quit R.

[Previously saved workspace restored]

> |
```

6. After the leaps package has loaded, the csv file containing the descriptor information and value that is desired to be correlated should be loaded into R. The column headers in the csv file will be used by R as names for the variable. Special characters are usually replaced by "X" and spaces are replaced by ".". To load the csv file, type the following command:

   pick a name = read.csv(file.choose())

   The name for the file is chosen by the user. A "Select file" window will pop up showing the user directory. Navigate to the csv file desired and select the file. Click Open.

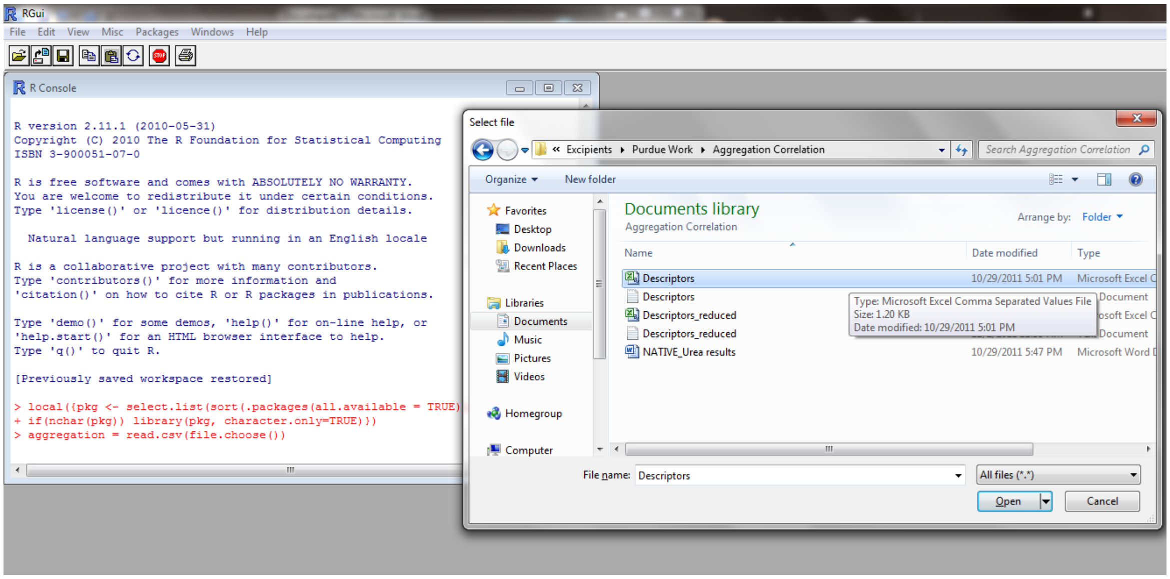

```
R version 2.11.1 (2010-05-31)
Copyright (C) 2010 The R Foundation for Statistical Computing
ISBN 3-900051-07-0

R is free software and comes with ABSOLUTELY NO WARRANTY.
You are welcome to redistribute it under certain conditions.
Type 'license()' or 'licence()' for distribution details.

  Natural language support but running in an English locale

R is a collaborative project with many contributors.
Type 'contributors()' for more information and
'citation()' on how to cite R or R packages in publications.

Type 'demo()' for some demos, 'help()' for on-line help, or
'help.start()' for an HTML browser interface to help.
Type 'q()' to quit R.

[Previously saved workspace restored]

> local({pkg <- select.list(sort(.packages(all.available = TRUE)
+ if(nchar(pkg)) library(pkg, character.only=TRUE)})
> aggregation = read.csv(file.choose())
```

Name	Date modified	Type
Descriptors	10/29/2011 5:01 PM	Microsoft Excel C
Descriptors		Document
Descriptors_reduced		osoft Excel C
Descriptors_reduced		Document
NATIVE_Urea results	10/29/2011 5:47 PM	Microsoft Word D

Type: Microsoft Excel Comma Separated Values File
Size: 1.20 KB
Date modified: 10/29/2011 5:01 PM

File name: Descriptors
All files (*.*)

7. To attach the column headers to the variable names in R, type the following command

   attach(*pick a name*)

   Using whatever name you had chosen in step 6. To check that the file is loaded correctly and to see the variable names that R is using, type

   pick a name

   Again using the name you had chosen in step 6. The csv file data will then display in R. Note the variable names for each column, as they will be used to create the correlation later.

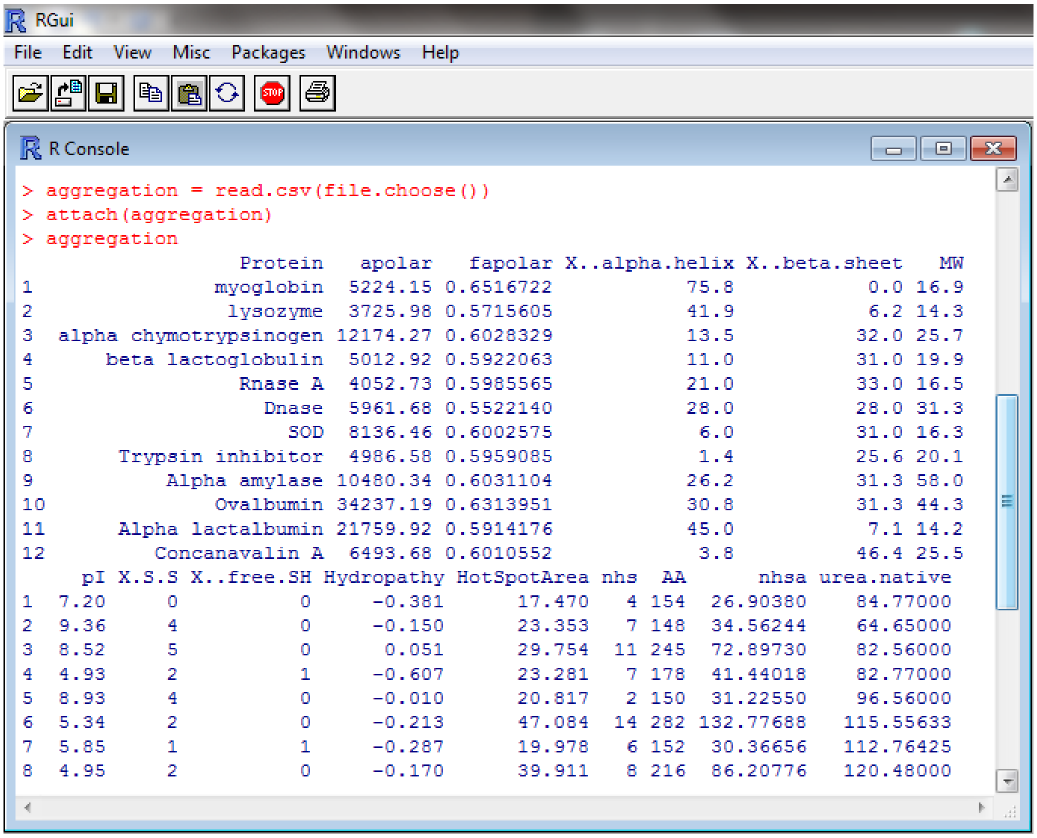

```
> aggregation = read.csv(file.choose())
> attach(aggregation)
> aggregation
                  Protein   apolar   fapolar X..alpha.helix X..beta.sheet   MW
1               myoglobin  5224.15 0.6516722           75.8           0.0 16.9
2                lysozyme  3725.98 0.5715605           41.9           6.2 14.3
3  alpha chymotrypsinogen 12174.27 0.6028329           13.5          32.0 25.7
4      beta lactoglobulin  5012.92 0.5922063           11.0          31.0 19.9
5                 Rnase A  4052.73 0.5985565           21.0          33.0 16.5
6                   Dnase  5961.68 0.5522140           28.0          28.0 31.3
7                     SOD  8136.46 0.6002575            6.0          31.0 16.3
8       Trypsin inhibitor  4986.58 0.5959085            1.4          25.6 20.1
9           Alpha amylase 10480.34 0.6031104           26.2          31.3 58.0
10              Ovalbumin 34237.19 0.6313951           30.8          31.3 44.3
11      Alpha lactalbumin 21759.92 0.5914176           45.0           7.1 14.2
12         Concanavalin A  6493.68 0.6010552            3.8          46.4 25.5
     pI X.S.S X..free.SH Hydropathy HotSpotArea nhs  AA      nhsa urea.native
1  7.20     0          0     -0.381      17.470   4 154  26.90380    84.77000
2  9.36     4          0     -0.150      23.353   7 148  34.56244    64.65000
3  8.52     5          0      0.051      29.754  11 245  72.89730    82.56000
4  4.93     2          1     -0.607      23.281   7 178  41.44018    82.77000
5  8.93     4          0     -0.010      20.817   2 150  31.22550    96.56000
6  5.34     2          0     -0.213      47.084  14 282 132.77688   115.55633
7  5.85     1          1     -0.287      19.978   6 152  30.36656   112.76425
8  4.95     2          0     -0.170      39.911   8 216  86.20776   120.48000
```

8. Next, a text file containing only the descriptor values must be loaded into R as a matrix. The matrix will be used for the descriptor selection. The number of columns in the text file must be inputted. To load the text file, type the following command:

   matrix name = matrix(scan(file.choose()),ncol=*number of columns in text file*,byrow=TRUE)

   Where *matrix name* is chosen by the user and *number of columns in text file* is entered as a number.

9. After the text file has been read, descriptor selection can be performed. Type the following command:

   leaps(*matrix name*,*correlated variable*,method=c("r2"),nbest=1,strictly.compatible=FALSE)

   Where *matrix name* is the name chosen in step 8 and *correlated variable* is the name of the dependent variable in the correlation being built. Two methods can be used. r2 choses the set of descriptors that maximizes the r^2 value. Cp chooses the set of descriptors that minimizes the C_p value, which is a measure of the lack of fit plus the number of descriptors used. Different values for what nbest is equal to can be selected and will determine how many different correlations/models of each size (# of descriptors) will be reported. For example, nbest=3 would report the three best models based upon the method chosen for each model size.

The output will display a matrix showing which descriptor was used for each correlation, as indicated by TRUE or FALSE. The score given by the method selected will also be displayed.

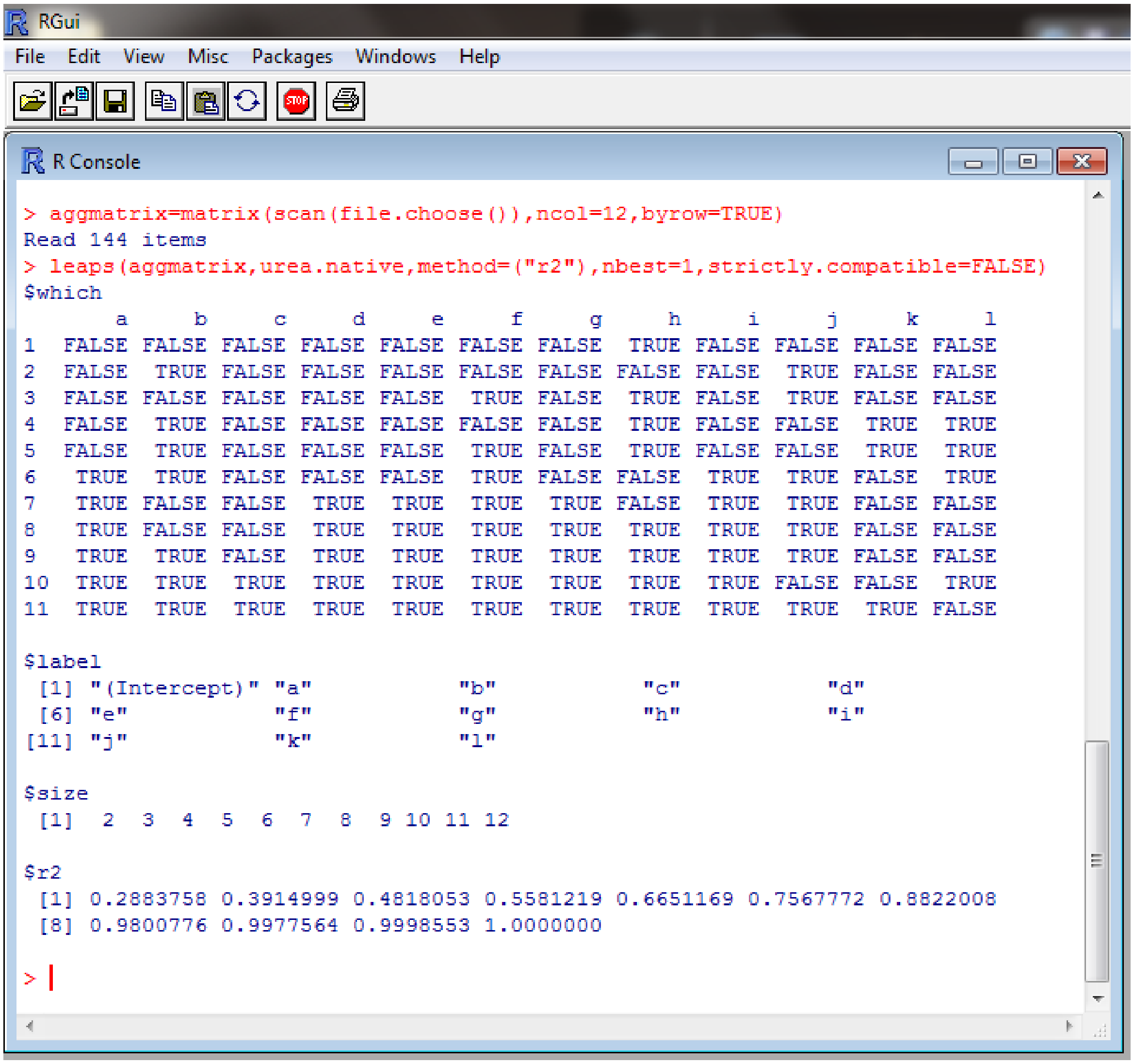

```
> aggmatrix=matrix(scan(file.choose()),ncol=12,byrow=TRUE)
Read 144 items
> leaps(aggmatrix,urea.native,method=("r2"),nbest=1,strictly.compatible=FALSE)
$which
        a     b     c     d     e     f     g     h     i     j     k     l
1   FALSE FALSE FALSE FALSE FALSE FALSE FALSE  TRUE FALSE FALSE FALSE FALSE
2   FALSE  TRUE FALSE FALSE FALSE FALSE FALSE FALSE FALSE  TRUE FALSE FALSE
3   FALSE FALSE FALSE FALSE FALSE  TRUE FALSE  TRUE FALSE  TRUE FALSE FALSE
4   FALSE  TRUE FALSE FALSE FALSE FALSE FALSE  TRUE FALSE FALSE  TRUE  TRUE
5   FALSE  TRUE FALSE FALSE FALSE  TRUE FALSE  TRUE FALSE FALSE  TRUE  TRUE
6    TRUE  TRUE FALSE FALSE FALSE  TRUE FALSE FALSE  TRUE  TRUE FALSE  TRUE
7    TRUE FALSE FALSE  TRUE  TRUE  TRUE  TRUE FALSE  TRUE  TRUE FALSE FALSE
8    TRUE FALSE FALSE  TRUE  TRUE  TRUE  TRUE  TRUE  TRUE  TRUE FALSE FALSE
9    TRUE  TRUE FALSE  TRUE  TRUE  TRUE  TRUE  TRUE  TRUE  TRUE FALSE FALSE
10   TRUE  TRUE  TRUE  TRUE  TRUE  TRUE  TRUE  TRUE  TRUE FALSE FALSE  TRUE
11   TRUE  TRUE  TRUE  TRUE  TRUE  TRUE  TRUE  TRUE  TRUE  TRUE  TRUE FALSE

$label
 [1] "(Intercept)" "a"           "b"           "c"           "d"
 [6] "e"           "f"           "g"           "h"           "i"
[11] "j"           "k"           "l"

$size
 [1]  2  3  4  5  6  7  8  9 10 11 12

$r2
 [1] 0.2883758 0.3914999 0.4818053 0.5581219 0.6651169 0.7567772 0.8822008
 [8] 0.9800776 0.9977564 0.9998553 1.0000000

> 
```

10. Select a desired model/correlation for further analysis. Note the descriptors used in the model. Build the correlation in R using the following command:

correlation name.lm <- lm(*correlated variable*~*var1*+*var2* +…+*var*X)

Where *correlation name* is selected by the user, *correlated variable* is the dependent variable, and *var1* to *varX* are the descriptors selected using leaps. X denotes the size of the model (# of descriptors).

11. The correlation information can be retrieved with the following command:

    summary(*correlation name*.lm)

    Where *correlation name* is the same as chosen in step 10.

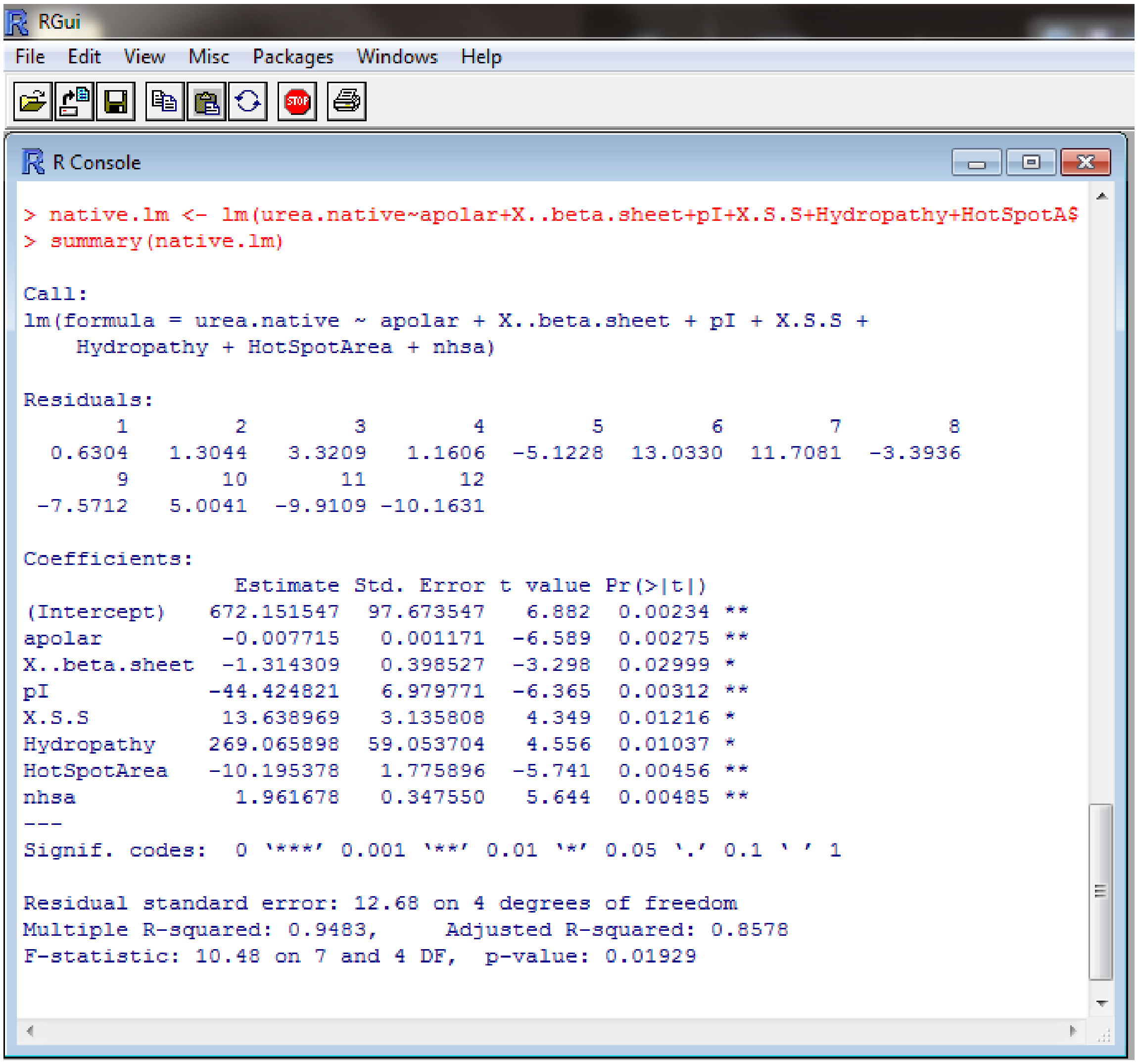

```
> native.lm <- lm(urea.native~apolar+X..beta.sheet+pI+X.S.S+Hydropathy+HotSpotA$
> summary(native.lm)

Call:
lm(formula = urea.native ~ apolar + X..beta.sheet + pI + X.S.S +
    Hydropathy + HotSpotArea + nhsa)

Residuals:
       1        2        3        4        5        6        7        8
  0.6304   1.3044   3.3209   1.1606  -5.1228  13.0330  11.7081  -3.3936
       9       10       11       12
 -7.5712   5.0041  -9.9109 -10.1631

Coefficients:
                Estimate Std. Error t value Pr(>|t|)
(Intercept)   672.151547  97.673547   6.882  0.00234 **
apolar         -0.007715   0.001171  -6.589  0.00275 **
X..beta.sheet  -1.314309   0.398527  -3.298  0.02999 *
pI            -44.424821   6.979771  -6.365  0.00312 **
X.S.S          13.638969   3.135808   4.349  0.01216 *
Hydropathy    269.065898  59.053704   4.556  0.01037 *
HotSpotArea   -10.195378   1.775896  -5.741  0.00456 **
nhsa            1.961678   0.347550   5.644  0.00485 **
---
Signif. codes:  0 '***' 0.001 '**' 0.01 '*' 0.05 '.' 0.1 ' ' 1

Residual standard error: 12.68 on 4 degrees of freedom
Multiple R-squared: 0.9483,     Adjusted R-squared: 0.8578
F-statistic: 10.48 on 7 and 4 DF,  p-value: 0.01929
```

12. To evaluate Q^2, you must create a csv file containing only the selected descriptors and correlated values. The variable names should remain the same to ensure that the correlation can be used for cross-validation.
13. Cross-validation can then be performed using the following command:

User-definedName.CVlm <- CVlm(*csv file name, correlationName.lm*, m=*number of folds*, plotit=TRUE, printit = TRUE)

14. The predicted and correlation values of each fold are used to calculate Q^2 (via excel).
15. To calculate the prediction intervals for a prediction, the prediction's descriptors must be entered as a new data frame:

Name of new data frame = data.frame(*descriptor1 = xxx*, *descriptor2 = xxx*, …)

16. The following command returns the prediction and the lower and upper interval value:

predict(*correlationName.lm*, *data frame name*, interval="predict")

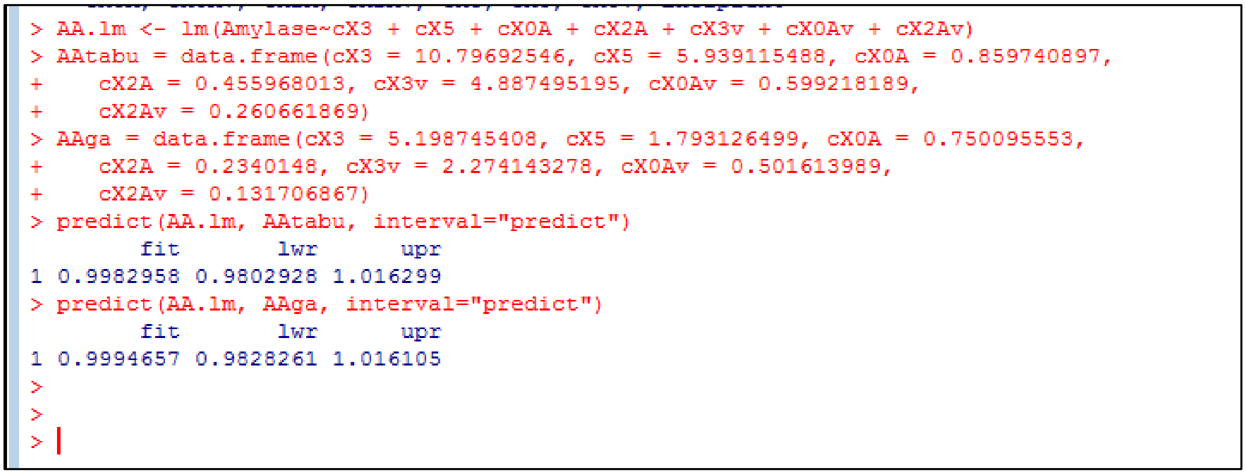

```
> AA.lm <- lm(Amylase~cX3 + cX5 + cX0A + cX2A + cX3v + cX0Av + cX2Av)
> AAtabu = data.frame(cX3 = 10.79692546, cX5 = 5.939115488, cX0A = 0.859740897,
+    cX2A = 0.455968013, cX3v = 4.887495195, cX0Av = 0.599218189,
+    cX2Av = 0.260661869)
> AAga = data.frame(cX3 = 5.198745408, cX5 = 1.793126499, cX0A = 0.750095553,
+    cX2A = 0.2340148, cX3v = 2.274143278, cX0Av = 0.501613989,
+    cX2Av = 0.131706867)
> predict(AA.lm, AAtabu, interval="predict")
        fit       lwr      upr
1 0.9982958 0.9802928 1.016299
> predict(AA.lm, AAga, interval="predict")
        fit       lwr      upr
1 0.9994657 0.9828261 1.016105
>
>
> 
```

An example code to complete the following steps is given below:

```
TIfields = read.csv(file.choose())
attach(TIfields)
TImatrix = matrix(scan(file.choose()),ncol=10,byrow=TRUE)
leaps(TImatrix,TI,method=c("Cp"),nbest=1,strictly.compatible=FALSE)
TI.lm <- lm(TI~cX4 + cX0A + cX1A + cX1v + cX3v + cX2Av + cX5Av)
summary(TI.lm)
TI.CVlm <- CVlm(TIfields, TI.lm, m=11, plotit=TRUE, printit = TRUE)
TItabu = data.frame(cX4 = 13.98383752, cX0A = 0.832184077,
                          cX1A = 0.603651, cX1v = 10.68623644, cX3v = 8.425098614,
                          cX2Av = 0.261058302, cX5Av = 0.057471174)
TIga = data.frame(cX4 = 7.903364617, cX0A = 0.846240068,
                          cX1A = 0.587963437, cX1v = 8.383716113, cX3v = 5.856908357,
                          cX2Av = 0.260155783, cX5Av = 0.067981002)
predict(TI.lm, TItabu, interval="predict")
predict(TI.lm, TIga, interval="predict")
```

C. POLYMER DESIGNER PROCEDURE

To open the Polymer Designer (pd2) executable, open the terminal in the pd2 Folder

Then in the terminal, type:

```
./pd2
```

In the program, you need to open a database. Click “Open Database” and then select the database you want to use.

To fill in the screen with info, click on “select columns”. Some useful columns are Info>Name and Descriptors> all the various connectivity indices. Then click Add Rows > Search and select the molecules you want to be shown. This can be used to calculate connectivity indices.

To add new correlations, you must do the following

- Close pd2
- Open >src>tabu>dp_tabu_01.cpp
- Scroll about ¾ of the way down and edit the correlations. Chii_# is the unweighted connectivity index and xi_# is the weighted connectivity index.
- Edit the cout information so your correlation values will be outputted
- If you add any new variables, make sure they are declared in this file
    - Then open >src>tabu>dp_tabu_01.hpp and define them there as well
- Close both the .cpp and .hpp files
- In the pd2 directory, delete the make file, pd2 executable file and pd2.pro file
- Then follow the instructions for installing the program found in (Eslick 2009).

To run the tabu search:

- Go to molecules>polymers>browse
- Select a starting molecule (such as Tabu BisGMA) and click view
- In the window that opens, go to the Toolbox and click on the graph tab. Then click Algorithm Test and select Tabu test. The search results will display in the terminal.

To view and save a tabu search solution:

- In pd2, go to Monomers>Browse>View and select anything
- Go to the graph tab and select “import” then “yes”
- Select your solution
- Rearrange the atoms and bonds to better view your solution
- Then close the molecule window
- Go to Monomers>Browse>Add and your molecule should appear. Change the name and add a description

To change the groups that will be used to build the tabu search solution:

- Go to molecules>monomers>edit
- Select a group from 09 to 18 to view. Only these are used by the program as building blocks.
- In the molecule viewer, you can edit the bond and atoms. An Atomic # = 0 makes the atom a connector. Every group must have at least one connector.

Ionic Liquid Groups Used in Polymer Designer

Cation Groups
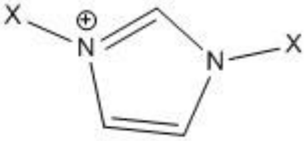 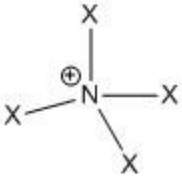 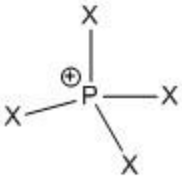
Anion Groups
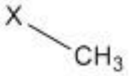 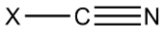 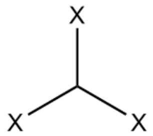 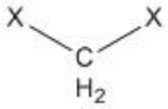 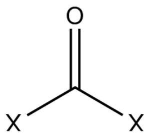

Excipient Groups Used in Polymer Designer

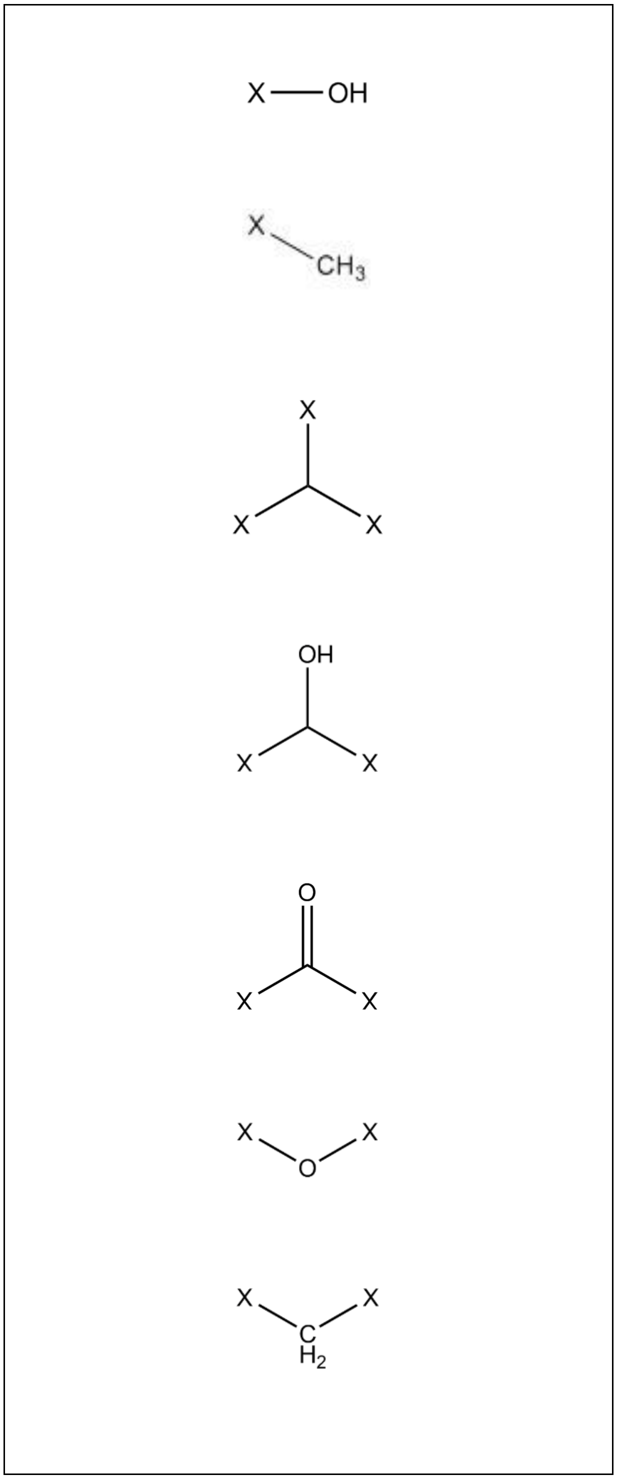

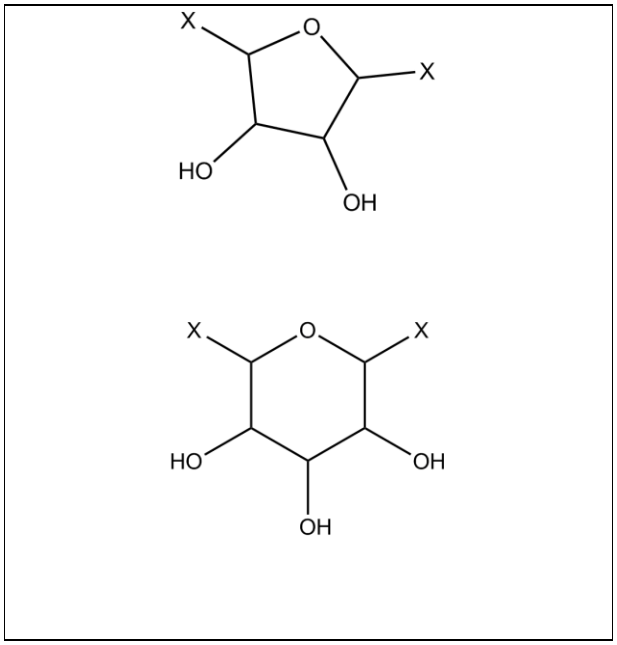
X
O
X
HO
OH
X
O
X
HO
OH
OH

D. CAMD Excipient Designer Source Code

The following code is written in VBA and contains all the code used to design carbohydrate excipient molecules for optimal *%Monomer* values. Modular programming was used with modules devoted to the following tasks: Running searches and building molecules, calculating descriptors, calculating properties, tabu search and genetic algorithm. In addition to the code provided here, data for each group is needed in worksheets. Comments are indicated by an apostrophe (').

CAMD Module Code

```
Public n As Long, n_minusrings As Long
Public m_max As Long
Public Declare Function GetTickCount Lib "kernel32.dll" () As Long  'Returns time elapsed since startup in miliseconds

Sub RunManyCAMD()

Dim i As Long, j As Long, runs As Long
Dim mol() As Long, mol_size As Long
Dim Final_Obj As Double
Dim t As Long

runs = 100

Range("B2:O101").ClearContents

For i = 1 To runs
   DoEvents    'Prevent not responding message
   t = GetTickCount
   Call CAMD(mol, Final_Obj)
   mol_size = UBound(mol)
   Cells(1 + i, 2) = i
   Cells(1 + i, 3) = Final_Obj
   Cells(1 + i, 4) = GetTickCount - t  'time elapsed while running code(and inserting i and obj values in excel - but that is negligible)
   Cells(1 + i, 5) = MW(mol)
   Cells(1 + i, 6) = HBD(mol)
   Cells(1 + i, 7) = HBA(mol)
   Cells(1 + i, 8) = Rings(mol)
   For j = 1 To mol_size
      Cells(1 + i, 8 + j) = mol(j)
   Next j
Next i
End Sub

Sub CAMD(mol() As Long, Final_Obj As Double)      'argument mol() As Long, Final_Obj As Double
```

```
Dim m As Long, size As Long
Dim i As Long, j As Long
'Dim mol() As Long, Final_Obj As Double   'arguments sometimes
Dim del() As Long, delv() As Long, nH() As Long
Dim AdjM() As Long, Chi(0 To 5) As Double, ChiV(0 To 5) As Double
Dim Chi_Avg(0 To 5) As Double, ChiV_Avg(0 To 5) As Double

m_max = 6 'maximum number of groups in molecule
n = 89 ' number of groups
n_minusrings = 9    'number of groups that are non-ring groups, also the first groups by order

'Create test solution -- For debugging
'Call InitialSolution(mol(), m)
'm = 5
'ReDim mol(1 To m)
'mol(1) = 1
'mol(2) = 37
'mol(3) = 3
'mol(4) = 71
'mol(5) = 1



'Create adjacency matrix and vectors to store del and delv values
'Call BuildMolecule(mol(), del(), delv(), nH(), AdjM(), m, size)
'Call GetConnectivity(del(), delv(), nH(), AdjM(), size, Chi(), ChiV(), Chi_Avg(), ChiV_Avg())
'Final_Obj = obj(mol, Chi(), ChiV(), Chi_Avg(), ChiV_Avg())
Call RunTabu(mol(), m, del(), delv(), nH(), AdjM(), size, Chi(), ChiV(), Chi_Avg(), ChiV_Avg(), Final_Obj)
'Call RunGA(mol(), m, del(), delv(), nH(), AdjM(), size, Chi(), ChiV(), Chi_Avg(), ChiV_Avg(), Final_Obj)
'MsgBox "Best solution was MW = " & MW(mol)

End Sub



Sub InitialSolution(mol() As Long, m As Long)
'Build Random Initial Solution

m = Int((m_max - 1 + 1) * Rnd + 1) ' groups in molecule

ReDim mol(1 To m) 'Vector to store types of groups

'Randomly assign groups in the molecule
For i = 1 To m
   If i > 1 Then
      If mol(i - 1) > n_minusriungs Then  'Make sure that you do not fuse two rings together
         mol(i) = Int((n_minusrings - 1 + 1) * Rnd + 1)  'Limits groups to non-ring groups
      Else
```

```
            mol(i) = Int((n - 1 + 1) * Rnd + 1) 'Entire selection of groups available
        End If
    Else
        mol(i) = Int((n - 1 + 1) * Rnd + 1) 'Entire selection of groups available for first group added
    End If
Next i

End Sub

Sub BuildMolecule(mol() As Long, del() As Long, delv() As Long, nH() As Long, AdjM() As Long, m As Long,
size As Long)
'Creates adjacency matrix, del and delv values for groups selected

Dim i As Long, j As Long, k As Long, jstart As Long, kstart As Long, jlag As Long
Dim terminal As Long

'Clear old Adjacency Matrix
Erase AdjM()

'Always will have two terminals
size = 2

'Calculate number of non-hydrogen atoms in the molecule
For i = 1 To m
    size = size + atoms(mol(i))
Next i

'Size adjacency matrix and del/delv vectors to proper size
ReDim AdjM(1 To size, 1 To size)
ReDim del(1 To size)
ReDim delv(1 To size)
ReDim nH(1 To size)

'Set terminals values for del and delv
'   This sets both terminals to -OH (hydroxyl) groups
del(1) = 8
del(size) = 8
delv(1) = 6
delv(size) = 6
nH(1) = 1
nH(size) = 1

'Set starting indices
jstart = 2  'used to store starting node for group being added to molecule
kstart = jstart
jlag = 1    'used to store terminal node from previous group added to molecule

For i = 1 To m
```

```
   AdjM(jlag, jstart) = 1   'Connects starting node from new group with terminal node from previous group
   AdjM(jstart, jlag) = 1

   'Obtains del/delv values and connectivity for group selected by accessing workbook
   For j = jstart To jstart + atoms(mol(i)) - 1
      del(j) = Worksheets(Name(mol(i))).Cells(3 + (j - jstart), 2).Value
      delv(j) = Worksheets(Name(mol(i))).Cells(3 + (j - jstart), 3).Value
      nH(j) = Worksheets(Name(mol(i))).Cells(3 + (j - jstart), 4).Value
      For k = kstart To kstart + atoms(mol(i)) - 1
         AdjM(j, k) = Worksheets(Name(mol(i))).Cells(2 + (j - jstart), 6 + (k - jstart)).Value
      Next k
   Next j

   'Finds terminal node for group added and node for next group to be added
   jlag = terminus(mol(i), jstart)
   jstart = jstart + atoms(mol(i))
   kstart = kstart + atoms(mol(i))

Next i

AdjM(jlag, size) = 1    'Connects terminal node from new group with terminal
AdjM(size, jlag) = 1




End Sub

Function atoms(molecule_group As Long) As Long
'Assigns number of atoms in group selected

Select Case molecule_group
   Case Is = 1
      atoms = 1
   Case 2 To 3
      atoms = 2
   Case Is = 4
      atoms = 1
   Case Is = 5
      atoms = 2
   Case 6 To 9
      atoms = 5
   Case 10 To 25
      atoms = 7
   Case 26 To 41
      atoms = 9
   Case 42 To 57
```

```
        atoms = 8
    Case 58 To 89
        atoms = 9
End Select

End Function

Function Name(molecule_group As Long) As String
'Assigns name to group selected

Select Case molecule_group
    Case Is = 1
        Name = "Group1"
    Case Is = 2
        Name = "Group2a"
    Case Is = 3
        Name = "Group2b"
    Case Is = 4
        Name = "Group3"
    Case Is = 5
        Name = "Group4"
    Case Is = 6
        Name = "Group5a"
    Case Is = 7
        Name = "Group5b"
    Case Is = 8
        Name = "Group5c"
    Case Is = 9
        Name = "Group5d"
    Case Is = 10
        Name = "Group6a"
    Case Is = 11
        Name = "Group6b"
    Case Is = 12
        Name = "Group6c"
    Case Is = 13
        Name = "Group6d"
    Case Is = 14
        Name = "Group6e"
    Case Is = 15
        Name = "Group6f"
    Case Is = 16
        Name = "Group6g"
    Case Is = 17
        Name = "Group6h"
    Case Is = 18
        Name = "Group6i"
    Case Is = 19
        Name = "Group6j"
    Case Is = 20
        Name = "Group6k"
    Case Is = 21
        Name = "Group6l"
    Case Is = 22
        Name = "Group6m"
    Case Is = 23
        Name = "Group6n"
    Case Is = 24
        Name = "Group6o"
    Case Is = 25
        Name = "Group6p"
    Case Is = 26
        Name = "Group7a"
    Case Is = 27
        Name = "Group7b"
    Case Is = 28
        Name = "Group7c"
    Case Is = 29
        Name = "Group7d"
    Case Is = 30
        Name = "Group7e"
    Case Is = 31
        Name = "Group7f"
    Case Is = 32
        Name = "Group7g"
    Case Is = 33
        Name = "Group7h"
    Case Is = 34
        Name = "Group7i"
    Case Is = 35
        Name = "Group7j"
    Case Is = 36
        Name = "Group7k"
    Case Is = 37
        Name = "Group7l"
    Case Is = 38
        Name = "Group7m"
    Case Is = 39
        Name = "Group7n"
    Case Is = 40
        Name = "Group7o"
    Case Is = 41
        Name = "Group7p"
    Case Is = 42
        Name = "Group8a"
    Case Is = 43
```

```
   Name = "Group8b"
Case Is = 44
   Name = "Group8c"
Case Is = 45
   Name = "Group8d"
Case Is = 46
   Name = "Group8e"
Case Is = 47
   Name = "Group8f"
Case Is = 48
   Name = "Group8g"
Case Is = 49
   Name = "Group8h"
Case Is = 50
   Name = "Group8i"
Case Is = 51
   Name = "Group8j"
Case Is = 52
   Name = "Group8k"
Case Is = 53
   Name = "Group8l"
Case Is = 54
   Name = "Group8m"
Case Is = 55
   Name = "Group8n"
Case Is = 56
   Name = "Group8o"
Case Is = 57
   Name = "Group8p"
Case Is = 58
   Name = "Group9a"
Case Is = 59
   Name = "Group9b"
Case Is = 60
   Name = "Group9c"
Case Is = 61
   Name = "Group9d"
Case Is = 62
   Name = "Group9e"
Case Is = 63
   Name = "Group9f"
Case Is = 64
   Name = "Group9g"
Case Is = 65
   Name = "Group9h"
Case Is = 66
   Name = "Group9i"
Case Is = 67
```

```
        Name = "Group9j"
    Case Is = 68
        Name = "Group9k"
    Case Is = 69
        Name = "Group9l"
    Case Is = 70
        Name = "Group9m"
    Case Is = 71
        Name = "Group9n"
    Case Is = 72
        Name = "Group9o"
    Case Is = 73
        Name = "Group9p"
    Case Is = 74
        Name = "Group9q"
    Case Is = 75
        Name = "Group9r"
    Case Is = 76
        Name = "Group9s"
    Case Is = 77
        Name = "Group9t"
    Case Is = 78
        Name = "Group9u"
    Case Is = 79
        Name = "Group9v"
    Case Is = 80
        Name = "Group9w"
    Case Is = 81
        Name = "Group9x"
    Case Is = 82
        Name = "Group9y"
    Case Is = 83
        Name = "Group9z"
    Case Is = 84
        Name = "Group9aa"
    Case Is = 85
        Name = "Group9ab"
    Case Is = 86
        Name = "Group9ac"
    Case Is = 87
        Name = "Group9ad"
    Case Is = 88
        Name = "Group9ae"
    Case Is = 89
        Name = "Group9af"
End Select

End Function
```

```
Function terminus(molecule_group As Long, jstart As Long) As String
'Finds right hand side terminal atom

Select Case molecule_group
   Case 1 To 9
      terminus = jstart
   Case 10 To 89
      terminus = jstart + atoms(molecule_group) - 1   'Different atom joins to next group than prior group
End Select

End Function
```

PROPERTY MODULE CODE

```
Function MW(mol) As Double

Dim sum As Long, size As Long
Dim i As Long

m = UBound(mol)

sum = 34

For i = 1 To m
   Select Case mol(i)
      Case Is = 1
         sum = sum + 14
      Case 2 To 3
         sum = sum + 30
      Case Is = 4
         sum = sum + 16
      Case Is = 5
         sum = sum + 28
      Case 6 To 9
         sum = sum + 3 * 12 + 2 * 16 + 6 * 1
      Case 10 To 25
         sum = sum + 4 * 12 + 3 * 16 + 6
      Case 26 To 41
         sum = sum + 5 * 12 + 4 * 16 + 8
      Case 42 To 57
         sum = sum + 5 * 12 + 3 * 16 + 8
      Case 58 To 89
         sum = sum + 5 * 12 + 4 * 16 + 8
   End Select
Next i

MW = sum
```

```
End Function
Function HBD(mol) As Double

Dim sum As Long, size As Long
Dim i As Long

m = UBound(mol)

sum = 2

For i = 1 To m
   Select Case mol(i)
      Case Is = 1
         sum = sum + 0
      Case 2 To 3
         sum = sum + 1
      Case Is = 4
         sum = sum + 0
      Case Is = 5
         sum = sum + 0
      Case 6 To 9
         sum = sum + 2
      Case 10 To 25
         sum = sum + 2
      Case 26 To 41
         sum = sum + 3
      Case 42 To 57
         sum = sum + 2
      Case 58 To 89
         sum = sum + 3
   End Select
Next i

HBD = sum

End Function
Function HBA(mol) As Double

Dim sum As Long, size As Long
Dim i As Long

m = UBound(mol)

sum = 2

For i = 1 To m
   Select Case mol(i)
      Case Is = 1
```

```
            sum = sum + 0
        Case 2 To 3
            sum = sum + 1
        Case Is = 4
            sum = sum + 1
        Case Is = 5
            sum = sum + 1
        Case 6 To 9
            sum = sum + 2
        Case 10 To 25
            sum = sum + 3
        Case 26 To 41
            sum = sum + 4
        Case 42 To 57
            sum = sum + 3
        Case 58 To 89
            sum = sum + 4
    End Select
Next i

HBA = sum

End Function
Function Rings(mol) As Double

Dim sum As Long, size As Long
Dim i As Long

m = UBound(mol)

sum = 0

For i = 1 To m
    Select Case mol(i)
        Case Is = 1
            sum = sum + 0
        Case 2 To 3
            sum = sum + 0
        Case Is = 4
            sum = sum + 0
        Case Is = 5
            sum = sum + 0
        Case 6 To 9
            sum = sum + 0
        Case 10 To 25
            sum = sum + 1
        Case 26 To 41
            sum = sum + 1
```

```
      Case 42 To 57
         sum = sum + 1
      Case 58 To 89
         sum = sum + 1
   End Select
Next i

Rings = sum

End Function


Function obj(mol, Chi() As Double, ChiV() As Double, Chi_Avg() As Double, ChiV_Avg() As Double) As
Double

Dim Prop_MW As Double, Prop_RNA As Double, Prop_BSA As Double, Prop_AA As Double, Prop_Ova As
Double, Prop_TI As Double
Dim Target_MW As Double, Target1 As Double, Prop_All As Double
Dim ASA As Double, ahelix As Double, bsheet As Double, MW_prot As Double, Tm As Double
'Design Targets
Target_MW = 342
Target1 = 1#   '1.64092082073789
'Target2 = 1#   '-0.99286646595339
'Protein Properties -- Read from user at later date
ASA = 4052
ahelix = 21
bsheet = 33
MW_prot = 16.5
Tm = 62.5
Penalty = 0

Prop_MW = MW(mol)

Prop_RNA = 12.271 + 0.0637 * Chi(1) + 0.5761 * Chi(3) - 0.1392 * Chi(5) - 18.2244 * Chi_Avg(0) + 3.9332
* Chi_Avg(2) + _
      6.0029 * Chi_Avg(5) + 0.6086 * ChiV(1) - 2.5101 * ChiV(2) + 3.5378 * ChiV(4) - 3.1432 * ChiV(5) + _
      36.8323 * ChiV_Avg(2) - 44.3452 * ChiV_Avg(3) - 19.6284 * ChiV_Avg(4) + 13.1564 * ChiV_Avg(5)

Prop_BSA = 5.9445 - 0.279 * Chi(3) - 0.3754 * Chi(5) - 10.0317 * Chi_Avg(0) + 7.5983 * Chi_Avg(1) -
16.2788 * Chi_Avg(4) + 23.4753 * Chi_Avg(5) + _
      0.2149 * ChiV(0) - 0.7594 * ChiV(1) - 0.1974 * ChiV(2) + 2.2207 * ChiV(3) - 0.7265 * ChiV(5) + _
      8.4658 * ChiV_Avg(2) - 21.0254 * ChiV_Avg(3)

Prop_AA = 0.6937 - 0.3134 * Chi(3) - 0.1253 * Chi(5) + 1.6912 * Chi_Avg(0) + 5.1275 * Chi_Avg(2) + _
      0.8448 * ChiV(3) - 2.3518 * ChiV_Avg(0) - 7.97 * ChiV_Avg(2)

Prop_Ova = 1.1102 - 0.0514 * Chi(2) + 0.5165 * Chi(4) + 1.0148 * Chi_Avg(2) - 7.149 * Chi_Avg(5) - _
      1.0949 * ChiV(4) - 0.4271 * ChiV_Avg(0) - 1.4052 * ChiV_Avg(4) + 16.5246 * ChiV_Avg(5)
```

```
Prop_TI = -6.786 + 0.1362 * Chi(4) + 13.9898 * Chi_Avg(0) - 11.5258 * Chi_Avg(1) + 0.0346 * ChiV(1) - _
    0.2911 * ChiV(3) + 16.7938 * ChiV_Avg(2) - 19.2179 * ChiV_Avg(5)


Prop_All = 0.0000251 * (-2.43 * Chi(0) + 6.52 * Chi(1) - 3.12 * Chi(2) - 94.32 * Chi_Avg(1) + 74.04 *
Chi_Avg(2)) * _
    (0.029 * ASA + 19.35 * ahelix - 60.34 * bsheet - 71.54 * MW_prot + 66.38 * Tm)


'Penalty Function
For i = 1 To UBound(mol)
  If mol(1) = 4 Or mol(UBound(mol)) = 4 Then  'Add penalty for O-OH bond
    Penalty = 1000
    Exit For
  End If
  If i > 1 Then
    If mol(i - 1) > n_minusrings And mol(i) > n_minusrings Then 'Add penalty if two rings are fused
together
      Penalty = 1000
      Exit For
    ElseIf mol(i - 1) = 4 And mol(i) = 4 Then   'Add penalty for O-O bond
      Penalty = 1000
      Exit For
    End If
  End If
Next i



obj = Abs(Prop_MW - Target_MW) / Abs(Target_MW) ' + Penalty

End Function



Function fitness(mol) As Double

Target_MW = 148
Lower_MW = 0
Higher_MW = 296
alpha = 0.001

fitness = Exp(-alpha * (MW(mol) - Target_MW) ^ 2 / (Higher_MW - Lower_MW) ^ 2)


End Function
```

```
Function RNAmonomer(groups As Range) As Double

Dim mol() As Long, m As Long, size As Long, i As Long
Dim del() As Long, delv() As Long, nH() As Long
Dim AdjM() As Long, Chi(0 To 5) As Double, ChiV(0 To 5) As Double
Dim Chi_Avg(0 To 5) As Double, ChiV_Avg(0 To 5) As Double

m = groups.Count
ReDim mol(1 To m)
For i = 1 To m
   mol(i) = groups(i).Value
Next i

Call BuildMolecule(mol(), del(), delv(), nH(), AdjM(), m, size)
Call GetConnectivity(del(), delv(), nH(), AdjM(), size, Chi(), ChiV(), Chi_Avg(), ChiV_Avg())

RNAmonomer = 12.271 + 0.0637 * Chi(1) + 0.5761 * Chi(3) - 0.1392 * Chi(5) - 18.2244 * Chi_Avg(0) +
3.9332 * Chi_Avg(2) + _
       6.0029 * Chi_Avg(5) + 0.6086 * ChiV(1) - 2.5101 * ChiV(2) + 3.5378 * ChiV(4) - 3.1432 * ChiV(5) + _
       36.8323 * ChiV_Avg(2) - 44.3452 * ChiV_Avg(3) - 19.6284 * ChiV_Avg(4) + 13.1564 * ChiV_Avg(5)

End Function

Function BSAmonomer(groups As Range) As Double

Dim mol() As Long, m As Long, size As Long, i As Long
Dim del() As Long, delv() As Long, nH() As Long
Dim AdjM() As Long, Chi(0 To 5) As Double, ChiV(0 To 5) As Double
Dim Chi_Avg(0 To 5) As Double, ChiV_Avg(0 To 5) As Double

m = groups.Count
ReDim mol(1 To m)
For i = 1 To m
   mol(i) = groups(i).Value
Next i

Call BuildMolecule(mol(), del(), delv(), nH(), AdjM(), m, size)
Call GetConnectivity(del(), delv(), nH(), AdjM(), size, Chi(), ChiV(), Chi_Avg(), ChiV_Avg())

BSAmonomer = 5.9445 - 0.279 * Chi(3) - 0.3754 * Chi(5) - 10.0317 * Chi_Avg(0) + 7.5983 * Chi_Avg(1) -
16.2788 * Chi_Avg(4) + 23.4753 * Chi_Avg(5) + _
       0.2149 * ChiV(0) - 0.7594 * ChiV(1) - 0.1974 * ChiV(2) + 2.2207 * ChiV(3) - 0.7265 * ChiV(5) + _
       8.4658 * ChiV_Avg(2) - 21.0254 * ChiV_Avg(3)

End Function

Function AAmonomer(groups As Range) As Double
```

```
Dim mol() As Long, m As Long, size As Long, i As Long
Dim del() As Long, delv() As Long, nH() As Long
Dim AdjM() As Long, Chi(0 To 5) As Double, ChiV(0 To 5) As Double
Dim Chi_Avg(0 To 5) As Double, ChiV_Avg(0 To 5) As Double

m = groups.Count
ReDim mol(1 To m)
For i = 1 To m
   mol(i) = groups(i).Value
Next i

Call BuildMolecule(mol(), del(), delv(), nH(), AdjM(), m, size)
Call GetConnectivity(del(), delv(), nH(), AdjM(), size, Chi(), ChiV(), Chi_Avg(), ChiV_Avg())

AAmonomer = 0.6937 - 0.3134 * Chi(3) - 0.1253 * Chi(5) + 1.6912 * Chi_Avg(0) + 5.1275 * Chi_Avg(2) + _
       0.8448 * ChiV(3) - 2.3518 * ChiV_Avg(0) - 7.97 * ChiV_Avg(2)

End Function

Function OVAmonomer(groups As Range) As Double

Dim mol() As Long, m As Long, size As Long, i As Long
Dim del() As Long, delv() As Long, nH() As Long
Dim AdjM() As Long, Chi(0 To 5) As Double, ChiV(0 To 5) As Double
Dim Chi_Avg(0 To 5) As Double, ChiV_Avg(0 To 5) As Double

m = groups.Count
ReDim mol(1 To m)
For i = 1 To m
   mol(i) = groups(i).Value
Next i

Call BuildMolecule(mol(), del(), delv(), nH(), AdjM(), m, size)
Call GetConnectivity(del(), delv(), nH(), AdjM(), size, Chi(), ChiV(), Chi_Avg(), ChiV_Avg())

OVAmonomer = 1.1102 - 0.0514 * Chi(2) + 0.5165 * Chi(4) + 1.0148 * Chi_Avg(2) - 7.149 * Chi_Avg(5) - _
       1.0949 * ChiV(4) - 0.4271 * ChiV_Avg(0) - 1.4052 * ChiV_Avg(4) + 16.5246 * ChiV_Avg(5)

End Function

Function TImonomer(groups As Range) As Double

Dim mol() As Long, m As Long, size As Long, i As Long
Dim del() As Long, delv() As Long, nH() As Long
Dim AdjM() As Long, Chi(0 To 5) As Double, ChiV(0 To 5) As Double
Dim Chi_Avg(0 To 5) As Double, ChiV_Avg(0 To 5) As Double

m = groups.Count
```

```
ReDim mol(1 To m)
For i = 1 To m
   mol(i) = groups(i).Value
Next i

Call BuildMolecule(mol(), del(), delv(), nH(), AdjM(), m, size)
Call GetConnectivity(del(), delv(), nH(), AdjM(), size, Chi(), ChiV(), Chi_Avg(), ChiV_Avg())

TImonomer = -6.786 + 0.1362 * Chi(4) + 13.9898 * Chi_Avg(0) - 11.5258 * Chi_Avg(1) + 0.0346 * ChiV(1)
- _
      0.2911 * ChiV(3) + 16.7938 * ChiV_Avg(2) - 19.2179 * ChiV_Avg(5)

End Function

Sub ReturnCI()

Dim mol() As Long, m As Long, size As Long, i As Long, groups As Range
Dim del() As Long, delv() As Long, nH() As Long
Dim AdjM() As Long, Chi(0 To 5) As Double, ChiV(0 To 5) As Double
Dim Chi_Avg(0 To 5) As Double, ChiV_Avg(0 To 5) As Double

Set groups = Application.InputBox("Select groups", Type:=8)
m = groups.Count
ReDim mol(1 To m)
For i = 1 To m
   mol(i) = groups(i).Value
Next i

Call BuildMolecule(mol(), del(), delv(), nH(), AdjM(), m, size)
Call GetConnectivity(del(), delv(), nH(), AdjM(), size, Chi(), ChiV(), Chi_Avg(), ChiV_Avg())

For i = 0 To 5
   ActiveCell.Offset(0, i) = Chi(i)
   ActiveCell.Offset(1, i) = ChiV(i)
   ActiveCell.Offset(2, i) = Chi_Avg(i)
   ActiveCell.Offset(3, i) = ChiV_Avg(i)
Next i

End Sub
```

CONNECTIVITY INDICES CALCULATOR CODE

```
Option Explicit

Sub GetConnectivity(del() As Long, delv() As Long, nH() As Long, AdjM() As Long, m As Long, Chi() As
Double, ChiV() As Double, _
               Chi_Avg() As Double, ChiV_Avg() As Double)

Dim i As Long, j As Long, k As Long, edgecount As Long
Dim path2count() As Double, path2sum As Double, p As Long
Dim path3count() As Double, path3sum As Double, i3 As Long
Dim path4count() As Double, path4sum As Double, i4 As Long
Dim path5count() As Double, path5sum As Double, i5 As Long
Dim av() As Double, avv() As Double, e() As Double, ev() As Double

'Clear old results
Erase Chi()
Erase ChiV()
Erase Chi_Avg()
Erase ChiV_Avg()

'ReDim all relevant arrays

ReDim av(1 To m)                        'Array for vertex degrees
ReDim avv(1 To m)                        'Array for valence vertex degrees
ReDim path2count(1 To m, 1 To m, 1 To m)    'Array for storing existence of 2-length paths
ReDim path3count(1 To m, 1 To m)    'Array for storing existence of 3-length paths
ReDim path4count(1 To m, 1 To m)    'Array for storing existence of 4-length paths
ReDim path5count(1 To m, 1 To m)    'Array for storing existence of 5-length paths

'Calculate valence vertex degrees
For i = 1 To m
   avv(i) = (delv(i) - nH(i)) / (del(i) - delv(i) - 1) + AdjM(i, i)
Next i

'Calculate vertex degrees and X0 and X0v
For i = 1 To m
   For j = 1 To m
      av(i) = AdjM(i, j) + av(i)
   Next j
   If av(i) = 0 Then
      MsgBox "Disconnected Atom", , "Error"
      Exit Sub
   End If
   Chi(0) = Chi(0) + 1 / (av(i) ^ 0.5)
   ChiV(0) = ChiV(0) + 1 / (avv(i) ^ 0.5)
Next i

'Count number of edges
For i = 2 To m
   For j = 1 To i - 1
      If AdjM(i, j) > 0 Then edgecount = edgecount + 1
   Next j
Next i

'Dimension array to size of number of edges
ReDim e(1 To edgecount)
ReDim ev(1 To edgecount)

'Calculate edge values and X1 and X1v
k = 1
For i = 2 To m
   For j = 1 To i - 1
      If AdjM(i, j) > 0 Then
         e(k) = av(i) * av(j)
         ev(k) = avv(i) * avv(j)
         Chi(1) = Chi(1) + 1 / (e(k) ^ 0.5)
         ChiV(1) = ChiV(1) + 1 / (ev(k) ^ 0.5)
         k = k + 1
      End If
   Next j
Next i

'Records existence of paths of length 2
For i = 1 To m
   For j = 1 To m
      If j <> i Then
         If AdjM(i, j) > 0 Then
            For k = 1 To m
               If k <> j And k <> i Then
                  If AdjM(j, k) > 0 Then
                     If path2count(k, j, i) > 0 Then
                        path2count(i, j, k) = 0
                     Else
                        path2count(i, j, k) = 1
                     End If
                  End If
               End If
            Next k
         End If
      End If
   Next j
Next i

'Calculate X2 and X2v
For i = 1 To m
   For j = 1 To m
      For k = 1 To m
         path2sum = path2sum + path2count(i, j, k)          'Count the number of paths of length 2 - Mainly
for debugging purposes
         If path2count(i, j, k) > 0 Then
            Chi(2) = Chi(2) + 1 / ((av(i) * av(j) * av(k)) ^ 0.5)
            ChiV(2) = ChiV(2) + 1 / ((avv(i) * avv(j) * avv(k)) ^ 0.5)
         End If
      Next k
   Next j
Next i

'Check for paths of length 3, 4 and 5
For i = 1 To m
   For j = 1 To m
      If j <> i Then
         If AdjM(i, j) > 0 Then
            For k = 1 To m
               If k <> j And k <> i Then
                  If AdjM(j, k) > 0 Then
                     For i3 = 1 To m
                        If i3 <> k And i3 <> j And i3 <> i Then
                           If AdjM(k, i3) > 0 Then
                              If path3count(i3, i) > 0 Then
                                 path3count(i, i3) = 0                              ' Avoids double counting paths
                              Else
                                 path3count(i, i3) = 1
                                 path3sum = path3sum + 1
                                 Chi(3) = Chi(3) + 1 / ((av(i) * av(j) * av(k) * av(i3)) ^ 0.5)
                                 ChiV(3) = ChiV(3) + 1 / ((avv(i) * avv(j) * avv(k) * avv(i3)) ^ 0.5)
                              End If
                              For i4 = 1 To m
                                 If i4 <> i3 And i4 <> k And i4 <> j And i4 <> i Then
                                    If AdjM(i3, i4) > 0 Then
                                       If path4count(i4, i) > 0 Then
                                          path4count(i, i4) = 0
                                       Else
                                          path4count(i, i4) = 1
                                          path4sum = path4sum + 1
                                          Chi(4) = Chi(4) + 1 / ((av(i) * av(j) * av(k) * av(i3) * av(i4)) ^ 0.5)
                                          ChiV(4) = ChiV(4) + 1 / ((avv(i) * avv(j) * avv(k) * avv(i3) * avv(i4)) ^ 0.5)
                                       End If
                                       For i5 = 1 To m
                                          If i5 <> i3 And i5 <> k And i5 <> j And i5 <> i4 And i5 <> i Then   'i5 cannot
equal i even if there is a five atom ring -- Paths not walks!
                                             If AdjM(i4, i5) > 0 Then
                                                If path5count(i5, i) > 0 Then
                                                   path5count(i, i5) = 0
                                                Else
                                                   path5count(i, i5) = 1
                                                   path5sum = path5sum + 1
                                                   Chi(5) = Chi(5) + 1 / ((av(i) * av(j) * av(k) * av(i3) * av(i4) * av(i5)) ^
0.5)

                                                   ChiV(5) = ChiV(5) + 1 / ((avv(i) * avv(j) * avv(k) * avv(i3) * avv(i4) *
avv(i5)) ^ 0.5)
                                                End If
                                             End If
                                          End If
                                       Next i5
                                    End If
                                 End If
                              Next i4
                           End If
                        End If
                     Next i3
                  End If
               End If
            Next k
         End If
      End If
   Next j
Next i


'Calculate XAs
'Molecule guarenteed to have path of length 2, but need to check if any path length > 2 to avoid overflow
Chi_Avg(0) = Chi(0) / m
Chi_Avg(1) = Chi(1) / edgecount
Chi_Avg(2) = Chi(2) / path2sum
If path3sum <> 0 Then
   Chi_Avg(3) = Chi(3) / path3sum
Else
   Chi_Avg(3) = 0
End If
If path4sum <> 0 Then
   Chi_Avg(4) = Chi(4) / path4sum
Else
   Chi_Avg(4) = 0
End If
If path5sum <> 0 Then
   Chi_Avg(5) = Chi(5) / path5sum
Else
   Chi_Avg(5) = 0
End If

ChiV_Avg(0) = ChiV(0) / m
ChiV_Avg(1) = ChiV(1) / edgecount
ChiV_Avg(2) = ChiV(2) / path2sum
If path3sum <> 0 Then
   ChiV_Avg(3) = ChiV(3) / path3sum
Else
   ChiV_Avg(3) = 0
End If
If path4sum <> 0 Then
```

```
   ChiV_Avg(4) = ChiV(4) / path4sum
Else
   ChiV_Avg(4) = 0
End If
If path5sum <> 0 Then
   ChiV_Avg(5) = ChiV(5) / path5sum
Else
   ChiV_Avg(5) = 0
End If


End Sub
```

TABU SEARCH CODE

```
ption Explicit

Sub RunTabu(mol() As Long, m As Long, del() As Long, delv() As Long, nH() As Long, AdjM() As Long, size
As Long, _
               Chi() As Double, ChiV() As Double, Chi_Avg() As Double, ChiV_Avg() As Double, Final_Obj As
Double)



Dim moves As Long, max_moves As Long, TabuCriterion As Double, Stop_Criterion As Double
Dim imax As Long, List_size As Long, Tabu_list() As Variant, Tabu_count As Long
Dim Neighbors() As Molecule, p() As Double
Dim Best_sol() As Long, Current_sol() As Long, Neighbor_sol() As Long
Dim Best_obj As Double, Current_obj As Double, Neighbor_obj As Double
Dim Neighbors_Chi(0 To 5) As Double, Neighbors_ChiV(0 To 5) As Double, Neighbors_Chi_Avg(0 To 5) As
Double, Neighbors_ChiV_Avg(0 To 5) As Double
Dim Current_Chi(0 To 5) As Double, Current_ChiV(0 To 5) As Double, Current_Chi_Avg(0 To 5) As
Double, Current_ChiV_Avg(0 To 5) As Double
Dim Best_Chi(0 To 5) As Double, Best_ChiV(0 To 5) As Double, Best_Chi_Avg(0 To 5) As Double,
Best_ChiV_Avg(0 To 5) As Double
Dim i As Long, j As Long, k As Long, iter As Long

imax = 100#  'Max number of non-improving iterations
List_size = 15#  'Size of tabu list
ReDim Tabu_list(1 To List_size, 1 To 2) 'Set length of tabu list.
'1st column is for molecule groups. 2nd column is for Chi0 values used in tabu check.
max_moves = 4#  'maximum number of moves to create neighbors
TabuCriterion = 0.2   'Criterion for making solution Tabu
Stop_Criterion = 0#     'Criterion for objective function being good enough to stop

'Create random initial solution
Call InitialSolution(mol(), m)

'Initial solution set as best solution and current solution
Best_sol = mol      'Stores structure
```

```
Current_sol = mol   'Stores structure
Call BuildMolecule(mol, del(), delv(), nH(), AdjM(), m, size)
Call GetConnectivity(del(), delv(), nH(), AdjM(), size, Chi(), ChiV(), Chi_Avg(), ChiV_Avg())
For k = 0 To 5
   Current_Chi(k) = Chi(k)
   Current_ChiV(k) = ChiV(k)
   Current_Chi_Avg(k) = Chi_Avg(k)
   Current_ChiV_Avg(k) = ChiV_Avg(k)
Next k
Best_obj = obj(mol, Chi(), ChiV(), Chi_Avg(), ChiV_Avg()) 'Stores objective value
Tabu_list(1, 1) = mol 'Put initial solution into tabu list
Tabu_list(1, 2) = Chi(0) 'Stores Chi0 for tabu solution

'Tabu Search
Do

DoEvents        'Prevent not responding


moves = Int((max_moves - 1 + 1) * Rnd + 1) 'Max number of neighbors evaluated
ReDim Neighbors(1 To moves) 'initialize array for storing neighbors
ReDim p(1 To moves) 'initialize array for storing objective function values of neighbors

'Create list of neighbors and neighbor properties
For j = 1 To moves
   Neighbors(j).mol = Make_Neighbor(Current_sol, m)
   Call BuildMolecule(Neighbors(j).mol, del(), delv(), nH(), AdjM(), m, size)
   Call GetConnectivity(del(), delv(), nH(), AdjM(), size, Chi(), ChiV(), Chi_Avg(), ChiV_Avg())
   For k = 0 To 5
      Neighbors(j).Chi(k) = Chi(k)
      Neighbors(j).ChiV(k) = ChiV(k)
      Neighbors(j).Chi_Avg(k) = Chi_Avg(k)
      Neighbors(j).ChiV_Avg(k) = ChiV_Avg(k)
   Next k
   p(j) = obj(Neighbors(j).mol(), Chi(), ChiV(), Chi_Avg(), ChiV_Avg())
Next j

Neighbor_obj = p(1) 'Arbitrarily sets first neighbor as best objective function value

'Determine best non-tabu neighbor
For j = 1 To moves
   Tabu_count = 0  'Initialize
   If p(j) <= Neighbor_obj Then 'If objective function of neighbor is better than previous best, replace
      For i = 1 To List_size  'Check against each member of tabu list
         If Abs(Neighbors(j).Chi(0) - Tabu_list(i, 2)) > TabuCriterion Then 'Tabu Check
            Tabu_count = 0 'Solution is not Tabu yet...
         Else
            Tabu_count = 1 'Solution is Tabu. Quit checking against Tabu List.
            Exit For
         End If
      Next i
      If Tabu_count = 0 Then 'Check to see if solution is tabu. If not, assign solution to surrent solution.
         Neighbor_sol = Neighbors(j).mol
         Neighbor_obj = p(j)
         For k = 0 To 5
            Neighbors_Chi(k) = Neighbors(j).Chi(k)
            Neighbors_ChiV(k) = Neighbors(j).ChiV(k)
            Neighbors_Chi_Avg(k) = Neighbors(j).Chi_Avg(k)
            Neighbors_ChiV_Avg(k) = Neighbors(j).ChiV_Avg(k)
         Next k
      ElseIf p(j) <= Best_obj Then 'Override Tabu Criterion if solution is best yet encountered
         Neighbor_sol = Neighbors(j).mol
         Neighbor_obj = p(j)
         For k = 0 To 5
            Neighbors_Chi(k) = Neighbors(j).Chi(k)
            Neighbors_ChiV(k) = Neighbors(j).ChiV(k)
            Neighbors_Chi_Avg(k) = Neighbors(j).Chi_Avg(k)
            Neighbors_ChiV_Avg(k) = Neighbors(j).ChiV_Avg(k)
         Next k
         If p(j) <= Stop_Criterion Then   'Stop search if you have found best possible/allowable solution
            Neighbor_sol = Best_sol
            Neighbor_obj = Best_obj
            Exit Do
         End If
      End If
   End If
Next j

'Aspirate if all neighbors are Tabu (i.e., no neighbor solution was found)
If isArrayEmpty(Neighbor_sol) Then
   Call InitialSolution(mol(), m)  'Randomly generate a new molecule to be pseudo-neighbor
   Neighbor_sol = mol

   Call BuildMolecule(mol, del(), delv(), nH(), AdjM(), m, size)
   Call GetConnectivity(del(), delv(), nH(), AdjM(), size, Chi(), ChiV(), Chi_Avg(), ChiV_Avg())
   For k = 0 To 5
      Neighbors_Chi(k) = Chi(k)
      Neighbors_ChiV(k) = ChiV(k)
      Neighbors_Chi_Avg(k) = Chi_Avg(k)
      Neighbors_ChiV_Avg(k) = ChiV_Avg(k)
   Next k
   Neighbor_obj = obj(mol, Neighbors_Chi(), Neighbors_ChiV(), Neighbors_Chi_Avg(),
Neighbors_ChiV_Avg())
End If

'Makes best non-tabu neighbor the current solution
```

```
Current_sol = Neighbor_sol
Current_obj = Neighbor_obj
m = UBound(Neighbor_sol)
For k = 0 To 5
   Current_Chi(k) = Neighbors_Chi(k)
   Current_ChiV(k) = Neighbors_ChiV(k)
   Current_Chi_Avg(k) = Neighbors_Chi_Avg(k)
   Current_ChiV_Avg(k) = Neighbors_ChiV_Avg(k)
Next k

Erase Neighbor_sol    'Clears out neighbor solution

'Check current solution against best solution
If Current_obj < Best_obj Then
   iter = 0                      'reset count on non-improving iterations
   Best_obj = Current_obj
   Best_sol = Current_sol
   For k = 0 To 5
      Best_Chi(k) = Current_Chi(k)
      Best_ChiV(k) = Current_ChiV(k)
      Best_Chi_Avg(k) = Current_Chi_Avg(k)
      Best_ChiV_Avg(k) = Current_ChiV_Avg(k)
   Next k
Else
   iter = iter + 1                  'increase count on non-improving iteration
End If

Call MakeTabuList(Current_sol, Current_Chi(0), Tabu_list(), List_size) 'Add newest solution to tabu list

Loop While iter <= imax

'Records best solution as solution molecule for output
mol = Best_sol
m = UBound(mol)
For k = 0 To 5
   Chi(k) = Best_Chi(k)
   ChiV(k) = Best_ChiV(k)
   Chi_Avg(k) = Best_Chi_Avg(k)
   ChiV_Avg(k) = Best_ChiV_Avg(k)
Next k
Final_Obj = Best_obj

End Sub

Sub MakeTabuList(mol, chi_0, Tabu_list(), List_size As Long)
'Add new solution to tabu list and delete oldest solution

Dim j As Long
```

```
For j = List_size To 2 Step -1
   Tabu_list(j, 1) = Tabu_list(j - 1, 1) 'move all tabu solutions down on the list
   Tabu_list(j, 2) = Tabu_list(j - 1, 2)
Next j

Tabu_list(1, 1) = mol 'put newest solution at top of tabu list
Tabu_list(1, 2) = chi_0 'record Chi0 value for use in future tabu checks

End Sub

Function Swap(mol() As Long, m As Long)
'Funtion to swap two existing groups

Dim i As Long, j As Long
Dim old_i As Long, old_j As Long

If m <= 1 Then Exit Function 'exit if molecule is comprised of only one group

' randomly select groups to swap
i = Int((m - 1 + 1) * Rnd + 1)
j = Int((m - 1 + 1) * Rnd + 1)

'Stores inital values of i and j
old_i = mol(i)
old_j = mol(j)

'Swaps values of i and j
mol(i) = old_j
mol(j) = old_i

Swap = mol 'returns new molecule

End Function

Function Insert(mol() As Long, m As Long)
'Function to insert group into existing molecule

Dim Insertion As Long, old_mol() As Long
Dim i As Long

If m >= m_max Then Exit Function

ReDim old_mol(1 To m) 'Exits if molecule is at maximum size

'Store old molecule
For i = 1 To m
   old_mol(i) = mol(i)
```

```
Next i

'Grow molecule by one
m = m + 1
ReDim mol(1 To m)

Insertion = Int((m - 1 + 1) * Rnd + 1) 'Randomly select insertion point

'Fills in groups prior to insertion
For i = 1 To Insertion - 1
   mol(i) = old_mol(i)
Next i

mol(Insertion) = Int((n - 1 + 1) * Rnd + 1) 'Insert random group at insertion point

'Fills in groups following insertion
For i = Insertion + 1 To m
   mol(i) = old_mol(i - 1)
Next i

Insert = mol 'returns new molecule

End Function

Function Delete(mol() As Long, m As Long)
'Function to insert group into existing molecule

Dim Deletion As Long, old_mol() As Long
Dim i As Long

If m <= 1 Then Exit Function 'Exits if molecule only contains one group

ReDim old_mol(1 To m)

'Store old molecule
For i = 1 To m
   old_mol(i) = mol(i)
Next i

'Shrink molecule by one
m = m - 1
ReDim mol(1 To m)

Deletion = Int((m - 1 + 1) * Rnd + 1) 'Randomly select deletion point

'Fills in groups prior to deletion
For i = 1 To Deletion - 1
   mol(i) = old_mol(i)
```

```
Next i

'Fills in groups following deletion
For i = Deletion To m
   mol(i) = old_mol(i + 1)
Next i

Delete = mol 'returns new molecule

End Function

Function Mutate(mol() As Long, m As Long)

Dim i As Long

i = Int((m - 1 + 1) * Rnd + 1)  'Randomly select mutation point
mol(i) = Int((n - 1 + 1) * Rnd + 1) 'Randomly select mutation

Mutate = mol    'returns new molecule

End Function

Function Make_Neighbor(mol() As Long, m As Long)
'Assigns number of atoms in group selected
Dim k As Long

If m = 1 Then
   k = 2   'Make sure you insert to find neighbor if molecule has only one group
ElseIf m = m_max Then
   k = 3   'Make sure you delete to find neighbor if molecule has max number of groups
Else
   k = Int((4 - 1 + 1) * Rnd + 1) 'Randomly select molecular operator
End If

Select Case k
   Case Is = 1
     Make_Neighbor = Swap(mol, m)
   Case Is = 2
     Make_Neighbor = Insert(mol, m)
   Case Is = 3
     Make_Neighbor = Delete(mol, m)
   Case Is = 4
      Make_Neighbor = Mutate(mol, m)
End Select

End Function

Public Function isArrayEmpty(parArray As Variant) As Boolean
```

```
'Returns true if:
'  - parArray is not an array
'  - parArray is a dynamic array that has not been initialised (ReDim)
'  - parArray is a dynamic array has been erased (Erase)

    If IsArray(parArray) = False Then isArrayEmpty = True
    On Error Resume Next
    If UBound(parArray) < LBound(parArray) Then
        isArrayEmpty = True
        Exit Function
    Else
        isArrayEmpty = False
    End If

End Function
```

GENETIC ALGORITHM CODE

```
Option Explicit

Sub RunGA(mol() As Long, m As Long, del() As Long, delv() As Long, nH() As Long, AdjM() As Long, size As
Long, _
            Chi() As Double, ChiV() As Double, Chi_Avg() As Double, ChiV_Avg() As Double, Final_Obj As
Double)

Dim Gen_Max As Long, Pop_Size As Long, Population() As Molecule, p() As Double, Max_Prob As Double
Dim Best_obj As Double, Best_Member As Long, p_total As Double, Stop_Criterion As Double
Dim Parents() As Molecule, Parent_selection() As Long, num_parents As Long, prob As Double
Dim Partner1() As Long, Partner2() As Long
Dim Parent_1 As Long, Parent_2 As Long, m_1 As Long, m_2 As Long, CX_1 As Long, CX_2 As Long
Dim i As Long, j As Long, k As Long


Gen_Max = 25#  'Maximum numbers of generations
Pop_Size = 50#  'Population size in each generation
Max_Prob = 100#   'Maximum probability to sample from for roulette selection
Stop_Criterion = 100#     'Criterion for objective function being good enough to stop
ReDim Population(1 To Pop_Size) 'Create array for storing population
ReDim p(1 To Pop_Size)  'Create array to store fitness values
i = 0 'Progenitors are zeroth generation

'Seed Population
For j = 1 To Pop_Size
    Call InitialSolution(Population(j).mol(), m)    'Randomly generate molecule
    Call BuildMolecule(Population(j).mol, del(), delv(), nH(), AdjM(), m, size)
    Call GetConnectivity(del(), delv(), nH(), AdjM(), size, Chi(), ChiV(), Chi_Avg(), ChiV_Avg())
    For k = 0 To 5
        Population(j).Chi(k) = Chi(k)
        Population(j).ChiV(k) = ChiV(k)
```

```
      Population(j).Chi_Avg(k) = Chi_Avg(k)
      Population(j).ChiV_Avg(k) = ChiV_Avg(k)
   Next k
Next j

'
'Genetic Algorithm
'
Do

DoEvents    'Suppress not responding

'Calculate Fitness
If obj(Population(1).mol, Population(1).Chi(), Population(1).ChiV(), Population(1).Chi_Avg(),
Population(1).ChiV_Avg()) = 0 Then
   p(1) = 1 / (obj(Population(1).mol, Population(1).Chi(), Population(1).ChiV(), Population(1).Chi_Avg(),
Population(1).ChiV_Avg()) + 0.001)
Else
   p(1) = 1 / obj(Population(1).mol, Chi(), ChiV(), Chi_Avg(), ChiV_Avg()) 'fitness(Population(1).mol)
End If
Best_obj = p(1)                'Set inital member of solution as best member
Best_Member = 1
p_total = p(1)
For j = 2 To Pop_Size
   If obj(Population(j).mol, Population(j).Chi(), Population(j).ChiV(), Population(j).Chi_Avg(),
Population(j).ChiV_Avg()) = 0 Then
      p(j) = 1 / (obj(Population(j).mol, Population(j).Chi(), Population(j).ChiV(), Population(j).Chi_Avg(),
Population(j).ChiV_Avg()) + 0.001)
   Else
      p(j) = 1 / obj(Population(j).mol, Population(j).Chi(), Population(j).ChiV(), Population(j).Chi_Avg(),
Population(j).ChiV_Avg()) 'fitness(Population(j).mol)
   End If
      p_total = p_total + p(j)
      If p(j) > Best_obj Then      'If current member has better obj than best, replace best with current
member
         Best_obj = p(j)
         Best_Member = j
      End If
   Next j

'Termination criteria
If i >= Gen_Max Or Best_obj > Stop_Criterion Then     'Check if generations have completed or if best
solution from generation is good enough to stop search
   mol = Population(Best_Member).mol             'If so, return best solution and exit GA
   For k = 0 To 5
      Chi(k) = Population(Best_Member).Chi(k)
      ChiV(k) = Population(Best_Member).ChiV(k)
      Chi_Avg(k) = Population(Best_Member).Chi_Avg(k)
      ChiV_Avg(k) = Population(Best_Member).ChiV_Avg(k)
   Next k
   Final_Obj = obj(mol, Chi(), ChiV(), Chi_Avg(), ChiV_Avg())
   Exit Do
End If

'Select Parents
num_parents = 0 'no parents selected yet
Erase Parents() 'erase old parents
ReDim Parent_selection(1 To Pop_Size)   'Create array for storing parent selection
k = 1   'counter for number of parents
For j = 1 To Pop_Size
   prob = 100 * p(j) / p_total               'Calculate probability of becoming parent
   If Int((Max_Prob - 1 + 1) * Rnd + 1) < prob Then 'Roulette selection
      Parent_selection(j) = 1
      num_parents = num_parents + 1
  End If
Next j

If num_parents = 0 Then      'If no parents selected, randomly choose two members of the population to
become parents
   ReDim Parents(1 To 2)
   Parents(1).mol = Population(Int((Pop_Size - 1 + 1) * Rnd + 1)).mol
   Parents(2).mol = Population(Int((Pop_Size - 1 + 1) * Rnd + 1)).mol
Else
   ReDim Parents(1 To num_parents)    'Dimension array for storing parents
   k = 1   'counter for number of parents
   For j = 1 To Pop_Size
      If Parent_selection(j) = 1 Then 'If memeber is selected as parent, add to parents array
         Parents(k).mol = Population(j).mol
         k = k + 1
      End If
   Next j
End If


'Reproduction
For j = 1 To Pop_Size
   If p(j) >= Best_obj Then    'Elitist Policy
      Population(j).mol = Population(j).mol
   Else
      Erase Partner1
      Erase Partner2
      Parent_1 = Int((num_parents - 1 + 1) * Rnd + 1)
      Parent_2 = Int((num_parents - 1 + 1) * Rnd + 1)
      m_1 = UBound(Parents(Parent_1).mol)
      m_2 = UBound(Parents(Parent_2).mol)
      Partner1 = Parents(Parent_1).mol
```

```
    Partner2 = Parents(Parent_2).mol
    Population(j).mol = Make_Offspring(Partner1, Partner2, m_1, m_2, k, CX_1, CX_2)
    If UBound(Population(j).mol) > m_max Then   'If new member of population is too large, kill off and replace with one of its two parents
      If Int((2 - 1 + 1) * Rnd + 1) = 1 Then
        Population(j).mol = Partner1
      Else
        Population(j).mol = Partner2
      End If
    ElseIf k = 5 And j <= (Pop_Size - 1) Then   'If crossover is selected, make sure next offspring is the other crossover result
      j = j + 1
      Partner1 = Parents(Parent_1).mol
      Partner2 = Parents(Parent_2).mol
      m_1 = UBound(Partner1)
      m_2 = UBound(Partner2)
      Population(j).mol = Crossover2(Partner1, Partner2, m_1, m_2, CX_1, CX_2)
    End If
  End If
Next j

'Calculate descriptors for next generation
For j = 1 To Pop_Size
  m = UBound(Population(j).mol)
  Call BuildMolecule(Population(j).mol, del(), delv(), nH(), AdjM(), m, size)
  Call GetConnectivity(del(), delv(), nH(), AdjM(), size, Chi(), ChiV(), Chi_Avg(), ChiV_Avg())
  For k = 0 To 5
    Population(j).Chi(k) = Chi(k)
    Population(j).ChiV(k) = ChiV(k)
    Population(j).Chi_Avg(k) = Chi_Avg(k)
    Population(j).ChiV_Avg(k) = ChiV_Avg(k)
  Next k
Next j


i = i + 1   'Increase generation
Erase Parent_selection

Loop

End Sub

Function Make_Offspring(Partner1() As Long, Partner2() As Long, m1 As Long, m2 As Long, k As Long, CX1 As Long, CX2 As Long)
'Assigns number of atoms in group selected

If m1 = 1 Then
  k = 2   'Make sure you insert to find neighbor if molecule has only one group
```

```
ElseIf m1 >= m_max Then
   k = 3   'Make sure you delete to find neighbor if molecule has max number of groups
Else
   k = Int((6 - 1 + 1) * Rnd + 1) 'Randomly select molecular operator
End If

Select Case k
   Case Is = 1
     Make_Offspring = Swap(Partner1, m1)
   Case Is = 2
     Make_Offspring = Insert(Partner1, m1)
   Case Is = 3
     Make_Offspring = Delete(Partner1, m1)
   Case Is = 4
      Make_Offspring = Mutate(Partner1, m1)
   Case Is = 5
      Make_Offspring = Crossover1(Partner1, Partner2, m1, m2, CX1, CX2)
   Case Is = 6
      Make_Offspring = Blend(Partner1, Partner2, m1, m2)
End Select

End Function

Function Crossover1(Partner1() As Long, Partner2() As Long, m1 As Long, m2 As Long, CX1 As Long, CX2 As Long)

Dim i As Long, j As Long, size As Long, mol() As Long

CX1 = Int(((m1 - 1) - 1 + 1) * Rnd + 1) 'Randomly choose crossover points
CX2 = Int(((m2 - 1) - 1 + 1) * Rnd + 1)
size = CX1 + (m2 - CX2)
ReDim mol(1 To size)

For i = 1 To CX1       'Offspring up to CX1 is taken from 1st parent
   mol(i) = Partner1(i)
Next i

For j = (CX2 + 1) To m2 'Offspring after CX1 is taken from 2nd parent
   mol(i) = Partner2(j)
   i = i + 1
Next j

Crossover1 = mol


End Function
```

```
Function Crossover2(Partner1() As Long, Partner2() As Long, m1 As Long, m2 As Long, CX1 As Long, CX2 As Long)

Dim i As Long, j As Long, size As Long, mol() As Long

size = CX2 + (m1 - CX1)
ReDim mol(1 To size)
i = 1
For j = (CX1 + 1) To m1      'Offspring past CX1 is taken from 1st parent
   mol(i) = Partner1(j)
   i = i + 1
Next j

For j = 1 To CX2 'Offspring before CX2 is taken from 2nd parent
   mol(i) = Partner2(j)
   i = i + 1
Next j

Crossover2 = mol

End Function

Function Blend(Partner1() As Long, Partner2() As Long, m1 As Long, m2 As Long)
'Add two parents together to yield offspring

Dim i As Long, j As Long, size As Long, mol() As Long

size = m1 + m2
ReDim mol(1 To size)

For i = 1 To m1
   mol(i) = Partner1(i)
Next i

For j = 1 To m2
   mol(i) = Partner2(j)
   i = i + 1
Next j

Blend = mol

End Function
```

E. UNIFAC-IL Interaction Parameters

Interaction parameters for the UNIFAC-IL model described in Sections 4 and 6 are given. The interaction parameters are used in calculation of the activity coefficient for any given binary mixture of interest.

Table E.1 UNIFAC-IL group interaction parameters Shaded regions indicate no parameter due to lack of experimental data points for regression. Interactions between ionic liquid groups are assumed to be zero.

	[Im]	[Py]	[N]	[DMP]	[BF$_4$]	[PF$_6$]	[Tf$_2$N]	[CF$_3$COO]	[CF$_3$SO$_3$]	[CH$_3$SO$_4$]	[CH$_3$CH$_2$SO$_4$]	[CH$_3$OC$_2$H$_4$SO$_4$]	[C$_2$H$_5$OC$_2$H$_4$SO$_4$]	[CH$_3$(OC$_2$H$_4$)$_2$SO$_4$]	[Br]	[Cl]	[I]	[SCN]
CH$_2$	65.08	-24.94	7783.26	879.73	703.25	219.44	19.68	154.79	694.19	331.64	595.73	465.54	221.23	89.02	-111.41	-4999.54	-1002.39	974.48
C=C	-68.40	-22.74	3650.75	909.19	719.15	204.21	127.07	336.73	318.83	338.97	5180.40	544.47	204.78	-158.71		1193.99		1121.71
C=-C	-165.32					-161.87	96.52	-249.93	374.09					-403.99		637.92		686.82
ACH	364.12	253.93	14507.69	495.39	231.68	-165.11	233.16	-95.77	599.35	194.86	-294.20	-264.31	188.60	-1491.59	-172.37	6678.72	0.10	1296.49
ACCH$_2$	-52.63	-172.52	9950.45	40.31	2040.01	-17.54	-50.86	527.38	560.87	253.24	3908.46	4183.35	65.94	2529.39		-3128.83		-11832.04
OH	-199.99	-147.61	5524.91	-33.36	-223.62	-61.13	-320.23	-126.41	91.85	-56.32					-777.58	-976.48	-1056.62	-442.46
CH$_2$CO	-266.87	-143.22	760.08	320.25	327.86	-206.22	142.35		443.95			-9.82	7845.25				-33.43	
COO	285.63						222.41											
CCOO	-46.38	37.17	7018.47		189.88		-220.76		163.17									
CH$_2$O	-220.86	-281.65	895.42	804.02	3716.54		7649.64		469.89									
CHO	-278.18		5425.81		26.26		-104.61											
CH$_3$OH	380.03	841.54	-350.11	-182.43	-348.29	-174.31	31.73	187.27	-335.72	-271.69				42.88	-6980.92	1582.04	-113.62	-770.70
H$_2$O	-914.38	-666.90		-650.60	-917.88	-97.63	-44.44	-67.07	-211.41									-1120.09
CNH$_2$	84.54						720.38										-1503.07	
DMF			651.48				97.51											
CCN	191.43	702.19	-526.00		-86.83		98.84		202.80									
CCl	342.41				585.17		-1965.24									-191.32		
CCl$_2$	70.75	-3.83	-114.66		850.59		-116.90		634.69						-159.10		-174.18	
CCl$_3$	120.91	-94.11	-1448.18		455.75		20.42		626.85								0.00	
CCl$_4$	-258.51	649.10			327.85		193.35		682.89					-1271.68				

	CH2	C=C	C=-C	ACH	ACCH2	OH	CH2CO	COO	CCOO	CH2O	CHO	CH3OH	H2O	CNH2	DMF	CCN	CCl	CCl2	CCl3	CCl4
[Im]	134.11	-116.48	8253.80	-177.56	100.96	737.69	438.53	187.36	909.57	-376.85	3047.06	0.05	0.00	-14.70		0.02	-363.62	119.34	0.06	584.82
[Py]	1269.62	-149.09		-25.31	4115.86	1789.95	507.94		678.44	-15.87		-224.11	-0.01			-285.53		704.34	3808.49	-1026.78
[N]	-791.24	-794.94		-784.43	-791.31	-417.34	2079.69		-619.82	1728.79	-119.95	646.15		327.43		448.44		-111.26	-2165.65	
[DMP]	-326.80	-351.56		-266.43	1017.65	64.06	-42.56			77.16		-211.21	1209.55							
[BF_4]	8730.62	2.92		216.79	895.71	32.29	-187.37		-208.82	-13.82	77.94	-0.04	0.01			0.00	141.59	-360.23	-143.79	3698.95
[PF_6]	-34.64	41.58	516.24	465.25	205.07	536.61	487.17					572.75	0.00							
[Tf_2N]	300.61	185.64	58.90	-122.81	325.93	636.96	-31.73	187.36	137.96	-113.90	292.40	0.01	0.00	456.99	220.08	-84.85	-155.53	304.09	71.51	-0.02
[CF_3COO]	816.71	15039.59	768.49	745.73	394.23	-28.95						-221.08	0.00							
[CF_3SO_3]	-285.94	205.33	-177.75	-328.36	-253.75	220.70	-191.88		-6.66	197.50		350.14	0.00			-208.43		-338.14	-338.39	-303.73
[CH_3SO_4]	-19.44	68.47		-49.92	133.36	-57.35						0.00								
[$CH_3CH_2SO_4$]	-229.99	6462.89		452.79	-2746.36															
[$CH_3OC_2H_4SO_4$]	-181.96	-192.08		6122.45	-2773.92		428.59													
[$C_2H_5OC_2H_4SO_4$]	-91.68	-71.57		-130.50	20.19		-264.88													
[$CH_3(OC_2H_4)_2SO_4$]	136.82	4934.10	5219.84	-8639.1	13185.19							60.01								2432.21
[Br]	69.02			-211.84		-941.81						-6981.27						-159.01		
[Cl]	-594.89	148.85	-377.18	-848.72	98.92	-678.25						0.26					0.00			
[I]	4498.45			0.10		7040.11	9999.95					-113.96				-4.58		-157.19	-189.98	
[SCN]	3528.75	6187.17	-360.91	-399.98	-2099.01	-119.73						0.00	0.01							

F. Summary of Experimental Data

Table F.1 summarizes the results obtained by Lavanya K. Iyer at Purdue University and used for model development for *%Monomer* as a function of protein structure (Roughton, Iyer *et al.* 2013). All other figures represent data obtained by the author.

Table F.1 Summary of experimental measures of protein aggregation via SEC (% monomer), UV- Vis (AI) and SDS-PAGE Values in parenthesis for SEC and A.I. are standard error about mean (SEM) for three observations.

Protein	Formulation																	
	Unlyophilized			*Buffer*			*Sucrose*			*Glycine*			*Urea*			*Gdn HCl*		
	SEC	A.I.	SDS-PAGE[a]	SEC	A.I.	SDS-PAGE[a]	SEC	A.I.	SDS-PAGE[a]	SEC	A.I.	SDS-PAGE[a]	SEC	A.I.	SDS-PAGE[a]	SEC	A.I.	SDS-PAGE[a]
Myoglobin	100 (0)	71 (31)	-	96 (3)	123 (59)	-, *dimer*	99 (3)	13 (1)	-, *dimer*	99 (1)	15 (2)	-, *dimer*	85 (6)	34 (15)	Pellet, *dimer*	0 (0)	24 (11)	Pellet, *dimer*
Lysozyme	100 (0)	5 (4)	-, *dimer*	80 (12)	11 (10)	-, *dimer*	77 (18)	7 (3)	-, *dimer*	97 (2)	1.9 (0.3)	-, *dimer*	65 (23)	18 (9)	-, *dimer*	0 (0)	2.1 (0.5)	-, *dimer*
Ovalbumin	100 (0)	43 (6)	+, *dimer, d*	98 (2)	245 (8)	+, *dimer, d*	97 (1)	5 (1)	+, *dimer, d*	99.7 (1.7)	113 (14)	+, *dimer, d*	16.5 (0.6)	413 (38)	Pellet, +, *dimer, d*	0 (0)	45 (14)	Pellet, +, *dimer*
RNase A	100 (0)	0.8 (0.3)	*dimer*	113 (5)	2.2 (0.2)	*dimer*	89 (10)	6 (1)	*dimer*	97 (12)	6.2 (0.1)	*dimer*	97 (9)	5.1 (0.3)	*dimer*	0 (0)	28 (19)	*dimer*
DNase I	100 (0)	6.6 (0.1)	-	107 (15)	109 (5)	-	86 (12)	9.9 (0.8)	-	62 (35)	59 (1)	-	116 (12)	239 (14)	-	0 (0)	44 (5)	-
α -chymotrypsinogen	100 (0)	7 (7)	-	102 (6)	13 (12)	-	95.6 (0.5)	1.05 (0.01)	-	103 (2)	24 (11)	-	83 (4)	12 (8)	-	0 (0)	9 (2)	Pellet, -
Cytochrome-C	100 (0)	159 (3)	-, *dimer*	30 (23)	3388 (1817)	-, *dimer*	33 (24)	120.4 (0.6)	-, *dimer*	127 (90)	61.5 (0.9)	-, *dimer*	0 (0)	193 (56)	-, *dimer*	0 (0)	65 (2)	+, *dimer*
Con A	100 (0)	23 (6)	-	103 (20)	9 (1)	-	122 (19)	20 (7)	-	121 (15)	26 (2)	-	21 (9)	80 (19)	-	45 (12)	388 (224)	-
Catalase	100 (0)	21 (13)	-	90 (5)	18 (12)	-	98 (6)	2.6 (0.2)	-	100 (2)	160 (16)	-	19 (2)	48 (22)	Pellet, +, d	0 (0)	10 (5)	Pellet, -
α-amylase	100 (0)	3.5 (0.5)	+	94 (3)	5 (1)	+	97 (4)	2.8 (0.2)	+	104 (2)	1.2 (0.4)	+	92 (4)	2.9 (0.6)	+	2.77 (0.02)	76 (6)	Pellet, +
α-lactalbumin	100 (0)	14 (10)	-, *dimer*	109 (11)	32.9 (0.5)	-, *dimer*	99 (2)	1.6 (0.5)	-, *dimer*	100 (4)	4.1 (0.8)	-, *dimer*	97 (2)	2.2 (0.2)	-, *dimer*	0 (0)	19 (5)	-
β-lactoglobulin	100 (0)	11 (9)	-, *dimer*	92 (6)	1.7 (0.4)	-, *dimer*	95 (3)	2.5 (0.8)	-, *dimer*	90 (6)	1.7 (0.2)	-, *dimer*	83 (3)	4.8 (3.1)	-, *dimer*	0 (0)	924 (179)	Pellet, +
SOD	100 (0)	3.5 (0.3)	-	89 (3)	3.65 (0.04)	-	99 (1)	0.7 (0.1)	-	100 (2)	15.9 (0.2)	-	113 (10)	155 (24)	-	48 (20)	51 (10)	+, d
BSA	100 (0)	65.1 (0.5)	+	94 (2)	66.4 (0.5)	+	96.5 (0.6)	3.6 (0.5)	+	93.2 (1.3)	3.1 (0.8)	+	77.2 (0.4)	3.2 (0.6)	+	117 (3)	18 (6)	Pellet, +
Trypsin Inhibitor	100 (0)	2.5 (0.3)	-	115 (16)	7 (1)	-	116 (15)	192 (5)	-	119 (13)	29 (1)	-	120 (15)	45 (4)	-	0 (0)	304 (216)	-

[a] 'Pellet' indicates formation of insoluble aggregates upon centrifugation of the reconstituted lyophilized formulation; presence of high molecular weight aggregate bands (greater than twice the molecular weight of the native protein) indicated by +; absence of high molecular weight aggregate bands indicated by -; presence of dimer band indicated by *dimer*; presence of disulfide-linked aggregates indicated by *d*

Figure F.1 Pxrd results for subset of formulations selected Each panel displays a protein–excipient pair selected for analysis. Panels with two X-Ray diffractograms represent formulations that were chosen for replication.

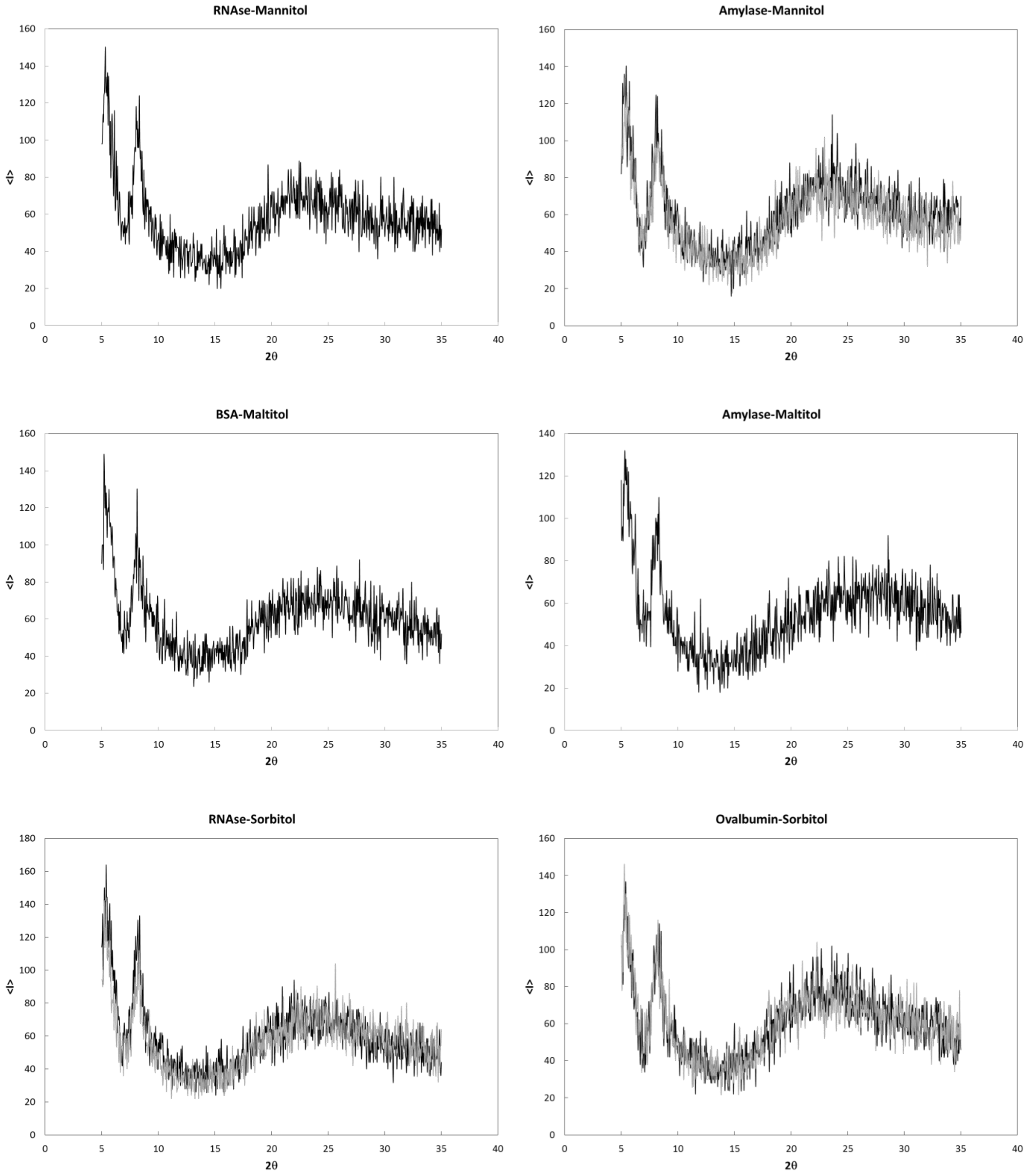

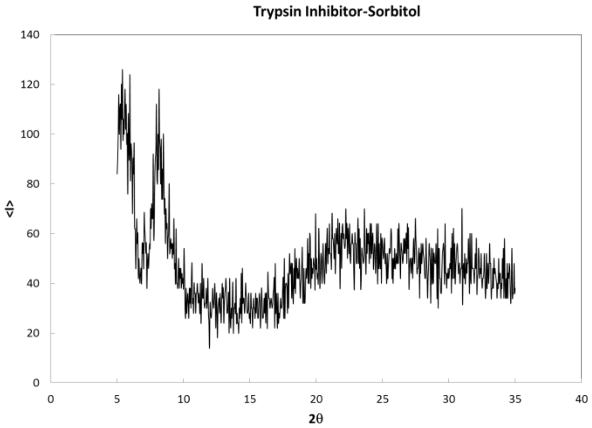
Trypsin Inhibitor-Sorbitol
<I>
0
20
40
60
80
100
120
140
0
5
10
15
20
25
30
35
40
2θ

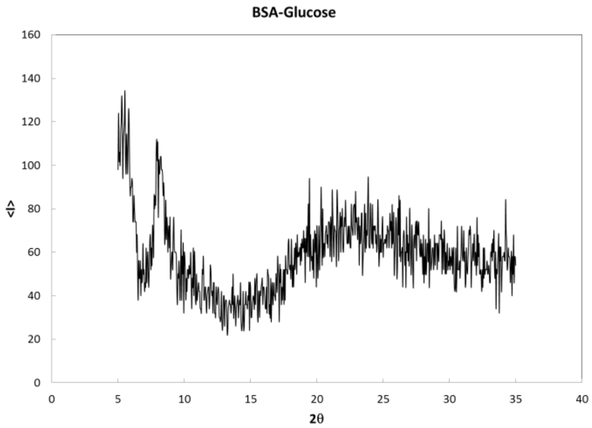
BSA-Glucose
<I>
0
20
40
60
80
100
120
140
160
0
5
10
15
20
25
30
35
40
2θ

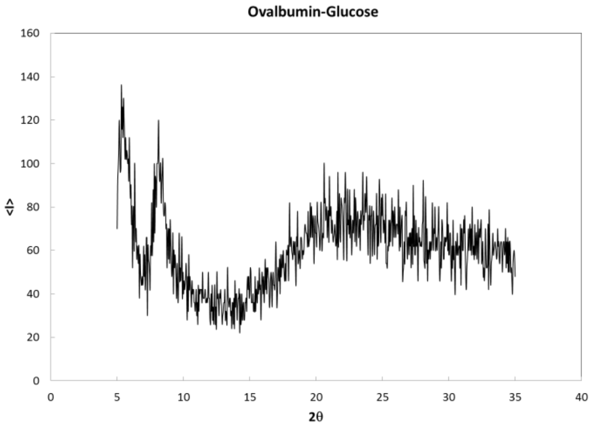
Ovalbumin-Glucose
<I>
0
20
40
60
80
100
120
140
160
0
5
10
15
20
25
30
35
40
2θ

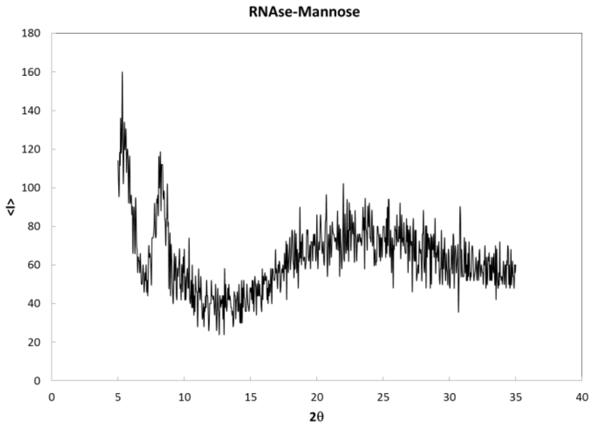
RNAse-Mannose
<I>
0
20
40
60
80
100
120
140
160
180
0
5
10
15
20
25
30
35
40
2θ

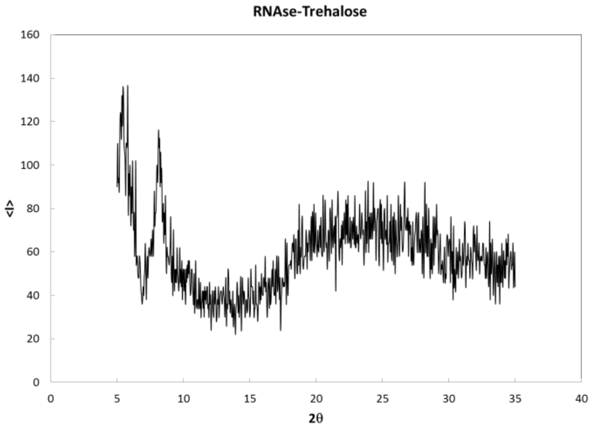
RNAse-Trehalose
<I>
0
20
40
60
80
100
120
140
160
0
5
10
15
20
25
30
35
40
2θ

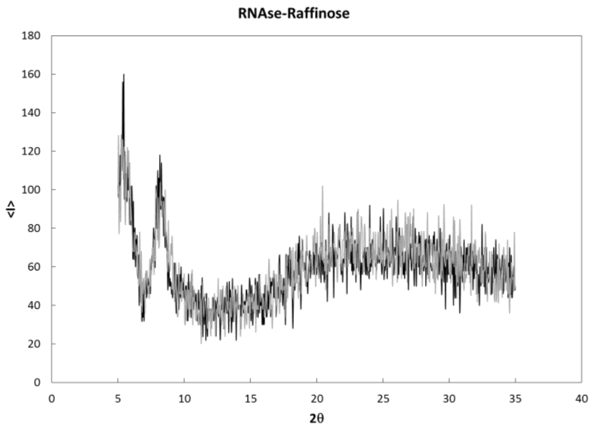
RNAse-Raffinose
<I>
0
20
40
60
80
100
120
140
160
180
0
5
10
15
20
25
30
35
40
2θ

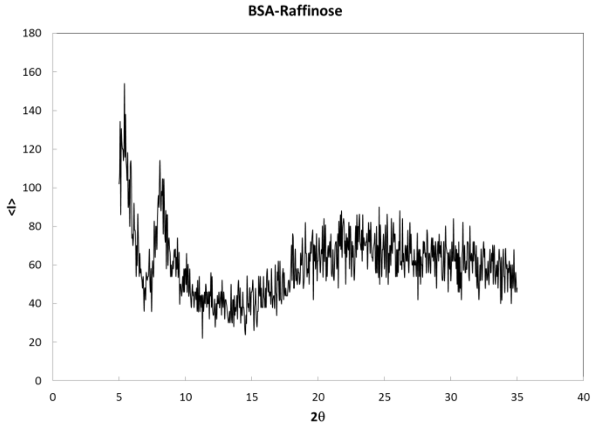

BSA-Raffinose

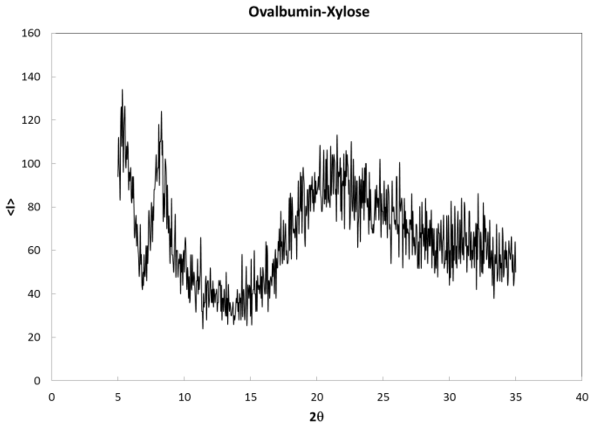

Ovalbumin-Xylose

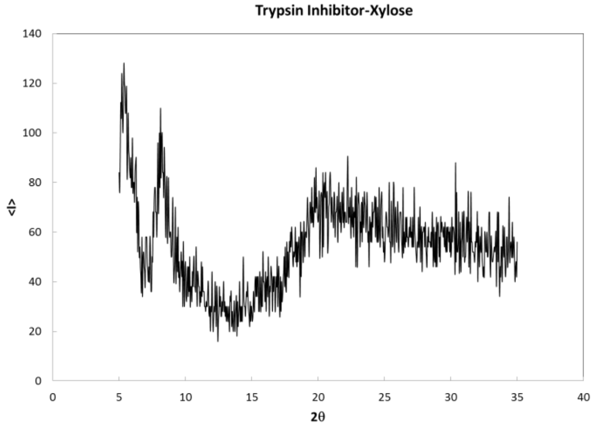

Trypsin Inhibitor-Xylose

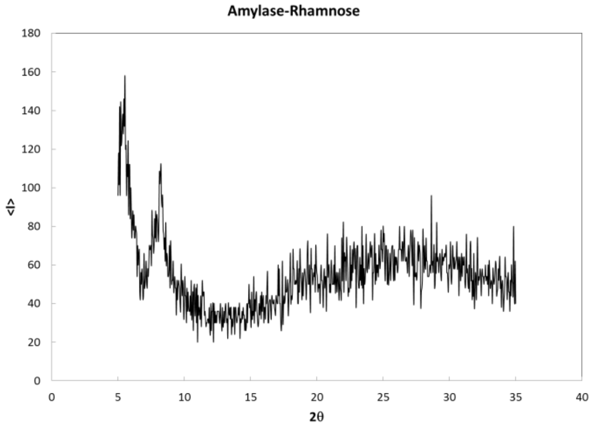

Amylase-Rhamnose

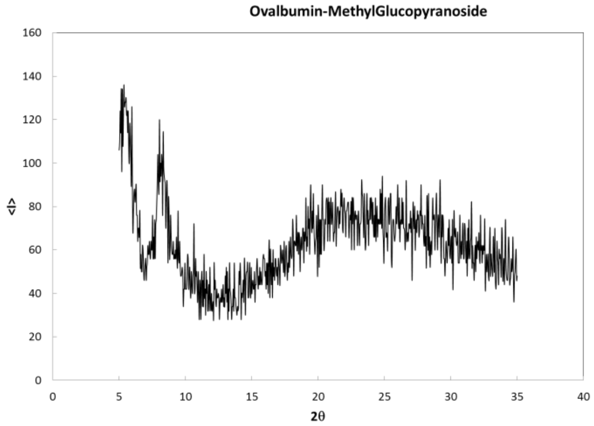

Ovalbumin-MethylGlucopyranoside

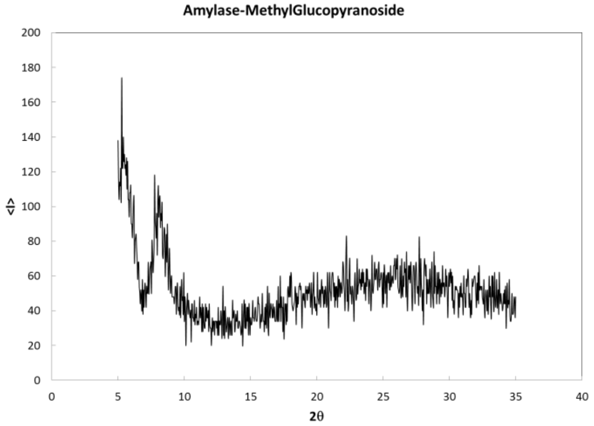

Amylase-MethylGlucopyranoside

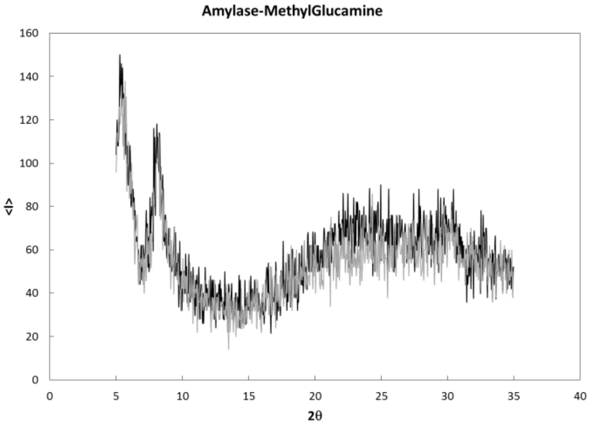
Amylase-MethylGlucamine
160
140
120
100
80
60
40
20
0
<I>
0
5
10
15
20
25
30
35
40
2θ

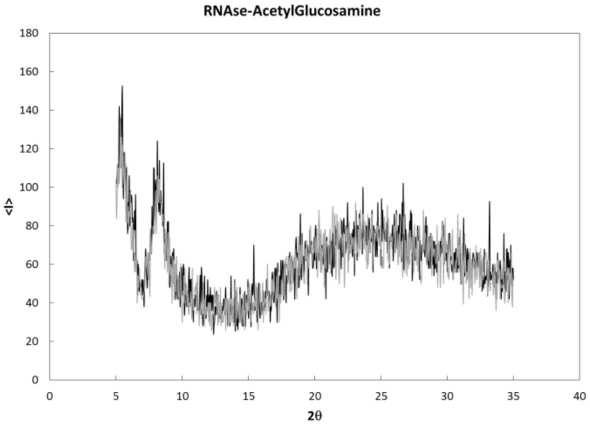
RNAse-AcetylGlucosamine
180
160
140
120
100
80
60
40
20
0
<I>
0
5
10
15
20
25
30
35
40
2θ

Table F.2 Experimental SEC results Value in parenthesis indicates standard error of the mean (SEM).

Excipient	**RNAse A**	**BSA**	**Ovalbumin**	**Trypsin Inhibitor**	**a-Amylase**
Sorbitol	99.3% (1.0%)	91.7% (1.1%)	99.6% (0.4%)	101.2% (2.1%)	98.1% (2.3%)
Mannitol	85.3% (1.7%)	82.6% (1.1%)	98.8% (0.7%)	88.9% (3.5%)	95.0% (1.2%)
Maltitol	86.6% (1.0%)	85.9% (2.3%)	92.5% (0.9%)	91.2% (0.3%)	93.5% (0.5%)
Methyl-glucamine	89.3% (0.2%)	94.0% (0.3%)	95.2% (1.1%)	95.5% (0.8%)	97.9% (0.8%)
Glucose	99.9% (0.5%)	88.8% (0.8%)	98.4% (0.5%)	91.8% (2.1%)	99.8% (2.5%)
Mannose	85.4% (0.2%)	92.5% (1.4%)	94.8% (0.8%)	94.7% (0.6%)	98.3% (3.6%)
Methyl-Glucopyranoside	89.2% (1.8%)	95.9% (0.6%)	95.3% (0.6%)	96.3% (0.8%)	88.2% (10.0%)
Xylose	83.0% (1.3%)	90.6% (0.6%)	95.7% (0.6%)	93.0% (0.5%)	94.8% (2.1%)
Rhamnose	97.0% (1.7%)	85.5% (3.0%)	95.6% (0.1%)	111.1% (0.8%)	92.4% (1.3%)
Acetyl-glucosamine	81.0% (1.7%)	92.8% (0.5%)	94.9% (0.3%)	91.6% (1.0%)	98.7% (1.2%)
Trehalose	91.5% (0.3%)	89.6% (0.6%)	98.4% (1.1%)	90.4% (0.9%)	92.1% (2.1%)
Raffinose	92.6% (1.7%)	90.8% (0.4%)	98.1% (0.5%)	86.5% (2.2%)	91.3% (4.1%)
Psicose	102.4% (2.6%)	95.1% (0.4%)			
Fructose	96.0% (0.4%)	92.3% (1.4%)			
2-deoxy-glucose	97.5% (0.3%)	95.1% (0.7%)			
2-deoxy-ribose	88.5% (0.6%)	93.5% (0.8%)			
Palatinose	98.2% (0.5%)	92.8% (1.6%)			
Melibiose	96.7% (1.9%)	95.1% (0.6%)			
Maltose	95.4% (0.6%)	92.8% (1.3%)			
N-Acetyl-Neuraminic Acid	95.5% (0.1%)	94.9% (1.2%)			
Ethyl-glycine	96.9% (0.2%)	92.8% (1.9%)			
n-acetyl-glycine	98.5% (0.4%)	93.1% (2.0%)			
Gly-gly	97.7% (0.6%)	91.6% (0.4%)			
Gly-leu	94.4% (0.6%)	93.4% (0.4%)			
Gly-ser	97.3% (0.9%)	92.5% (0.4%)			
Gly-glu	97.2% (0.6%)	88.6% (0.6%)			

Table F.3 SDS-PAGE Results under non-reducing and reducing conditions Reducing conditions were not used for α-amylase as it does not contain cysteine residues. Results for reducing conditions are given in parenthesis.

Excipient	RNAse A	BSA	Ovalbumin	Trypsin Inhibitor	α-Amylase
Sorbitol	Dimer + Larger Aggregates (Dimer)	Dimer + Larger Aggregates (Dimer + Larger Aggregates)	Large Aggregates (None)	None (None)	Large Aggregates
Mannitol	Dimer (Dimer)	Dimer + Larger Aggregates (Dimer + Larger Aggregates)	Large Aggregates (None)	None (None)	Large Aggregates
Maltitol	Dimer (Dimer)	Dimer + Larger Aggregates (Dimer + Larger Aggregates)	Large Aggregates (None)	None (None)	Large Aggregates
Methyl-glucamine	Dimer (Dimer)	Dimer + Larger Aggregates (Dimer + Larger Aggregates)	Large Aggregates (None)	None (None)	Large Aggregates
Glucose	Dimer + Larger Aggregates (Dimer)	Dimer + Larger Aggregates (Dimer + Larger Aggregates)	Large Aggregates (None)	None (None)	Large Aggregates
Mannose	Dimer (Dimer)	Dimer + Larger Aggregates (Dimer + Larger Aggregates)	Large Aggregates (None)	None (None)	Large Aggregates
Methyl-glucose	Dimer (Dimer)	Dimer + Larger Aggregates (Dimer + Larger Aggregates)	Large Aggregates (None)	None (None)	Large Aggregates
Xylose	Dimer (Dimer)	Dimer + Larger Aggregates (Dimer + Larger Aggregates)	Large Aggregates (None)	None (None)	Large Aggregates
Rhamnose	Dimer + Larger Aggregates (Dimer)	Dimer + Larger Aggregates (Dimer + Larger Aggregates)	Large Aggregates (None)	None (None)	Large Aggregates
Acetyl-glucosamine	Dimer (Dimer)	Dimer + Larger Aggregates (Dimer + Larger Aggregates)	Large Aggregates (None)	None (None)	Large Aggregates
Trehalose	Dimer + Larger Aggregates (Dimer)	Dimer + Larger Aggregates (Dimer + Larger Aggregates)	Large Aggregates (None)	None (None)	Large Aggregates
Raffinose	Dimer + Larger Aggregates (Dimer)	Dimer + Larger Aggregates (Dimer + Larger Aggregates)	Large Aggregates (None)	None (None)	Large Aggregates